Web-Based Radio Fading Channel Modeling, Estimation and Identification

Jun Zhan

Supervisor: Professor Dr. C.D. Charalambos

A thesis submitted to the Faculty of Graduate and Postdoctoral Studies
in partial fulfillment of the requirements for the degree of
Master's Program in Systems Science

Systems Science Program
School of Information Technology and Engineering
University of Ottawa
Ottawa, Ontario, K1N 6N5
Canada

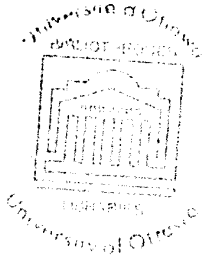

Abstract

This thesis focuses on the practical implementation issues for modeling, simulation, estimation and system identification of wireless fading channels.

The state space models are introduced to describe fading channels including flat fading and frequency-selective fading channels.

Without measurement data, simulation and estimation of fading channels are related to the motion of the transmitter or the receiver. The state space realizations and the Kalman filtering are derived for Rayleight fading, Ricean fading and frequency-selective fading channels. The inphase, quadrature and envelope components of the received signals are simulated and estimated through the state space realizations and the Kalman filtering. These model parameters are defined by the transfer function of a given Doppler power spectral density (DPSD) associated to several physical factors such as carried frequency, mobile moving speed, signal-to-noise ratio (SNR), an angle and an interval time.

With measurement data, system identification is based on the Expectation-Maximization (EM) algorithm together with the Kalman filtering. These system parameters are computed recursively. Various identified results illustrate the processes of system identification for flat fading and frequency-selective fading channels based on the measurement data provided by Communications Research Center Canada (CRC). Measurement data could also be input by users.

Finally, a web-based wireless fading channel simulation and estimation system is analyzed, designed and implemented using UML™ techniques and Java™ programming language. The web-based system can provide friendly interfaces to complete modeling, simulation, estimation and system identification of fading channels. The Web-based simulation and estimation system can be run on the following site:

http://www.site.uottawa.ca/~jzhan037/onlineSystem.html or

http://www.site.uottawa.ca/~chadcha/onlineSystem.html.

Keywords: fading channel, Rayleigh fading, Ricean fading, flat fading, frequency-selective fading, state space model, Kalman filter, Expectation-Maximization algorithm, system identification, measurement data, web application, Java and UML.

Acknowledgements

I am grateful to my supervisor, Professor Dr. C. D. Charalambous since he has been particularly helpful in guiding my research. Due to his valuable suggestions and essential support, I have completed this research.

I would like to thank Mr. Xin Li for explaining his master's thesis results. From these results, I obtained value ideas in building mathematical models.

I would also like to thank Mr. Alireza Farhadi for discussing the Expectation Maximization algorithm.

Many thanks to Mr. Shili Lu, Mr. Yongshen Yang and many others at the Broadband Wireless and Internetworking Research Lab.

I would also like to thank Dr. Jean-Michel Thizy, director of the Systems Science, for his help.

Special thanks to my wife, Chunling Shi. Without her encouragement and support, I could not have studied for the master's program. From a software engineer's view, she has also given me many excellent suggestions about software development. I would also thank my sons, Gerry and Jimmy, because they have given me a very happy life during my hard work. Thanks also to my parents and my parents-in-law for their love and care.

Acronyms and Abbreviations

API:	*Application Programming Interface*
AWGN:	*Additive White Gaussian Noise*
CRC:	*Communications Research Center Canada*
DPSD:	*Doppler power spectral density*
EM:	*Expectation-Maximization*
FFT:	*Fast Fourier Transform*
GUI:	*Graphics User Interface*
LOS:	*Line-of-Sight*
JDK:	*Java Development Kit*
JFC:	*Java Foundation Class*
JVM:	*Java Visual Machine*
MLE:	*Maximum Likelihood Estimation*
NLOS:	*Non-Line-of-Sight*
OOP:	*Object-Oriented Programming*
SNR:	*Signal-to-Noise*
WFSE:	*Web-Based Fading Channel Simulation and Estimation System*
WSS:	*Wide Sense Stationary*
UML:	*Unified Modeling Language*

Table of Contents

List of Figures

List of Tables

Chapter 1

Introduction

This chapter introduces basic knowledge of mobile radio channel and fading channels, and presents objectives and organization of this thesis.

1.1 Mobile Radio Channel

Wireless communication has become one of the most important fields in our daily life and it is also the fastest growing segment of the communication industry. It provides high-speed, high-quality information exchange between portable devices located anywhere in the world. It has also been applied to many fields such as voice communication, high-speed internet access, web browsing, paging and short messaging, file transfer, device interconnection, smart homes and appliances, video teleconferencing, and autonomous sensor networks.

Figure 1-1, adapted from [JAK74], is a block of a wireless communication link which includes three components such as a transmitter, a receiver and a channel. The transmitter sends messages (data source) to the receiver through a channel. A channel is established to provide a communication path between the transmitter and the receiver; and it can be defined as *frequency band* in the frequency domain or *digital time slot equivalent* in the time domain [PRO00].

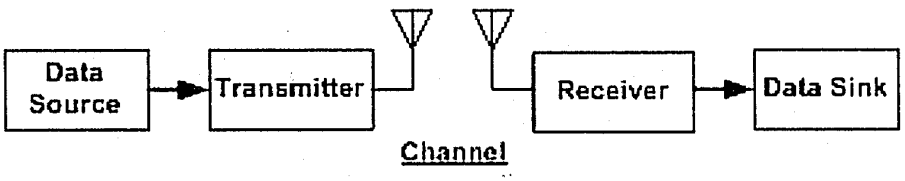

Figure 1-1 Block Diagram of the Wireless Communication Link

The mobile radio channel places fundamental limitations on the performance of wireless communication systems. Wireless communications have different characteristics from wired communication. The mobile radio channel is extremely unpredictable and variable, while wired channel is predictable and stable. Fading and interference are two important problems in wireless communication, while they are not significant in wired communication [AKA97].

Because of the natural and man-made objects, there exists no direct line-of-sight path between the transmitter and receiver in wireless communications, this property is called fading. The fading causes the received signal power to change with time and the received signal is the combination of multipath components [BIG99]; the fading rate depends on the velocity of the receiver.

The interference of wireless communications is due to wireless communicates over the air. The interference can be between transmitters communicating with a common receiver, such as uplink of a cellular system; or between signals from a signal transmitter to multiple receivers, such as downlink of a cellular system; or between different transmitter-receiver pairs, such as interference between users in different cells [RAP96].

This thesis will focus on studying the fading channel only. Modeling and computer simulation are the tools used for understanding and studying the mobile radio fading channel.

1.2 Fading Channels

In order to ensure reliable and high performance communications over a mobile radio channel, wireless communication systems have to be designed for minimizing the effects of mulitpath fading and interference. This section presents concepts of the fading channel such as multipath propagation, characteristics, types, parameters and classification, etc.

1.2.1 Multipath Propagation

Multipath fading is a common phenomenon in the radio channel. When a signal is transmitted at very high frequency over a radio channel, the received signal arrives from various directions over a multiplicity of paths. This phenomenon is called *multipath propagation* [GAR96]. Multipath is connected with the relative motion of the receiver, which results in variation of received signal amplitude and phase. Multipath is usually described as *Line-of-Sight* (LOS) and *Non-Line-of-Sight* (NLOS). LOS is the direct path between the transmitter and the receiver; in addition, NLOS is the path arriving after reflection from reflectors.

There are three basic propagation mechanisms of multipath fading such as *reflection*, *diffraction* and *scattering*. Reflection occurs when the signal is reflected from a smooth surface with significantly larger dimensions than the signal wavelength. Diffraction occurs when the signal encounters an object larger than the wavelength of the signal, causing secondary waves to be formed behind the object. Scattering occurs when a radio wave impinges on either: a large rough surface; or any surface whose dimensions are on the order of the signal wavelength; or small rough surface, causing the reflected energy to spread out in all directions.

As a consequence of reflections, diffraction, and scattering, the received signals arrive at the receiver from many directions and with amplitude, phase fluctuations and time delay. Examples of such situations occur in indoor propagation, when the electromagnetic waves are perturbed by structures inside the building; and in terrestrial mobile radio, when mulitpath is caused by large fixed or moving objects such as buildings, hills, vehicles, etc [JAK74]

1.2.2 Characteristics of the Fading Channels

The radio channels are a time varying, multipath fading channel, and its main characteristics are *time spread* and *time variation*.

The *time spread* of fading channels is due to the multipath property. The transmitted signal travels through many paths from a transmitter to a receiver, and each

received pulse arrives at the receiver via different paths. For example, when an ideal impulse is transmitted over a time-varying multipath channel, the received signal might appear as a train of impulse having different attenuation, different phase and different delay time [RAP96].

The *time variation* of fading channels is due to the environmental changes as time passes between the transmitter and receiver. If the pulse-sounding experiment is repeated over time under the same conditions, the received pulse train will be differences. These differences include the sizes of the individual pluses, the relative delays among the pluses, and the number of impulses observed, as well, the time variation appears to be unpredictable. Therefore, the multipath fading channel is characterized statistically [RAP96].

1.2.3 Fading Types: Large-scale Fading and Small-scale Fading

The fading channels can be divided into two types: *Large-scale fading* and *Small-scale fading*.

Large-scale fading characterizes signal strength over large transmitter-receiver (T-R) separation distances [RAP96].

Small-scale fading represents the rapid fluctuations of the received signal strength over very short travel distances or short time durations. In this case, the received signal is a sum of many contributions coming from different directions at slightly different times. The small-scale fading is usually described as Rayleigh fading or Rice fading.

This thesis will focus on the small-scale fading.

1.2.4 Classification of Fading Channels

These parameters, such as *delay spread*, *coherence bandwidth*, *Doppler spread* and *coherence time*, are used to describe the features of the fading channels.

The *delay spread* and *coherence bandwidth* describe the time spreading nature of fading channels in a local area [BAR98]. Delay spread T_m is a measure characterizing the

time-dispersive properties of the channel. Coherence Bandwidth B_c is a statistical measure of the range of frequencies over which the channel can be considered constant or flat.

The *Doppler spread* and *coherence time* describe the time varying nature of fading channels in a small-scale region [RAP96]. Doppler spread B_D is a measure of the spectral broadening caused by the time rate of change of the mobile radio channel and is defined as the range of frequencies over which the received Doppler spectrum is essentially non-zero. Coherence time T_C is used to characterize the time varying nature of the frequency dispersiveness of the channel in the time domain.

Fading channels will undergo different types of fading according to the relation between the signal parameters and the channel parameters. Based on multipath time spreading, the fading channel is classified as *frequency nonselective fading channel* and *frequency-selective fading channel*; according to Doppler spread, however, the fading channels are classified as *fast fading channel* and *slow fading channel*. Figure 1-2 shows the fading channel classification, adapted from [RAP96]. Figure 1-2 (a) is based on the time domain, and Figure 1-2 (b) is based on the frequency domain.

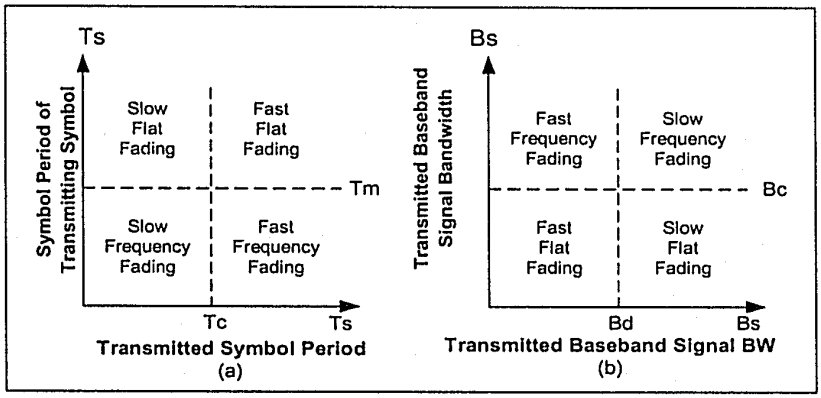

Figure 1-2. Illustrating Types of Fading Classification

Frequency non-selective fading and Frequency selective fading describe the characteristics of the frequency variation. Frequency non-selective fading, also known as *flat fading channel*, indicates that the radio channel has a constant gain and a linear phase

response over a bandwidth that is larger than that of the transmitted signal. *Frequency selective fading* refers to the relationship between the coherence bandwidths. [RAP96].

Fast fading and slow fading channels describe characteristics of the time variation. In a fast fading channel, the channel impulse response changes rapidly within the symbol duration; and the coherence time of the channel is smaller than the symbol period of the transmitted signal. The fast fading causes frequency dispersion due to Doppler spreading. In a slow fading channel, the channel impulse response changes at a rate much slower than the transmitted baseband signal; and the Doppler spread of the channel is much less than the bandwidth of the baseband signal. The slow fading channel may be assumed to be static over one or several reciprocal bandwidth intervals [RAP96, PRO00].

Therefore, there can be four types of fading channels: *Slow and Flat fading channel, Fast and Flat fading channel*, *Slow and Frequency-selective fading channel*, and *Fast and frequency-selective fading channel* [BIG99].

\Specifically, these four types of fading channels are described as follows:

(1) Flat Slow Fading Channel

If $T_s > T_m$ and $T_s < T_c$ or if $B_s < B_c$ and $B_s > B_D$, then this channel is characterized as the flat slow fading channel. In this case, all of the propagation paths are received within one symbol period, and all of the signal frequency components are equally affected by the channel.

(2) Flat Fast Fading Channel

If $T_s > T_m$ and $T_s > T_c$ or if $B_s < B_c$ and $B_s < B_D$, then this channel is characterized as the flat fast fading. This channel varies during the symbol period. It is very difficult to compensate effectively.

(3) Frequency-selective Slow Fading Channel

This channel is characterized as the frequency-selective slow fading if $T_s < T_m$ and $T_s < T_c$ or if $B_s > B_c$ and $B_s > B_D$. In this channel, all the frequency components are not equally affected

(4) Frequency-selective Fast Fading Channel

This channel is characterized as frequency-selective fast fading, if $T_s < T_m$ and $T_s > T_c$, or if $B_s > B_c$ and $B_s < B_D$. This case is the worst type of channel for the receiver because the received symbol is spread over many symbol periods and the channel varies during the symbol period as well.

1.3 Objectives

Wireless communication systems offer many effective services and benefits to humans, but they are expensive for us to design, build and maintain. Therefore, manufacturers have been looking at alternatives so as to avoid these perhaps unnecessary costs. One of these alternatives is to simulate a real wireless communication system, of which the fading channel model is one of the key simulation components. For these reasons, the purposes of this thesis are to build a web-based fading channel simulation and estimation system.

According to the above wireless communication concepts and their explanations, this thesis will make full use of the existing wireless communication technologies and present the specific thesis topic as the following aspects [CHA03]:

(1) *Development of mathematical models of fading channels that are related to the motion of the receiver.*

The mathematical models are important in the development of a novel channel simulator which would replicate wireless channel characteristics, and are related to the motion of the receiver through the *Doppler power spectral density* (DPSD) function. A state space models are used to represents fading channels that can be flat fading (Rayleigh fading or Ricean fading) and frequency-selective fading.

(2) *Descriptions of the Kalman filter to estimate the least square components of the received signal.*

The Kalman filter is employed to estimate inphase, quadrature, envelope and phase components of the received signal without the measurement data. In this case, the model parameters are assumed to be known.

(3) *Development of the Expectation Maximization (EM) algorithm related to system identification.*

Together with the Kalman filter, the EM algorithm can be used to analyze and identify the model parameters based on the measured data provided by the Communications Research Centre of Canada (CRC). In addition, the purpose of the EM algorithm is to estimate the inphase and quadrature components of the received signal when the model parameters are unknown.

(4) *Employment of the EM algorithm and the Kalman filter.*

The EM algorithm is developed in the state space models which when fed with white noise, and is generated outputs that have the statistical characteristics of both the inphase and quadrature components of the measured data.

(5) *Development of a web-based software system to model, estimate and identify the fading channel.*

The web-based application is designed for the radio fading channel simulation, estimation and identification based on the above (1)~(4) descriptions and the web-based application is implemented using Java programming. Its purpose is that anyone can use this web-based system to analyze characteristics of fading channels anywhere and anytime; it is more important that users can use their own measurement data to model, estimate and identify fading channels.

1.4 Organization

This thesis includes six chapters as follows:

Chapter 1, *Introduction*, introduces the basic knowledge of mobile radio channels and fading channels such as their concept, characteristics, parameters and classifications; it also presents the objectives of the thesis.

Chapter 2, *Wireless Fading Channel Models, Simulation and Estimation*, describes mathematical models of the fading channels in state space form and the Kalman filters; and these system parameters are related to the physical factors of the motion of the receiver. These models and the Kalman filters are employed to estimate the inphase, quadrature, envelope and phase components; and they are suited to the Rayleigh fading, the Ricean fading channels and the frequency-selective fading. Several estimated results are also presented to verify the state space models and the Kalman filters.

Chapter 3, *System Identification via Expectation Maximization Algorithm and Kalman Filter*, describes the Expectation-Maximum (EM) algorithm together with the Kalman filter to estimate system parameters in state space form. An example shows how to use the EM algorithm; and a table lists the verification results of the EM algorithm with some samples. Furthermore, the model based on the measurement data provided by the CRC is also discussed for flat fading and frequency-selective fading; and several estimated results are indicated.

Chapter 4, *Web-based System Analysis, Design and Implementation*, presents software analysis, design and implementation for this web-based wireless fading channel simulation and estimation system. It introduces basic concepts about Object-oriented and UML, analyzes the web-based system's requirements, and presents the system's user case diagrams, class diagrams and sequence diagrams using UML techniques. Additionally, for software implementation, this chapter also introduces Java architecture, Java Applet and its related techniques such as Java Plug-in, Java Swing, Java 2D Graphics, and Java I/O operations.

Chapter 5, *Summary and Future Work*, summaries the research work and indicates future research.

Appendix A, *System Identification Estimated Results for the Flat Fading Based on the Measurement Data*, illustrates the estimated results for the flat fading channel models based on the measurement data.

Appendix B, *System Identification Estimated Results for the Frequency-selective Fading Based on the Measurement Data*, shows the estimated results for the frequency-selective fading channel model based on the measurement data.

Appendix C, *Web-based Simulation and Estimation Operating Guide*, presents operating the web-based wireless fading channel simulation and estimation system. It introduces the system's functions, Graphics User Interface (GUI) and operation steps.

Appendix D, *Installing CD-ROM*, introduces CD-ROM installation that this CD-ROM contains the author's Java source and the measurement data provided by CRC.

Chapter 2

Wireless Fading Channel Mathematical Models, Simulation and Estimation

Wireless fading channels have historically been one of the most difficult tasks of mobile radio communications. Most models and simulators for radio fading channels are typically modulated in a statistical fashion. However, the analysis of various measurement data reveals that the channel process changes as a result of the motion of the transmitter or the receiver. Accordingly, these models and simulators are often inappropriate and inaccurate [CHA03]. It is very important to develop a novel channel simulator that replicates wireless channel characteristics and produces varying outputs in a similar manner to a real-world channel.

This chapter discusses the development of better fading channel models that are based on state space models that are associated with the motion of the receiver. Section 2.1 introduces the mathematical representation and the characteristics of the fading channels, and also describes a simulation structure of the fading channel in the frequency domain; Section 2.2 presents the state space realization for flat fading and frequency-selective fading, especially the Rayleigh fading and the Ricean fading channel; Section 2.3 discusses the Kalman filter's applications for estimating the fading channels described in the above; Section 2.4 describes estimating process of these fading channel models and illustrates several estimated results to verify the state space models and the Kalman filter's equations.

2.1 Mathematical Description of Fading Channels

The mobile radio channel is actually the combination of the multipath propagation. The multipath effect causes the radio fading channel to be much more difficult to simulate than the AWGN channel [BIG99].

This section introduces mathematical representation and characteristics of the fading channel; and presents a simulation structure of the fading channel in the frequency domain.

2.1.1 Mathematical Representation for Fading Channels

A typical multipath fading channel is generally characterized by a time-varying (equivalent low-pass) impulse response $C_\ell(t,\tau)$ or a time-varying frequency response filter $C_\ell(t,f)$.

If $\{s_l(t)\}_{t \geq 0}$ denotes a low-pass signal with carried frequency f_c transmitted via multipath fading channels, the equivalent low-pass received signal can be expressed as the following [CHA991, CHA01]:

$$\begin{aligned} y_t(t) &= \sum_{n=1}^{N} r_n(t,\tau_n(t))\, e^{j\phi_n(t,\tau_n(t))} s_t(t-\tau_n(t)) + v_t(t) \\ &= \int_{-\infty}^{+\infty} C_t(t,\tau) s_t(t-\tau_n(t))\, d\tau + v_t(t) \end{aligned} \qquad (2.1)$$

Here, $C_\ell(t,\tau)$ denotes the response of the fading channel at time t, due to an impulse applied at time (t-τ); and $\{v_\ell(t)\}_{t\geq 0}$ is the AWGN process.

From the equation (2.1), a statistical model of the fading channel is presented as [CHA991, CHA01]:

$$C_\ell(t,\tau) = \sum_{n=1}^{N} r_n(t,\tau_n(t)) e^{j\phi_n(\tau,\tau_n(t))} \delta(\tau-\tau_n(t)) \qquad (2.2)$$

In this equation, $r_n(t,\tau_n(t))$, $\phi_n(t,\tau_n(t))$ and $\tau_n(t)$ denote the attenuation, phase and propagation time delay on the n^{th} path at time t; whereas, N is the total number of multipath components.

If $s_\ell(t) = 1$ for all time t, the received signal in the equation (2.1) can be expressed by [PRO00]:

$$y_\ell(t) = \sum_{n=1}^{N} r_n(t, \tau_n(t))\, e^{j\phi_n(t,\tau_n(t))} + v_\ell(t) \tag{2.3}$$

The equation (2.3) shows that the received signal of the fading channel is composed of the sum of a number of time-variant vectors with their amplitudes $r_n(t, \tau_n(t))$ and phases $\phi_n(t, \tau_n(t)) = 2\pi f_c \tau_n(t)$.

Similarly, the received band pass signal can also be expressed as [PRO00]:

$$\begin{aligned} y(t) &= \mathrm{Re}\left\{ y_\ell(t)\, e^{j2\pi f_c t} \right\} \\ &= \mathrm{Re}\left\{ \left(\sum_{n=1}^{N} r_n(t, \tau_n(t)) e^{j\phi_n(t,\tau_n(t))} s_\ell(t - \tau_n(t)) + v_\ell(t) \right) e^{j\omega_c t} \right\} \end{aligned}$$

Further, the band pass representation of the received signal can be given by [CHA99]:

$$\begin{aligned} y(t) &= \sum_{n=1}^{N} \left(I_n(t, \tau_n(t)) \cos(\omega_c t) - Q_n(t, \tau_n(t)) \sin(\omega_c t) \right) s\left(t - \tau_n(t)\right) + v_I \cos(\omega_c t) - v_Q(t) \sin(\omega_c t) \\ &= \left(I(t,\tau) \cos(\omega_c t) - Q(t,\tau) \sin(\omega_c t) \right) s\left(t - \tau_n(t)\right) + v_I \cos(\omega_c t) - v_Q(t) \sin(\omega_c t) \end{aligned} \tag{2.4}$$

In this case, $\left\{ I_n\left(t, \tau_n(t)\right) \right\}_{t \geq 0}$ and $\left\{ Q_n\left(t, \tau_n(t)\right) \right\}_{t \geq 0}$ are the inphase and quadrature components of the received signal at n^{th} path, and they can be expressed as:

$$\begin{aligned} I_n\left(t, \tau_n(t)\right) &= r_n\left(t, \tau_n(t)\right) \cos\left(\phi_n(t, \tau_n(t))\right) \\ Q_n\left(t, \tau_n(t)\right) &= r_n\left(t, \tau_n(t)\right) \sin\left(\phi_n(t, \tau_n(t))\right) \end{aligned}$$

The total inphase and quadrature components of the received signal are illustrated by $\left\{ I(t) \right\}_{t \geq 0}$ and $\left\{ Q(t) \right\}_{t \geq 0}$, and they are given by the following equation:

$$\begin{aligned} I(t,\tau) &= \sum_{n=1}^{N} I_n\left(t, \tau_n(t)\right) = \sum_{n=1}^{N} r_n\left(t, \tau_n(t)\right) \cos\left(\phi_n(t, \tau_n(t))\right) \\ Q(t,\tau) &= \sum_{n=1}^{N} Q_n\left(t, \tau_n(t)\right) = \sum_{n=1}^{N} r_n\left(t, \tau_n(t)\right) \sin\left(\phi_n(t, \tau_n(t))\right) \end{aligned} \tag{2.5}$$

Furthermore, $\{v_I(t)\}_{t\geq 0}$ and $\{v_Q(t)\}_{t\geq 0}$ are two independent and identically distributed (iid) AWGN with the density $N(0,\sigma_v^2)$ and $\omega_c = 2\pi f_c$.

2.1.2 Mathematical Characterization of Fading Channels

This subsection analyzes three mathematical characteristics of the fading channels: statistical characterization, received signal amplitude distribution, and LOS components.

- **Statistical Characterization**

According to the central limit theorem, when there are a number of paths in which N is large, $y_t(t)$ may be modeled as a complex-valued Gaussian random process. This means that the time-variant impulse response $C_t(t,\tau)$ is also a complex-valued Gaussian random process in the time variable t. Similarly, the inphase component $\{I(t)\}_{t\geq 0}$ and the quadrature component $\{Q(t)\}_{t\geq 0}$ are also Gaussian random variables with the same mean and variance, and their probability densities are given as the following:

$$f(x) = \frac{1}{\sqrt{2\pi\sigma}} e^{-(x-u)^2/2\sigma^2}, \quad x \geq 0$$

In this equation, $u = E[I(t)] = E[Q(t)]$ denote the mean values and $\sigma^2 = Var(I(t)) = Var(Q(t))$ denote the variances of the inphase and quadrature components.

- **Received Signal Amplitude Distribution**

The envelope of the received signal of the fading channel is $|r(t)|$.

Depending on the traveling wave environment, the envelope of the received signal can be described by a Rayleigh or a Ricean distribution. If the inphase and quadrature components are zero-mean ($\mu = 0$), the received signal amplitude distribution corresponds to the Rayleigh distribution, and the phase is uniformly distributed in the interval (0, 2π). Conversely, if the inphase and quadrature components are not zero-mean ($\mu \neq 0$), the received signal amplitude distribution corresponds to the Ricean distribution.

- **LOS Component**

In the Rayleigh fading channel, there is no LOS component between the transmitter and the receiver. Thus, the inphase component $\{I(t)\}_{t\geq 0}$ and the quadrature component $\{Q(t)\}_{t\geq 0}$ do not include a LOS component, and they are Gaussian random variables with zero-means.

However, in the Ricean fading channel, there exists a direct LOS component between the transmitter and the receiver. Therefore, the inphase component $\{I(t)\}_{t\geq 0}$ and the quadrature component $\{Q(t)\}_{t\geq 0}$ are composed of a LOS component, but they are still Gaussian random variables with non-zero means.

2.1.3 Autocorrelation Function and Doppler Power Spectral Density Function

The autocorrelation function and Doppler power spectral density (DPSD) function are usually used to describe characteristics of the fading channel.

- **Autocorrelation Function [PRO00]**

If the equivalent low pass impulse response $C_t(t,\tau)$ is assumed to be WSS, then, the *autocorrelation function* of $C_t(t,\tau)$ is defined as:

$$\phi_c(\tau_1,\tau_2;\Delta t) = E[C_t^{T}(\tau_1;t)\, C_t(\tau_2;t+\Delta t)] \tag{2.6}$$

Further, if the attenuation and the phase shift of the received signal of the fading channel at path delay τ_1 is uncorrelated with the received signal at path delay τ_2, the autocorrelation function can be also expressed as:

$$\phi_c(\tau_1,\tau_2;\Delta t) = \phi_c(\tau_1;\Delta t)\delta(\tau_1-\tau_2) \tag{2.7}$$

In this equation (2.7), $\phi_c(\tau;\Delta t)$ denotes the average power output as a function of time-delay (τ) and time difference (Δt). If $\Delta t = 0$, $\phi_c(\tau;0) \equiv \phi_c(\tau)$ denotes the average power output as a function of time-delay (τ), then $\phi_c(\tau)$ is called *the multipath intensity profile.*

The time variant transfer function of the fading channel is obtained by taking the Fourier transform of $C_t(t,\tau)$ and it can be expressed via:

$$C_t(t,f) = \int_{-\infty}^{\infty} C_t(t;\tau)e^{-j2\pi f_c \tau} d\tau$$

In this case, variable (f) denotes frequency, and $C_t(t,f)$ has the same statistics characteristics as $C_t(t,\tau)$.

Similarly, if it is assumed that there are the same conditions as $C_t(t,\tau)$, the autocorrelation function of $C_t(t,f)$ in frequency domain can be expressed as:

$$\phi_C(f_1,f_2;\Delta t) = E[C_t^{\ T}(f_1;t)\, C_t(f_2;t+\Delta t)] = \phi_C(\Delta f;\Delta t) \qquad (2.8)$$

The equation (2.8) is meant that the autocorrelation function of $C_t(t,f)$ is a function of the frequency difference ($\Delta f = f_2 - f_1$) and the time difference (Δt). $\phi_C(\Delta f;\Delta t)$ is called *the spaced-frequency, spaced-time correlation function* of the fading channel. But only if $\Delta t = 0$, $\phi_C(\Delta f;\Delta t) \equiv \phi_C(\Delta f)$.

The relationship between $\phi_c(\tau)$ and $\phi_C(\Delta f)$ is given as:

$$\phi_C(\Delta f) = \int_{-\infty}^{\infty} \phi_c(\tau)e^{-j2\pi \Delta f \tau} d\tau \qquad (2.9)$$

- **Doppler Shift**

The time variations of the fading channel can be related directly to the motion of the receiver and indirectly to the *Doppler* effects.

Due to mobile motion, the rate of the phase change is apparent as a *Doppler frequency shift* or *Doppler Shift* in each propagation path. Figure 2-1, adapted from [PAP96], illustrates the Doppler shift.

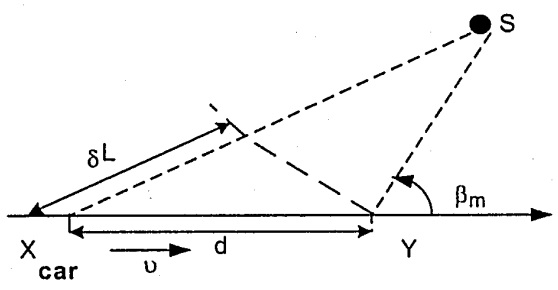

Figure 2-1. Illustration of Doppler Effect

For instance, a mobile moves with velocity υ along the path XY, and receives a wave from a scatter S, therefore, the phase change can be defined as [PAP96]:

$$\Delta\phi = -\frac{2\pi}{\lambda}\Delta l = -\frac{2\pi\upsilon\Delta t}{\lambda}\cos\beta_m \tag{2.10}$$

Here, $\lambda = {}^{1}/_{f_c}$ is wavelength of carried frequency.

The Doppler shift can be described as the apparent change in frequency. It is defined as [PAP96]:

$$f = -\frac{1}{2\pi\lambda}\frac{\Delta\phi}{\Delta t} = -\frac{\upsilon}{\lambda}\cos\beta_m \tag{2.11}$$

This equation (2.11) means that the Doppler shift will depend on the carrier frequency, the mobile velocity, and the spatial angle between the wave and the direction of motion.

In this case, the maximum Doppler shift is obtained by $f_{\max} = -{}^{\upsilon}/_{\lambda}$.

- **Doppler Power Spectrum [PRO00, RAP96]**

In order to relate the Doppler shift effects to the time variations for the fading channel, the function $S_C(\Delta f, \lambda)$ is defined as the Fourier transform of $\phi_C(\Delta f; \Delta t)$, with respect to the variable Δt.

$$S_C(\Delta f, \lambda) = \int_{-\infty}^{\infty} \phi_C(\Delta f, \Delta t) e^{-j2\pi\lambda\Delta t} d\Delta t \tag{2.12}$$

If $\Delta f = 0$, then $S_C(0;\lambda) \equiv S_C(\lambda)$ and the equation can be expressed simply as:

$$S_C(\lambda) = \int_{-\infty}^{\infty} \phi_C(0, \Delta t) e^{-j2\pi\lambda\Delta t} d\Delta t = \int_{-\infty}^{\infty} \phi_C(\Delta t) e^{-j2\pi\lambda\Delta t} d\Delta t \tag{2.13}$$

Here, $S_C(\lambda)$ is called *the Doppler power spectrum* that gives the signal intensity as a function of the Doppler frequency λ. If the channel is time invariant, $\phi_C(\Delta t) = 1$, then $S_C(\lambda) = \delta(\lambda)$ (delta function). This means that there are no time variations in the fading channel, and there is no spectral broadening observed in the transmission of a pure frequency tone.

Under certain conditions, the Doppler power spectral densities of the inphase and quadrature components are expressed by [CHA03, LIX02]:

$$S_I(f)=S_Q(f)=\begin{cases}0; & |f|>\frac{\upsilon(t)}{\lambda} \\ \frac{E_0}{2}\frac{1}{2\sin\beta_m(t)}\frac{\lambda}{\upsilon(t)}; & \frac{\upsilon(t)}{\lambda}\cos\beta_m(t)\le|f|\le\frac{\upsilon(t)}{\lambda} \\ \frac{E_0}{2}\frac{1}{2\sin\beta_m(t)}\frac{\lambda}{\upsilon(t)}\left[\frac{\pi}{2}-\arcsin\frac{2\cos^2\beta_m(t)-1-(\frac{f\lambda}{\upsilon(t)})^2}{1-(\frac{f\lambda}{\upsilon(t)})^2}\right]; & |f|<\frac{\upsilon(t)}{\lambda}\cos\beta_m(t)\end{cases} \quad (2.14)$$

In this equation, $\upsilon(t)$ is the velocity of a moving mobile; $\beta_m(t)$ is the maximum assumed spatial angle; λ is the wave length associated with the carrier frequency; $f_d = \upsilon/\lambda$ is the maximum Doppler shift, and E_0 controls the attenuation of $S_I(f)$ or $S_Q(f)$ at zero frequency. These variables are associated with each path component.

The Doppler power spectral density function $S(f)$ describes how the multipath propagation spreads the spectrum of the transmitted signal and also indicates how fast the fading process is.

2.1.4 Simulation Structure of Fading Channels in Frequency Domain

The fading channel is assumed to be WSS both in time domain and frequency domain, and the different propagation paths are also assumed to be uncorrelated. Therefore, a simple simulation structure for the fading phenomenon can be built from several functions, such as multipath intensity profile function, spaced-frequency correlation function, spaced-time correlation function and Doppler power spectrum [RAP96].

[LIX02] introduces the state space model from the rational transfer function which is related to the Doppler power spectral density functions. Figure 2-2, adapted from [LIX02], describes the bandpass fading channel's simulation structure in frequency domain.

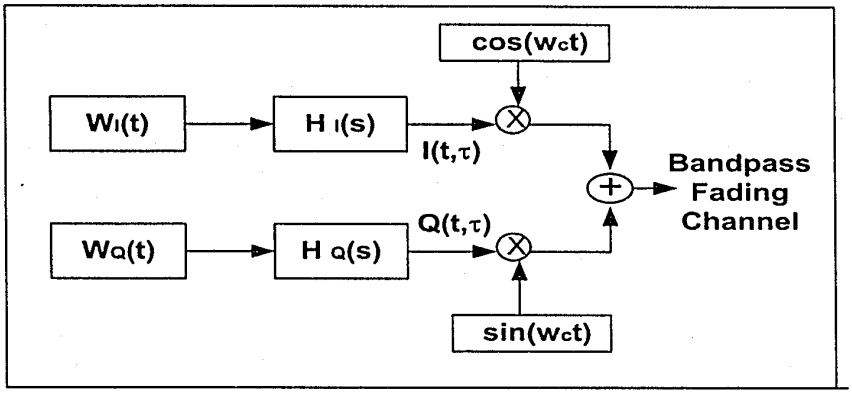

Figure 2-2. The Bandpass Channel Model in Frequency Domain

In this figure, $W_I(t)$ and $W_Q(t)$ are AWGN, $H_I(s)$ and $H_Q(s)$ denote rational transfer functions.

2.2 State Space Realization of Fading Channels

In mobile communication systems, the mobile radio channel models have been studied over 40 years. Several fading channel models are suggested to explain the observed statistical characteristics of the electromagnetic fields and the envelope and phase of the received signal. For instance, Ossana's model was used to explain the interference of wave incident and reflected from the flat sides of randomly-located buildings, but this model is rather inflexible and inappropriate for urban areas [OSS64]. Clarke's model was one of the most widely uses of 2-dimensional model, which assumed the field incident on the mobile antenna was composed of a number of horizontally traveling plane waves of random phase; this model assumes that a fixed transmitter with a vertically polarized antenna uses[CLA68]. Aulin was the first to show that the introduction of a third dimension, extruding the ring of scatterers into a cylinder, brought better agreement with empirical results [AUL79].

This section describes the fading channel models based on the state space equation for flat and frequency-selective fading channels.

2.2.1 General State Space Model

The state space model has been widely used in many fields such as real-time optimal controls and wireless communications. A state space model can be expressed as the following equation [DAZ95, OGA02]:

$$\begin{cases} \dfrac{dx(t)}{dt} = A(t)x(t) + G(t)u(t) + B(t)w(t) \\ y(t) = C(t)x(t) + D(t)v(t) \end{cases} \tag{2.15}$$

In this equation, the system parameters $\{A(t), G(t), B(t), C(t), D(t)\}$ are defined as the following: $A(t) \in \Re^{n \times n}$ denotes the state matrix, $G(t) \in \Re^{n \times q}$ denotes the input matrix, $B(t) \in \Re^{n \times m}$ denotes the process noise matrix, $C(t) \in \Re^{r \times n}$ denotes the output matrix, and $D(t) \in \Re^{r \times q}$ denotes the measurement noise matrix. Additionally, $x(t) \in \Re^{n}$ is the state of the system, $u(t) \in R^{m}$ and $y(t) \in R^{p}$ are vectors of the input and output signals, $w(t) \in \Re^{m}$ and $v(t) \in \Re^{r}$ are sequences of uncorrelated random variables with zero-mean and covariance σ^2, and the initial state variable x_0 is assumed to be uncorrelated with the process noise [OGA02].

$$\begin{cases} m_0 = E[x(0)] \\ \sigma^2 = E\left[(x(0) - m_0)(x(0) - m_0)^T\right] \end{cases}$$

A zero-input state space model can be rewritten as:

$$\begin{cases} \dfrac{dx(t)}{dt} = A(t)x(t) + B(t)w(t) \\ y(t) = C(t)x(t) + D(t)v(t) \end{cases} \tag{2.16}$$

The state space models are realized from a rational transfer function $H(s)$. However, the state space realizations are not unique. There exist several realizations for the state space such as controllable and observable canonical forms.

For example, a second-order rational transfer function can be given by:

$$H(s) = \frac{k(t)}{s^2 + 2\varsigma(t)\omega_n(t)s + \omega_n^2(t)} \tag{2.17}$$

Let $I(s) = H(s)H^T(s)$, a second-order stochastic differential equation which can be obtained from the rational transfer function $H(s)$ and it can be written as:

$$\begin{cases} \dfrac{d^2x(t)}{dt^2} + 2\xi(t)\omega_n(t)\dfrac{dx(t)}{dt} + \omega_n(t)x(t) = k(t)w(t); \\ \dfrac{dx(t)}{dt}\Big|_{t=0},\ x(0)\ \textit{are given} \end{cases} \tag{2.18}$$

Further, the stochastic differential equation is related to the state space realization with two canonical forms.

For the controllable canonical form, the state space realization can be expressed as [OGA02]:

$$\begin{aligned} \frac{dx(t)}{dt} &= \begin{bmatrix} 0 & 1 \\ -\omega_n^2 & -2\xi\omega_n \end{bmatrix} x(t) + \begin{bmatrix} 0 \\ k \end{bmatrix} w(t) \\ y(t) &= \begin{bmatrix} 1 & 0 \end{bmatrix} x(t) \end{aligned} \tag{2.19}$$

In this case, the system parameters can be given as following form:

$$A = \begin{bmatrix} 0 & 1 \\ -\omega_n^2 & -2\xi\omega_n \end{bmatrix},\quad B = \begin{bmatrix} 0 \\ k \end{bmatrix},\quad C = \begin{bmatrix} 1 & 0 \end{bmatrix} \tag{2.20}$$

In addition, for the observable canonical form, the state-space realization can also be expressed [OGA02]:

$$\begin{aligned} \frac{dx(t)}{dt} &= \begin{bmatrix} 0 & -\omega_n^2 \\ 1 & -2\xi\omega_n \end{bmatrix} x(t) + \begin{bmatrix} k \\ 0 \end{bmatrix} w(t) \\ y(t) &= \begin{bmatrix} 0 & 1 \end{bmatrix} x(t) \end{aligned} \tag{2.21}$$

Similarly, in this case, the system parameters can be given as following form:

$$A = \begin{bmatrix} 0 & -\omega_n^2 \\ 1 & -2\xi\omega_n \end{bmatrix},\quad B = \begin{bmatrix} k \\ 0 \end{bmatrix},\quad C = \begin{bmatrix} 0 & 1 \end{bmatrix} \tag{2.22}$$

A discrete-time linear systems of the state space formulation in the equation (2.16) can be presented as [OGA02]:

$$\begin{cases} x(t_{n+1}) = A(t_n)x(t_n) + B(t_n)w(t_n) \\ y(t_n) = C(t_n)x(t_n) + D(t_n)v(t_n) \end{cases} \tag{2.23}$$

Here t_n denotes discrete time.

The state space model in the equation (2.16), which is related to the Doppler power spectral density function in the equation (2.14), is used to generate the inphase and quadrature components for the fading channel [CHA01, LIX02]. Therefore, there is a state space representation corresponding to the inphase and quadrature components of the fading channel.

In the following subsection, the state space realization of the flat and frequency-selective fading channels will be introduced.

2.2.2 State Space Realization for Flat Fading Channels

In the flat fading channel, the bandwidth of the transmitted signal is less than the coherence bandwidth of the fading channel. Therefore, the envelope of the received signal of the flat fading channel is assumed to follow Rayleigh or Ricean distribution.

In this case, the transmitted signal is considered to be a narrow signal, for instance, $s(t) = 1, \forall\ t \geq 0$, thus the received signal of the flat fading channel is a special case of $N = 1$ in (2.4), and it can be rewritten as:

$$y(t) = \left(I(t,\tau)\cos(\omega_c t) - Q(t,\tau)\sin(\omega_c t)\right)s(t-\tau) + v_I \cos(\omega_c t) - v_Q(t)\sin(\omega_c t) \tag{2.24}$$

2.2.2.1 State-Space Realization for Rayleight Fading Channel

The channel is said to be a *Rayleigh fading channel* if the envelope of the received signal follow the Rayleigh distribution. There is no LOS component, but there exists a number of plane waves with independent and identically distributed inphase and quadrature components with zero-means. The type of fading channel follows quite well with empirical observations for macrocellular applications [RAP96].

Following the equation (2.23), the discrete-time state space models for the inphase and quadrature components of the flat fading channel are easy obtained.

For the inphase component, the state space model for the flat fading channel can be written as:

$$\begin{cases} x_I(t_{n+1}) = A_I(t_n)x_I(t_n) + B_I(t_n)w_I(t_n) \\ y_I(t_n) = C_I(t_n)x_I(t_n) + D_I(t_n)v_I(t_n) \end{cases} \tag{2.25}$$

Additionally, for the quadrature component, the state space model for the flat fading channel can be written as:

$$\begin{cases} x_Q(t_{n+1}) = A_Q(t_n)x_{Qi}(t_n) + B_Q(t_n)w_Q(t_n) \\ y_Q(t_n) = C_Q(t_n)x_Q(t_n) + D_Q(t_n)v_Q(t_n) \end{cases} \tag{2.26}$$

Further, considering a combination of the inphase and quadrature components for the fading channel, the state space model can be given as [LIX02]:

$$\begin{cases} x(t_{n+1}) = \begin{pmatrix} x_I(t_{n+1}) \\ x_Q(t_{n+1}) \end{pmatrix} = \begin{bmatrix} A_I(t_n) & 0 \\ 0 & A_Q(t_n) \end{bmatrix} \begin{pmatrix} x_I(t_n) \\ x_Q(t_n) \end{pmatrix} + \begin{bmatrix} B_I(t_n) & 0 \\ 0 & B_Q(t_n) \end{bmatrix} \begin{pmatrix} w_I(t_n) \\ w_Q(t_n) \end{pmatrix} \\ y(t_n) = y_I(t_n) + y_Q(t_n) = \begin{bmatrix} C_I(t_n) & C_Q(t_n) \end{bmatrix} \begin{pmatrix} x_I(t_n) \\ x_Q(t_n) \end{pmatrix} + \begin{bmatrix} D_I(t_n) & D_Q(t_n) \end{bmatrix} \begin{pmatrix} v_I(t_n) \\ v_Q(t_n) \end{pmatrix} \end{cases} \tag{2.27}$$

The equation (2.27) can be also rewritten in the same way as the equation (2.23):

$$\begin{cases} x(t_{n+1}) = A(t_n)x(t_n) + B(t_n)w(t_n) \\ y(t_n) = C(t_n)x(t_n) + D(t_n)v(t_n) \end{cases} \tag{2.28}$$

Here the system parameters $\{A(t_n), B(t_n), C(t_n), D(t_n)\}$ can be expressed as [LIX02]:

$$\begin{aligned} A(t_n) &= \begin{bmatrix} A_I(t_n) & 0 \\ 0 & A_Q(t_n) \end{bmatrix}, \quad B(t_n) = \begin{bmatrix} B_I(t_n) & 0 \\ 0 & B_Q(t_n) \end{bmatrix}, \\ C(t_n) &= [C_I(t_n) \quad C_Q(t_n)], \quad D(t_n) = [D_I(t_n) \quad D_Q(t_n)] \end{aligned} \tag{2.29}$$

The parameters $\{A_I(t_n), B_I(t_n), C_I(t_n), D_I(t_n)\}$ and $\{A_Q(t_n), B_Q(t_n), C_Q(t_n), D_Q(t_n)\}$ are defined as two forms in the equations (2.20) or (2.22). In addition, the state variables are redefined as the following: $y(t_n)$ is a sequence of the measurement data, $x(t_n) = \begin{bmatrix} x_I(t_n) & x_Q(t_n) \end{bmatrix}^T$ denotes a sequence of interpreting the inphase and quadrature components, $w(t_n) = \begin{bmatrix} w_I(t_n) & w_Q(t_n) \end{bmatrix}^T$ denotes the AWGN process with the density $N(0,1)$, and $v(t_n) = \begin{bmatrix} v_I(t_n) & v_Q(t_n) \end{bmatrix}^T$ denotes the measurement AWGH with the density $N(0,1)$.

In this case, the inphase and quadrature components of the flat fading channel are obtained from the following equation:

$$I(t_n) = \begin{bmatrix} 1 & 0 & 0 & 0 \end{bmatrix} x(t)$$
$$Q(t_n) = \begin{bmatrix} 0 & 0 & 1 & 0 \end{bmatrix} x(t) \tag{2.30}$$

2.2.2.2 State Space Realization for Ricean Fading Channel

This channel is said to be a *Ricean fading channel* if the envelope of the received signal follows the Ricean distribution. The Ricean fading model is similar to the Rayleigh fading model, but the received signal is composed of different components made up of MLOS multiple components plus a significant LOS component. Accordingly, this means that $I(t)$ and $Q(t)$ both have a non-zero mean. The type of fading channel is often observed in microcellular applications [RAP96].

Let $\{I^R(t)\}_{t\geq 0}$ and $\{Q^R(t)\}_{t\geq 0}$ represent the inphase and quadrature components of the Ricean fading channel, thus these components can be generated through the following equation [LIX02]:

$$E\left[I^R(t)\right] = r_0 \cos(\omega_0 t + \theta_0)$$
$$E\left[I^R(t)\right] = r_0 \sin(\omega_0 t + \theta_0) \tag{2.31}$$

In this case, the parameters $\{r_0, \omega_0, \theta_0\}$ correspond to the LOS component.

Considering a LOS component, the state variables of the inphase and quadrature components are rewritten as [LIX02]:

$$x_I^R(t_n) = x_I(t_n) + r_0 \cos(\omega_0 t + \theta_0)\begin{bmatrix} 1 \\ 0 \end{bmatrix}$$
$$x_Q^R(t_n) = x_Q(t_n) + r_0 \sin(\omega_0 t + \theta_0)\begin{bmatrix} 1 \\ 0 \end{bmatrix} \tag{2.32}$$

Similarly, the state space realization for the Ricean fading channel can be expressed as [LIX02]:

$$\begin{cases} x(t_{n+1}) = A(t_n)x(t_n) + B(t_n)w(t_n) + L(t_n) \\ y(t_n) \quad = C(t_n)x(t_n) + D(t_n)v(t_n) \end{cases} \tag{2.33}$$

In this equation, $L(t_n)$ denotes the LOS component and it can be defined as [LIX02]:

$$L(t_n) = \begin{bmatrix} -r_0\omega_0 \sin(\omega_0 t + \theta_0) \\ r_0\omega_n^2 \cos(\omega_0 t + \theta_0) \\ r_0\omega_0 \cos(\omega_0 t + \theta_0) \\ r_0\omega_n^2 \sin(\omega_0 t + \theta_0) \end{bmatrix} \tag{2.34}$$

Therefore, the inphase and quadrature components can be computed from the following equation:

$$\begin{aligned} I^R(t) &= \begin{bmatrix} 1 & 0 & 0 & 0 \end{bmatrix} x^R(t) \\ Q^R(t) &= \begin{bmatrix} 0 & 0 & 1 & 0 \end{bmatrix} x^R(t) \end{aligned} \tag{2.35}$$

2.2.3 State Space Realization for Frequency-selective Fading Channel

The frequency-selective fading channel consists of N multipath components. If it is assumed that the envelope of the received signal for each component follows the Rayleigh or Ricean distributions, then the frequency-selective fading channel can also be represented through the state space model. In this case, the transmitted signal is considered to be a wideband, thus the received signal in the equation (2.4) can be rewritten as:

$$y(t) = \sum_{n=1}^{N} \left(I_n(t, \tau_n(t)) \cos(\omega_c t) - Q_n(t, \tau_n(t)) \sin(\omega_c t) \right) s\left(t - \tau_n(t)\right) + v_I \cos(\omega_c t) - v_Q(t) \sin(\omega_c t) \tag{2.36}$$

Further, it is assumed that the envelope of the received signal of one component follows the Ricean distribution, and others follow the Rayleigh distribution. As previously analyzed in the subsection 2.2.1 and 2.2.2, the state space realization for the frequency-selective fading channel can be expressed as [LIX02]:

$$\begin{cases} x(t_{n+1}) = A(t_n)x(t_n) + B(t_n)w(t_n) + L(t_n) \\ y(t_n) = \sum_{i=1}^{N} C_i(t_n)s(t - \tau_i)x(t_n) + D(t_n)v(t_n) \end{cases} \tag{2.37}$$

In the same way, the state space model parameters are redefined as [LIX02]:

$$A(t_n)=\begin{bmatrix} A_1(t_n) & 0 & \cdots & 0 \\ 0 & A_2(t_n) & \cdots & 0 \\ \vdots & \vdots & \cdots & \vdots \\ 0 & 0 & \cdots & A_N(t_n) \end{bmatrix},\quad B(t_n)=\begin{bmatrix} B_1(t_n) & 0 & \cdots & 0 \\ 0 & B_2(t_n) & \cdots & 0 \\ \vdots & \vdots & \cdots & \vdots \\ 0 & 0 & \cdots & B_N(t_n) \end{bmatrix}$$

$$C(t_n)=[C_1(t_n)s(t-\tau_1)\quad C_2(t_n)s(t-\tau_2)\quad \cdots\quad C_N(t_n)s(t-\tau_N)],$$

$$D(t_n)=[D_1(t_n)\quad D_2(t_n)\quad \cdots\quad D_N(t_n)]$$

$$L(t_n)=\left[L_1(t_n)\quad \overbrace{0\ 0\ 0\ 0}^{2}\quad \cdots\quad \overbrace{0\ 0\ 0\ 0}^{N}\right] \tag{2.38}$$

In addition, the inphase and quadrature components on the k^{th} path can be obtained from the following equation:

$$I_k(t_n)=\left[0\ 0\ 0\ 0\ \cdots\ \overbrace{1\ 0\ 0\ 0}^{k}\ \cdots\ 0\ 0\ 0\ 0\right]x(t_n)$$

$$Q_k(t_n)=\left[0\ 0\ 0\ 0\ \cdots\ \overbrace{0\ 0\ 1\ 0}^{k}\ \cdots\ 0\ 0\ 0\ 0\right]x(t_n) \tag{2.39}$$

In short, the state space model can be applied to modeling the fading channels including the Rayleigh fading, the Ricean fading and the frequency-selective fading. For these fading channel models, the state space realizations are obtained from the rational transfer function, and they are used to generate the inphase and quadrature components of the received signal. Naturally, the envelope and phase components of the received signal are also computed easily through the inphase and quadrature components.

2.3 Application of Kalman Filter to Fading Channels

In 1960, R.E. Kalman described a recursive solution to the discrete-data linear filtering problem. Currently the Kalman filter has been the subject of extensive research and application, particularly in the area of autonomous or assisted navigation. The Kalman filter is a set of mathematical equations that provides an efficient computational (recursive) solution of the least-squares method. The filter is very powerful in several aspects: it supports estimations of past, present, and even future states, and it can do so even when the precise nature of the modeled system is unknown [DAV85].

This section presents the Kalman filter for the state space models of the fading channels described in the Section 2.2.

2.3.1 Kalman Filter Theory

It is the most general problem to estimate a state $\hat{x}(t|t)$ with a known state $x(t)$ in engineering applications. This problem can be represented as [BRO98]:

$$J(t) = E\left[\left(x(t) - \hat{x}(t \mid t)\right)^T \left(x(t) - \hat{x}(t \mid t)\right)\right] \tag{2.40}$$

where $\hat{x}(t|t)$ denotes the estimated state of a known state $x(t)$.

This problem is minimize the estimation error criterion $J(t)$ in (2.40) and Kalman provided a solution to this problem. Kalman defined the state estimation $\hat{x}(t|t)$ as the conditional mean of a known state $x(t)$ given the observation data $Y_N(t)$. The state estimation $\hat{x}(t|t)$ can be expressed as [DAV85]:

$$\hat{x}(t|t) = E\left[x(t)|Y_N(t)\right] \tag{2.41}$$

The following subsections will introduce the Kalman filter for the fading channel models described in Section 2.2.

2.3.2 The Discrete-time Kalman Filter for Rayleigh Fading Channel

Based on the state space realization of the Rayleigh fading channel, the Kalman filter equations provide solutions for estimating the least-square components of the received signal, such as inphase component, quadrature component, envelope component and phase component, $\{I(t_n), Q(t_n), r^2(t_n), \phi(t_n)\}_{t_n \geq 0}$.

The Kalman filter equations for the Rayleigh channels are presented as the following [CHA03, LIX02].

- Initialization Conditions:

$$\hat{x}(0) = E\left[x(0)\right],\ \sigma^2 = Var(x(0)); \tag{2.42}$$

- Error Covariance (Riccati Equation):

$$P(t_{n+1}) = AP(t_n)A^T + BQB^T - AP(t_n)C^T\left[CP(t_n)C^T + DRD^T\right]^{-1}CP(t_n)A^T$$
$$P_0 = \sigma^2 \tag{2.43}$$

In this case, $R = \frac{E_0}{10^{\frac{(SNR)_{dB}}{10}}}\begin{bmatrix}1 & 0\\ 0 & 1\end{bmatrix}$, $Q = \begin{bmatrix}1 & 0\\ 0 & 0\end{bmatrix}$, E_0 is a constant and SNR denotes *Signal to Noise Ratio.*

- Filter Gain:

$$K(t_n) = AP(t_n)C^T\left[CP(t_n)C^T + DRD^T\right]^{-1} \tag{2.44}$$

- Estimation of the State:

$$\hat{x}(t_{n+1}|t_{n+1}) = A\hat{x}(t_n|t_n) + K(t_n)\left[y(t_n) - C\hat{x}(t_n|t_n)\right] \tag{2.45}$$

- Estimations of the Inphase and Quadrature Components:

$$\hat{I}(t_n) = E[I(t_n)|Y_N(t)] = [1\ 0\ 0\ 0]\hat{x}(t_n|t_n)$$
$$\hat{Q}(t_n) = E[Q(t_n)|Y_N(t)] = [0\ 0\ 1\ 0]\hat{x}(t_n|t_n) \tag{2.46}$$

- Estimation of the Square-Envelope Component:

$$\hat{r^2}(t_n) = \hat{I^2}(t_n) + \hat{Q^2}(t_n) + e_I^2(t_n) + e_Q^2(t_n) \tag{2.47}$$

In this equation, $e_I^2(t_n)$ and $e_Q^2(t_n)$ denote the mean square errors (MSEs), and they are defined as the following:

$$e_I^2(t_n) = E\left[\left(I(t_n) - \hat{I}(t_n)\right)^2\right] \text{ and } e_Q^2(t) = E\left[\left(Q(t_n) - \hat{Q}(t_n)\right)^2\right]$$

In addition, $I(t_n)$ and $Q(t_n)$ are defined in the equation (2.30).

- Estimation of Phase Component:

$$\hat{\phi}(t_n) = \tan^{-1}\left(\frac{\hat{Q}(t_n)}{\hat{I}(t_n)}\right) \tag{2.48}$$

The error covariance sequence $P(t_n)$, the gain matrix $K(t_n)$ and the state $\hat{x}(t_n|t_n)$ should be done recursively in order to implement the Kalman filter $\hat{x}(t_{n+1}|t_{n+1})$,.

2.3.3 The Discrete-time Kalman Filter for Ricean Fading Channel

The discrete-time Kalman filter equations for the Ricean fading channel are similar to those of Rayleigh channels. However, the Ricean fading channel contains a LOS component, thus the estimation of the state can be expressed as [LIX02]:

$$\hat{x}(t_{n+1}|t_{n+1}) = A\hat{x}(t_n|t_n) + K(t_n)\left[y(t_n) - C\hat{x}(t_n|t_n) - L(t_n)\right] \tag{2.49}$$

Other Kalman filter's equations are the same as in the list in Subsection 2.3.2

2.3.4 The Discrete-time Kalman Filter of the Frequency-selective Fading Channel

Furthermore, the discrete-time Kalman filter equations for the frequency-selective fading channels can be presented as the following [LIX02]:

- Error Covariance (Riccati Equation):

$$\begin{aligned} P(t_{n+1}) &= AP(t_n)A^T + BQB^T - AP(t_n)C^T\left[CP(t_n)C^T + DRD^T\right]^{-1}CP(t_n)A^T \\ P_0 &= \sigma^2 \end{aligned} \tag{2.50}$$

In this case,

$$R = \frac{E_s}{10^{\frac{(SNR)_{dB}}{10}}}\begin{bmatrix} 1 & 0 & \cdots & 0 \\ \vdots & \vdots & \cdots & \vdots \\ 0 & 0 & \cdots & 1 \end{bmatrix}_{N\times N} \quad \text{and} \quad Q = \begin{bmatrix} 1 & 0 & \cdots & 0 \\ \vdots & \vdots & \cdots & \vdots \\ 0 & 0 & \cdots & 1 \end{bmatrix}_{N\times N}.$$

- Filter Gain:

$$K(t_n) = AP(t_n)C^T\left[CP(t_n)C^T + DRD^T\right]^{-1} \tag{2.51}$$

- Estimation of the State:

$$\hat{x}(t_{n+1}|t_{n+1}) = A\hat{x}(t_n|t_n) + K(t_n)\left[y(t_n) - C\hat{x}(t_n|t_n) - L(t_n)\right] \tag{2.52}$$

- Estimations of the Inphase and Quadrature Components on the i[th] path:

$$\hat{I}_i(t_n) = E\left[I_i(t_n)|Y_N(t)\right] = \left[0\ 0\ 0\ 0\ \cdots\ \overbrace{1\ 0\ 0\ 0}^{i}\ \cdots\ 0\ 0\ 0\ 0\right]\hat{x}(t_n|t_n)$$
$$\hat{Q}_i(t_n) = E\left[Q_i(t_n)|Y_N(t)\right] = \left[0\ 0\ 0\ 0\ \cdots\ \overbrace{0\ 0\ 1\ 0}^{i}\ \cdots\ 0\ 0\ 0\ 0\right]\hat{x}(t_n|t_n) \quad (2.53)$$

- Estimation of Square-Envelope Component on the i[th] path:

$$\hat{r}_i^2(t_n) = \hat{I}_i^2(t_n) + \hat{Q}_i^2(t_n) + e_{I_i}^2(t_n) + e_{Q_i}^2(t_n) \quad (2.54)$$

In this equation, $e_{Ii}^2(t_n)$ and $e_{Qi}^2(t_n)$ denote the mean square errors (MSEs) on the i[th] path, and they are defined as the following:

$$e_{Ii}^2(t_n) = E\left[\left(I_i(t_n) - \hat{I}_i(t_n)\right)^2\right]$$

$$e_{Qi}^2(t) = E\left[\left(Q_i(t_n) - \hat{Q}_i(t_n)\right)^2\right]$$

Additionally, $I_i(t_n)$ and $Q_i(t_n)$ are defined in the equation (2.39).

- Estimation of Phase Component on the i[th] path:

$$\hat{\phi}_i(t_n) = \tan^{-1}\left(\frac{\hat{Q}_i(t_n)}{\hat{I}_i(t_n)}\right) \quad (2.55)$$

In summary, the Kalman filter theory can be used to estimate the least-squares components of the received signal for different fading channel models in the state space forms. These components include inphase, quadarture, envelope, phase and MSEs components.

2.4 Simulation and Estimation of Fading Channels

The system parameters $\{A, B, C, D\}$ of the state space model are assumed to be known, then the characteristics of the fading channel are very easy to simulate and estimate using the state space models described in Section 2.2 together with the Kalman filters described in Section 2.3.

This section presents how to simulate and estimate the inphase, quadrature, envelope and phase components $\{I(t_n), Q(t_n), r^2(t_n), \phi(t_n)\}_{t_n \geq 0}$ of the received signal of the fading channel, and illustrates several estimated results to verify the state space models and the Kalman filters for the Rayleigh fading, the Ricean fading and the frequency-selective fading.

2.4.1 Definition of System Parameters

The state space models of the fading channel are related to the motion of the receiver or the transmitter. The characteristics of the fading channel can be affected by several physical factors such as the carried frequency (f_c), the velocity of the transmitter or the receiver (υ), the signal-to-noise ratio (SNR), and the spatial angle (β_m) between the transmitter and the receiver. In addition, these factors are associated to the Doppler power spectral density function (DPSD). Furthermore, an interval time (Δt) is considered in the discrete-time state space models and the Kalman filters.

In order to simulate and estimate the characteristics of the fading channel, it is necessary to find the relationship between the physical factors and the system parameters of the state space model.

As previous described, the system parameters $\{A, B, C, D\}$ can be defined two canonical forms in the equations (2.20) and (2.22). However, it is essential to first compute these variables $\{\omega_n, \zeta, k\}$. The following equations show how to compute these variables $\{\omega_n, \zeta, k\}$ from the DPSD function $S(f)$ in (2.14) [LIX02]:

$$\begin{aligned} \zeta &= \sqrt{\frac{1}{2}\left[1 - \sqrt{1 - \frac{S_D(0)}{S_D(f_{\max})}}\right]} \\ \omega_n &= \frac{2\pi f_{\max}}{\sqrt{1 - 2\zeta^2}} \\ k &= \omega_n^2 \sqrt{S_D(0)} \end{aligned} \tag{2.56}$$

In this case,

$$
\begin{aligned}
f_{\max} &= f_d \cos\beta_m; \\
f_d &= \upsilon/\lambda; \\
S_D(f_{\max}) &= \frac{E_0}{4 f_d \sin\beta_m}; \\
S_D(0) &= \frac{E_0}{4\pi f_d \sin\beta_m}\left[\frac{\pi}{2} - \arcsin(2\cos^2\beta_m - 1)\right];
\end{aligned}
\tag{2.57}
$$

Therefore, the system parameters can be computed using the equations (2.20) or (2.22), (2.56) and (2.57).

2.4.2 Simulation and Estimation Results of Fading Channels

This section presents several simulation and estimation results for the different fading channel models using the state space models and the Kalman filters.

The following figures illustrate these simulation and estimation results of the least-square components for different fading channel models. The least-square components $\{I(t_n), Q(t_n), r^2(t_n), \phi(t_n)\}_{t_n \geq 0}$ denote the simulation results that are generated using the state space models; the least-square components $\left\{\hat{I}(t_n), \hat{Q}(t_n), \hat{r}^2(t_n), \hat{\phi}(t_n)\right\}_{t_n \geq 0}$ denote the estimation results that are computed using the Kalman filters. In theory, the two least-square components should be equal. In fact, these simulation results and the estimation results of the two least-square components are very close.

Figure 2-3 and Figure 2-4 show the simulated and estimated results for a Rayleigh fast fading channel, which only different from the moving velocities of the mobile. Figure 2-5 presents the simulated and estimated results for a Ricean slow fading channel. Figure 2-6 compares the simulated and estimated results for a frequency-selective slow fading channel with six paths. These figures are plotted using Java Graphics 2D implementation.

Figure 2-3 illustrates the simulated and estimated results for a Rayleigh fast fading channel with the physical factors: u=60km/h, SNR=10 dB, β=10° (degree) and Δt=0.25ms.

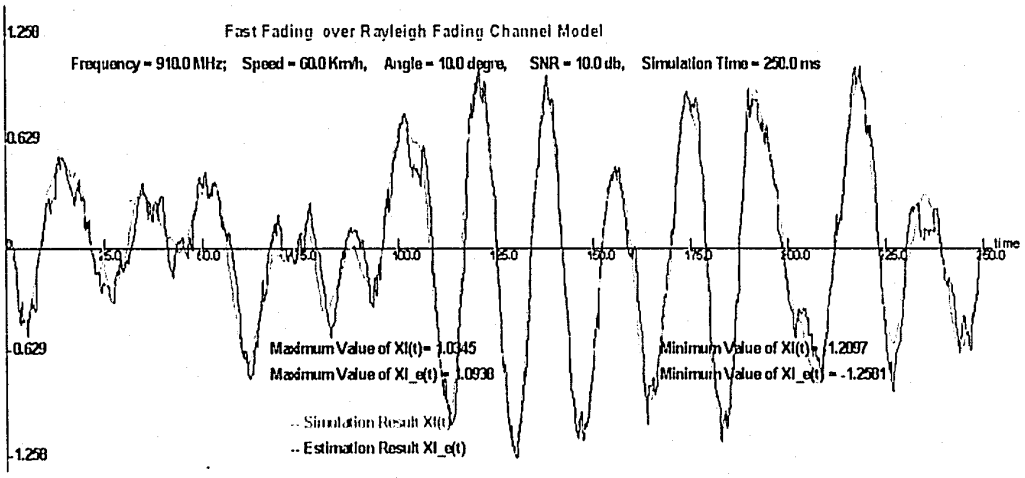

Figure 2-3 (a). Inphase Components: $I(t_n)$ **vs.** $\hat{I}(t_n)$

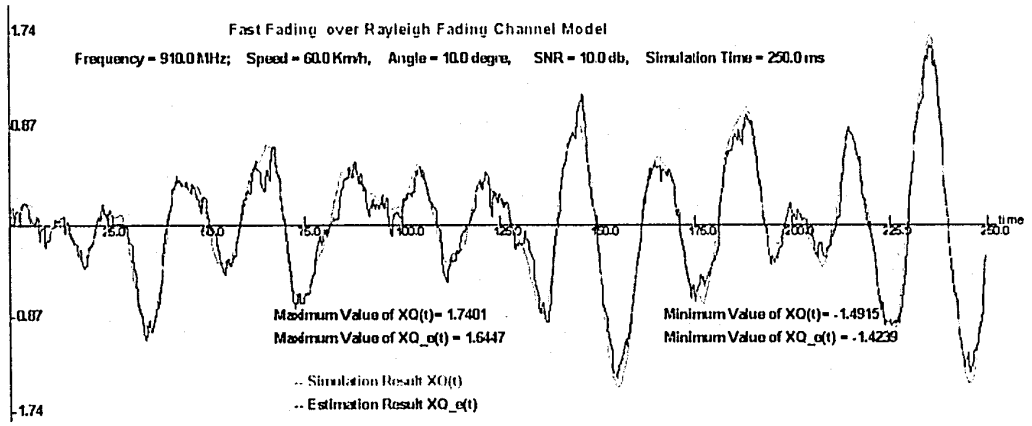

Figure 2-3 (b). Quadrature Components : $Q(t_n)$ **vs.** $\hat{Q}(t_n)$

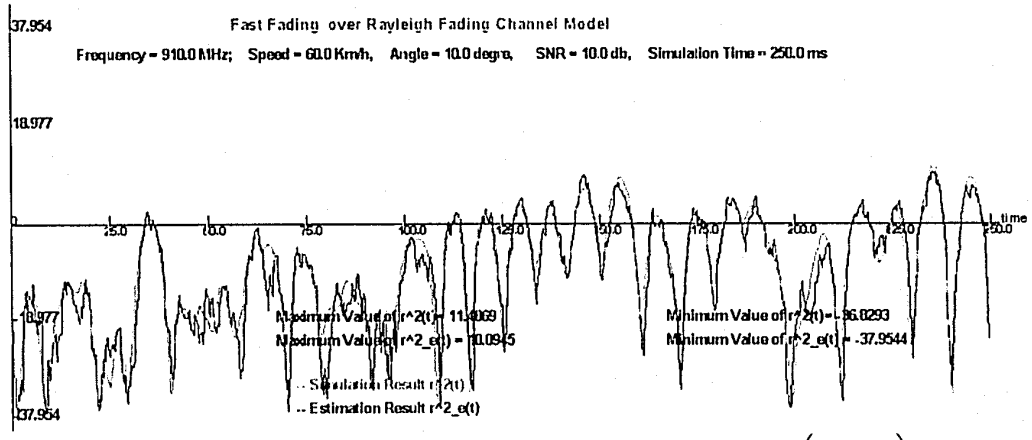

Figure 2-3 (c). Envelope Components: $10\log\left(r^2(t_n)\right)$ **vs.** $10\log\left(\hat{r}^2(t_n)\right)$ **(dB)**

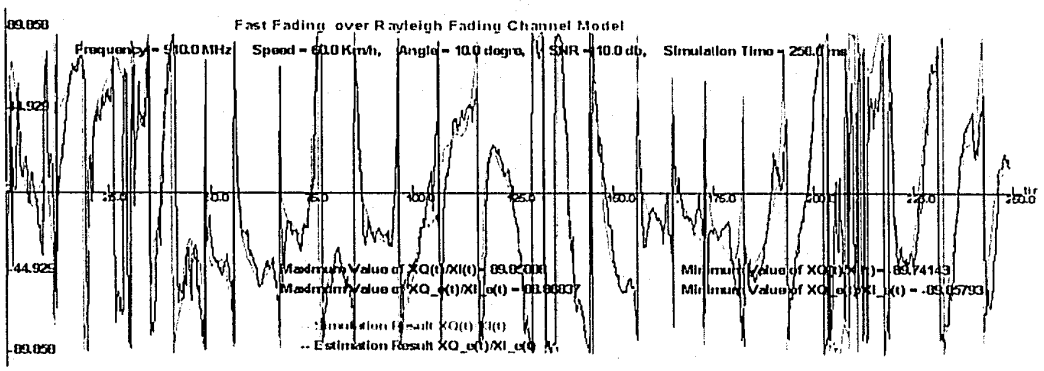

Figure 2-3 (d). Phase Components: $\phi(t_n)$ **vs.** $\hat{\phi}(t_n)$ **(°)**

Figure 2-3. Rayleigh Fast Fading Channel ($T_s >> T_c$)**:**

u=60 km/h, SNR=10 dB, β=10 °and Δt=250 ms

Figure 2-4 illustrates the simulated and estimated results for a Rayleigh fast fading channel with the physical factors: u=120km/h, SNR=10 dB, β=10 ° and Δt=0.25ms.

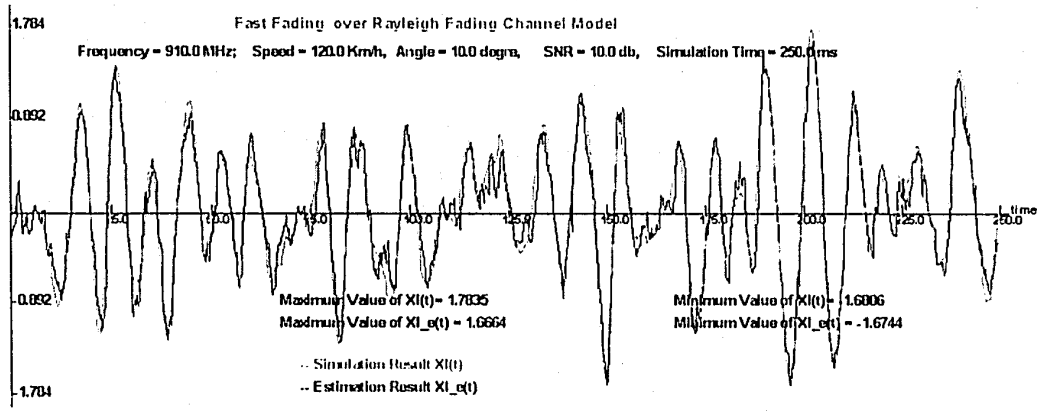

Figure 2-4 (a). Inphase Components: $I(t_n)$ **vs.** $\hat{I}(t_n)$

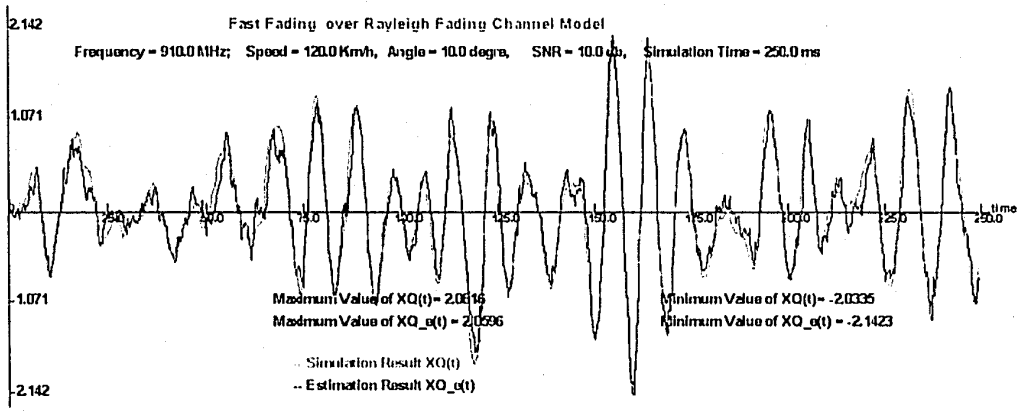

Figure 2-4 (b). Quadrature Components: $Q(t_n)$ **vs.** $\hat{Q}(t_n)$

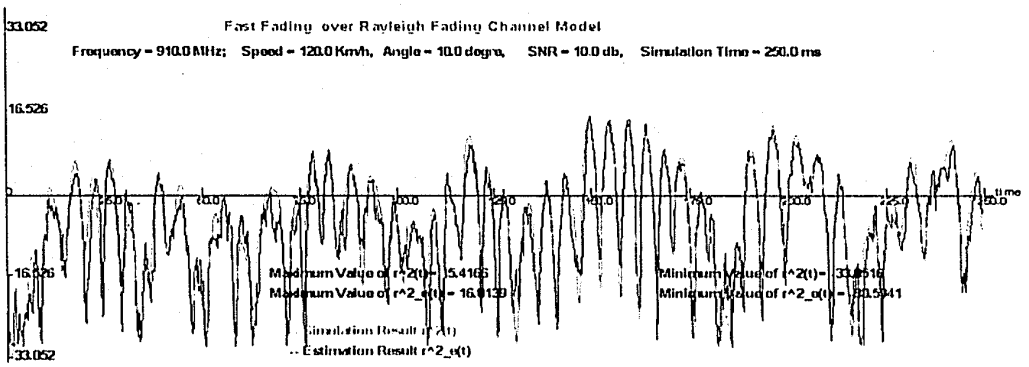

Figure 2-4 (c). Envelope Components : $10\log\left(r^2(t_n)\right)$ **vs.** $10\log\left(\hat{r}^2(t_n)\right)$ **(dB)**

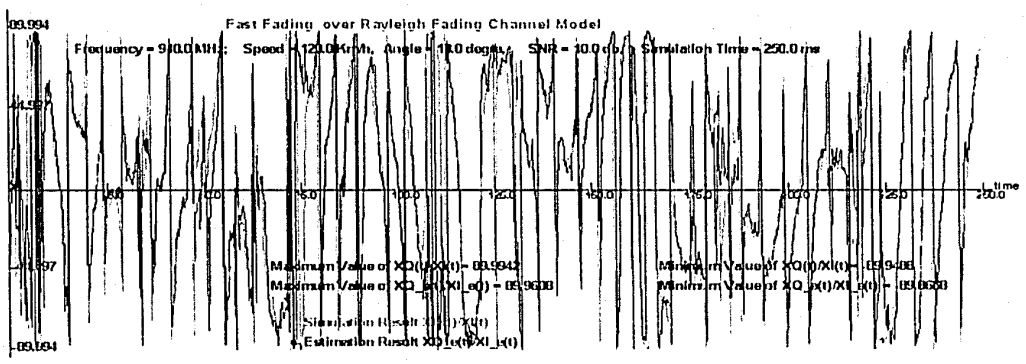

Figure 2-4 (d). Phase Components: $\phi(t_n)$ **vs.** $\hat{\phi}(t_n)$ **(°)**

Figure 2-4. Rayleigh Fast Fading Channel ***($T_s >> T_c$):***

u=120 km/h, SNR=10 dB, β=10 and Δt=250 ms

Figure 2-5 illustrates the simulated and estimated results for a Ricean slow fading channel with the physical factors: u=60km/h, SNR=10 dB, β=10 ° and Δt=0.6ms.

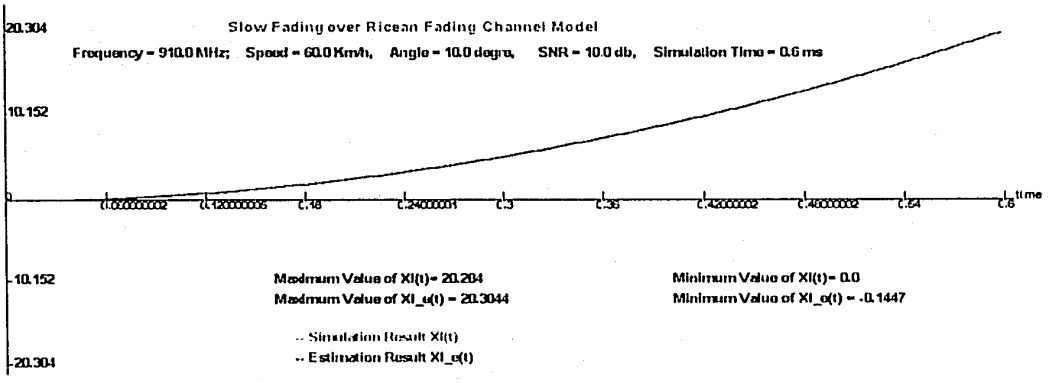

Figure 2-5 (a). Inphase Components: $I(t_n)$ **vs.** $\hat{I}(t_n)$

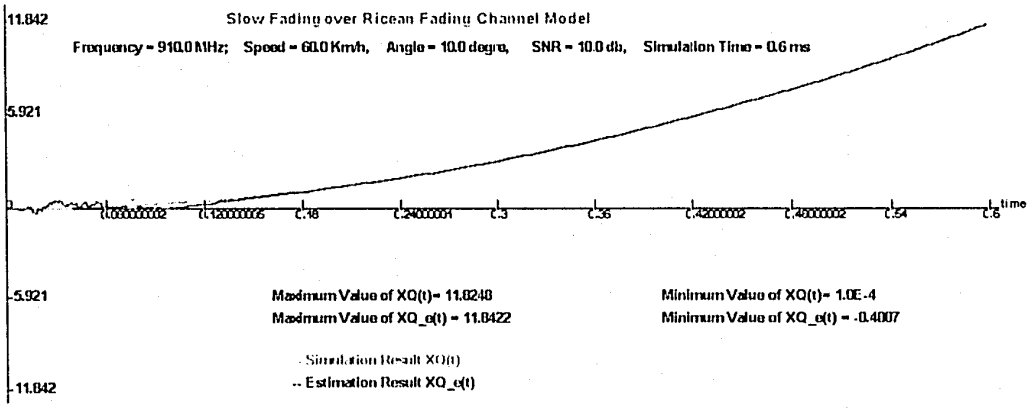

Figure 2-5 (b) . Quadrature Components: $Q(t_n)$ vs. $\hat{Q}(t_n)$

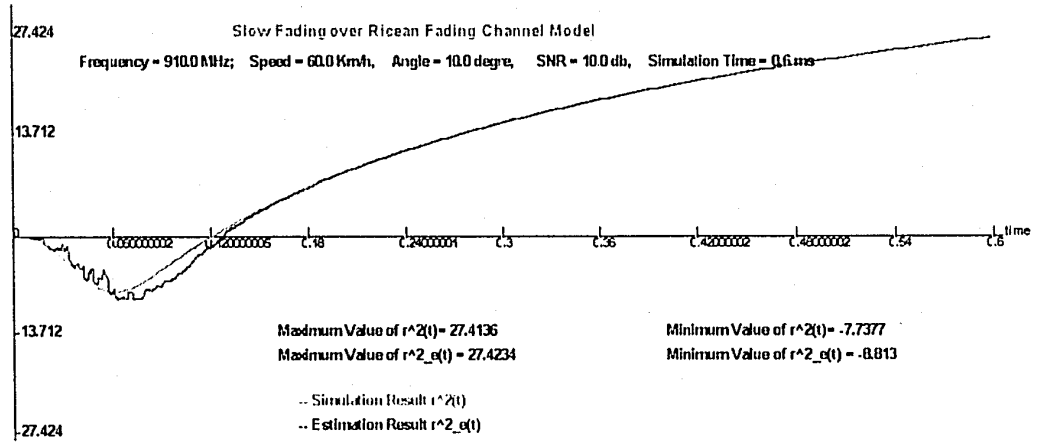

Figure 2-5 (c). Envelope Components : $10\log\left(r^2(t_n)\right)$ vs. $10\log\left(\hat{r^2}(t_n)\right)$ (dB)

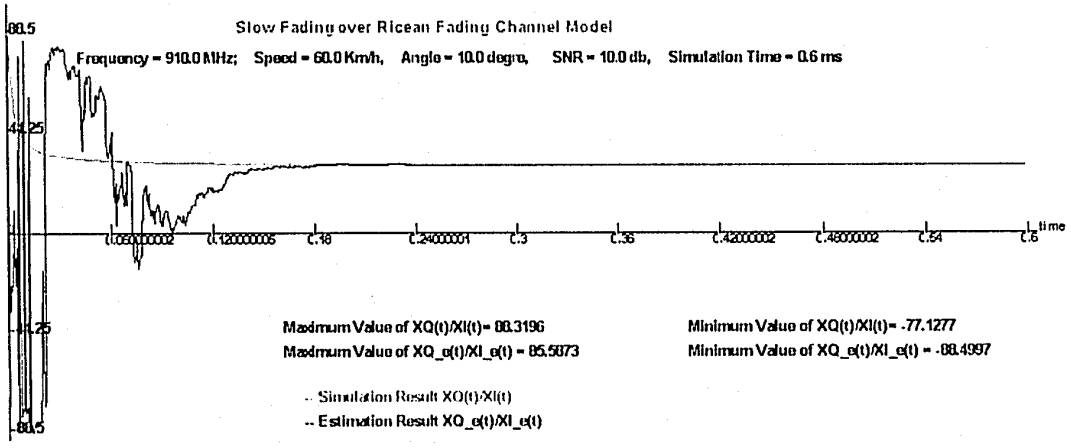

Figure 2-5 (d) . Phase Components: $\phi(t_n)$ vs. $\hat{\phi}(t_n)$ (°)

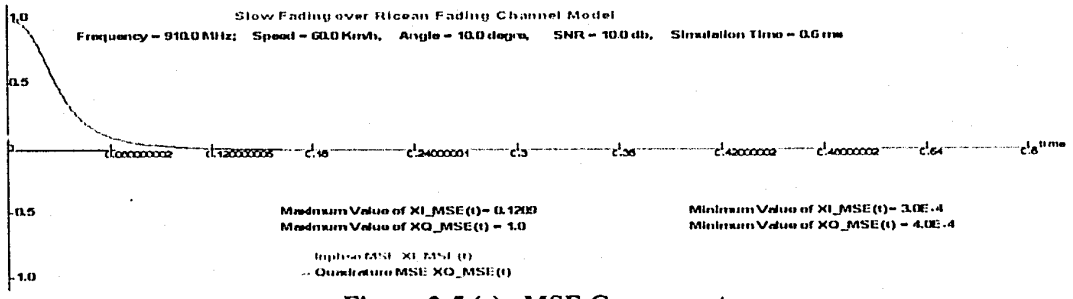

Figure 2-5 (e). MSE Components

Figure 2-5. Ricean Slow Fading Channel ($T_s << T_c$):
u=60 km/h, SNR=10 dB, β=10 ° and Δt=0.600 ms

Figure 2-6 is the simulated and estimated results of a frequency-selective slow fading channel containing six paths with the physical factors: u=60km/h, SNR=10 dB, β=10° and Δt=0.3ms.

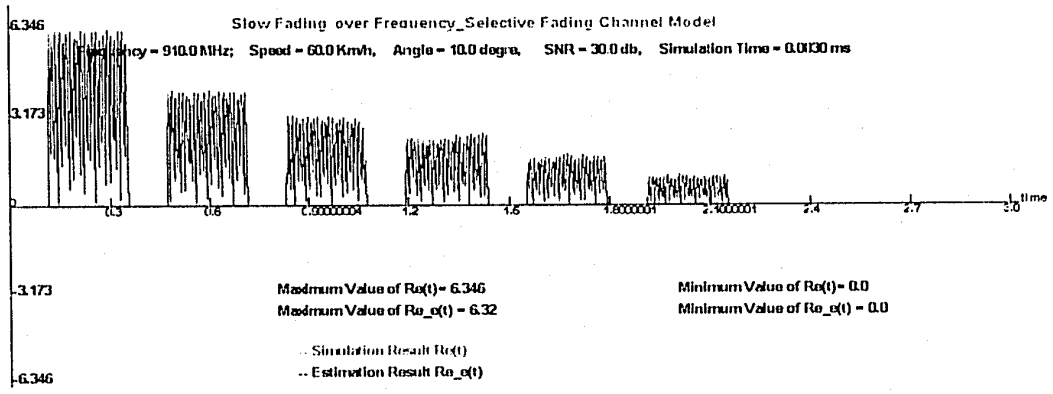

Figure 2-6 (a). Received signals without noise: $y(t_n)$ vs. $\hat{y}(t_n)$

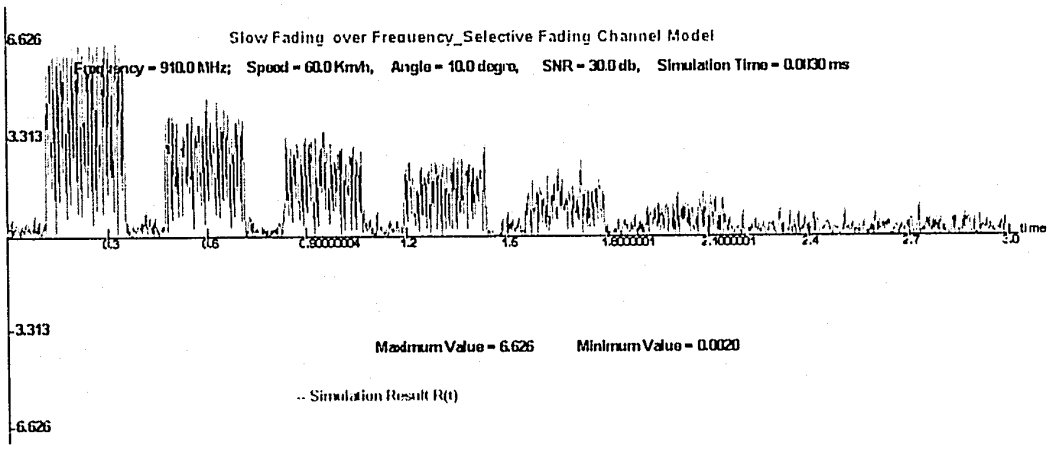

Figure 2-6 (b). Received signals with noise: $y_0(t_n)$ vs. $\hat{y}_0(t_n)$

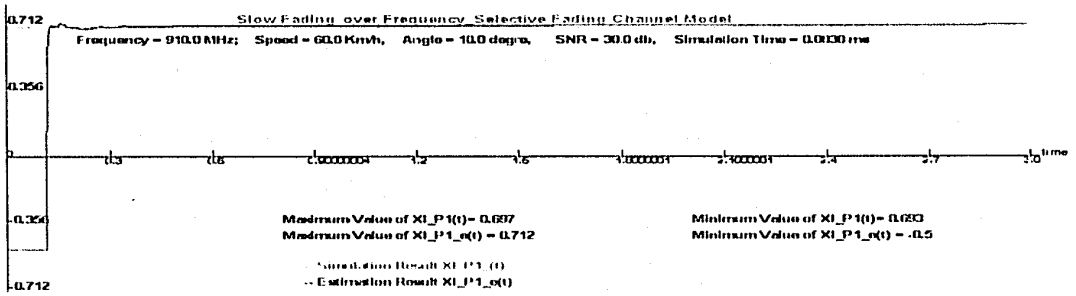

Figure 2-6 (c). Inphase components on 1st path: $I_1(t_n)$ vs. $\hat{I}_1(t_n)$

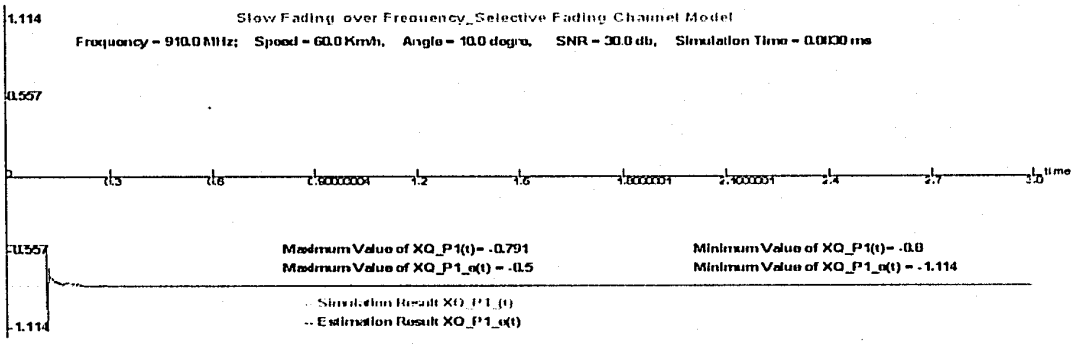

Figure 2-6 (d). Quadrature components on 1st path: $Q_1(t_n)$ vs. $\hat{Q}_1(t_n)$

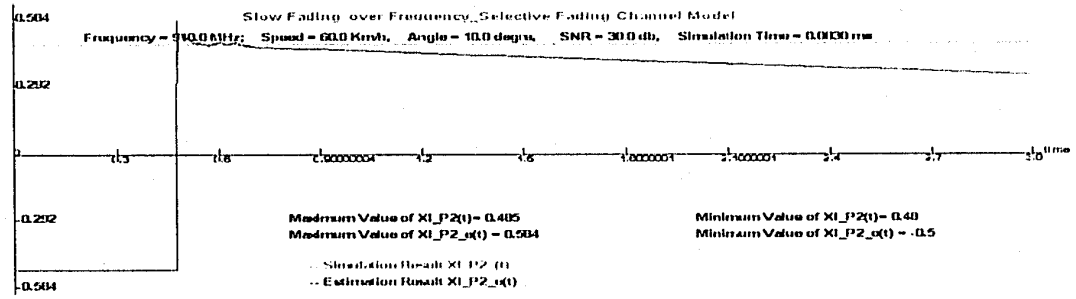

Figure 2-6 (e). Inphase components on 2nd path: $I_2(t_n)$ vs. $\hat{I}_2(t_n)$

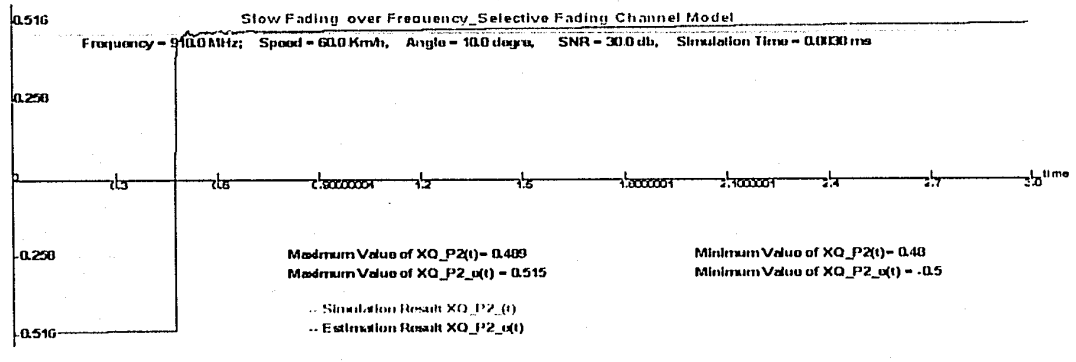

Figure 2-6 (f). Quadrature components on 2nd path: $Q_2(t_n)$ vs. $\hat{Q}_2(t_n)$

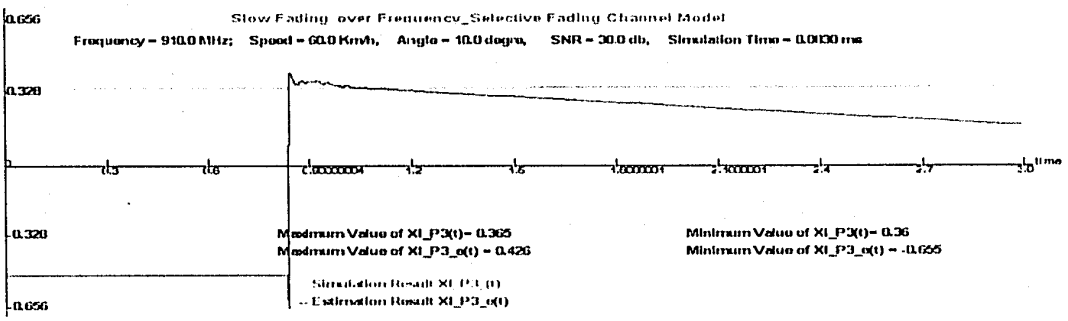

Figure 2-6 (g). Inphase components on 3rd path: $I_3(t_n)$ vs. $\hat{I}_3(t_n)$

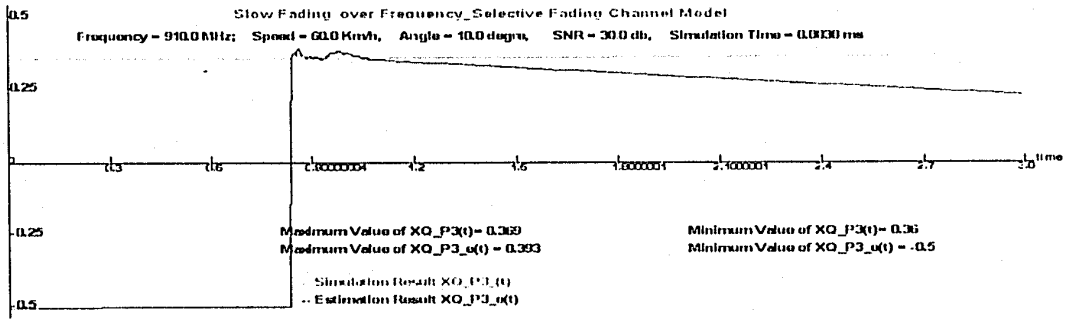

Figure 2-6 (h). Quadrature components on 3rd path: $Q_3(t_n)$ vs. $\hat{Q}_3(t_n)$

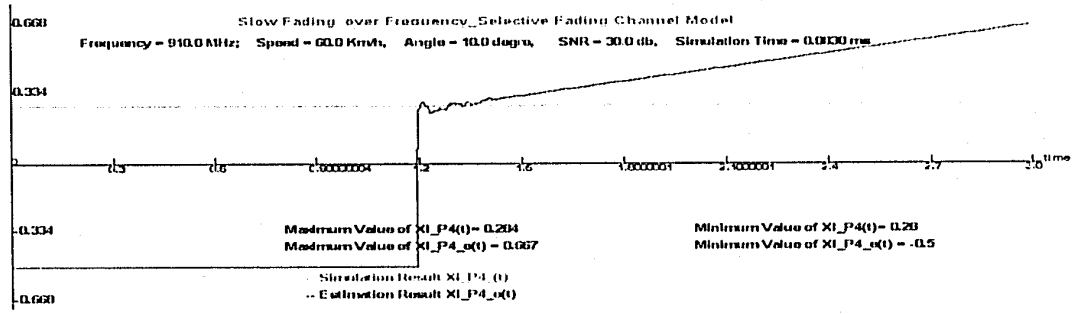

Figure 2-6 (i) . Inphase components on 4th path: $I_4(t_n)$ vs. $\hat{I}_4(t_n)$

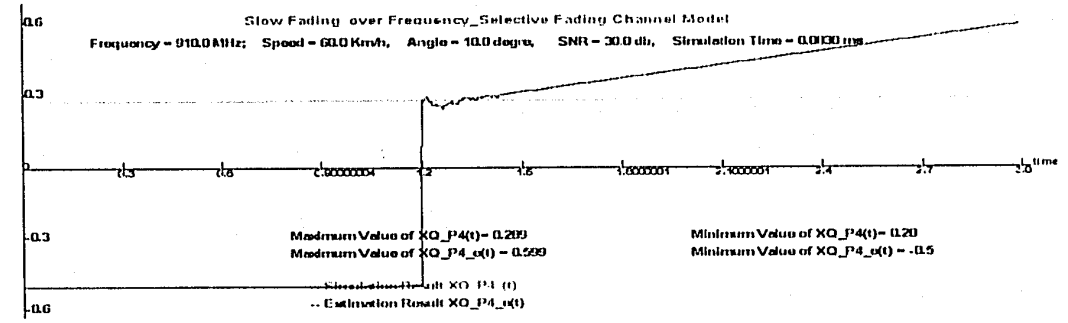

Figure 2-6 (g). Quadrature components on 4th path: $Q_4(t_n)$ vs. $\hat{Q}_4(t_n)$

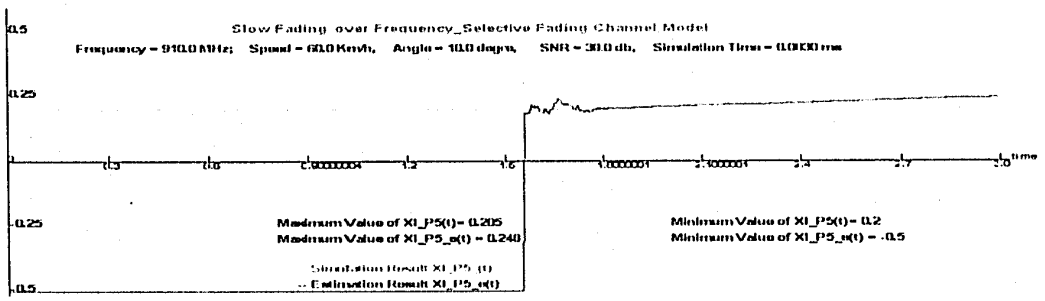

Figure 2-6 (k) . Inphase components on 5th path: $I_5(t_n)$ vs. $\hat{I}_5(t_n)$

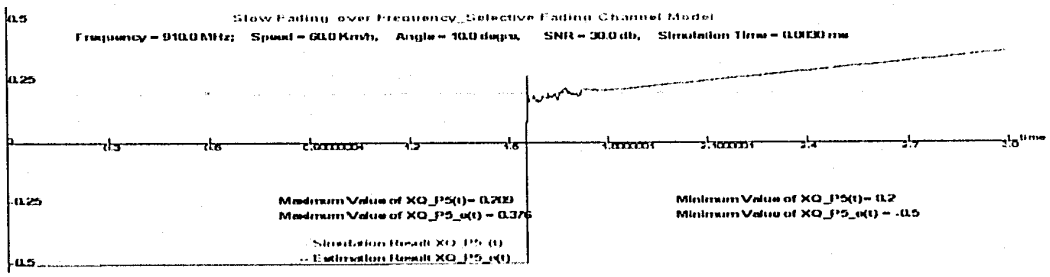

Figure 2-6 (l) . Quadrature components on 5th path: $Q_5(t_n)$ vs. $\hat{Q}_5(t_n)$

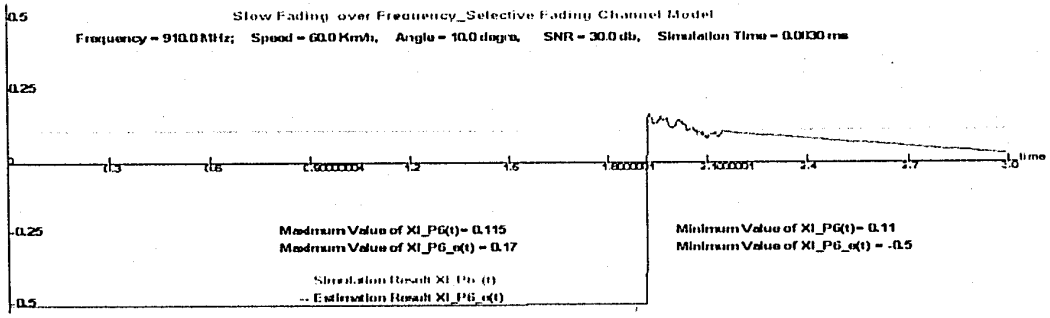

Figure 2-6 (m). Inphase components on 6th path: $I_6(t_n)$ vs. $\hat{I}_6(t_n)$

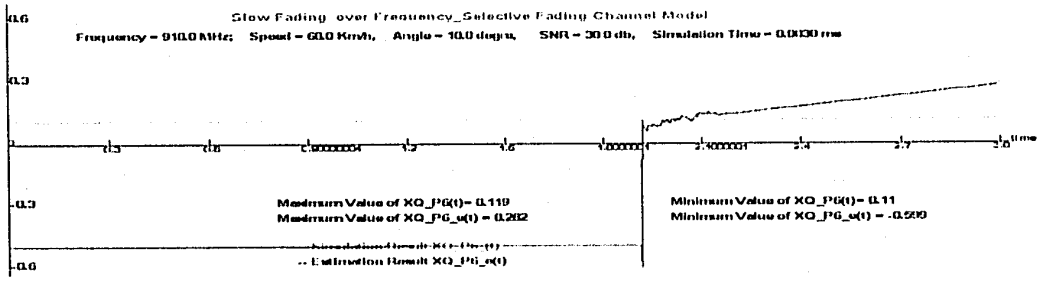

Figure 2-6 (n). Quadrature components on 6th path: $Q_6(t_n)$ vs. $\hat{Q}_6(t_n)$

Figure 2-6. Frequency-Selective Slow Fading Channel *($T_s << T_c$):*
u=60 km/h, SNR=10 dB, β=10 and Δt=0.300 ms

In this case, the envelopes, phases and MSEs components of the received signal are also simulated, estimated and plotted on each path. But the section does not include these results.

From these simulated and estimated listed in the above figures, it is easy to know that the state space models and the Kalman filters are better matched.

Chapter Summary

The state space models are used to describe the characteristics of the fading channel such as the flat and frequency-selective fading channels.

The Kalman filters are the best description for estimating the least square components such as the inphase, quadrature, envelope and phase components of the received signal for the fading channel.

The simulation and estimation computation are based on the state space models and the Kalman filters. Additionally, their model parameters are defined with respect to several physical factors of the motion of the receiver or the transmitter.

The simulation and estimation results are presented for the Rayleigh fading, the Ricean fading and the frequency-selective fading with six-path.

Chapter 3

System Identification via Expectation Maximization Algorithm and Kalman Filter

System identification or parameter estimation is a common problem in process modeling. It is also an important research area in wireless communications.

This chapter will present a system identification algorithm which is employed to extract the various parameters of the fading channel models; and indicate the mathematical models based on the measurement data provided by the Communications Research Centre of Canada (CRC) [BUL01]. Section 3.1 introduces basic concepts of system identification; Section 3.2 states the Expectation Maximization (EM) algorithm together with the Kalman filter applied to system identification; Section 3.3 verifies the EM algorithm and illustrates estimated results with several samples; Section 3.4 presents the system identification mathematical models and estimated results for the flat fading channel based on the measurement data; and Section 3.5 addresses the system identification mathematical models and estimated results for the frequency-selective fading channel based the measurement data; in addition, the transmitted signal of the frequency-selective fading channel is considered as the narrowband signal and the wideband signal; furthermore, the frequency-selective fading can be considered as fast or slow fading.

3.1 Introduction to System Identification

System identification is a process of constructing a mathematical model for a dynamic system from observations and prior knowledge. The basic idea is assumed that there exist some "true" values of the system parameters which provide a perfect description of the mathematical model and it is best fit to the measurement data [DIN97].

System identification is generally based on the least-square or maximum likelihood criterion with mathematical models and tools. Computer programs are often used to find general mathematical descriptions that give the best fit to a series of recorded input and output signals. In practical situations, the observation process is monitored at discrete times only, but the system identification could be determined with either continuous-time or discrete-time [DAV85].

System identification has some advantages. Firstly, the mathematical models via system identification are usually accurate because they are based on observed data rather than assumptions. Secondly, the process of system identification is fast, predictable and completely universal.

3.1.1 Description of System Identification

System identification is usually formulated as an optimization problem. Figure 3-1, adapted from [DAV85], illustrates the process of system identification. It is assumed that the unknown system is needed to be identified, and the adaptive filter is a known system. The variable $x(t_n)$ is usually a random variable. When $x(t_n)$ is fed to both the unknown system and the adaptive filter, the unknown system gives response $y(t_n)$, the adaptive filter gives output $f(t_n)$, and their difference between the two is called the error signal $\varepsilon(t_n)$. The adaptive filter coefficients are updated according to some mathematical algorithms in order to minimize $\varepsilon(t_n)$. If $\varepsilon(t_n)$ is less than a very small given value, the adaptive filter response is said to give good estimation of the unknown system.

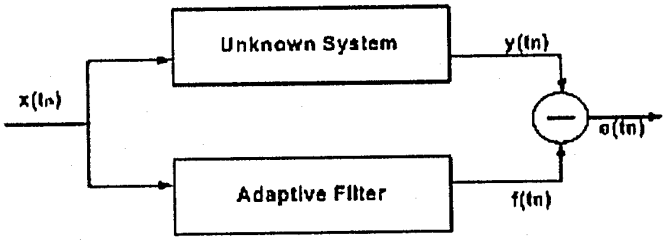

Figure 3-1 the System Identification Problem

The algorithms of the updating adaptive filter coefficients are the main subject of the system identification problem. Many different algorithms, which different from their convergence speed, computational complexity, performance and stability [DAZ95], have been considered. For example, the maximum likelihood estimation (MLE) is the most robust of system identification techniques.

3.1.2 Maximum Likelihood Estimation (MLE)

The basic idea of the *maximum likelihood estimation* (MLE) is to obtain the most likely values of system parameters for a given distribution that will best describe the samples. It means that the MLE is to determine the system parameters which maximize the probability (likelihood) of the samples.

Let $\Theta = (\theta_1, \theta_2, \cdots, \theta_k)$ denotes the k unknown system parameters need to be estimated, $Y_k = \{y_{k1}, y_{k2}, \cdots, y_{kN}\}$ denote an observed sequence, and $f(y_i;\Theta)$ is an independent probability density function of a random variable. Therefore, the likelihood function can be expressed as the following equation [DAV85]:

$$L(y_{k1}, y_{k2}, \cdots, y_{kN} | \theta_1, \theta_2, \cdots, \theta_k) = L = \prod_{i=1}^{N} f(y_i;\Theta); \quad i = 1, 2, \cdots, N$$

In the same way, the logarithmic likelihood function of L can be given as:

$$\Lambda = \ln L = \sum_{i=1}^{N} \ln f(y_i, \Theta)$$

A necessary condition to maximize Λ is given as the following equation:

$$\frac{\partial(\Lambda)}{\partial\theta_i} = 0; \quad i = 1, 2, \cdots, k$$

The above equation is known as the maximum likelihood equation. The system parameters $\Theta = (\theta_1, \theta_2, \cdots, \theta_k)$ can be obtained by maximizing L or Λ.

The MLE is computed recursively using first or second order derivatives of the log-likelihood function with respect to the unknown system parameter. It is clear that the sample size determines the accuracy of an estimator. If the sample size equals the whole population, then the estimator is the true value.

3.2 Expectation Maximization (EM) Algorithm

The Expectation Maximization (EM) algorithm uses a bank of Kalman filters to yield a maximum likelihood parameter estimation of the Gaussian state space model. This section introduces a system identification model for the fading channel, and presents the EM algorithm and its computing process. In addition, an example is discussed to show how to use the EM algorithm.

3.2.1 Fading Channel Models for System Identification

As discussed in Chapter 2, the state space model can be used to described fading channels. For a linear discrete-time, time-invariant Gauss-Markov system, the state space model can be rewritten in the following form:

$$\begin{aligned} x_{t+1} &= A_t x_t + B_t w_t; \quad x_0 \sim N(\mu, \sigma^2) \\ y_t &= C_t x_t + D_t \upsilon_t \end{aligned} \tag{3.1}$$

In this equation, $x_t \in \Re^n$ is a state vector, $y_t \in \Re^d$ is a measurement vector, $w_t \in \Re^m$ is a state noise, and $\upsilon_t \in \Re^d$ is a measurement noise. The noises, $\{w_t\}_{t\geq 0}$ and $\{\upsilon_t\}_{t\geq 0}$, are assumed to be independent identification Gaussian processes with the probability density functions [CHA98]:

$$f_w(w) = (2\pi)^{-m/2} \exp\left(\frac{-w_t^T w_t}{2}\right);$$

$$f_\upsilon(\upsilon) = (2\pi)^{-d/2} \exp\left(\frac{-\upsilon_t^T \upsilon_t}{2}\right)$$

Further, the noises are independent of the initial state x_0, which is assumed to be Gaussian distributed with $N \sim (\mu, \sigma^2)$.

The unknown system parameters $\theta_t = \{A_t, B_t, C_t, D_t\}$ or $\theta = \{A, B, C, D\}$ can be estimated through a realization of the measured data. The methodology employed is based on the EM algorithm together with the Kalman filter.

3.2.2 Description of the Expectation Maximization Algorithm

Let $\theta = \{A, B, C, D\}$ denote system parameters in the equation (3.1); P_0 denotes a fixed probability measurement; and $\{P_\theta; \theta \in \Theta\}$ denotes a family of probability measures induced by the system parameters θ. If the original model is a white noise sequence, then $\{P_\theta; \theta \in \Theta\}$ is absolutely continuous with respect to P_0 [CHA98, CHA03]. It can be expressed as:

$$P_0: \quad \begin{cases} x_{t+1} = w_t \\ y_t = v_t \end{cases}$$

The EM algorithm is an iterative scheme for computing the maximum likelihood estimate of the system parameters θ with given data $Y_N = \{y_1, y_2, \ldots, y_N\}$. Specifically, each iteration of the EM algorithm consists of the following steps:

(1) Expectation Step

This step is use to evaluate the conditional expectation of the log-likelihood function under the complete data. This can be expressed as:

$$\Lambda(\theta, \theta_t) = E_{\theta_t}\{\log \frac{dP_\theta}{dP_{\theta_t}} | y_T\}$$

(2) Maximization Step

This step is use to find $\theta_{t+1} \in \arg\max_{\theta \in \Theta} \Lambda(\theta, \theta_t)$.

The expectation and maximization steps are repeated until the convergence of the system parameters $\|\theta_t - \theta_{t-1}\| \leq \varepsilon$.

Based on the state space model, the EM algorithm is described by the following equations [CHA98]:

$$\hat{A} = E\left(\sum_{t=1}^{N} \hat{x}_t \hat{x}_{t-1}^T \middle| Y_N\right) \times \left[E\left(\sum_{t=1}^{N} \hat{x}_t \hat{x}_t^T \middle| Y_N\right)\right]^{-1} \tag{3.2}$$

$$\begin{aligned}\hat{B}^2 &= \frac{1}{N} E\left(\sum_{t=0}^{N} \left(\hat{x}_t - A\hat{x}_{t-1}\right)\left(\hat{x}_t - A\hat{x}_{t-1}\right)^T \middle| Y_N\right) \\ &= \frac{1}{N} E\left(\sum_{t=0}^{N} \left((\hat{x}_t \hat{x}_t^T) - A(\hat{x}_t \hat{x}_{t-1}^T)^T - (\hat{x}_t \hat{x}_{t-1}^T)A^T + A(\hat{x}_{t-1} \hat{x}_{t-1}^T)A^T\right) \middle| Y_N\right)\end{aligned} \tag{3.3}$$

$$C = E\left(\sum_{t=1}^{N} y_t \hat{x}_t^T \middle| Y_N\right) \times \left[E\left(\sum_{t=1}^{N} \hat{x}_t \hat{x}_t^T \middle| Y_N\right)\right]^{-1} \tag{3.4}$$

$$\begin{aligned}\hat{D}^2 &= \frac{1}{N} E\left(\sum_{t=1}^{N} \left(y_t - C\hat{x}_t\right)\left(y_t - C\hat{x}_t\right)^T \middle| Y_N\right) \\ &= \frac{1}{N} E\left(\sum_{t=1}^{N} \left(y_t y_t^T - (y_t \hat{x}_t^T)C^T - C(y_t \hat{x}_t^T)^T + C(x_t x_t^T)C^T\right) \middle| Y_N\right)\end{aligned} \tag{3.5}$$

In this case, $B^2 = BB^T$ and $D^2 = DD^T$. In addition, $E(x)$ denotes the expectation operator of variable (x), $Y_N = \{y_1, y_2, y_3, \cdots, y_N\}$ denote a sequence of the observed data, N denotes the total number of the observed samples, and $\hat{x}_t$ denotes the estimated value at time t that is computed using the Kalman filter; and $\theta_t = \{\hat{A}_t, \hat{B}_t^2, \hat{C}_t, \hat{D}_t^2\}$ denotes the estimated system parameters at the ℓ^{th} iteration.

The main advantage of the EM algorithm is that the computation process of system parameters is less expensive than the Newton-Raphson method, because the updated system parameters of the EM algorithm at each iteration are linear.

3.2.3 Definitions of the EM Algorithm and the Kalman Filter

In order to identify system parameters, the Kalman filter and a new class of finite dimensional filters are defined.

(1) The Kalman Filter

For given system parameters $\theta = \{A, B^2, C, D^2\}$, the Kalman filter can be expressed as the following [CHA98]:

$$\begin{aligned}
\hat{x}_{t|t} &= A\hat{x}_{t-1|t-1} + P_{t|t}C^T D^{-2}\left(y_t - CA\hat{x}_{t-1|t-1}\right) \\
\hat{x}_{t|t-1} &= A\hat{x}_{t-1|t-1} \\
\hat{x}_{0|0} &= m_0 \quad t = 0, 1, 2, \ldots N
\end{aligned} \tag{3.6}$$

The sequence $P_{t|t}$ can also be given as the following [CHA98]:

$$\begin{aligned}
\overline{P}_{t|t}^{-1} &= P_{t-1|t-1}^{-1} + A^T B^{-2} A \\
P_{t|t}^{-1} &= C^T D^{-2} C + B^{-2} - B^{-2}\overline{P}_{t|t}A^T B^{-2} \\
P_{t|t-1} &= AP_{t-1|t-1}A^T + B^2
\end{aligned} \tag{3.7}$$

The calculation of $P_{t|t}$ and $\hat{x}_{t|t}$ can be computed recursively.

(2) Definition of the New Class of Filters

A new class of finite dimensional filters is defined as the following [CHA98]:

$$L_N^{(1)} = E\left\{\sum_{t=1}^{N} x_t^T Q x_t \middle| Y_N\right\} \tag{3.8}$$

$$L_N^{(2)} = E\left\{\sum_{t=1}^{N} x_{t-1}^T Q x_{t-1} \middle| Y_N\right\} \tag{3.9}$$

$$L_N^{(3)} = E\left\{\sum_{t=1}^{N} \left[x_t^T R x_{t-1} + x_{t-1}^T R^T x_t\right] \middle| Y_N\right\} \tag{3.10}$$

$$L_N^{(4)} = E\left\{\sum_{t=1}^{N} \left[x_t^T S y_t + y_t^T S^T x_t\right] \middle| Y_N\right\} \tag{3.11}$$

In addition, matrixes Q, R and S are defined as the following:

$$Q \equiv \left\{\frac{e_i e_j^T + e_j e_i^T}{2}; i, j = 1,2,\ldots\ldots,m\right\} \tag{3.12}$$

$$R \equiv \left\{\frac{e_i e_j^T}{2}; i, j = 1,2,\ldots\ldots,m\right\} \tag{3.13}$$

$$S \equiv \left\{\frac{e_i e_n^T}{2}; i = 1,2,\ldots\ldots,m; n = 1,2,\ldots\ldots,d\right\} \tag{3.14}$$

In these equations, e_i is the unit vector in the Euclidean space; it means that $e_i = 1$ in the i^{th} position and $e_i = 0$ in other positions.

Further, the new class of finite dimensional filters should be obtained.

(3) Filter Estimation of $L_N^{(1)}$

The filter estimation of $L_N^{(1)}$ is derived as the following [CHA98]:

$$\begin{aligned} L_N^{(1)} &= E\left\{\sum_{t=1}^{N} x_t^T Q x_t \,\middle|\, Y_N\right\} \\ &= -\frac{1}{2}Tr\left(N_N^{(1)} P_{N|N}\right) - \frac{1}{2}\sum_{t=1}^{N} Tr\left(N_{t-1}^{(1)} \overline{P}_{t|t}\right) \\ &\quad -\frac{1}{2}\sum_{t=1}^{N}\left[-2x_{t|t}^T P_{t|t}^{-1} r_t^{(1)} + 2x_{t|t-1}^T P_{t|t-1}^{-1} r_{t|t-1}^{(1)} - x_{t|t}^T N_t^{(1)} x_{t|t} + x_{t|t-1}^T B^{-2} A\overline{P}_{t|t} N_{t-1}^{(1)} \overline{P}_{t|t} A^T B^{-2} x_{t|t-1}\right] \end{aligned} \tag{3.15}$$

In this equation, $r_t^{(1)}$ satisfies the following recursions:

$$\begin{cases} r_t^{(1)} = \left(A - P_{t|t} C^T D^{-2} CA\right) r_{t-1}^{(1)} + 2P_{t|t} Q x_{t|t-1} - P_{t|t} N_t^{(1)} P_{t|t} C^T D^{-2}\left(y_t - C x_{t|t-1}\right) \\ r_{t|t-1}^{(1)} = A r_t^{(1)} \\ r_0^{(1)} = 0_{m\times 1} \end{cases} \tag{3.16}$$

Furthermore, $N_t^{(1)}$ also satisfies the following recursions:

$$\begin{cases} N_t^{(1)} = B^{-2} A\overline{P}_{t|t} N_{t-1}^{(1)} \overline{P}_{t|t} A^T B^{-2} - 2Q \\ N_0^{(1)} = 0_{m\times m} \end{cases} \tag{3.17}$$

(4) Filter Estimation of $L_N^{(2)}$

The filter estimation of $L_N^{(2)}$ is derived as the following [CHA98]:

$$\begin{aligned} L_N^{(2)} &= E\left\{\sum_{t=1}^{N} x_{t-1}^T Q x_{t-1} \,\middle|\, Y_N\right\} \\ &= E_\theta\left\{x_0^T Q x_0 \,\middle|\, Y_N\right\} + E_\theta\left\{\sum_{t=2}^{N} x_{t-1}^T Q x_{t-1} \,\middle|\, Y_N\right\} \\ &= E_\theta\left\{x_0^T Q x_0 \,\middle|\, Y_N\right\} + E_\theta\left\{\sum_{t=1}^{N} x_t^T Q x_t \,\middle|\, Y_N\right\} - E_\theta\left\{x_N^T Q x_N \,\middle|\, Y_N\right\} \end{aligned} \tag{3.18}$$

Therefore, $L_N^{(2)}$ can be obtained from the filter of $L_N^{(1)}$. x_N is computed using the equation (3.6)

(5) Filter Estimation of $L_N^{(3)}$

The filter estimation of $L_N^{(3)}$ is also expressed as the following [CHA98]:

$$\begin{aligned} L_N^{(3)} &= E\left\{\sum_{t=1}^{N}\left(x_t^T R x_{t-1} + x_{t-1}^T R^T x_t\right)\middle| Y_N\right\} \\ &= -\frac{1}{2}Tr\left(N_N^{(2)} P_{N|N}\right) - \frac{1}{2}\sum_{t=1}^{N} Tr\left(N_{t-1}^{(2)} \overline{P}_{t|t}\right) \\ &\quad -\frac{1}{2}\sum_{t=1}^{N}\left[-2x_{t|t}^T P_{t|t}^{-1} r_t^{(2)} + 2x_{t|t-1}^T P_{t|t-1}^{-1} r_{t|t-1}^{(2)} - x_{t|t}^T N_t^{(2)} x_{t|t} + x_{t|t-1}^T B^{-2} A \overline{P}_{t|t} N_{t-1}^{(2)} \overline{P}_{t|t} A^T B^{-2} x_{t|t-1}\right] \end{aligned} \tag{3.19}$$

In this case, $r_t^{(3)}$ satisfies the following recursions:

$$\begin{cases} r_t^{(3)} = \left(A - P_{t|t} C^T D^{-2} CA\right) r_{t-1}^{(3)} - P_{t|t} N_t^{(3)} P_{t|t} C^T D^{-2}\left(y_t - C x_{t|t-1}\right) + \left(2P_{t|t} R + 2P_{t|t} B^{-2} A \overline{P}_{t|t} R^T A\right) x_{t-1|t-1} \\ r_{t|t-1}^{(3)} = A r_t^{(3)} \\ r_0^{(3)} = 0_{m\times 1} \end{cases} \tag{3.20}$$

Furthermore, $N_t^{(3)}$ also satisfies the following recursions:

$$\begin{cases} N_t^{(3)} = B^{-2} A \overline{P}_{t|t} N_{t-1}^{(3)} \overline{P}_{t|t} A^T B^{-2} - 2R\overline{P}_{t|t} A^T B^{-2} - 2B^{-2} A \overline{P}_{t|t} R^T \\ N_0^{(3)} = 0_{m\times m} \end{cases} \tag{3.21}$$

(6) Filter Estimation of $L_N^{(4)}$

The filter estimation of $L_N^{(4)}$ is given as the following [CHA98]:

$$L_N^{(4)} = E\left\{\sum_{t=1}^{N}\left(x_t^T S y_t + y_t^T S^T x_t\right)\middle| Y_N\right\} = \sum_{t=1}^{N}\left(x_{t|t}^T P_{t|t}^{-1} r_t^{(4)} - x_{t|t-1}^T P_{t|t-1}^{-1} r_{t|t-1}^{(4)}\right) \tag{3.22}$$

In this equation, $r_t^{(4)}$ satisfies the following recursions:

$$\begin{cases} r_t^{(4)} = \left(A - P_{t|t} C^T D^{-2} CA\right) r_{t-1}^{(4)} + 2P_{t|t} S y_t \\ r_{t|t-1}^{(4)} = A r_t^{(4)} \\ r_0^{(4)} = 0_{m\times 1} \end{cases} \tag{3.23}$$

Using these definitions of $L_N^{(i)}$ ($i = 1,2,3,4$) and the Kalman filter described in the above equations, it is easy to estimate system parameters $\theta = \{A, B^2, C, D^2\}$ through the EM algorithm described in the equations (3.2)-(3.5).

3.2.4 An Example of the EM Algorithm

An example shows how to estimate system parameters using the EM algorithm together with the Kalman filter presented in Subsection 3.2.3.

Considering a second order form ($n = m = 2, d = 1$) of the state space model in the equation (3.1), these system parameters can be expressed as the following forms:

$$A = \begin{bmatrix} a_{11} & a_{12} \\ a_{21} & a_{22} \end{bmatrix}, \quad B = \begin{bmatrix} b_{11} & b_{12} \\ b_{21} & b_{22} \end{bmatrix}, \quad C = \begin{bmatrix} c_{11} & c_{12} \end{bmatrix}, \quad D = \begin{bmatrix} d_1 \end{bmatrix}$$
$$x_t = \begin{bmatrix} x_{t1} & x_{t2} \end{bmatrix}^T, \quad y_t = \begin{bmatrix} y_{t1} \end{bmatrix} \tag{3.24}$$

In this case, the following derived equations are related to the EM algorithm in the equations (3.2) to (3.5):

$$E\left(\sum_{t=1}^{N} x_t x_t^T \middle| Y_N\right) = E\left(\sum_{t=1}^{N} \begin{bmatrix} x_{t1}x_{t1} & x_{t1}x_{t2} \\ x_{t2}x_{t1} & x_{t2}x_{t2} \end{bmatrix} \middle| Y_N\right) = \begin{pmatrix} E\left(\sum_{t=1}^{N} x_{t1}x_{t1} \middle| Y_N\right) & E\left(\sum_{t=1}^{N} x_{t1}x_{t2} \middle| Y_N\right) \\ E\left(\sum_{t=1}^{N} x_{t2}x_{t1} \middle| Y_N\right) & E\left(\sum_{t=1}^{N} x_{t2}x_{t2} \middle| Y_N\right) \end{pmatrix} \tag{3.25}$$

$$E\left(\sum_{t=1}^{N} x_{t-1} x_{t-1}^T \middle| Y_N\right) = E\left(\sum_{t=1}^{N} \begin{bmatrix} x_{t1-1}x_{t1-1} & x_{t1-1}x_{t2-1} \\ x_{t2-1}x_{t1-1} & x_{t2-1}x_{t2-1} \end{bmatrix} \middle| Y_N\right) = \begin{pmatrix} E\left(\sum_{t=1}^{N} x_{t1-1}x_{t1-1} \middle| Y_N\right) & E\left(\sum_{t=1}^{N} x_{t1-1}x_{t2-1} \middle| Y_N\right) \\ E\left(\sum_{t=1}^{N} x_{t2-1}x_{t1-1} \middle| Y_N\right) & E\left(\sum_{t=1}^{N} x_{t2-1}x_{t2-1} \middle| Y_N\right) \end{pmatrix} \tag{3.26}$$

$$E\left(\sum_{t=1}^{N} x_t x_{t-1}^T \middle| Y_N\right) = E\left(\sum_{t=1}^{N} \begin{bmatrix} x_{t1}x_{t1-1} & x_{t1}x_{t2-1} \\ x_{t2}x_{t1-2} & x_{t2}x_{t2-1} \end{bmatrix} \middle| Y_N\right) = \begin{pmatrix} E\left(\sum_{t=1}^{N} x_{t1}x_{t1-1} \middle| Y_N\right) & E\left(\sum_{t=1}^{N} x_{t1}x_{t2-1} \middle| Y_N\right) \\ E\left(\sum_{t=1}^{N} x_{t2}x_{t1-2} \middle| Y_N\right) & E\left(\sum_{t=1}^{N} x_{t2}x_{t2-1} \middle| Y_N\right) \end{pmatrix} \tag{3.27}$$

$$E\left(\sum_{t=1}^{N} y_t \hat{x}_t^T \middle| Y_N\right) = E\left(\sum_{t=1}^{N} \begin{bmatrix} y_{t1}\hat{x}_{t1} & y_{t1}\hat{x}_{t2} \end{bmatrix} \middle| Y_N\right) = \begin{bmatrix} E\left(\sum_{t=1}^{N} y_{t1}\hat{x}_{t1} \middle| Y_N\right) & E\left(\sum_{t=1}^{N} y_{t1}\hat{x}_{t2} \middle| Y_N\right) \end{bmatrix} \tag{3.28}$$

In order to get computing results in the equation (3.25) to (3.28), the computing process is described in the following steps:

(1) Defining Matrix Q to Compute $L_N^{(1)}$ and $L_N^{(2)}$

The matrix Q can be defined for different values in the equation (3.12). For instance,

If $Q = \begin{bmatrix} 1 & 0 \\ 0 & 0 \end{bmatrix}$, then $L_N^{(1)} = E\left\{\sum_{t=1}^{N} x_t^T Q x_t \middle| Y_N\right\} = E\left\{\sum_{t=1}^{N} x_{t1}x_{t1} \middle| Y_N\right\}$

If $Q = \begin{bmatrix} 0 & \frac{1}{2} \\ \frac{1}{2} & 0 \end{bmatrix}$, then $L_N^{(1)} = E\left\{\sum_{t=1}^{N} x_t^T Q x_t \middle| Y_N\right\} = E\left\{\sum_{t=1}^{N} x_{t1}x_{t2} \middle| Y_N\right\} = E\left\{\sum_{t=1}^{N} x_{t2}x_{t1} \middle| Y_N\right\}$

$$\text{If } Q=\begin{bmatrix}0 & 0\\ 0 & 1\end{bmatrix}, \text{ then } L_N^{(1)} = E\left\{\sum_{t=1}^{N} x_t^T Q x_t \middle| Y_N\right\} = E\left\{\sum_{t=1}^{N} x_{t2}x_{t2} \middle| Y_N\right\}$$

With these various Q values, the different filter estimation of $L_N^{(1)}$ can be obtained through the equations (3.15) to (3.17). Similarly, the different filtered estimation of $L_N^{(2)}$ can also be computed by the equation (3.18). The equation (3.25) and (3.26) can be computed using the above computing results.

(2) Defining Matrix R to Compute $L_N^{(3)}$

The matrix R can be defined for different values in the equation (3.13). For example,

$$\text{If } R=\begin{bmatrix}\frac{1}{2} & 0\\ 0 & 0\end{bmatrix}, \text{ then } L_N^{(3)} = E\left\{\sum_{t=1}^{N}\left[x_t^T R x_{t-1} + x_{t-1}^T R^T x_t\right] \middle| Y_N\right\} = E\left\{\sum_{t=1}^{N} x_{t1}x_{t1-1} \middle| Y_N\right\}$$

$$\text{If } R=\begin{bmatrix}0 & \frac{1}{2}\\ 0 & 0\end{bmatrix}, \text{ then } L_N^{(3)} = E\left\{\sum_{t=1}^{N}\left[x_t^T R x_{t-1} + x_{t-1}^T R^T x_t\right] \middle| Y_N\right\} = E\left\{\sum_{t=1}^{N} x_{t1}x_{t2-1} \middle| Y_N\right\}$$

$$\text{If } R=\begin{bmatrix}0 & 0\\ \frac{1}{2} & 0\end{bmatrix}, \text{ then } L_N^{(3)} = E\left\{\sum_{t=1}^{N}\left[x_t^T R x_{t-1} + x_{t-1}^T R^T x_t\right] \middle| Y_N\right\} = E\left\{\sum_{t=1}^{N} x_{t1-1}x_{t2} \middle| Y_N\right\}$$

$$\text{If } R=\begin{bmatrix}0 & 0\\ 0 & \frac{1}{2}\end{bmatrix}, \text{ then } L_N^{(3)} = E\left\{\sum_{t=1}^{N}\left[x_t^T R x_{t-1} + x_{t-1}^T R^T x_t\right] \middle| Y_N\right\} = E\left\{\sum_{t=1}^{N} x_{t2}x_{t2-1} \middle| Y_N\right\}$$

Thus, the values of $L_N^{(3)}$ can be obtained using the equations (3.19) to (3.21) with these different matrix R values. The equation (3.27) can be computed using the above computing results.

(3) Defining Matrix S to Compute $L_N^{(4)}$

The matrix S can be defined for different values in the equation (3.14). For instance,

$$\text{If } S=\begin{bmatrix}\frac{1}{2} & 0\end{bmatrix}, \text{ then } L_N^{(4)} = E\left\{\sum_{t=1}^{N}\left[x_t^T S y_t + y_t^T S^T x_t\right] \middle| Y_N\right\} = E\left\{\sum_{t=1}^{N} y_t x_{t1} \middle| Y_N\right\}$$

$$\text{If } S=\begin{bmatrix}0 & \frac{1}{2}\end{bmatrix}, \text{ then } L_N^{(4)} = E\left\{\sum_{t=1}^{N}\left[x_t^T S y_t + y_t^T S^T x_t\right] \middle| Y_N\right\} = E\left\{\sum_{t=1}^{N} y_t x_{t2} \middle| Y_N\right\}$$

The values of $L_N^{(4)}$ can be obtained using the equations (3.22) to (3.23) with these different S values. Thus, the equation (3.28) can be obtained using the above computing results.

(4) Estimating System Parameters

The equations (3.25) to (3.28) should be known after completing the computation (1), (2) and (3) described above. Therefore, it is very easy to estimate the system parameters in the equation (3.24) using the equations (3.2) to (3.5).

Similarly, it is also easy to estimate system parameters with 3rd-order or 4th-order or even higher order form of the state space models through the EM algorithm and the Kalman filter.

3.3 Verification of the EM Algorithm and the Kalman Filter

This section introduces the computing process of the EM algorithm and presents the estimated results with several samples.

3.3.1 Computing Process of the EM Algorithm

In order to verify the success of the EM algorithm in identifying system parameters, the computation processes are presented as the following:

(1) Setting a True Model

A true model with system parameters $\theta_{true} = \{A_t, B_t, C_t, D_t\}$ is assumed to be known; then a sequence of observed $Y_N = \{y_1, y_2, \ldots, y_N\}$ can be generated using the equation (3.1) with the known system parameters.

(2) Guessing an Initial Model

An initial model with system parameters $\theta_0 = \{A_0, B_0, C_0, D_0\}$ can be guessed, and they can be any values.

(3) Estimating New System Parameters θ_t

New system parameters $\theta_t = \{\hat{A}_t, \hat{B}_t^2, \hat{C}_t, \hat{D}_t^2\}$ can be estimated using the EM algorithm and the Kalman filter defined in Sections 3.2 and 3.3.

The estimated system parameters are compared between θ_t and θ_{t-1}. If $\|\theta_t - \theta_{t-1}\| \leq \varepsilon$, then $\theta_t = \{\hat{A}_t, \hat{B}_t^2, \hat{C}_t, \hat{D}_t^2\}$ can be considered as the final estimated results; otherwise, this step is repeated until $\|\theta_t - \theta_{t-1}\| \leq \varepsilon$. Here, ε is a very small value; and it determines the computing precision.

(4) Comparing Estimated Results

After completing the estimated process, the estimated system parameters are displayed. In addition, several results are also compared between the true model and the estimated model.

3.3.2 Analysis of the Estimated Results for System Identification

The identified system is in the controllable canonical form or the observable canonical form in the state space models.

Table 3.1 shows the estimated results of the various system parameters with different order's models (n = 2, 3, 4 and only considered single output d=1 case).

Figure 3-2 shows an example of the estimated results for verifying the EM Algorithm. Figure 3-2 (a) is the results of the sequence $P_{t|t}$, it means that the values of the sequence are constant after a time t_k. Figure 3-2 (b) compares the output sequences obtained by using different system parameters between the true system parameters and the identification system parameters.

Table 3.1: Verification of the Estimated Results for System Identification

Order		System Parameters for True Model	Estimated System Parameters via the EM Algorithm
1st		$A = 0.90, B = 25, BB^T = 625$ $C = 9.5,\ D = 4, DD^T = 16$	$\hat{A} = 0.91,\ \hat{BB^T} = 637.98$ $\hat{C} = 9.47,\ \hat{DD^T} = 15.93$
		$A = 0.90, B = 9, BB^T = 81$ $C = 1.0,\ D = 0.8, DD^T = 0.64$	$\hat{A} = 0.893,\ \hat{BB^T} = 80.943$ $\hat{C} = 0.998,\ \hat{DD^T} = 0.622$
2nd	Controllable	$A = \begin{bmatrix} 0 & 1 \\ 0.5 & 0.2 \end{bmatrix}, BB^T = \begin{bmatrix} 0.0005 & 0.0026 \\ 0.0026 & 0.0409 \end{bmatrix}$ $C = [1\ \ 0],\quad DD^T = [0.0025]$	$\hat{A} = \begin{bmatrix} -0.0003 & 0.925 \\ 0.5819 & 0.1406 \end{bmatrix}, \hat{BB^T} = \begin{bmatrix} 0.0006 & 0.0041 \\ 0.0041 & 0.0447 \end{bmatrix}$ $\hat{C} = [0.9801\ \ 0.0129],\ \hat{DD^T} = [0.0024]$
	Observable	$A = \begin{bmatrix} 0 & 0.5 \\ 1 & 0.5 \end{bmatrix}, BB^T = \begin{bmatrix} 25 & 50 \\ 50 & 101 \end{bmatrix}$ $C = [0\ \ 1],\quad D = [1]$	$\hat{A} = \begin{bmatrix} 0.099 & 0.449 \\ 1.171 & 0.462 \end{bmatrix}, \hat{BB^T} = \begin{bmatrix} 26.150 & 51..260 \\ 51.260 & 104.428 \end{bmatrix}$ $\hat{C} = [0.009\ \ 0.996],\ \hat{DD^T} = [0.979]$
3rd	Controllable	$A = \begin{bmatrix} 0 & 1 & 0 \\ 0 & 0 & 1 \\ 0.3 & 0.1 & 0.2 \end{bmatrix}; BB^T = \begin{bmatrix} 0.0014 & 0.0011 & 0.0065 \\ 0.0011 & 0.0014 & 0.0038 \\ 0.0065 & 0.0038 & 0.0905 \end{bmatrix},$ $C = [1\ \ 0\ \ 0];\ DD^T = [0.0016]$	$\hat{A} = \begin{bmatrix} -0.079 & 0.983 & 0.042 \\ -0.092 & 0.047 & 0.983 \\ 0.3618. & 0.131 & 0.191 \end{bmatrix}; \hat{BB^T} = \begin{bmatrix} 0.007 & 0.002 & 0.008 \\ 0.002 & 0.007 & 0.006 \\ 0.009 & 0.006 & 0.097 \end{bmatrix},$ $\hat{C} = [1.0\ \ 0.0\ \ 0.0];\ \hat{DD^T} = [0.0016]$
	Observable	$A = \begin{bmatrix} 0 & 0 & 0.3 \\ 1 & 0 & 0.3 \\ 0 & 1 & 0.3 \end{bmatrix}; BB^T = \begin{bmatrix} 6 & 13 & 18 \\ 13 & 30 & 40 \\ 18 & 40 & 59 \end{bmatrix},$ $C = [0\ \ 0\ \ 1];\ DD^T = [2.0]$	$\hat{A} = \begin{bmatrix} 0.094 & -0.127 & 0.345 \\ 1.092 & -0.186 & 0.380 \\ 0.188. & 0.780 & 0.413 \end{bmatrix}; \hat{BB^T} = \begin{bmatrix} 5.735 & 12.995 & 17.881 \\ 12.995 & 31.399 & 41.577 \\ 17.881 & 41.577 & 61.384 \end{bmatrix}$ $\hat{C} = [0.017\ \ 0.050\ \ 0.959];\ \hat{DD^T} = [3.703]$
4th	Controllable	$A = \begin{bmatrix} 0 & 1 & 0 & 0 \\ 0 & 0 & 1 & 0 \\ 0 & 0 & 0 & 1 \\ 0.3 & 0.2 & 0.1 & 0.2 \end{bmatrix},$ $BB^T = \begin{bmatrix} 0.0030 & 0.0024 & 0.0021 & 0.0046 \\ 0.0024 & 0.0030 & 0.0023 & 0.0078 \\ 0.0021 & 0.0023 & 0.0030 & 0.0133 \\ 0.0046 & 0.0078 & 0.0133 & 0.0914 \end{bmatrix}$ $C = [1\ \ 0\ \ 0\ \ 0];\quad DD^T = [0.25]$	$\hat{A} = \begin{bmatrix} -0.0609 & 1.0007 & 0.0148 & 0.0168 \\ -0.0430 & 0.0165 & 1.0020 & 0.0116 \\ -0.0517 & 0.0226 & 0.0075 & 1.0118 \\ 0.2989 & 0.2208 & 0.0856 & 0.2065 \end{bmatrix}$ $\hat{BB^T} = \begin{bmatrix} 0.0089 & 0..0055 & 0.0056 & 0.0101 \\ 0.0055 & 0.0062 & 0.0054 & 0.0129 \\ 0.0056 & 0.0054 & 0.0070 & 0.0204 \\ 0.0101 & 0.0129 & 0.0204 & 0.1427 \end{bmatrix}$ $\hat{C} = [1.0\ \ 0.0\ \ 0.0\ \ 0.0];\ \hat{DD^T} = [0.2286]$
	Observable	$A = \begin{bmatrix} 0 & 0 & 0 & 0.2 \\ 1 & 0 & 0 & 0.2 \\ 0 & 1 & 0 & 0.3 \\ 0 & 0 & 1 & 0.3 \end{bmatrix};$ $BB^T = \begin{bmatrix} 10 & 17 & 16 & 19 \\ 17 & 35 & 27 & 31 \\ 16 & 27 & 45 & 32 \\ 19 & 31 & 32 & 46 \end{bmatrix}$ $C = [0\ \ 0\ \ 0\ \ 1];$ $DD^T = [4.0]$	$\hat{A} = \begin{bmatrix} 0.029 & -0.026 & -0.091 & 0.239 \\ 1.060 & -0.025 & 0.018 & 0.164 \\ 0.304 & 0.782 & -0.181 & 0.345 \\ 0.294 & -0.061 & 0.863 & 0.269 \end{bmatrix}$ $\hat{BB^T} = \begin{bmatrix} 8.008 & 15.168 & 14.867 & 17.543 \\ 15.168 & 35.104 & 29.135 & 33.695 \\ 14.867 & 29.135 & 48.759 & 35.708 \\ 17.543 & 33.695 & 35.708 & 51.733 \end{bmatrix}$ $\hat{C} = [-0.037\ \ 0.015\ \ 0.028\ \ 0.958];$ $\hat{DD^T} = [3.821]$

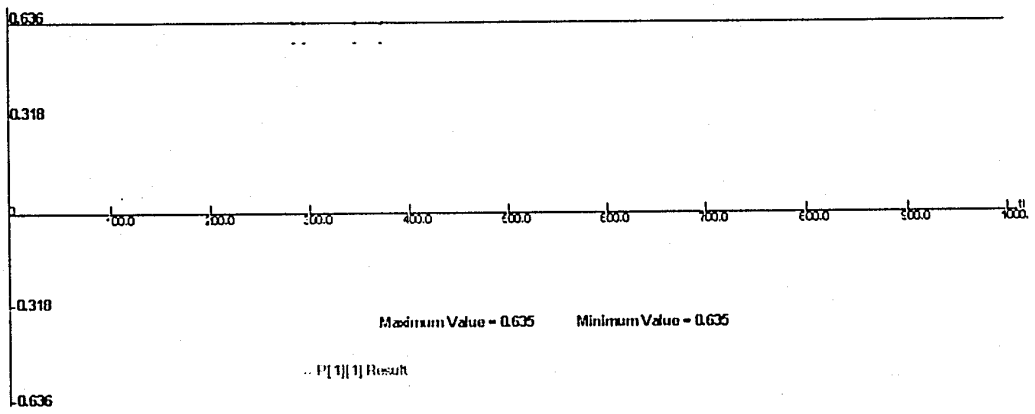

Figure 3-2 (a) the sequence of $P_{t|t}$

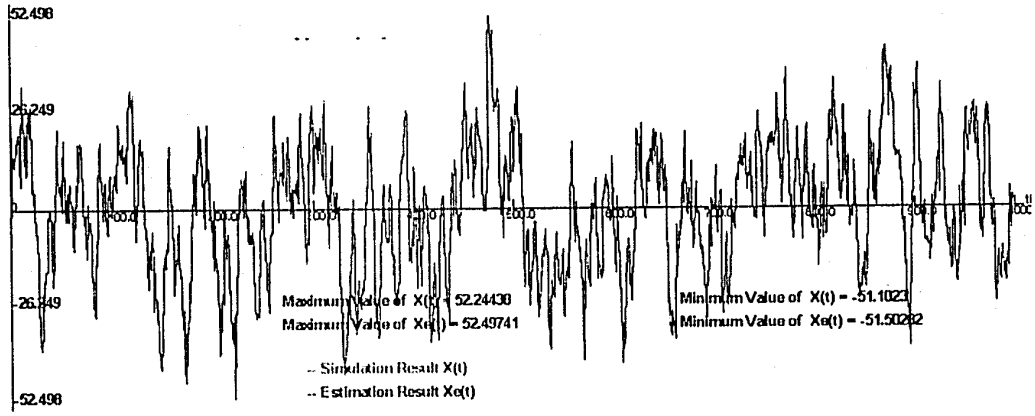

Figure 3-2 (b) compares the state variables between $x_{t|t}$ and $\hat{x}_{t|t}$.

Figure 3-2 An Example of the Estimated Results for Verifying the EM Algorithm.

These estimated results show that the estimated system parameters are very close to the true system parameters. Therefore, it can indicate that the EM algorithm is a very effective method for system identification.

In these estimated results, the observed data are generated using the true system parameters. However, system identification can be more interesting based on the real measurement data.

The following sections will present system identification for the fading channel based on the real measurement data provided by the CRC.

3.4 System Identification for Flat Fading Channels Based on Measurement Data

This section introduces the mathematical models for the flat fading channel based on the measurement data provided by the CRC. For a set of the measurement data, each model is employed to identify system parameters using the EM algorithm together with the Kalman filter. In addition, their Doppler power spectral densities (DPSD) are also computed and compared between the measurement data and the estimated system parameters.

3.4.1 Description of Identified Mathematical Models of Flat fading Channels

Using the measurement data, the mathematical models are identified based on the state space model in the equation (3.1). For a set of data, the following models and estimations are presented:

(1) the second-order estimation ($n = m = 2, d = 1$)

(2) the third-order estimation ($n = m = 3, d = 1$)

(3) the fourth-order estimation ($n = m = 4, d = 1$)

(4) the fourth-order estimation for combination

For cases (1), (2) and (3), the model can be employed as the following:

$$y_t = F_t + v_t \tag{3.29}$$

In this equation, F_t denotes the inphase component I_t or the quadrature component Q_t from the measurement data, and v_t is a white noise with Gaussian process.

Specifically, the parameters B and D are not computed directly; whereas the parameters BB^T and DD^T are computed in the EM algorithm. Therefore, the form of parameter BB^T is different from the form defined in Chapter 2. Several variables ε_{ij} $(i, j = 1,2,3,4)$, having very small values (closed to zero), are added to the BB^T form in order to make matrix (BB^T) inverse.

If the controllable canonical form is considered, then the system parameters in the state space model can be expressed as the following:

For the second order model, the system parameters are defined as the following:

$$A=\begin{bmatrix}0 & 1\\ \alpha_1 & \alpha_2\end{bmatrix},\quad B=\begin{bmatrix}\varepsilon_{11} & \varepsilon_{12}\\ k & \varepsilon_{22}\end{bmatrix},\quad C=\begin{bmatrix}1 & 0\end{bmatrix},\quad D=[d] \tag{3.30}$$

For the third order model, the system parameters are defined as the following:

$$A=\begin{bmatrix}0 & 1 & 0\\ 0 & 0 & 1\\ \alpha_1 & \alpha_2 & \alpha_3\end{bmatrix},\quad B=\begin{bmatrix}\varepsilon_{11} & \varepsilon_{12} & \varepsilon_{13}\\ \varepsilon_{21} & \varepsilon_{22} & \varepsilon_{23}\\ k & \varepsilon_{32} & \varepsilon_{33}\end{bmatrix},\quad C=\begin{bmatrix}1 & 0 & 0\end{bmatrix},\quad D=[d] \tag{3.31}$$

For the fourth order model, the system parameters are defined as the following:

$$A=\begin{bmatrix}0 & 1 & 0 & 0\\ 0 & 0 & 1 & 0\\ 0 & 0 & 0 & 1\\ \alpha_1 & \alpha_2 & \alpha_3 & \alpha_4\end{bmatrix},\quad B=\begin{bmatrix}\varepsilon_{11} & \varepsilon_{12} & \varepsilon_{13} & \varepsilon_{14}\\ \varepsilon_{21} & \varepsilon_{22} & \varepsilon_{23} & \varepsilon_{24}\\ \varepsilon_{31} & \varepsilon_{32} & \varepsilon_{33} & \varepsilon_{34}\\ k & \varepsilon_{42} & \varepsilon_{43} & \varepsilon_{44}\end{bmatrix}, \tag{3.32}$$

$$C=\begin{bmatrix}1 & 0 & 0 & 0\end{bmatrix},\quad D=[d]$$

For case (4), the model employed can be expressed as the following:

$$y_t=\left(I_t\cos(\omega_c t)-Q_t\sin(\omega_c t)\right)s(t)+v_{It}\cos(\omega_c t)-v_{Qt}\sin(\omega_c t) \tag{3.33}$$

In this case, I_t and Q_t are the inphase and the quadrature components; and the system parameters $\theta_t=\{A_t,B_t,C_t,D_t\}$ are represented as the following:

$$A_t=\begin{bmatrix}0 & 1 & 0 & 0\\ a_1 & a_2 & 0 & 0\\ 0 & 0 & 0 & 1\\ 0 & 0 & a_3 & a_4\end{bmatrix};\quad B_t=\begin{bmatrix}\varepsilon_{11} & \varepsilon_{12} & \varepsilon_{13} & \varepsilon_{14}\\ k_1 & \varepsilon_{22} & \varepsilon_{23} & \varepsilon_{24}\\ \varepsilon_{31} & \varepsilon_{32} & \varepsilon_{33} & \varepsilon_{34}\\ \varepsilon_{41} & k_2 & \varepsilon_{43} & \varepsilon_{44}\end{bmatrix} \tag{3.34}$$

$$C_t=[\cos(\omega_c t)\quad 0\quad -\sin(\omega_c t)\quad 0],\qquad D_t=[d]$$

Of course, the system parameters can be represented as the observable canonical form and can also be a higher order model. In this thesis, the mathematical models are just considered as the controllable canonical form with 2nd, 3rd and 4th orders.

3.4.2 Analysis of Identified Results for Flat Fading Channels

As previously described, the estimation of system identification for the flat fading channel is considered in the four cases for each set of the measurement data. The estimated results include the identified system parameters and the comparison curves between the measurement data and the estimated results.

In the above (1), (2) and (3) cases, the measurement data is responded the inphase component or the quadrature component. In the case (4), the measurement data is responded a combination from the inphase component and the quadrature component.

The measurement data provided by CRC contains 98 data files. The data files are classified as the inphase components and the quadrature components. Furthermore, each component includes seven groups and each group also includes seven data files. For instance, I3.2 denotes the data file is from the second data file of the third group in the inphase component.

For example, considering the 2^{nd}, 3^{rd}, and 4^{th} orders of the state space models based on the measurement data files I1.1 and Q1.1 that the data files include 766 samples. The estimated system parameters are presented in the following table; and their compared results are also plotted in the following figures. These figures are compared the output sequences and the Doppler power spectral densities (DPSDs) between the measurement data (real data) and the computed results using the estimated system parameters.

Many estimated results for the different measurement data files are listed in Appendix A.

Table 3.2: the Estimated Results Based on the Measurement Data I1.1 and Q1.1

Order		Estimated Model Parameters	Estimated Figures
I(k)	2nd	$\hat{A}=\begin{bmatrix}0 & 1\\ 0.0468 & 0.0132\end{bmatrix}$, $\hat{BB}^T=\begin{bmatrix}0.0957 & 0.0027\\ 0.0027 & 0.0963\end{bmatrix}$ $\hat{C}=[1\ \ 0]$, $\hat{DD}^T=[0.0961]$	Figure 3-3
	3rd	$\hat{A}=\begin{bmatrix}0.0 & 1.0 & 0.0\\ 0.0 & 0.0 & 1.0\\ 0.5989 & -0.0159 & 0.2072\end{bmatrix}$, $\hat{BB}^T=\begin{bmatrix}0.0037 & 0.00081 & 0.00085\\ 0.00081 & 0.0039 & 0.00095\\ 0.00085 & 0.00095 & 0.0040\end{bmatrix}$ $\hat{C}=[1\ \ 0\ \ 0]$, $\hat{DD}^T=[0.0029]$	Figure 3-4
	4th	$\hat{A}=\begin{bmatrix}0 & 1 & 0 & 0\\ 0 & 0 & 1 & 0\\ 0 & 0 & 0 & 1\\ 0.5684 & -0.0889 & 0.0199 & 0.0245\end{bmatrix}$, $\hat{BB}^T=\begin{bmatrix}0.0288 & 0.0010 & 0.0020 & 0.0030\\ 0.0010 & 0.0289 & 0.0020 & 0.0020\\ 0.0020 & 0.0020 & 0.0316 & 0.0010\\ 0.0030 & 0.0020 & 0.0010 & 0.0316\end{bmatrix}$ $\hat{C}=[1\ \ 0\ \ 0\ \ 0]$, $\hat{DD}^T=[0.0078]$	Figure 3-5
Q(k)	2nd	$\hat{A}=\begin{bmatrix}0 & 1\\ 0.7281 & 0.1853\end{bmatrix}$, $\hat{BB}^T=\begin{bmatrix}0.0026 & 0.00083\\ 0.00083 & 0.0029\end{bmatrix}$ $\hat{C}=[1\ \ 0]$, $\hat{DD}^T=[0.0019]$	Figure 3-6
	3rd	$\hat{A}=\begin{bmatrix}0.0 & 1.0 & 0.0\\ 0.0 & 0.0 & 1.0\\ 0.5925 & 0.0325 & 0.2068\end{bmatrix}$, $\hat{BB}^T=\begin{bmatrix}0.0060 & 0.0011 & 0.0011\\ 0.0011 & 0.0063 & 0.0013\\ 0.0011 & 0.0013 & 0.0066\end{bmatrix}$ $\hat{C}=[1\ \ 0\ \ 0]$, $\hat{DD}^T=[0.0050]$	Figure 3-7
	4th	$\hat{A}=\begin{bmatrix}0 & 1 & 0 & 0\\ 0 & 0 & 1 & 0\\ 0 & 0 & 0 & 1\\ 0.6710 & -0.0759 & 0.0383 & 0.0359\end{bmatrix}$, $\hat{BB}^T=\begin{bmatrix}0.0291 & 0.0010 & 0.0020 & 0.0030\\ 0.0010 & 0.0293 & 0.0020 & 0.0020\\ 0.0020 & 0.0020 & 0.0320 & 0.0010\\ 0.0030 & 0.0020 & 0.0010 & 0.0321\end{bmatrix}$ $\hat{C}=[1\ \ 0\ \ 0\ \ 0]$, $\hat{DD}^T=[0.0078]$	Figure 3-8
Combination		$\hat{A}=\begin{bmatrix}0 & 1 & 0 & 0\\ 0.5154 & 0.0668 & 0 & 0\\ 0 & 0 & 0 & 1\\ 0 & 0 & 0.5262 & 0.0915\end{bmatrix}$, $\hat{BB}^T=\begin{bmatrix}0.0506 & 0.0071 & 0.0036 & 0.0017\\ 0.0071 & 0.0523 & 0.0012 & 0.0037\\ 0.0036 & 0.0012 & 0.0482 & 0.0081\\ 0.1017 & 0.0037 & 0.0081 & 0.0496\end{bmatrix}$ $\hat{C}=[1\ \ 0\ \ 1\ \ 0]$, $\hat{DD}^T=[0.0019]$	Figure 3-9

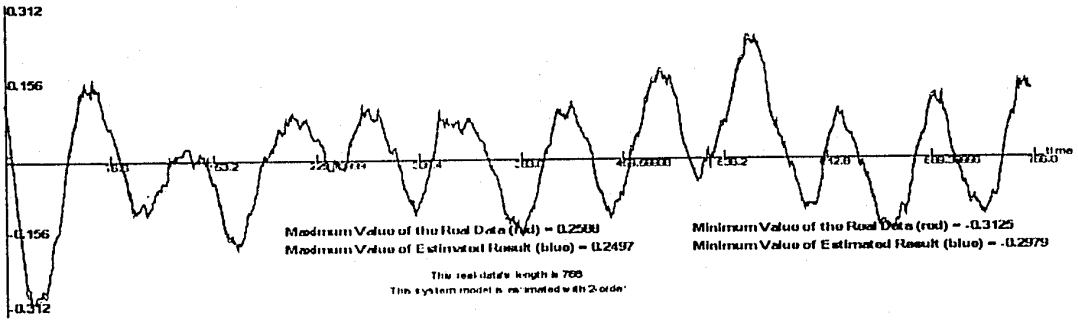

Figure 3-3 (a). The Estimated Result $\hat{I}_{t|t}$ vs. The Measured data $I_{t|t}$

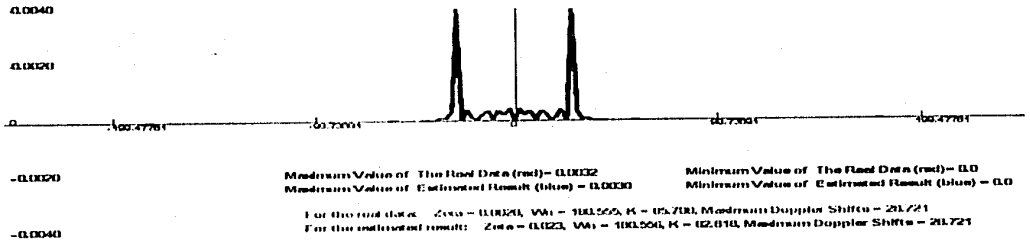

Figure 3-3 (b). DPSDs for $\hat{I}_{t|t}$ vs. $I_{t|t}$

Figure 3-3. the real inphase component vs. estimate value in 2nd-order (I1.1)

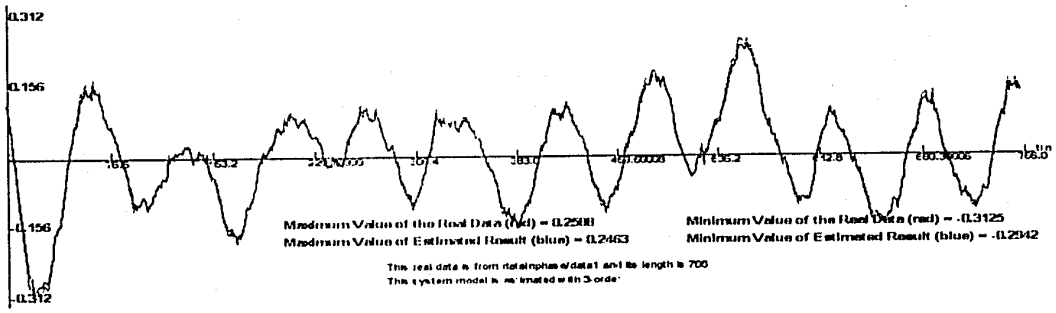

Figure 3-4 (a). The Estimated Result $\hat{I}_{t|t}$ vs. the Measured data $I_{t|t}$

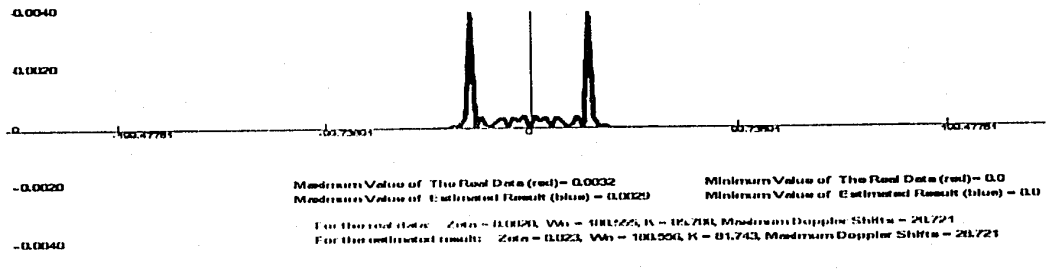

Figure 3-4 (b). DPSDs for $\hat{I}_{t|t}$ vs. $I_{t|t}$

Figure 3-4. The real inphase component vs. estimate result in 3rd-order (I1.1)

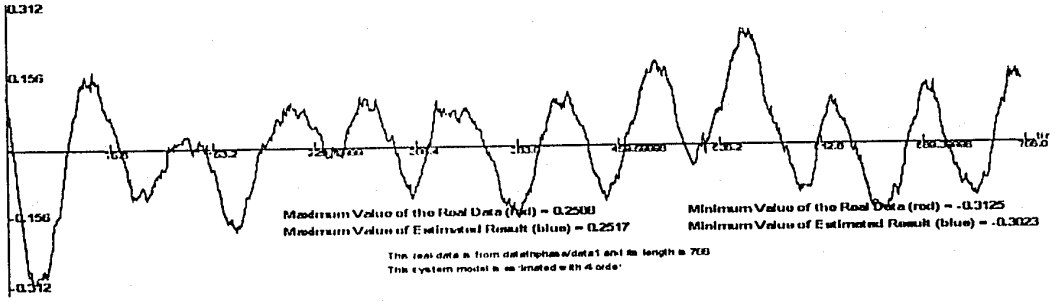

Figure 3-5 (a). The Estimated Result $\hat{I}_{t|t}$ vs. The Measured data $I_{t|t}$

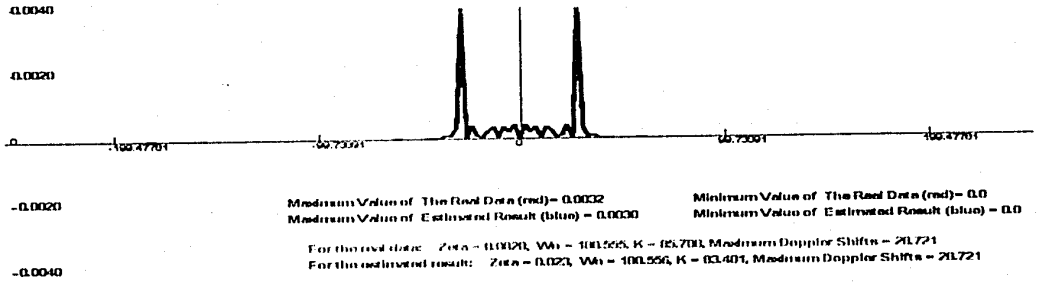

Figure 3-5 (b). DPSDs for $\hat{I}_{t|t}$ vs. $I_{t|t}$

Figure 3-5. The real inphase components vs. estimate result in 4th-order (I1.1)

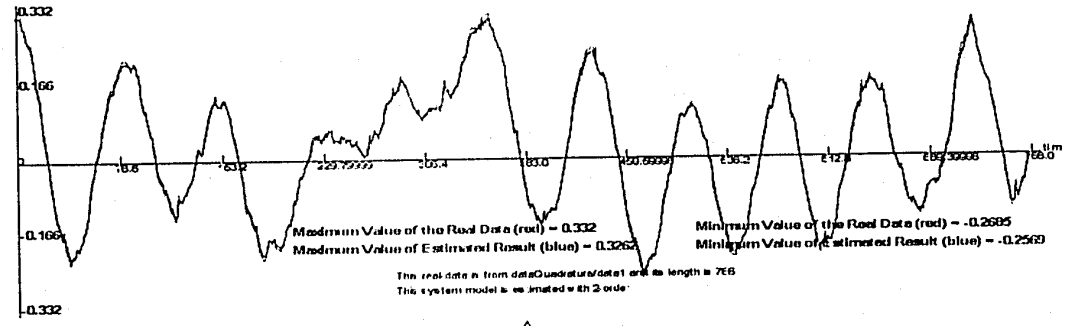

Figure 3-6 (a). The Estimated $\hat{Q}_{t|t}$ vs. The Measurement Data $Q_{t|t}$

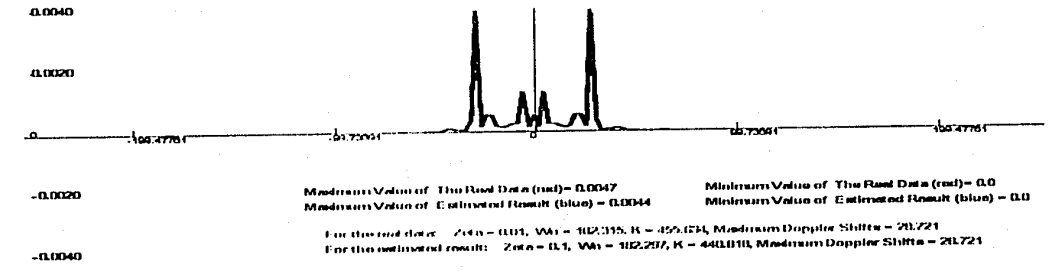

Figure 3-6 (b). DPSDs for $\hat{Q}_{t|t}$ vs. $Q_{t|t}$

Figure 3-6. The real quadrature component vs. estimate result in 2nd-order (Q1.1)

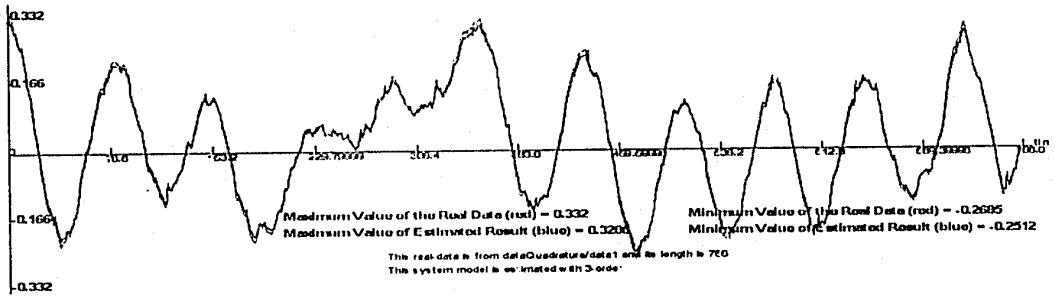

Figure 3-7 (a). The Estimated $\hat{Q}_{t|t}$ vs. The Measurement Data $Q_{t|t}$

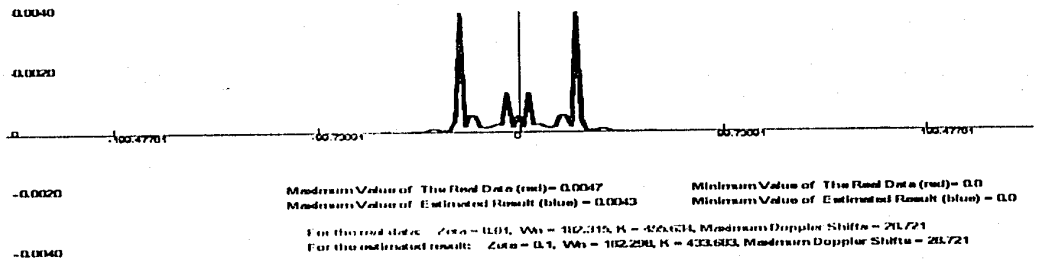

Figure 3-7 (b). DPSDs for $\hat{Q}_{t|t}$ vs. $Q_{t|t}$

Figure 3-7. The real quadrature component vs. estimate result in 3rd-order (Q1.1)

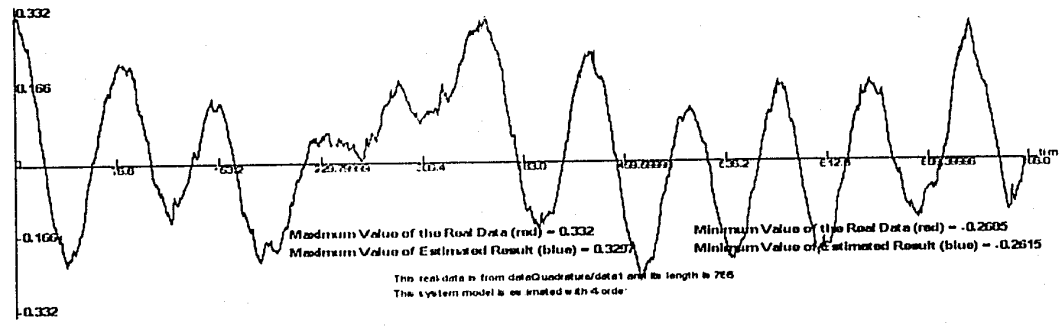

Figure 3-8 (a). The Estimated $\hat{Q}_{t|t}$ vs. The Measurement Data $Q_{t|t}$

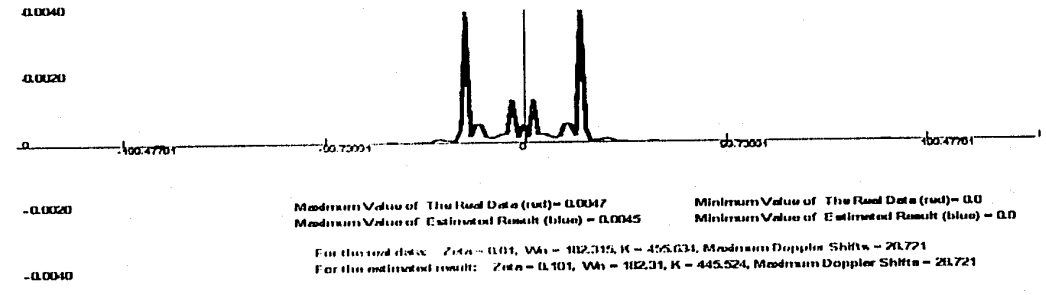

Figure 3-8 (b). DPSDs for $\hat{Q}_{t|t}$ vs. $Q_{t|t}$

Figure 3-8. The real quadrature component vs. estimate result in 4th-order (Q1.1)

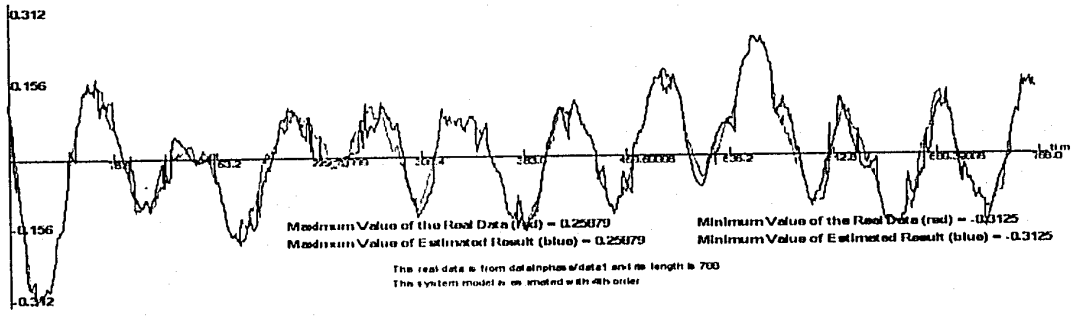

Figure 3-9 (a). Inphase Components: $\hat{I}_{t|t}$ vs. $I_{t|t}$

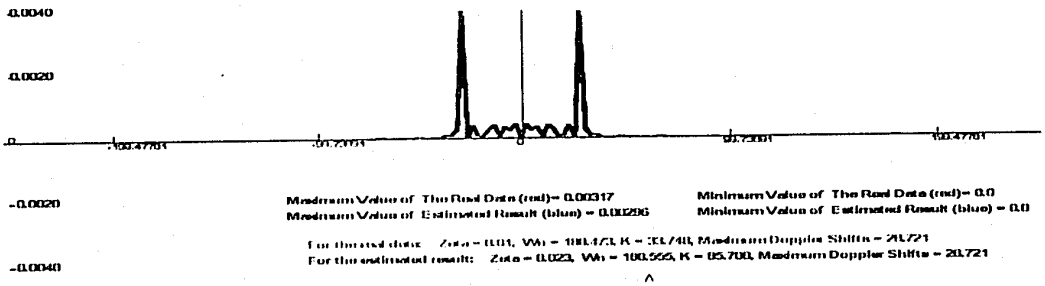

Figure 3-9 (b). DPSDs for $\hat{I}_{t|t}$ vs. $I_{t|t}$

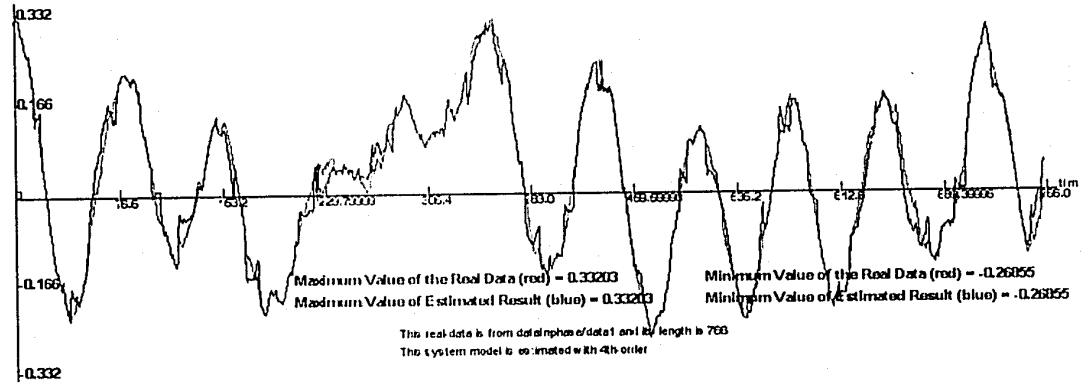

Figure 3-9 (c). Quadrature Components: $\hat{Q}_{t|t}$ vs. $Q_{t|t}$

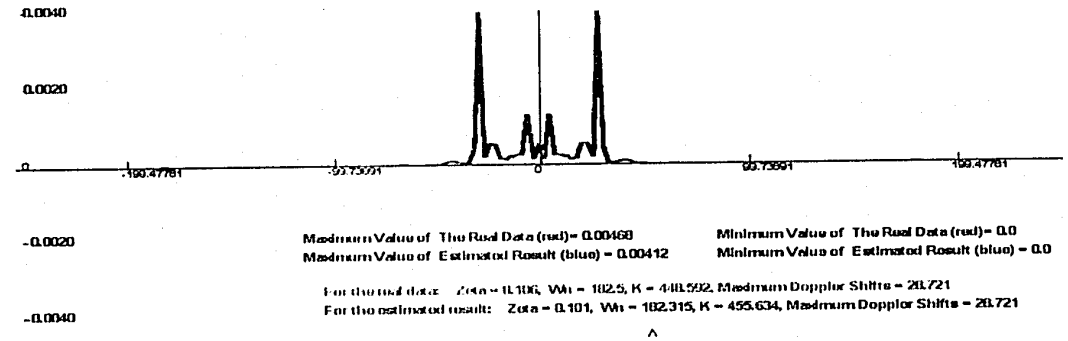

Figure 3-9 (d). DPSDs for $\hat{Q}_{t|t}$ vs. $Q_{t|t}$

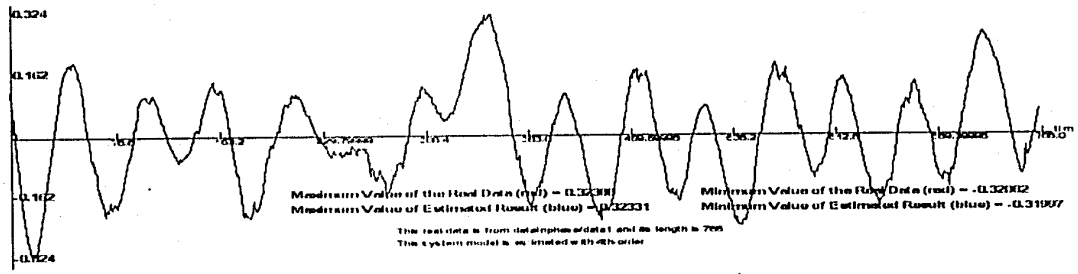

Figure 3-9 (e). Combination Components: $\hat{y}_{t|t}$ vs. $y_{t|t}$

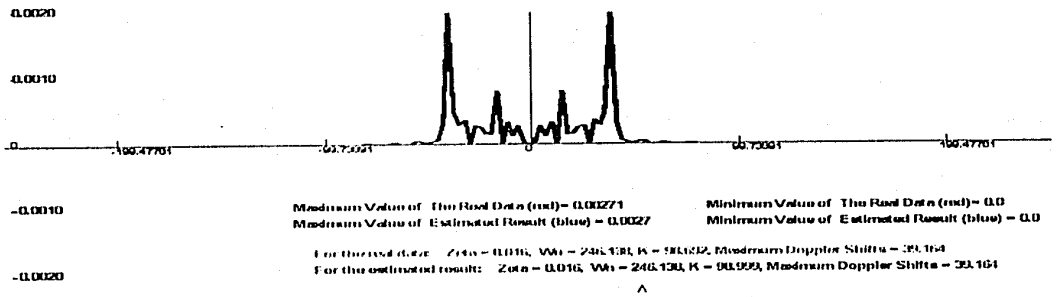

Figure 3-9 (f). DPSDs for $\hat{y}_{t|t}$ vs. $y_{t|t}$

Figure 3-9. The real Inphase and quadrature component vs. estimate result in 4th-order

In these figures, the red curves denote the measured data corresponding to the measured data files; and the blue curves denote the estimated results.

The above estimated results can illustrate that nothing is gained by increasing the order of the state space models. It is also concluded that the models of the measured data can be generated with very high accuracy through a simple second-order discrete time stochastic differential equation.

3.5 System Identification for Frequency-Selective Fading Channels Based on Measurement Data

This section will address system identification for the frequency-selective fading channel which is also based on the measurement data provided by CRC.

3.5.1 Identified Mathematical Model for Frequency-Selective Fading Channels

The received signal of the frequency-selective fading channel is represented as the following equation described in Chapter 2:

$$y_t = \sum_{k=1}^{N} \left(I_{k(t,\tau_k)} \cos(\omega_c t) - Q_{k(t,\tau_k)} \sin(\omega_c t) \right) s_{(t-\tau_k)} + v_{It} \cos(\omega_c t) - v_{Qt} \sin(\omega_c t) \tag{3.35}$$

In this case, the state space model in the equation (3.1) can be modified as the following [CHA03]:

$$\begin{aligned} x_{i(t+1)} &= A_{i(t)} x_{i(t)} + B_{i(t)} w_{i(t)}; \quad x_{i(0)} \sim N(\mu_i, \Sigma_{i(0)}) \\ x_{t+1} &= A_t x_t + B_t w_t; \\ y_t &= \sum_{i=1}^{N} C_{i(t)} x_{i(t)} s_{(t-\tau_i)} + D_t v_t = C_t x_t + D_t v_t \end{aligned} \tag{3.36}$$

In this equation, the noises of w_{it} and v_t are also independent white noises with $N(0,1)$; and the system parameters are given as the following equation [CHA03, LIX02]:

$$\begin{aligned} A_t &= \begin{bmatrix} A_{1t} & 0 & \cdots & 0 \\ 0 & A_{2t} & \cdots & 0 \\ \vdots & \vdots & \cdots & \vdots \\ 0 & 0 & \cdots & A_{Nt} \end{bmatrix}, \quad B_t = \begin{bmatrix} B_{1t} & 0 & \cdots & 0 \\ 0 & B_{2t} & \cdots & 0 \\ \vdots & \vdots & \cdots & \vdots \\ 0 & 0 & \cdots & B_{Nt} \end{bmatrix}, \\ C_t &= \begin{bmatrix} C_{1t} s_{t-\tau_1} & C_{2t} s_{t-\tau_2} & \cdots & C_{Nt} s_{t-\tau_N} \end{bmatrix}, \\ D_t &= \begin{bmatrix} \cos(\omega_c t) & -\sin(\omega_c t) \end{bmatrix} \end{aligned} \tag{3.37}$$

On the other hand, A_{it}, B_{it} and C_{it} are defined as the following:

$$\begin{aligned} A_{it} &= \begin{bmatrix} 0 & 1 & 0 & 0 \\ a_{11} & a_{12} & 0 & 0 \\ 0 & 0 & 0 & 1 \\ 0 & 0 & a_{21} & a_{22} \end{bmatrix}, \quad B_{it} = \begin{bmatrix} \varepsilon_{11} & \varepsilon_{12} & \varepsilon_{13} & \varepsilon_{14} \\ k_1 & \varepsilon_{22} & \varepsilon_{23} & \varepsilon_{24} \\ \varepsilon_{31} & \varepsilon_{32} & \varepsilon_{33} & \varepsilon_{34} \\ \varepsilon_{41} & k_2 & \varepsilon_{42} & \varepsilon_{43} \end{bmatrix}, \\ C_{it} &= \begin{bmatrix} \cos(\omega_c t) & 0 & -\sin(\omega_c t) & 0 \end{bmatrix} \end{aligned} \tag{3.38}$$

3.5.2 Analysis of Identified Results for Frequency-Selective Fading Channels

The system identification of the frequency-selective fading channel is estimated in the same process as the flat fading channel; but it is assumed that the total channel number can be N = 2, 3, 4, 5, 6, 7 in the equation (3.35).

In addition, the transmitted signal can considered as a narrow band signal or a wide band signal; the system identification process can thus be determined with the two cases. Furthermore, the frequency-selective fading can be considered as a fast fading or a slow

fading. Therefore, the system identification can be estimated using these different cases: the narrowband transmitted signal, the wideband transmitted signal and the slow fading.

This section only presents the estimated results for $N = 6$ case. In this case, the inphase component and quadrature component are considered as a combination with six paths; and the measurement data is selected from the data group 1 with 385 samples.

Many estimated results for the frequency-selective fading channel are listed in Appendix B.

In the following figures, the inphase component and the quadrature component are compared between the measured data and the estimation on each path. The output sequences $\{y_t\}_{t=1}^{N}$ are obtained from the equation (3.35), and the estimated results $\{\hat{C}\hat{x}_t\}_{t=1}^{N}$ are computed from the equation (3.36).

(1) Wide Band Transmitted Signal

Considered the transmitted signal is a wide band signal, the estimated system parameters are computed as following:

$$\hat{A} = \begin{bmatrix} \hat{A}_1 & 0 & \cdots & 0 \\ 0 & \hat{A}_2 & \cdots & 0 \\ \vdots & \vdots & \vdots & 0 \\ 0 & 0 & \cdots & \hat{A}_6 \end{bmatrix}, \quad \hat{BB}^T = \begin{bmatrix} \hat{BB}_1^T & 0 & \cdots & 0 \\ 0 & \hat{BB}_2^T & \cdots & 0 \\ \vdots & \vdots & \cdots & 0 \\ 0 & 0 & \cdots & \hat{BB}_6^T \end{bmatrix},$$

$$\hat{C} = \begin{bmatrix} \hat{C}_1 & \hat{C}_2 & \cdots & \hat{C}_6 \end{bmatrix}, \quad \hat{DD}^T = 0.0023$$

Here, $\left\{\hat{A}_l, \hat{BB}_l^T, \hat{C}_l\right\}$ are defined as the following:

$$\hat{A}_1 = \begin{bmatrix} 0 & 1 & 0 & 0 \\ 0.1953 & -0.0278 & 0 & 0 \\ 0 & 0 & 0 & 1 \\ 0 & 0 & 0.1605 & -0.1328 \end{bmatrix}, \quad \hat{A}_2 = \begin{bmatrix} 0 & 1 & 0 & 0 \\ 0.2071 & 0.1199 & 0 & 0 \\ 0 & 0 & 0 & 1 \\ 0 & 0 & -0.1628 & 0.0970 \end{bmatrix}$$

$$\hat{A}_3 = \begin{bmatrix} 0 & 1 & 0 & 0 \\ 0.1950 & -0.0274 & 0 & 0 \\ 0 & 0 & 0 & 1 \\ 0 & 0 & 0.1882 & -0.2785 \end{bmatrix}, \quad \hat{A}_4 = \begin{bmatrix} 0 & 1 & 0 & 0 \\ 0.2935 & 0.0654 & 0 & 0 \\ 0 & 0 & 0 & 1 \\ 0 & 0 & 0.3664 & -0.0877 \end{bmatrix}$$

$$\hat{A}_5 = \begin{bmatrix} 0 & 1 & 0 & 0 \\ 0.2001 & -0.0272 & 0 & 0 \\ 0 & 0 & 0 & 1 \\ 0 & 0 & 0.1920 & -0.2836 \end{bmatrix}, \quad \hat{A}_6 = \begin{bmatrix} 0 & 1 & 0 & 0 \\ 0.2966 & 0.0753 & 0 & 0 \\ 0 & 0 & 0 & 1 \\ 0 & 0 & 0.3766 & -0.0937 \end{bmatrix}$$

$$\hat{BB}_1^T = \begin{bmatrix} 0.0884 & 0.0112 & 0.0164 & 0.0149 \\ 0.0112 & 0.1763 & 0.0275 & -0.0133 \\ 0.0164 & 0.0275 & 0.0905 & 0.0135 \\ 0.0149 & -0.0133 & 0.0135 & 0.3449 \end{bmatrix}, \quad \hat{BB}_2^T = \begin{bmatrix} 0.2952 & 0.0196 & 0.0018 & 0.0117 \\ 0.0196 & 0.2651 & 0.0297 & -0.0059 \\ 0.0018 & 0.0297 & 0.1733 & 0.0149 \\ 0.0117 & -0.0059 & 0.0149 & 0.0796 \end{bmatrix}$$

$$\hat{BB}_3^T = \begin{bmatrix} 0.1797 & 0.0202 & 0.0135 & 0.0038 \\ 0.0202 & 0.2598 & 0.0144 & -0.0062 \\ 0.0135 & 0.0144 & 0.1768 & 0.0240 \\ 0.0038 & -0.0062 & 0.0240 & 0.1771 \end{bmatrix}, \quad \hat{BB}_4^T = \begin{bmatrix} 0.2770 & 0.0042 & 0.0096 & 0.0008 \\ 0.0042 & 0.0955 & 0.0338 & 0.0065 \\ 0.0096 & 0.0338 & 0.3411 & 0.0054 \\ 0.0008 & 0.0065 & 0.0054 & 0.3394 \end{bmatrix}$$

$$\hat{BB}_5^T = \begin{bmatrix} 0.1824 & 0.0209 & 0.0150 & 0.0042 \\ 0.0209 & 0.2651 & 0.0152 & -0.053 \\ 0.0150 & 0.0152 & 0.1815 & 0.0253 \\ 0.0042 & -0.0053 & 0.0253 & 0.1819 \end{bmatrix}, \quad \hat{BB}_6^T = \begin{bmatrix} 0.2927 & 0.0024 & 0.0084 & 0.0009 \\ 0.0024 & 0.0975 & 0.0357 & 0.0051 \\ 0.0084 & 0.0356 & 0.3602 & 0.0058 \\ 0.0009 & 0.0051 & 0.0058 & 0.3581 \end{bmatrix}$$

$$\hat{C}_1 = \hat{C}_2 = \hat{C}_3 = \hat{C}_4 = \hat{C}_5 = \hat{C}_6 = \begin{bmatrix} 1 & 0 & 1 & 0 \end{bmatrix}$$

Figure 3-10 shows the compared results between the measurement data and the estimated results on each path.

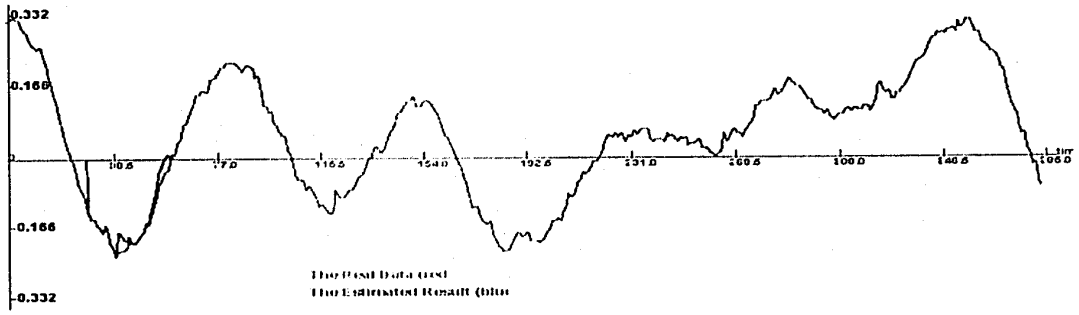

Figure 3-10 (a). Inphase Components on 1st path:

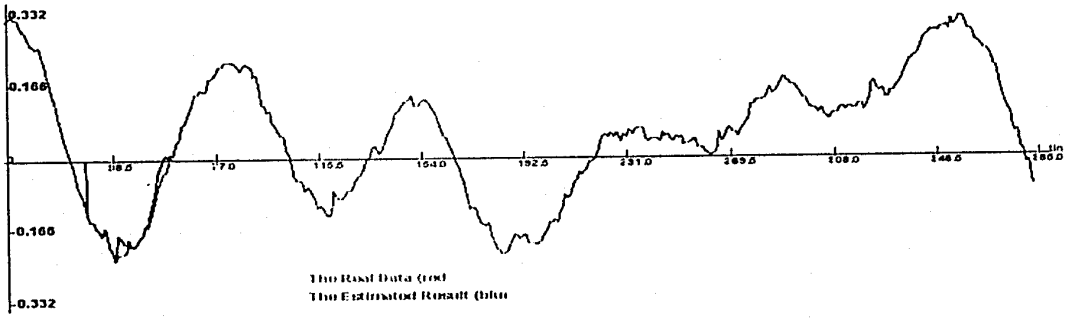

Figure 3-10 (b). Quadrature Components on 1st path

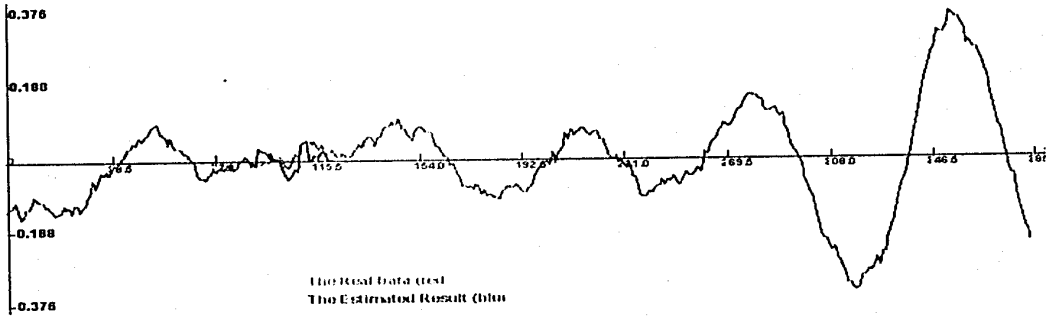

Figure 3-10 (c). Inphase Components on 2nd path

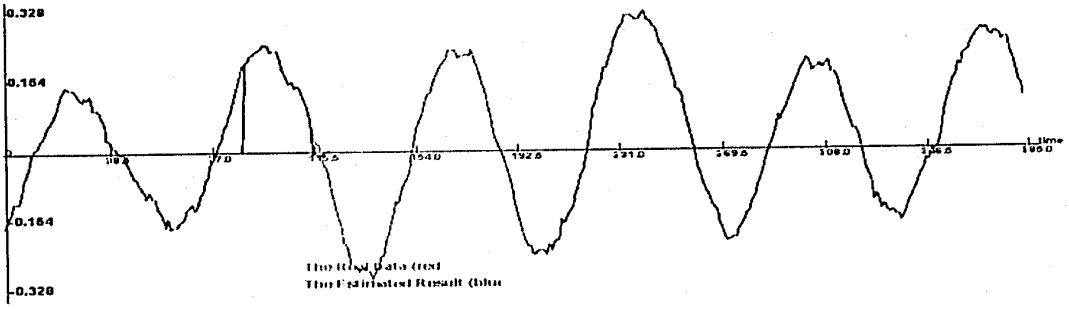

Figure 3-10 (d). Quadrature Components on 2nd path

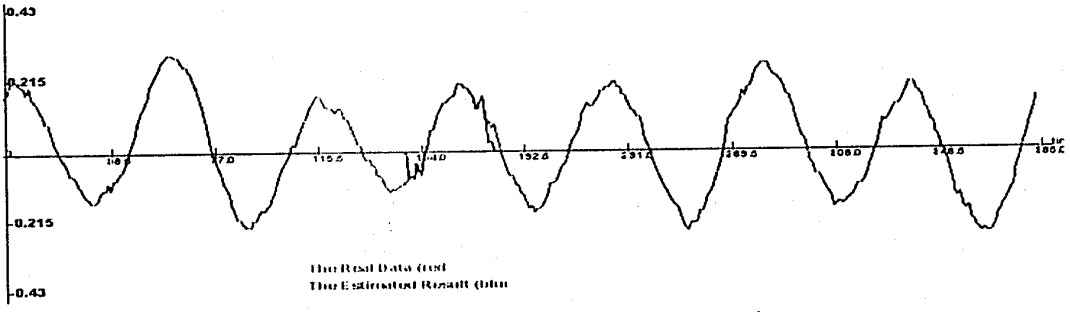

Figure 3-10 (e). Inphase Components on 3rd path

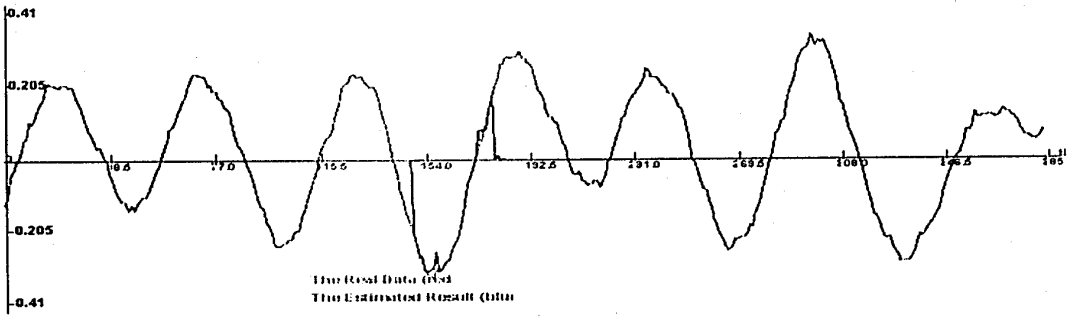

Figure 3-10 (f). Quadrature Components on 3rd path

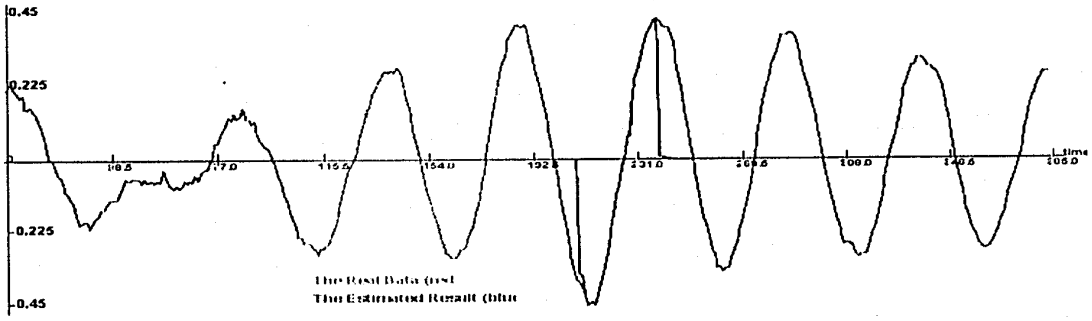

Figure 3-10 (g). Inphase Components on 4th path

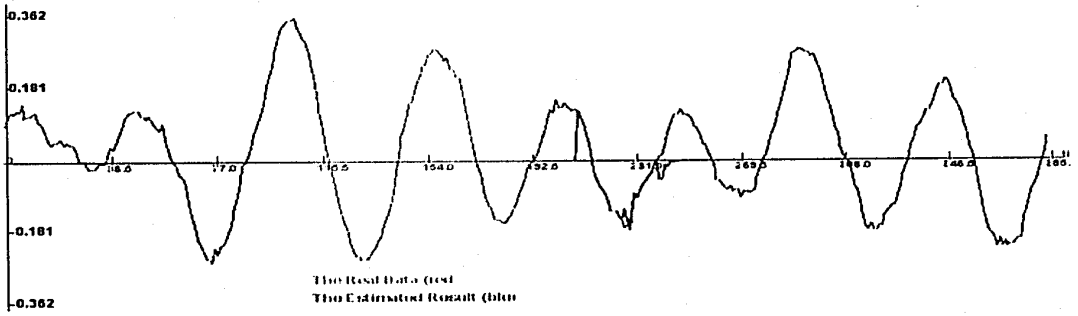

Figure 3-10 (h). Quadrature Components on 4th path

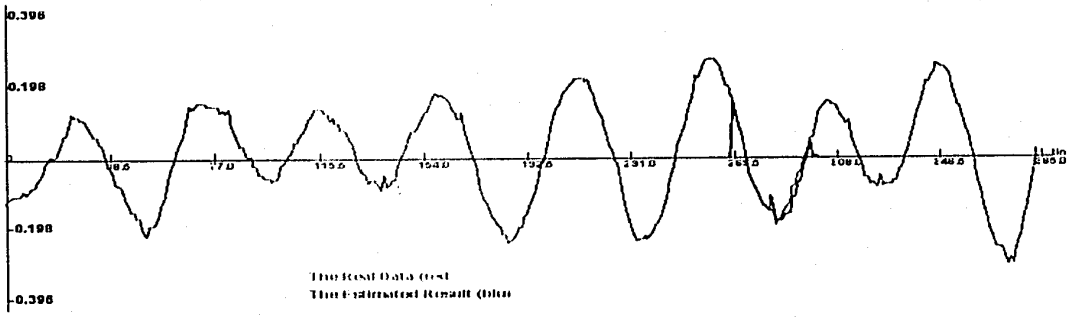

Figure 3-10 (i). Inphase Components on 5th path

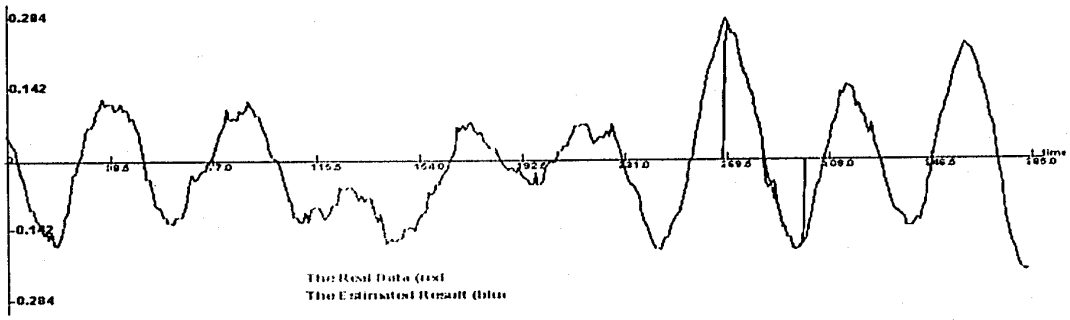

Figure 3-10 (j). Quadrature Components on 5th path

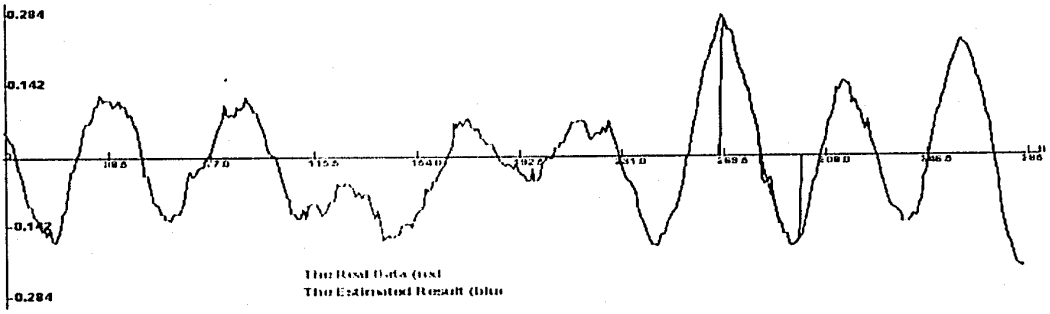

Figure 3-10 (k). Inphase Components on 6th path

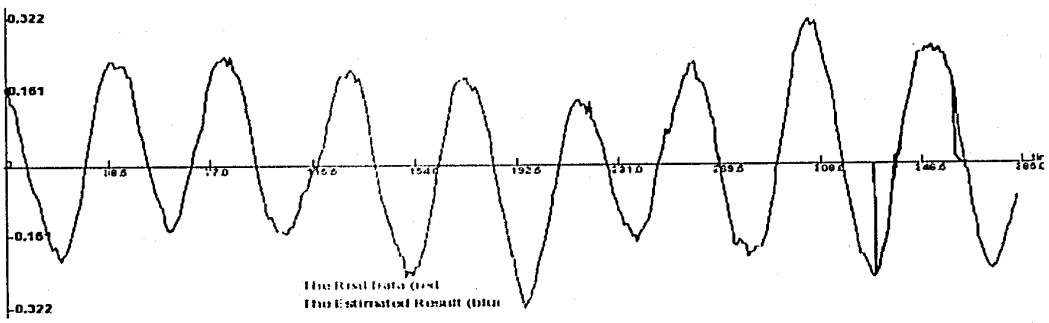

Figure 3-10 (l). Quadrature Components on 6th path

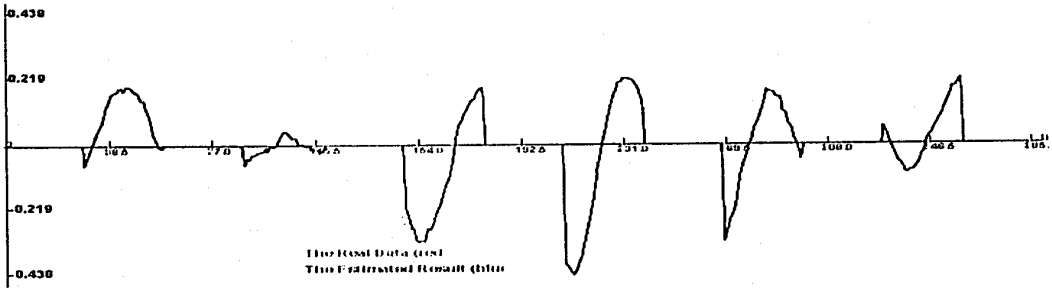

Figure 3-10 (m). the Output Sequences $y(t)$ vs. $\hat{y}(t)$

Figure 3-10. the Estimated Results for Frequency-selective Fading Channel (N=6 case) On the Wide Band Transmitted Signal

(2) Narrow Band Transmitted Signal

Considered the transmitted signal is a narrow band signal, the estimated system parameters are computed as following:

$$\hat{A} = \begin{bmatrix} \hat{A}_1 & 0 & \cdots & 0 \\ 0 & \hat{A}_2 & \cdots & 0 \\ \vdots & \vdots & \vdots & 0 \\ 0 & 0 & \cdots & \hat{A}_6 \end{bmatrix}, \quad \hat{BB}^T = \begin{bmatrix} \hat{BB}_1^T & 0 & \cdots & 0 \\ 0 & \hat{BB}_2^T & \cdots & 0 \\ \vdots & \vdots & \cdots & 0 \\ 0 & 0 & \cdots & \hat{BB}_6^T \end{bmatrix},$$

$$\hat{C} = \begin{bmatrix} \hat{C}_1 & \hat{C}_2 & \cdots & \hat{C}_6 \end{bmatrix}, \quad \hat{DD}^T = 0.0023$$

Here, $\left\{ \hat{A}_i, \hat{BB}_i^T, \hat{C}_i \right\}$ are defined as the following:

$$\hat{A}_1 = \begin{bmatrix} 0 & 1 & 0 & 0 \\ 0.1829 & -0.0652 & 0 & 0 \\ 0 & 0 & 0 & 1 \\ 0 & 0 & 0.1484 & -0.0966 \end{bmatrix}, \quad \hat{A}_2 = \begin{bmatrix} 0 & 1 & 0 & 0 \\ 0.1968 & 0.0556 & 0 & 0 \\ 0 & 0 & 0 & 1 \\ 0 & 0 & -0.1569 & 0.0564 \end{bmatrix}$$

$$\hat{A}_3 = \begin{bmatrix} 0 & 1 & 0 & 0 \\ 0.1903 & -0.0598 & 0 & 0 \\ 0 & 0 & 0 & 1 \\ 0 & 0 & 0.1806 & -0.2572 \end{bmatrix}, \quad \hat{A}_4 = \begin{bmatrix} 0 & 1 & 0 & 0 \\ 0.2921 & 0.0566 & 0 & 0 \\ 0 & 0 & 0 & 1 \\ 0 & 0 & 0.3575 & -0.0693 \end{bmatrix}$$

$$\hat{A}_5 = \begin{bmatrix} 0 & 1 & 0 & 0 \\ 0.2023 & -0.0594 & 0 & 0 \\ 0 & 0 & 0 & 1 \\ 0 & 0 & 0.1881 & -0.2669 \end{bmatrix}, \quad \hat{A}_6 = \begin{bmatrix} 0 & 1 & 0 & 0 \\ 0.2960 & 0.0693 & 0 & 0 \\ 0 & 0 & 0 & 1 \\ 0 & 0 & 0.3734 & -0.0804 \end{bmatrix}$$

$$\hat{BB}_1^T = \begin{bmatrix} 0.0795 & 0.0056 & 0.0157 & 0.0043 \\ 0.0056 & 0.1632 & 0.0218 & -0.0256 \\ 0.0157 & 0.0218 & 0.0824 & 0.0076 \\ 0.0043 & -0.0256 & 0.0076 & 0.2597 \end{bmatrix}, \quad \hat{BB}_2^T = \begin{bmatrix} 0.2540 & 0.0017 & 0.0006 & 0.0062 \\ 0.0017 & 0.2298 & 0.0182 & -0.0033 \\ 0.0006 & 0.0182 & 0.1429 & 0.0077 \\ 0.0062 & -0.0033 & 0.0077 & 0.0722 \end{bmatrix}$$

$$\hat{BB}_3^T = \begin{bmatrix} 0.1638 & 0.0115 & 0.0094 & 0.0004 \\ 0.0115 & 0.2329 & 0.0077 & -0.0107 \\ 0.0094 & 0.0077 & 0.1541 & 0.0192 \\ 0.0004 & -0.0107 & 0.0192 & 0.1547 \end{bmatrix}, \quad \hat{BB}_4^T = \begin{bmatrix} 0.2561 & 0.0013 & 0.0077 & -0.0134 \\ 0.0013 & 0.0921 & 0.0254 & 0.0015 \\ 0.0077 & 0.0254 & 0.2959 & 0.0056 \\ -0.0134 & 0.0015 & 0.0056 & 0.2969 \end{bmatrix}$$

$$\hat{BB}_5^T = \begin{bmatrix} 0.1699 & 0.0129 & 0.0122 & 0.0009 \\ 0.0129 & 0.2451 & 0.0087 & -0.0103 \\ 0.0122 & 0.0087 & 0.1628 & 0.0213 \\ 0.0009 & -0.0103 & 0.0213 & 0.1637 \end{bmatrix}, \quad \hat{BB}_6^T = \begin{bmatrix} 0.2871 & 0.0004 & 0.0044 & -0.0181 \\ 0.0004 & 0.0961 & 0.0287 & -0.0004 \\ 0.0044 & 0.0287 & 0.3310 & 0.0069 \\ -0.0181 & -0.0004 & 0.0069 & 0.3334 \end{bmatrix}$$

$$\hat{C}_1 = \hat{C}_2 = \hat{C}_3 = \hat{C}_4 = \hat{C}_5 = \hat{C}_6 = \begin{bmatrix} 1 & 0 & 1 & 0 \end{bmatrix}$$

Figure 3-11 shows the compared results between the measurement data and the estimated results on each path.

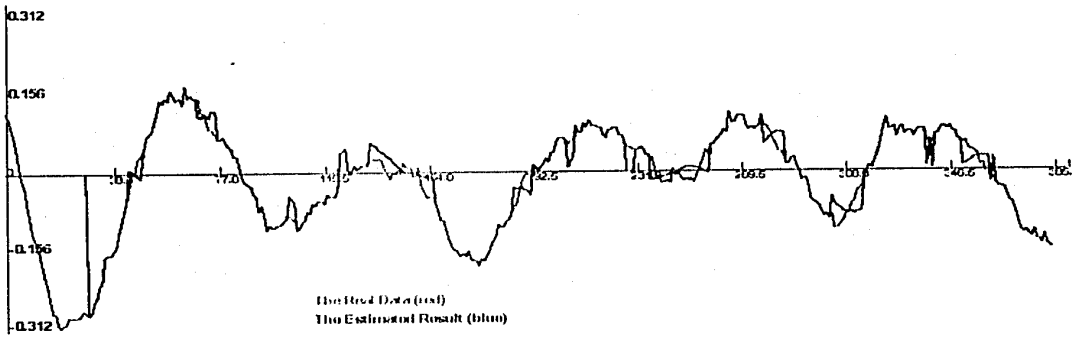

Figure 3-11 (a). Inphase Components on 1st path

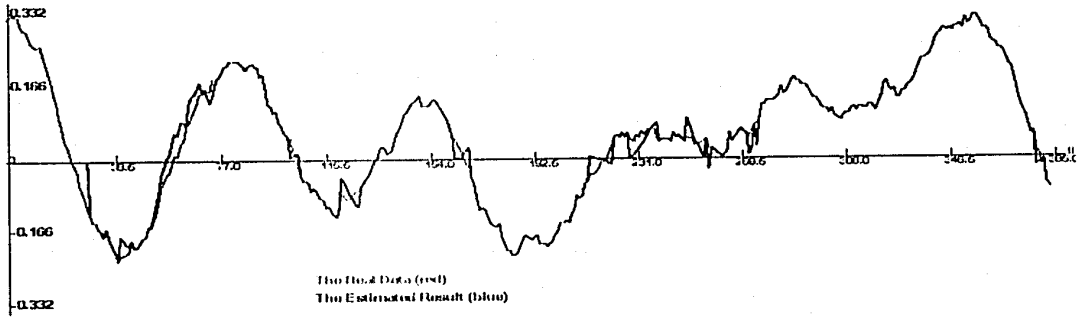

Figure 3-11 (b). Quadrature Components on 1st path

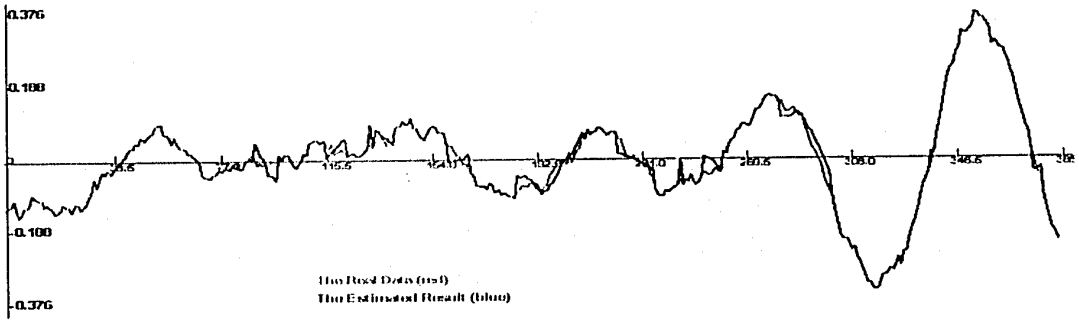

Figure 3-11 (c). Inphase Components on 2nd path

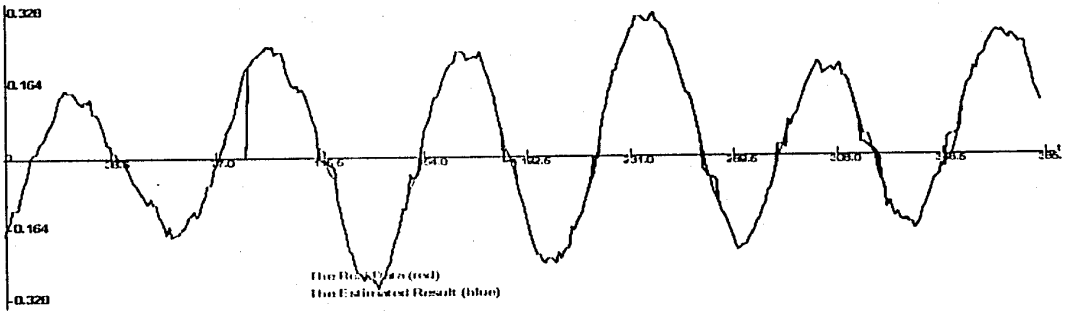

Figure 3-11 (d). Quadrature Components on 2nd path

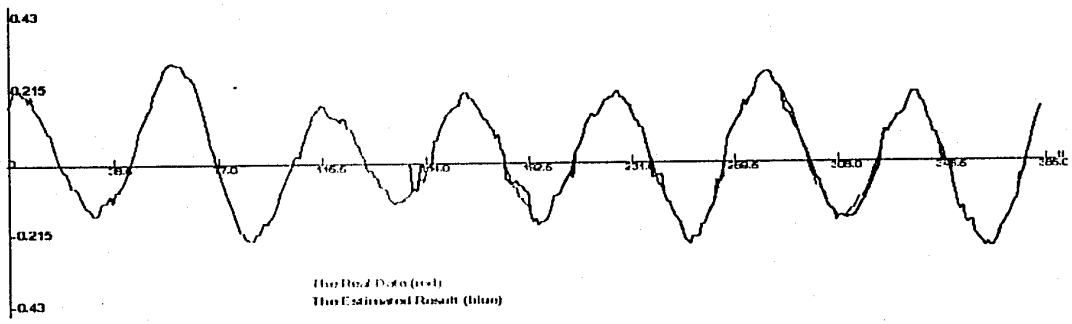

Figure 3-11 (e). Inphase Components on 3rd path

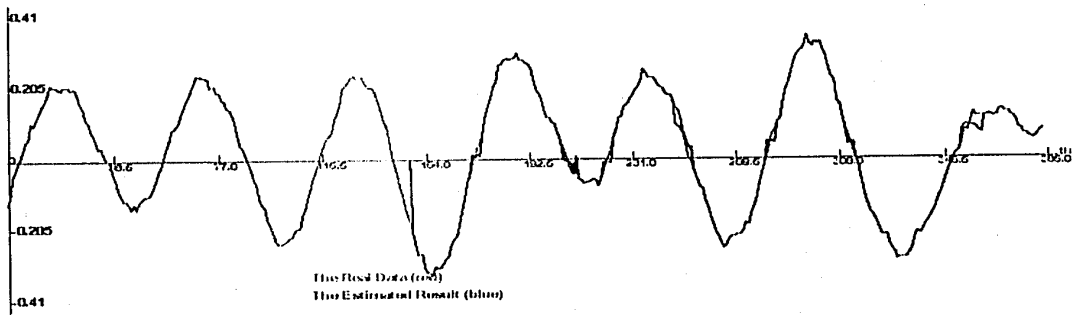

Figure 3-11 (f). Quadrature Components on 3rd path

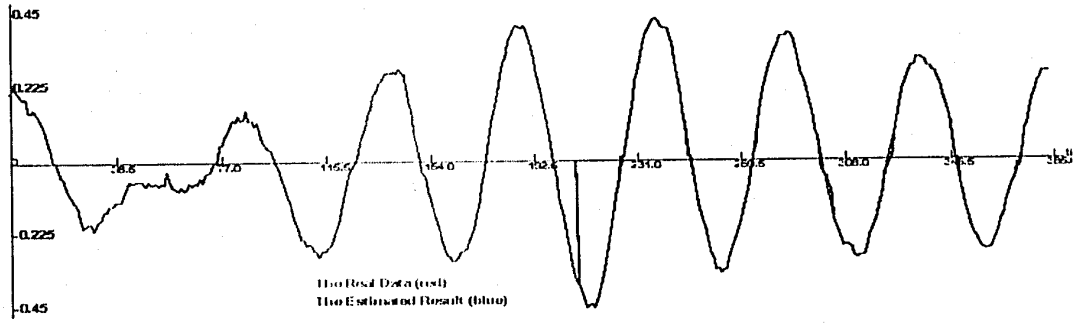

Figure 3-11 (g). Inphase Components on 4th path

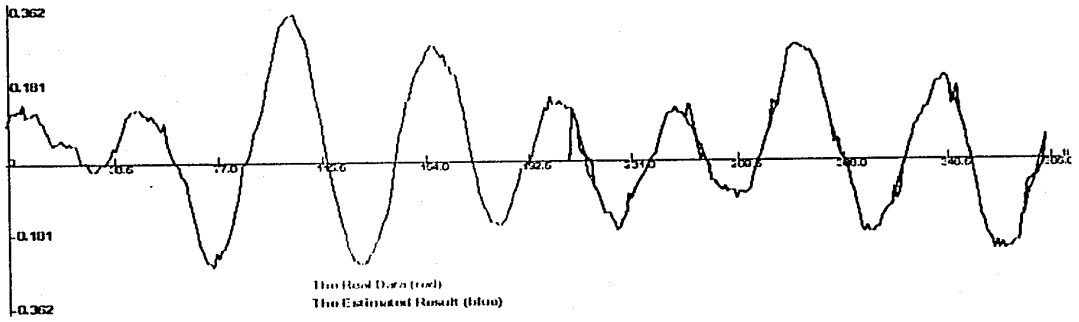

Figure 3-11 (h). Quadrature Components on 4th path

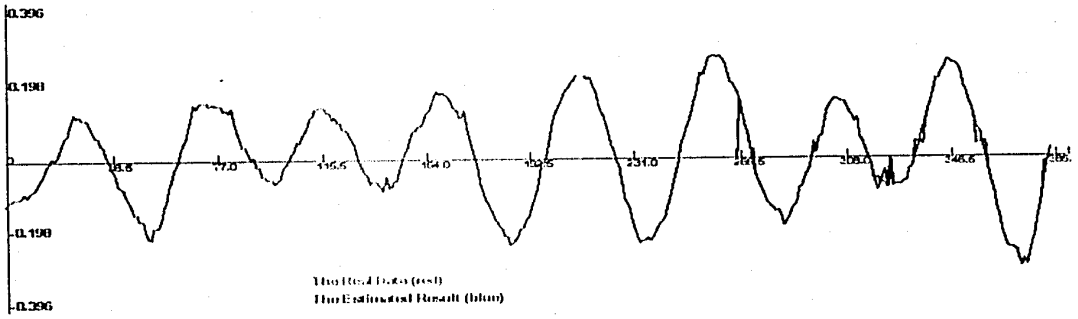

Figure 3-11 (i). Inphase Components on 5th path

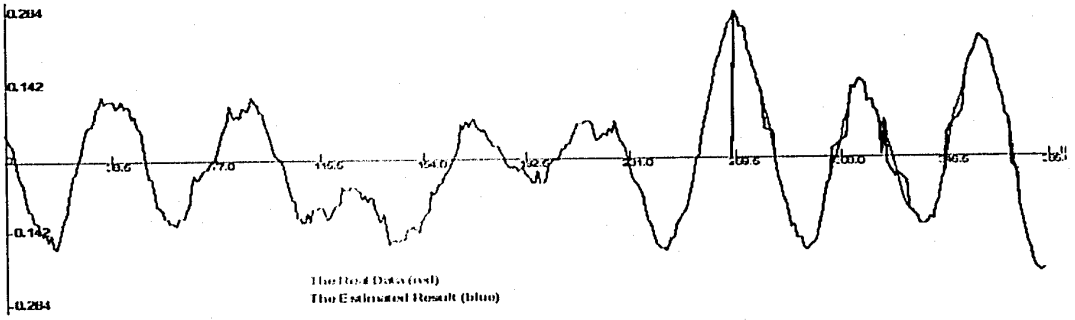

Figure 3-11 (j). Quadrature Components on 5th path

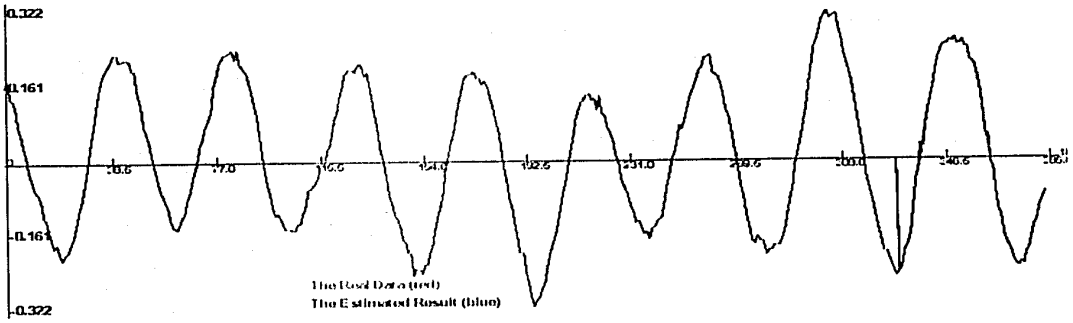

Figure 3-11 (k). Inphase Components on 6th path

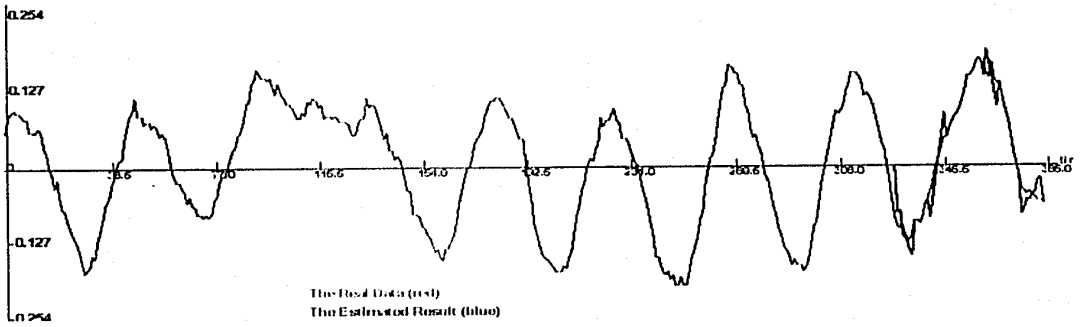

Figure 3-11 (l). Quadrature Components on 6th path

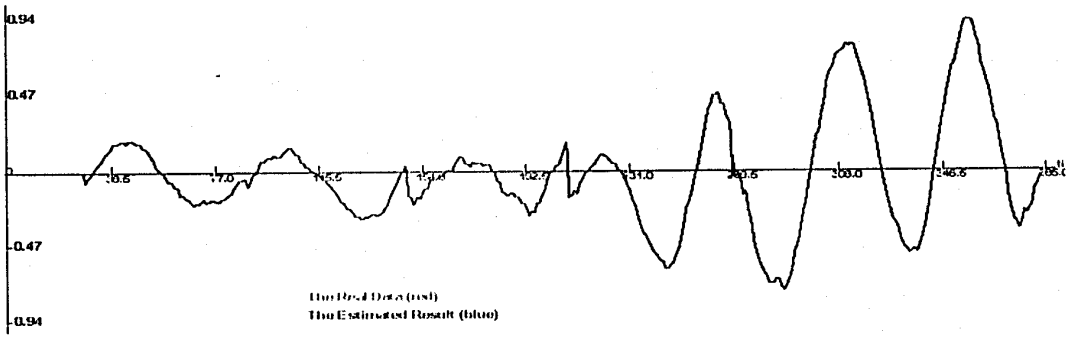

Figure 3-11 (m). the Output Sequences $y(t)$ vs. $\hat{y}(t)$

Figure 3-11. the Estimated Results for Frequency-selective Fading Channel (N=6 case) On the Narrow Band Transmitted Signal

(3) Slow Fading with Narrow Band Transmitted Signal

The estimated system parameters of the frequency-selective slow fading are computed as following:

$$\hat{A} = \begin{bmatrix} \hat{A}_1 & 0 & \cdots & 0 \\ 0 & \hat{A}_2 & \cdots & 0 \\ \vdots & \vdots & \vdots & 0 \\ 0 & 0 & \cdots & \hat{A}_6 \end{bmatrix}, \quad \hat{BB^T} = \begin{bmatrix} \hat{BB_1^T} & 0 & \cdots & 0 \\ 0 & \hat{BB_2^T} & \cdots & 0 \\ \vdots & \vdots & \cdots & 0 \\ 0 & 0 & \cdots & \hat{BB_6^T} \end{bmatrix},$$

$$\hat{C} = \begin{bmatrix} \hat{C}_1 & \hat{C}_2 & \cdots & \hat{C}_6 \end{bmatrix}, \qquad \hat{DD^T} = 0.0023$$

Here, $\left\{ \hat{A}_i, \hat{BB_i}^T, \hat{C}_i \right\}$ are defined as the following:

$$\hat{A}_1 = \begin{bmatrix} 0 & 1 & 0 & 0 \\ 0.2104 & -0.0228 & 0 & 0 \\ 0 & 0 & 0 & 1 \\ 0 & 0 & 0.1789 & -0.1458 \end{bmatrix}, \quad \hat{A}_2 = \begin{bmatrix} 0 & 1 & 0 & 0 \\ 0.0811 & 0.0325 & 0 & 0 \\ 0 & 0 & 0 & 1 \\ 0 & 0 & -0.1409 & 0.0419 \end{bmatrix}$$

$$\hat{A}_3 = \begin{bmatrix} 0 & 1 & 0 & 0 \\ 0.2084 & -0.0242 & 0 & 0 \\ 0 & 0 & 0 & 1 \\ 0 & 0 & 0.2013 & -0.3022 \end{bmatrix}, \quad \hat{A}_4 = \begin{bmatrix} 0 & 1 & 0 & 0 \\ 0.3034 & 0.0736 & 0 & 0 \\ 0 & 0 & 0 & 1 \\ 0 & 0 & 0.3814 & -0.0954 \end{bmatrix}$$

$$\hat{A}_5 = \begin{bmatrix} 0 & 1 & 0 & 0 \\ 0.2084 & -0.0242 & 0 & 0 \\ 0 & 0 & 0 & 1 \\ 0 & 0 & 0.2013 & -0.3022 \end{bmatrix}, \quad \hat{A}_6 = \begin{bmatrix} 0 & 1 & 0 & 0 \\ 0.3038 & 0.0849 & 0 & 0 \\ 0 & 0 & 0 & 1 \\ 0 & 0 & 0.3801 & -0.0972 \end{bmatrix}$$

$$\hat{BB}_1^T = \begin{bmatrix} 0.0745 & 0.0141 & 0.0213 & 0.0154 \\ 0.0141 & 0.1823 & 0.0305 & 0.0003 \\ 0.0213 & 0.0305 & 0.0823 & 0.0139 \\ 0.0154 & 0.0003 & 0.0139 & 0.3121 \end{bmatrix}, \quad \hat{BB}_2^T = \begin{bmatrix} 1.6505 & 0.0414 & -0.2051 & -0.0342 \\ 0.0414 & 0.3151 & 0.0334 & -0.0096 \\ -0.2051 & 0.0334 & 0.1746 & 0.0278 \\ -0.0342 & -0.0096 & 0.0278 & 0.0881 \end{bmatrix}$$

$$\hat{BB}_3^T = \begin{bmatrix} 0.1809 & 0.0253 & 0.0186 & 0.0048 \\ 0.0253 & 0.2876 & 0.0178 & -0.0054 \\ 0.0186 & 0.0178 & 0.1862 & 0.0342 \\ 0.0048 & -0.0054 & 0.0342 & 0.1964 \end{bmatrix}, \quad \hat{BB}_4^T = \begin{bmatrix} 0.2830 & 0.0031 & 0.0108 & 0.0019 \\ 0.0031 & 0.0971 & 0.0403 & 0.0077 \\ 0.0108 & 0.0403 & 0.3797 & 0.0087 \\ 0.0019 & 0.0077 & 0.0087 & 0.3845 \end{bmatrix}$$

$$\hat{BB}_5^T = \begin{bmatrix} 0.1809 & 0.0253 & 0.0186 & 0.0048 \\ 0.0253 & 0.2876 & 0.0178 & -0.0054 \\ 0.0186 & 0.0178 & 0.1862 & 0.0342 \\ 0.0048 & -0.0054 & 0.0342 & 0.1965 \end{bmatrix}, \quad \hat{BB}_6^T = \begin{bmatrix} 0.2827 & 0.0010 & 0.0128 & 0.0024 \\ 0.0010 & 0.0973 & 0.0402 & 0.0070 \\ 0.0128 & 0.0402 & 0.3795 & 0.0083 \\ 0.0024 & 0.0070 & 0.0083 & 0.3839 \end{bmatrix}$$

$$\hat{C}_1 = \hat{C}_2 = \hat{C}_3 = \hat{C}_4 = \hat{C}_5 = \hat{C}_6 = \begin{bmatrix} 1 & 0 & 1 & 0 \end{bmatrix}$$

Figure 3-12 shows the compared results between the measurement data and the estimated results on each path for the frequency-selective slow fading.

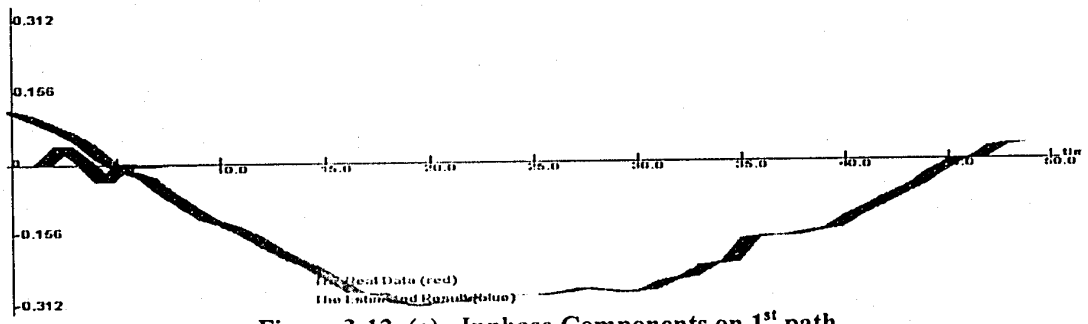

Figure 3-12 (a). Inphase Components on 1st path

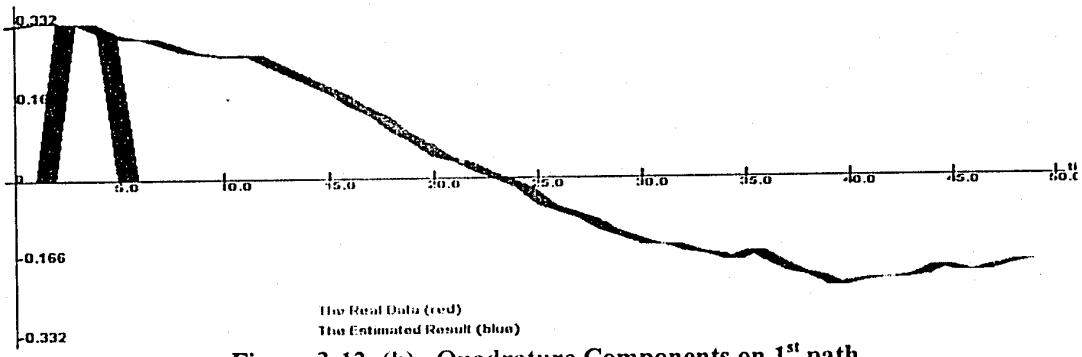

Figure 3-12 (b). Quadrature Components on 1st path

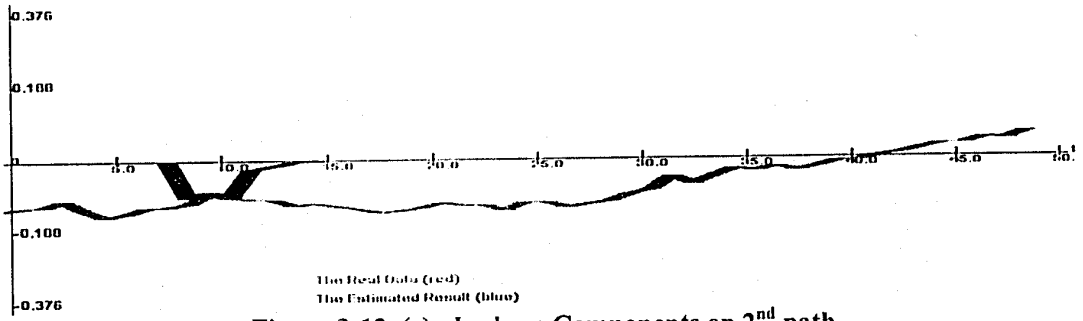

Figure 3-12 (c). Inphase Components on 2nd path

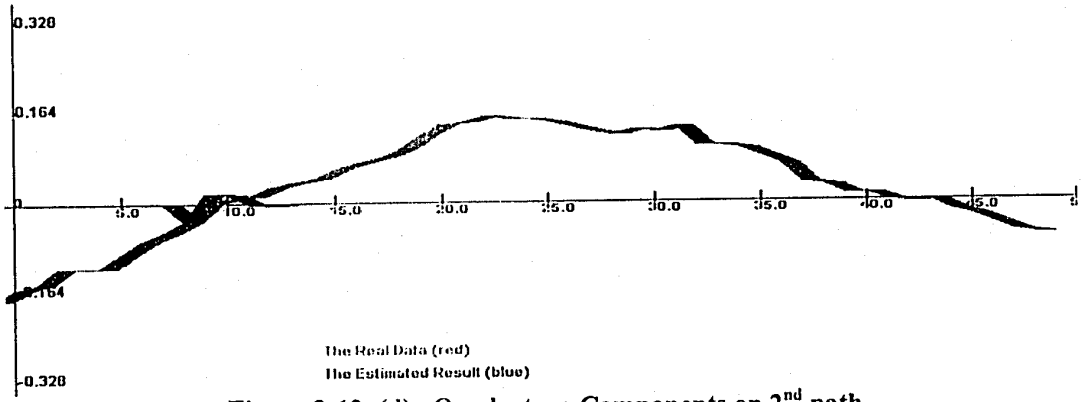

Figure 3-12 (d). Quadrature Components on 2nd path

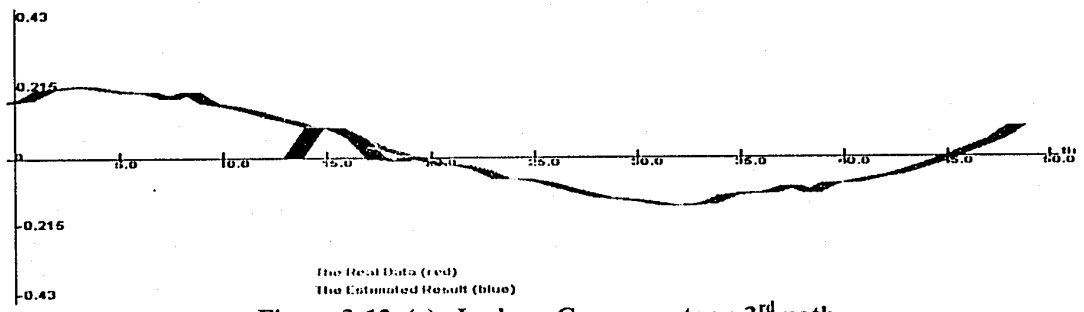

Figure 3-12 (e). Inphase Components on 3rd path

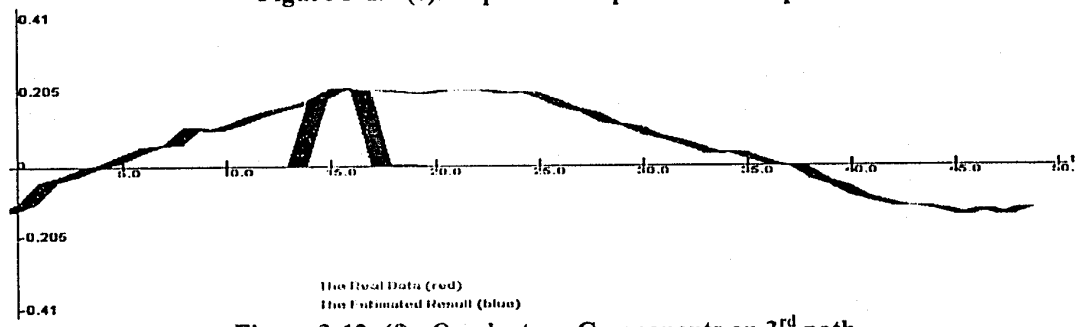

Figure 3-12 (f). Quadrature Components on 3rd path

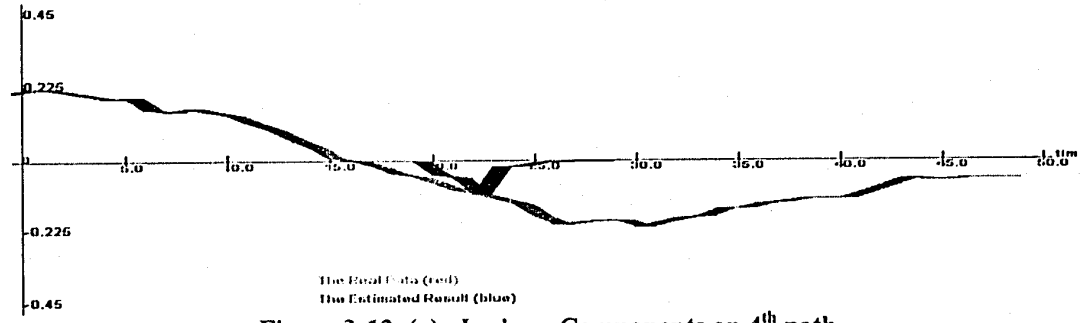

Figure 3-12 (g). Inphase Components on 4th path

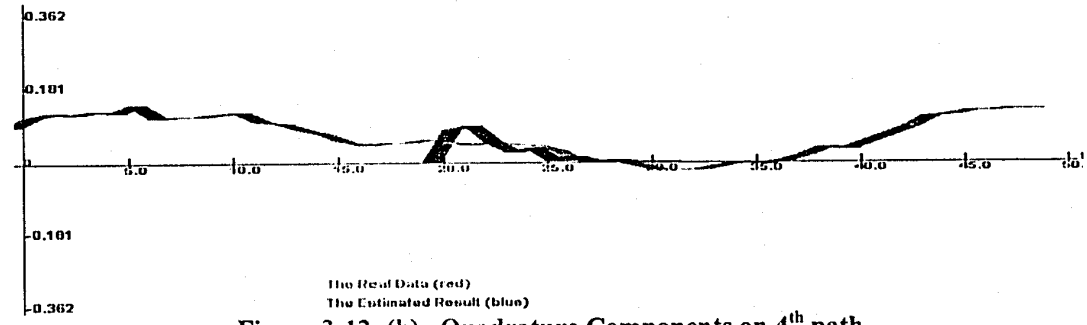

Figure 3-12 (h). Quadrature Components on 4th path

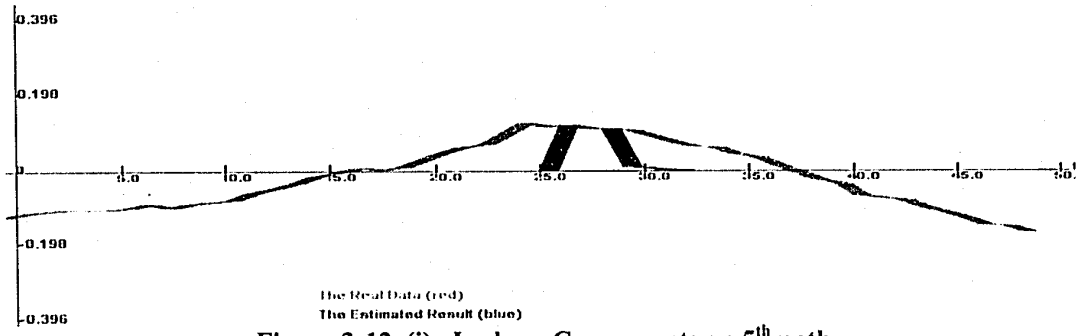

Figure 3-12 (i) . Inphase Components on 5th path

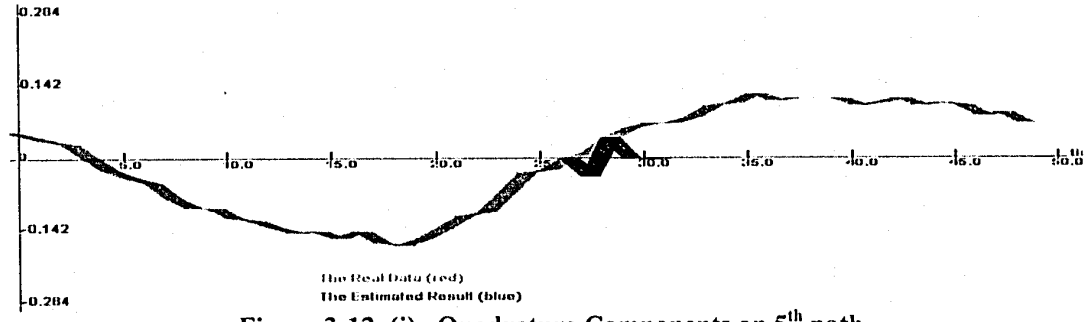

Figure 3-12 (j). Quadrature Components on 5th path

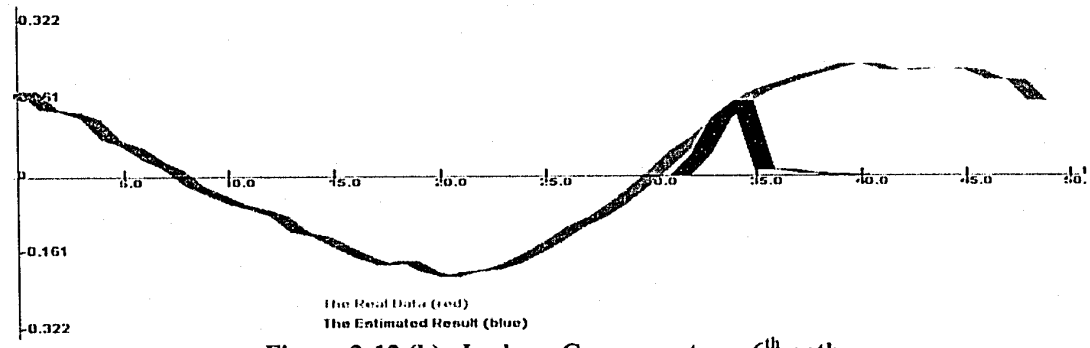

Figure 3-12 (k). Inphase Components on 6th path

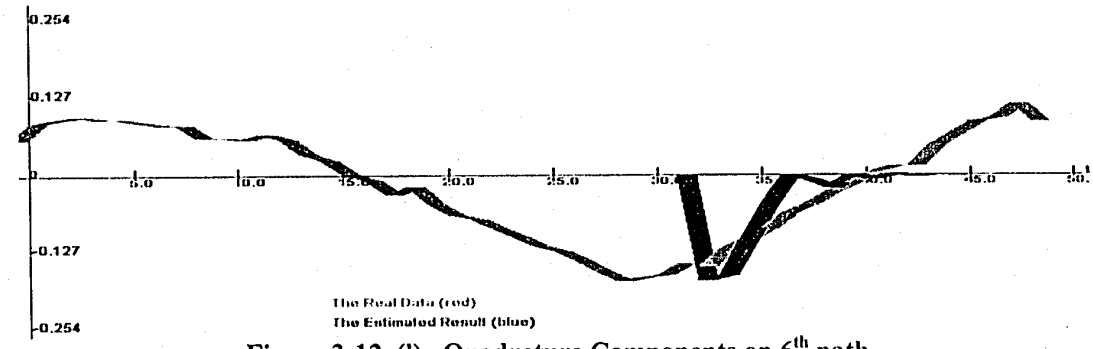

Figure 3-12 (l). Quadrature Components on 6th path

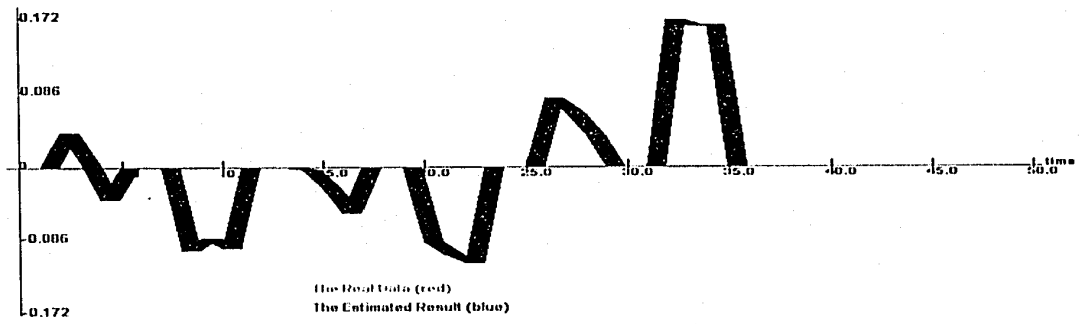

Figure 3-12 (m). the Output Sequences $y(t)$ vs. $\hat{y}(t)$

Figure 3-12. the Estimated Results for Frequency-selective Slow Fading Channel (N=6 case)

The estimated results for the flat and frequency-selective fading models based on the measurement data are also indicated the state space models, the EM algorithm and the Kalman filter are good matched the real fading channel environment.

Chapter Summary

System identification is a process of constructing a mathematical model for a dynamic system from observations and prior knowledge.

The Expectation Maximization (EM) algorithm uses a bank of Kalman filters to yield maximum-likelihood parameter estimation of the state space model.

Based on measurement data models, the system identification is considered for the flat fading channel and frequency-selective fading channel.

The system parameters of flat fading channels are identified with the different order's models. The system parameters of frequency-selective fading channels are identified with the different total numbers of the multipath (N=2, 3, 4, 5, 6, 7) and the different transmitted signals (narrowband and wideband).

The estimated results are very well matched to the measurement data provided by CRC. Therefore, this means that the EM algorithm is a very effect method in system identification of fading channels.

Chapter 4

Web-based System Analysis, Design and Implementation

Various estimated results, based on several computation tools such as Matlab™, have been presented in the fading channel models and system identification. However, these computations did not provide web-based tools. Therefore, one of the thesis's aims is to develop a web-based system, called *the web-based fading channel simulation and estimation system* (WFSE) system, to model, simulate, estimate and identify the characteristics of the fading channel using the state space models and the EM algorithm presented in Chapter 2 and Chapter 3. The WFSE system is a web-based application and is implemented using Java ™ techniques.

Based on the software development process and *Unified Modeling Language*™ (UML) techniques [COO91, SAT00], this chapter will present analysis, design and implementation for the WFSE system. Section 4.1 introduces basic concepts, advantages and technologies of web applications; Section 4.2 analyzes the WFSE system's requirements including functional and non-functional requirements; Section 4.3 presents system analysis and design using UML techniques including user case diagrams, sequence diagrams and class diagrams; Section 4.4 describes software implementation with Java techniques such as Java Applet, Java Graphics2D, Java Swing, Java Input/Output and Exception handling.

4.1 Basic Concepts of Web Application

A web application is a computer program that is accessed via a web interface. Web applications have been become an important part of the modern technologies. This section introduces concept, advantages and technologies of web applications

Web applications are evolved from websites or web systems. A web-based application should contain three principal components: a web server, a network connection, and one or more client browsers. The web server is used to distribute pages of formatted information to clients that request it, and these pages implement the system requirements. The request is made over a network connection and uses the HTTP protocol; and users interact with a website via browsers [HAE00].

Web applications have more advantages than desktop applications. For example, web applications can be accessed from anywhere that has a web connection and can be easily expanded and revised at any time.

Web technologies, particularly the Internet, have become an important part of the business world over the past few years. Web browsers are a standard way of accessing the vast amount of information available through the Internet. Server-side programming is to develop Web applications. Several server-side technologies exist today such as *Common Gateway Interface* (CGI), *Active Server Pages* (ASP), Java Applet, Java Servlets and *Java Server Pages* (JSP) [SUNWB].

Java has become the dominant web programming language due to its complete class library and easy to use syntax.

The process for creating, deploying, and executing a Web application can be summarized as follows [SUNWB]:

- Develop the Web component code
- Build the Web application components along with any static resources and helper classes referenced by the component
- Install or deploy the application into a Web container
- Access a URL that references the Web application

4.2 System Requirements

A requirement model expresses a behavior or a property that the system should have [CON99]. The requirements can be categorized as functional or nonfunctional requirements. The functional requirements declare an action that the system should perform. The nonfunctional requirements make the system easier to understand and track [CHE01].

The section analyzes the WFSE system requirements for the fading channel simulation and estimation.

4.2.1 Functional Requirements

The functional requirements of the WFSE system should complete the following main functions:

- To provide different fading channel models.

These fading channel models are based on the state space models; and these models include the flat fading (the Rayleigh and Ricean fading) and the frequency-selective fading.

- To generate and estimate the inphase, quadrature and envelope components.

The inphase, quadrature and envelope components of the received signal are generated using the state space models. In the same way, the inphase, quadrature and envelope components of the received signal are estimated using the Kalman filters.

- To identify system parameters based on the measurement data.

Based on the measurement data, the system identification of the fading channel is estimated through the EM algorithm together with the Kalman filter.

- To analyze the Doppler Power Spectral Density (DPSD).

The DPSD of the fading channel is analyzed with respect to the motion of the receiver or the transmitter. In addition, the DPSD is also computed in system identification based on the measurement data.

- To plot all of computation results.

All of the computation results are necessary to display. These figures can be printed and resized by enlarging or reducing.

- To provide an online help tool

An online help tool provides solutions for common problems in running the WFSE system.

4.2.2 System Non-Functional Requirements

The nonfunctional requirements of the WFSE system should be usability, performance, robustness or reliability, security, efficiency, maintainability and deployment. In the other hand, the system should have user-interface friendly, simple operations and can be easy understood.

4.3 System Analysis and Design

System analysis is a process of examining system requirements and building a conceptual model. The elements of system analysis include user case diagrams, sequence diagrams, state diagrams and activity diagrams. On the other hand, system design is a process of making analysis model to be realizable in software. Its tasks are to define system architecture, build user interface prototypes and make object-oriented designs [CON99].

This section introduces basic concepts of object-oriented programming and UML designs, and presents the user case diagram, the sequence diagrams and the class diagram of the WFSE system.

4.3.1 Concepts of Object-Oriented Programming and UML Design

The Object-oriented concept has been widely applied to system analysis, design and implementation. An object is a key to understand object-oriented. Objects are like real-world entities that they have attributes and behaviors. A software object maintains its

attributes with variables and implements its behavior with methods [SUNBA]. For instance, an object of the fading channel model can be defined by the variables such as the carried frequency, the mobile speed, the SNR, the spatial angle and an interval time. Additionally, many methods can be implemented by the object such as the computation of the Kalman filters, plot computation results, etc. Figure 4-1 is an example of a fading channel model's object.

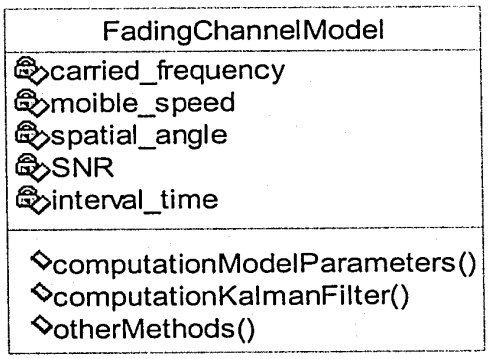

Figure 4-1. An Example of Defining an Object

Object-oriented programming (OOP) was designed to simplify the process of building complex real-world applications. It addresses application's issues by the object, and these objects are grouped into classes. A class describes the structure and properties of an object. OOP is easier to read, understand, correct, modify and reuse than the traditional structural programs [FOW99, STA00].

UML is an industrial standard visual modeling language for specifying, visualizing, constructing and documenting the artifacts of a software system. UML is used to understand, design, browse, configure, maintain, and control information about software system [RUM98]. UML is a user-case driven, and it focuses on development activities of models. In addition, UML also takes an iterative approach to the software development life cycle and embeds object-oriented techniques [HAR018].

4.3.2 User Case Diagram

User cases present the system functional requirements from the actor's view. A user case diagram considers a system as a black box; in addition, it describes the interactions

between the actors and the system, and covers all behaviors and exceptional conditions together with the desired response [SAT00].

Figure 4-2 indicates the user case diagram of the WFSE system. These user cases will be described as the following.

(1) *FCEstimation* User Case

The *FCEstimation* user case is used to analyze the characteristics of the fading channel related to the motion of mobiles; the system parameters can be computed through several physical factors. This user case includes two extend user cases: *FadingChanEstimation* and *DPSDAnalysis*.

Further, the *FadingChanEstimation* user case is employed to simulate and estimate the inphase, uuadrature and envelope components of the received signal of the fading channel with the known system parameters; this user case also includes three extend user cases for the fading channel models, such as the flat fading (the Rayleigh and Ricean fading) and frequency-selective fading.

The *DPSDAnalysis* user case is applied to compute the Doppler Power Spectral Density (DPSD) of the fading channel models.

(2) *SIVerification* User Case

The *SIVerification* user case is used to verify the EM algorithm and the Kalman filters in system identification. This user case includes two extend user cases: *SystemIdentificationVerfication* and *KalmanFilterVerification*.

The *SystemIdentificationVerfication* user case is applied to verify the EM algorithm through comparing the identified system parameters with the given system parameters.

The *KalmanFilterVerification* user case is applied to verify the Kalman filter via comparing the output sequences. One output sequence is computed through the Kalman filters and the identified system parameters; the other output sequence is obtained using the state space model and the given system parameters.

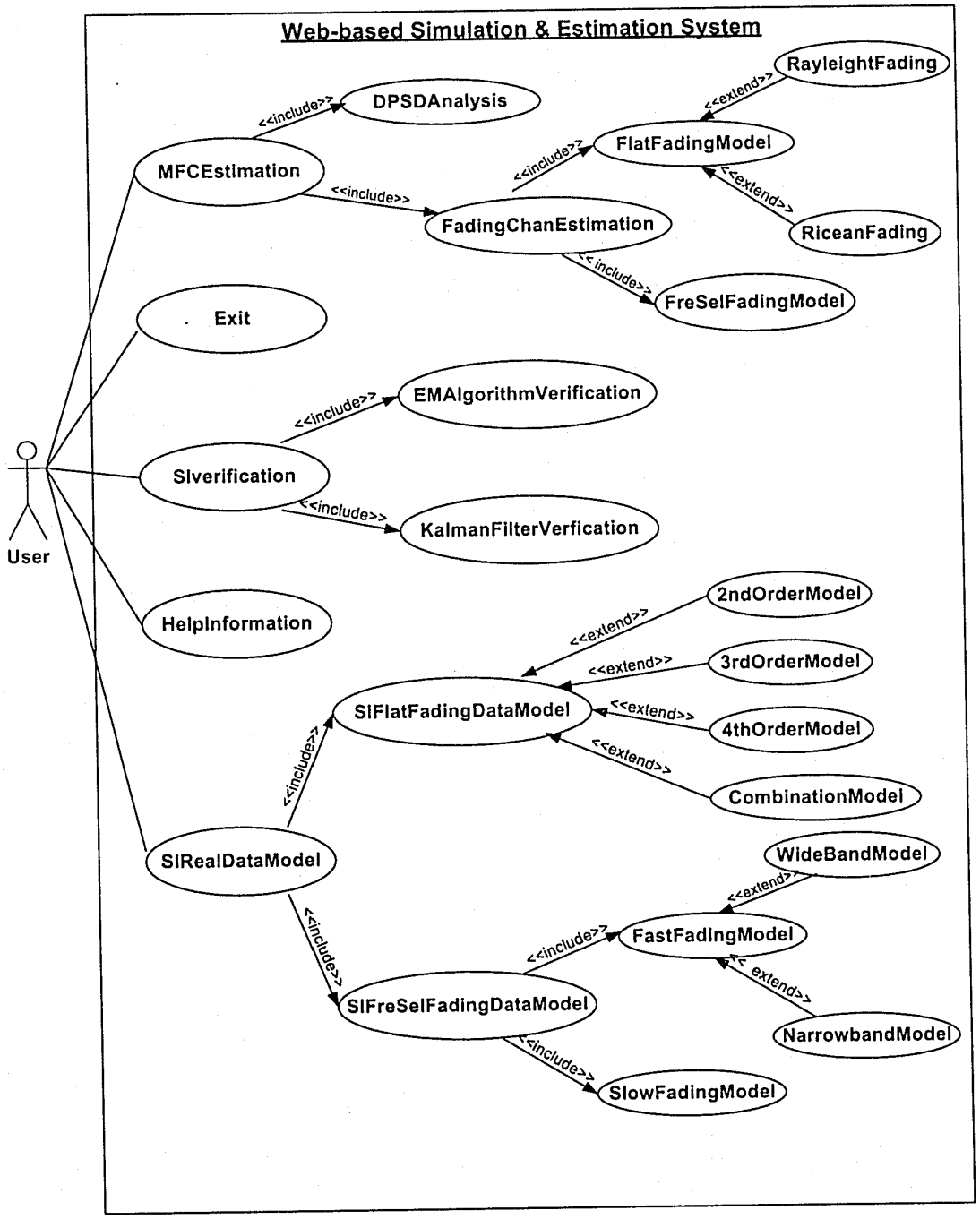

Figure 4-2. the User Case Diagram

(3) *SIRealDataModel* User Case

The *SIRealDataModel* user case is used to identify system parameters via the EM algorithm based on the measurement data models. The models include the flat fading channel and the frequency-selective fading channel. Therefore, this user case also includes two extend user cases: *FlatFadingDataModel* and *FreSelFadingDataModel*.

The *FlatFadingDataModel* user case is used to identify system parameters for the flat fading channel. In this case, a set of the measurement data can be identified with the different model's orders.

The *FreSelFadingDataModel* user case is employed to identify system parameters for the frequency-selective fading channel. A set of the measurement data can be identified with the different total numbers of multipath. In addition, the frequency-selective fading channel can be considered as the fast fading and the slow fading channel. Furthermore, the transmitted signal can be classified as the narrowband signal and the wideband signal. Therefore, this user case contains three extend user cases: *SlowFadingModel*, *NarrowbandModel* and *WidebandModel*.

(4) *HelpInformation* User Case

The *HelpInformation* user case is employed to list the common questions and their solutions about the WFSE system. For example, there are some questions such as how to enter values of the physical factors, how to run this system, how to select a real data file from the measurement data list, how to understand computation results, and so on.

(5) Exit User Case

The *Exit* user case is used to exit the WFSE system and close the current window.

4.3.3 Sequence Diagrams

Sequence diagrams are commonly used for both analysis and design purposes, and they model the flow of logic within a system in a visual manner. Additionally, sequence diagrams are the most popular UML artifact for dynamic modeling, which focuses on identifying the behavior within a system. The sequence diagrams describe how objects

interact over the course of time through an exchange of messages. A single sequence diagram often represents the flow of events for a single user case [RUM98].

The following sequence diagrams present the time component of interactions between the entities of the system for the main user cases described in Subsection 4.3.2.

Figure 4-3 is a sequence diagram of the *FadingChanEstimation* user case. It describes the simulation and estimation process of the fading channel with known system parameters.

Figure 4-4 is a sequence diagram of the *SystemIdentificationVerification* user case. It presents the verification process of system identification using the EM algorithm.

Figure 4-5 is a sequence diagram of the *FlatFadingDataModel* user case. It addresses the estimation process of system identification for the flat fading based on the measurement data models.

Figure 4-6 is a sequence diagram of the *FreSelFadingDataModel* user case. It addresses the estimation process of system identification for the frequency-selective fading based on the measurement data models.

4.3.4 Class Diagram

Class diagrams are the mainstay of object-oriented analysis and design. Class diagrams are used for a wide variety of purposes, including both conceptual/domain modeling and detailed design modeling [RUM98]. A class diagram describes the classes of the system, their interrelationships, and the operations and attributes of the classes [SAT00]. These classes of the WFSE system can be categorized as five types: *Graphics User Interface* (GUI) classes, computation classes, input/output operations classes, plotting results classes and exception classes.

Figure 4-7 shows the class diagram of the WFSE system.

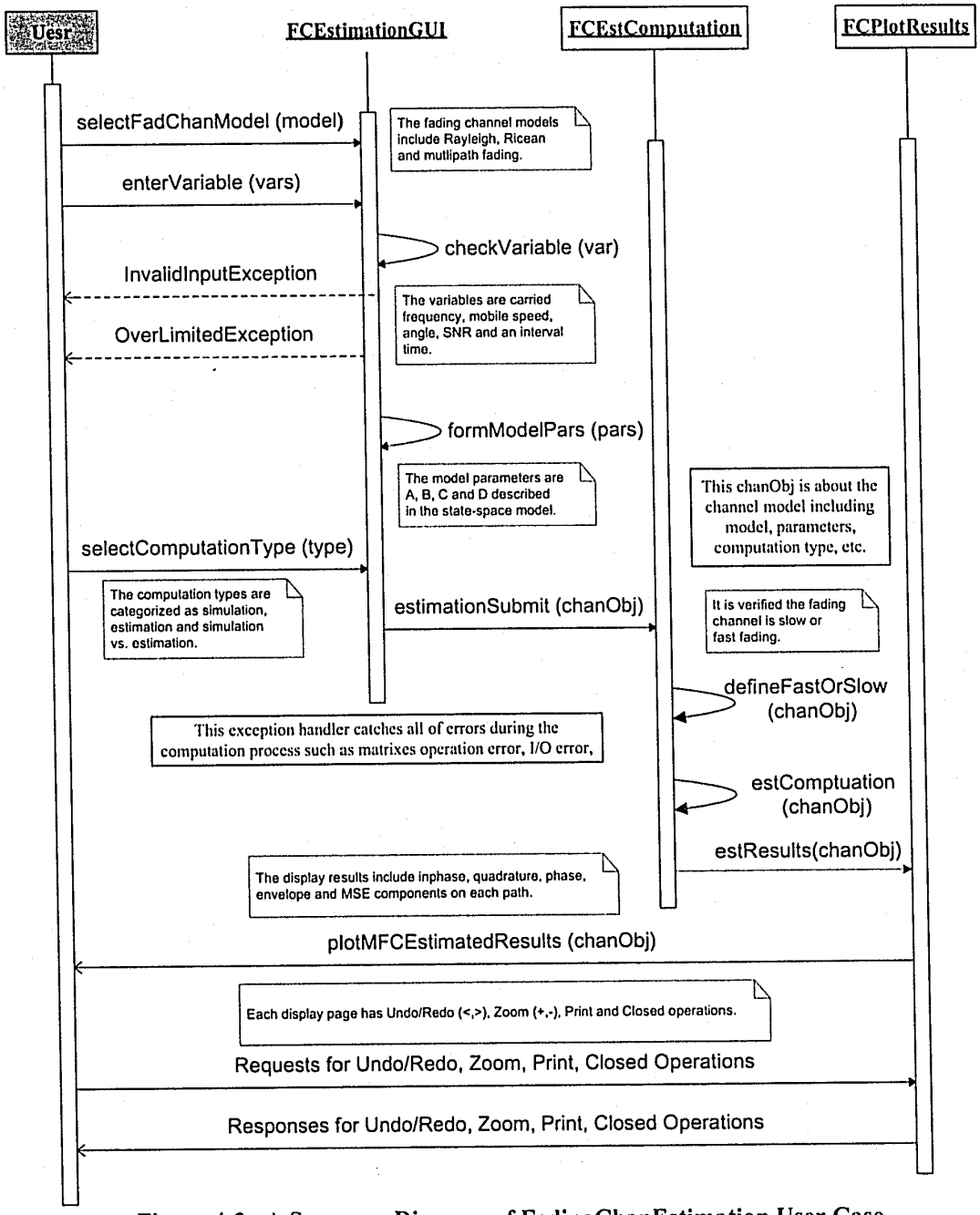

Figure 4-3. A Sequence Diagram of FadingChanEstimation User Case

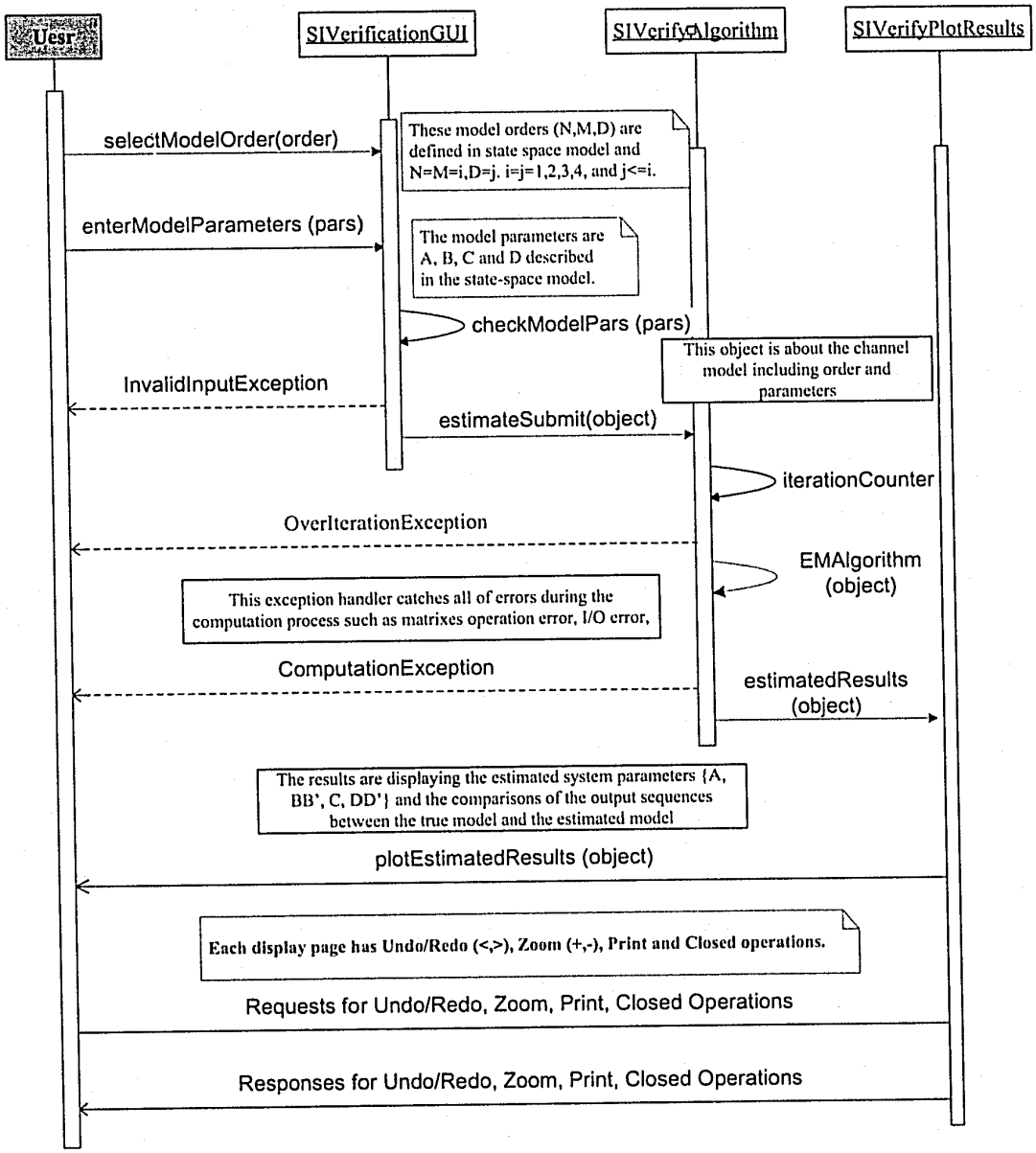

Figure 4-4. A Sequence Diagram of System Identification Verification User Case

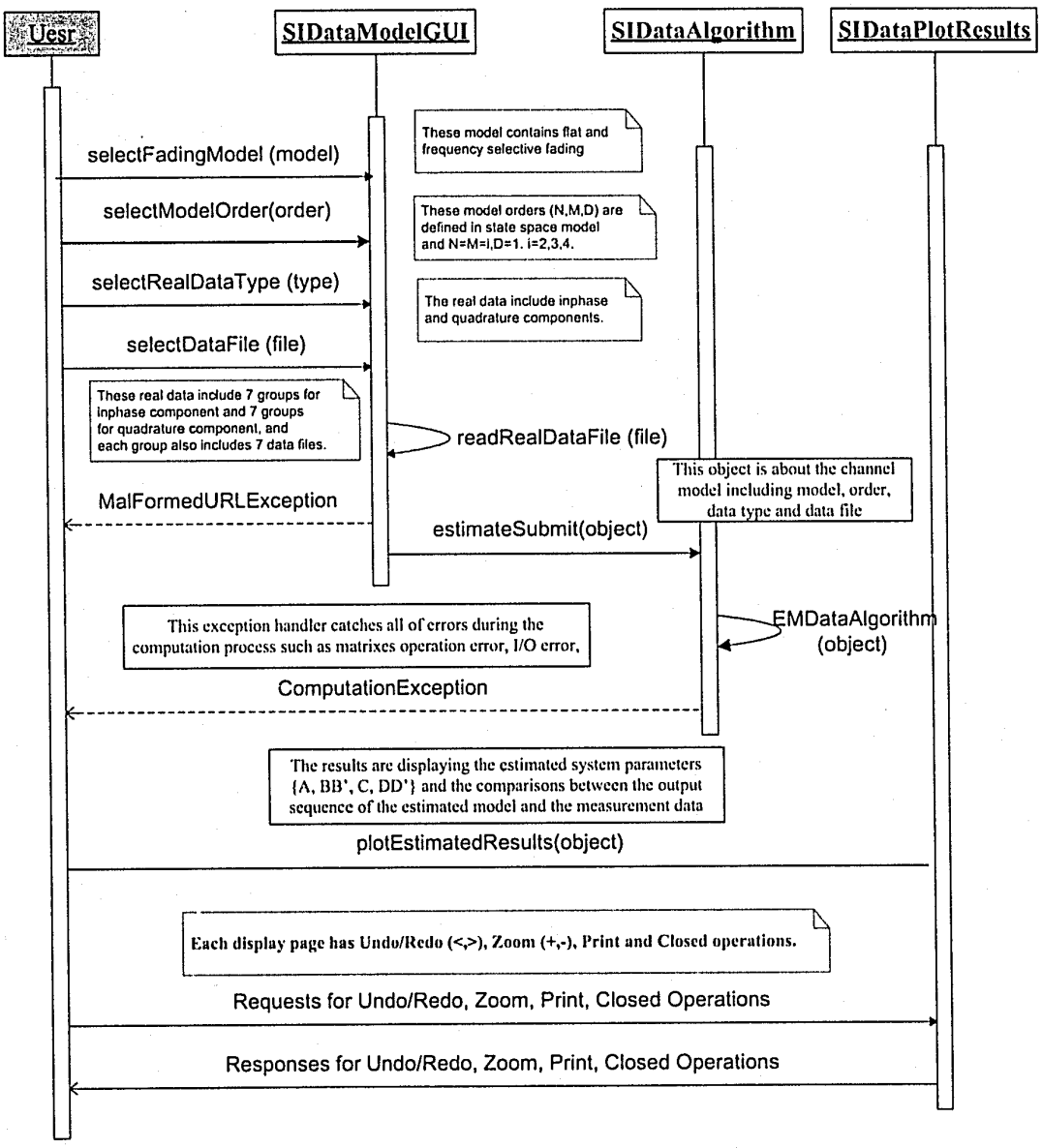

Figure 4-5 A Sequence Diagram of System Identification for the Flat Fading Based on Real Data Model User Case

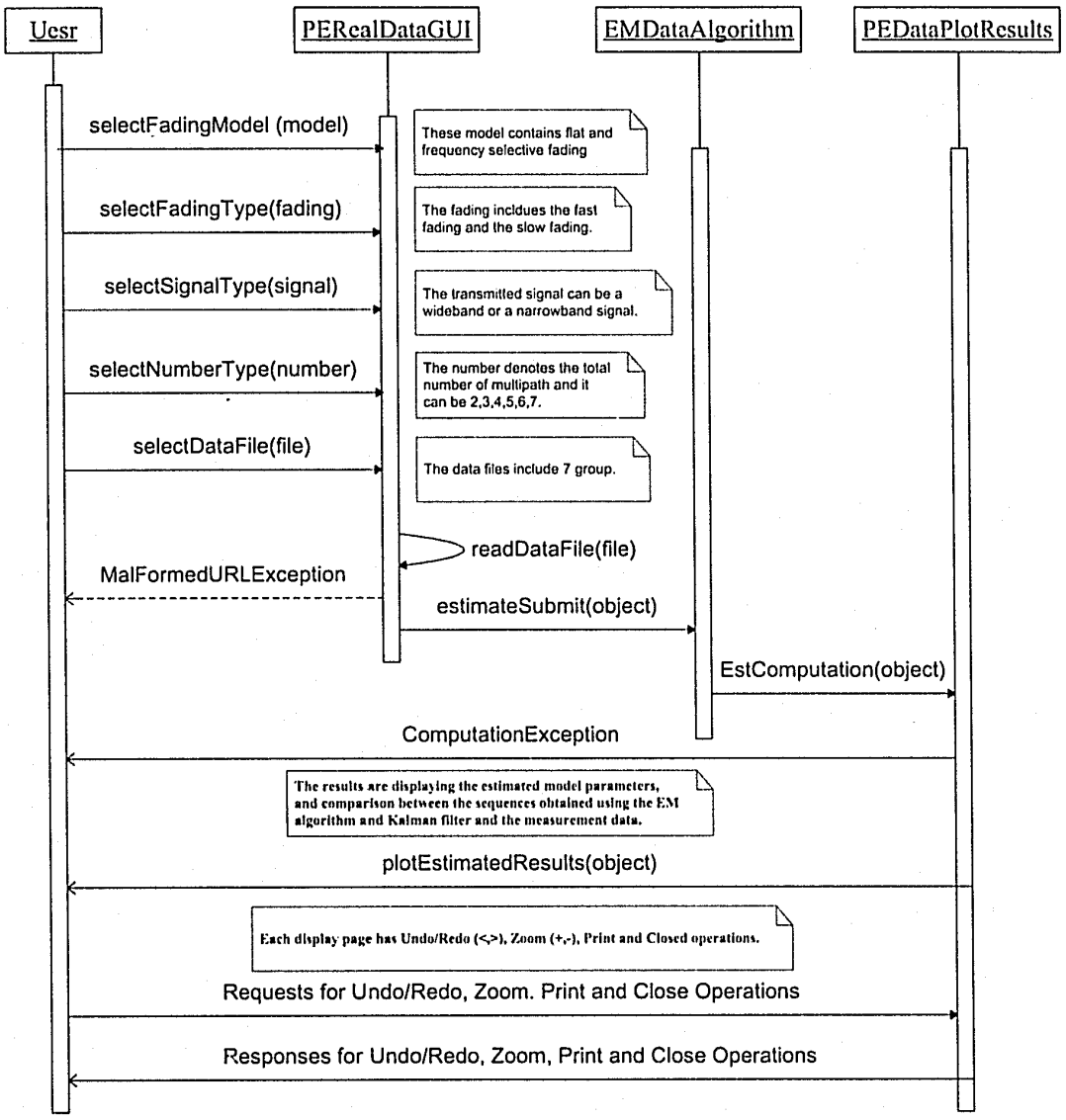

Figure 4-6 A Sequence Diagram of System Identification for the Flat Fading Based on Real Data Model User Case

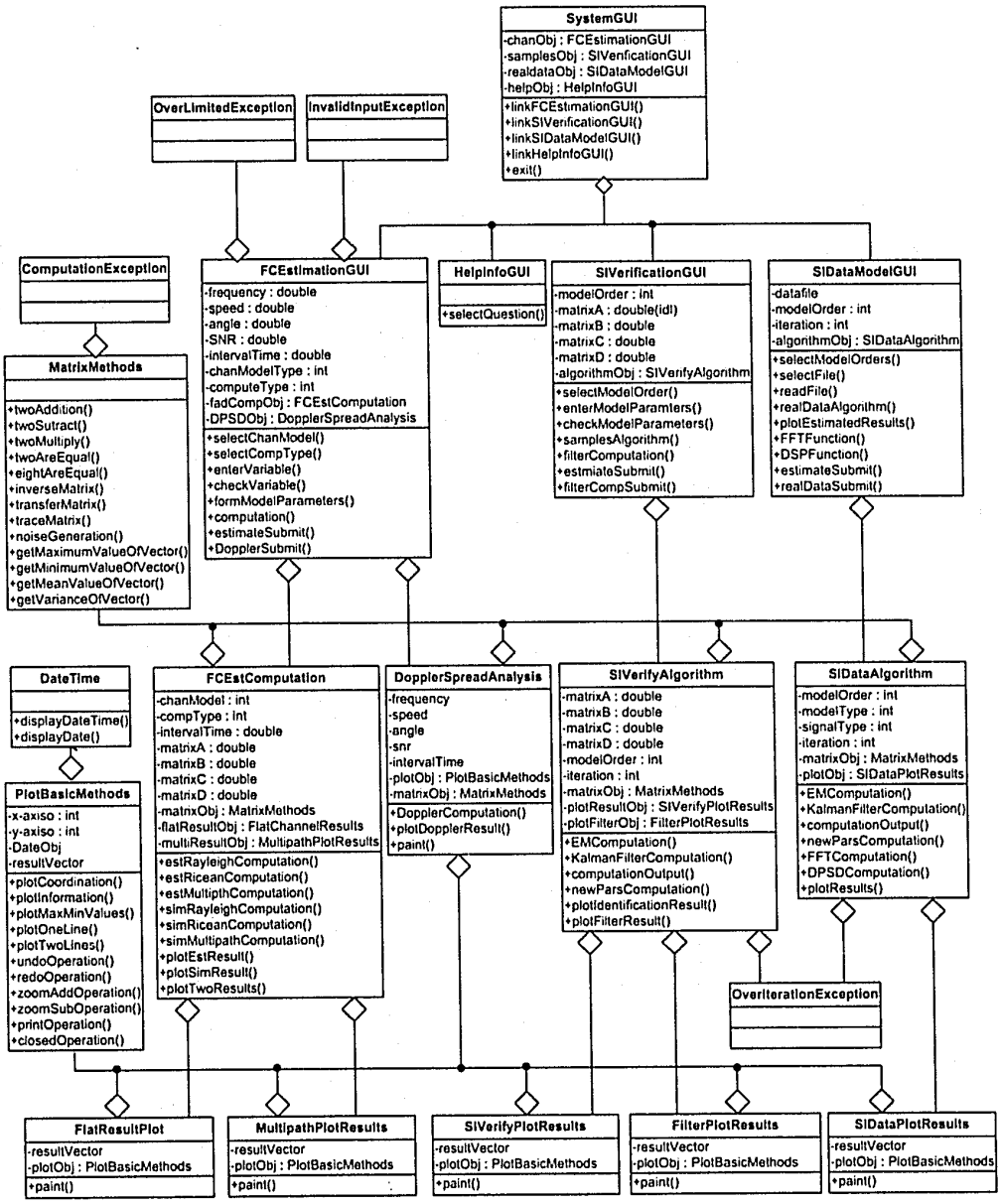

Figure 4-7 the Class Diagram

(1) GUI Classes

The GUI classes define human-machine interfaces in order to communicate information between users and system through the input/output operations. These GUIs are designed to make easily accessible the most used functionality.

The WFSE system includes a system GUI and three subsystem GUIs. The system GUI defines the WFSE system structure and integrates these four subsystems: the fading channel simulation and estimation subsystem (*FCEstimation Subsystem*), the system identification for verifying subsystem (*SIVerfication Subsystem*), the system identification for the measurement data subsystem (*SIRealDataModel Subsystem*), and the help information subsystem (*HelpInfo Subsystem*).

The *FCEstimationGUI* class is an interface for the fading channel simulation and estimation related to the motion of the receiver or the transmitter.

The *SIVerficationGUI* class is an interface for verifying system identification using the EM algorithm. It is implemented through users setting system parameters.

The *SIRealDataModelGUI* class is an interface for system identification based the measurement data.

The *HelpInfoGUI* class is an interface providing helping information for users. The information is applied to solve several common problems.

(2) Computation Classes

The WFSE system defines many computation classes and implements various computation methods based on matrix operations. The matrix operations are also implemented including addition, subtraction, multiplication, inversion, transformation, and so on..

(3) Input/Output and Read Files Operation Class

The WFSE system defines several input/output operations. The input operations include entering values of the system variables, selecting an operation such as a type of the fading channel model or a data file, reading a data file and pushing a submit button.

In addition, these input operations throw exception when the operation contains errors. The output operations are used to display error warnings and other information.

The read files operation is used to read data files from the web servers.

(4) Plot Results Classes

The WFSE system defines the drawing graphics classes. These drawing classes are used to plot computation results as curves and related information as strings. For example, the *PlotFlatFadingResults* class is employed to display the simulated and estimated results for the flat fading channel model, and the *PlotFreSelFadingResults* class is employed to plot the simulated and estimated results for the frequency-selective fading channel.

(5) Exception Classes

The exception classes are to control the flows of a software system and manage software risks. The WFSE system predefines several types of exception classes such as *ComputationException*, *InputInvalidException*, *OverLimitedValueException* and *OverIterationException*.

The *ComputationException* class is called when the computation process include error operations. For instance, two matrixes having different row or column are operated in the addition or subtraction.

The *InputInvalidException* class handles an error when inputting a non-digital or dot (.) letter.

The *OverLimitedValueException* class is used to handle an error when inputting value is over the limited value. For example, if the input value is larger than the set maximum value or less then the set minimum value, then the inputting value is considered as over limited, and the *OverLimitedValueException* will occur.

The *OverIterationException* class will handle an error when the iteration of the computation times is over the given value in the EM algorithm.

In addition, Java provides many kinds of exception classes in the class libraries; for example, an *I/O exception*, a *MarFormedException*, and so on.

4.4 Software Implementation using Java ™

The task of software implementation is used to map the artifacts of analysis and design into executable codes. This section introduces Java architecture and presents Java techniques that are used in the WFSE system including Java Applet and Java Plug-in, Java Swing, Java Graphics 2D, Java I/O file and Java Exception handler.

4.4.1 Java ™ Architecture

Java was designed by Sun Microsystem® in order to create reliable network applications and to run securely over a network. Java is a simple, object oriented, distributed, interpreted, portable, robust, secure, architecture neutral, multithreaded, platform independence, high performance and dynamic programming language [GIL97]. Java has been widely applied to business applications, server and client applications, and n-tier applications.

Java can work on a wide range of platforms. The Java's platform independence is one of the significant advantages over other programming languages because it introduced *Java Visual Machine* (JVM). The JVM is the component of the technology responsible for hardware independence and operating system independence [HAE00]. The JVM is an abstract machine that may be thinking as a translator between Java codes and computers. The JVM avoids both the binary distribution problem and the version problem. Furthermore, the JVM also allows a Java applet to run on any operating systems and anywhere in the network [SMI98].

The *Java Development Kit* (JDK) is an original Java development environment. The JDK contains libraries of standard classes for building, testing and documenting Java programs; it also can create and display full graphics applications. There are many Java *Integrated Development Environments* (IDEs) such as JBuilder, Visual J++, VisualAge, Java Studio and Java Work Shop. In this thesis, all Java programs are edited, compiled, debugged, and run on JBuilder version7 developed by Borland® Inc. The JBuilder is the leading, cross-platform environment for building industrial-strength enterprise Java applications [BORBD].

4.4.2 Java Applet and Plug-in

Java web application technologies include Applets, Servlet, JavaServerPages (JSP) and JavaBeans. However, Java Applet has been widely used in web applications, since it can provide more complex user interfaces than Servlet or JSP.

The Java Applet is applied for the WFSE system. This subsection introduces basic concept and applications of Java Applet and Java Plug-in technology.

(1) Java Applet

Java program contains *Applets* and *Applications*. Java Applications are installed on the user's machine and can access to all system resources. Java Applets are stored on an Internet or intranet server, and they are referenced with web pages using <applet> and </applet> tags in *Hypertext Markup Language* (HTML).

Figure 4-8, adapted from [VAN96], shows how Java Applets work on the Internet.

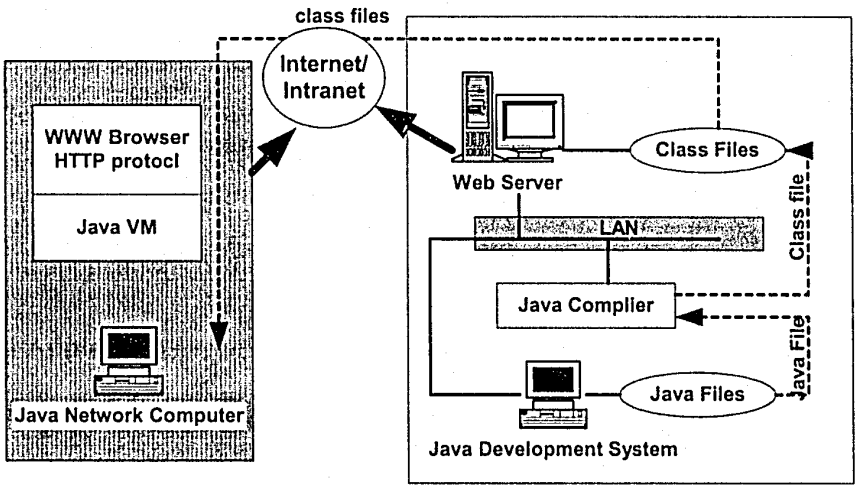

Figure 4-8. The Java System Flow Diagram

Java developers write Java Applet source codes with Java files. The class files are generated after compiling these Java files and stored on the web server. Java Applets are downloaded to multiple client platforms where they are run in the JVM provided by the browser on the client machine. When the browser encounters a web page with an applet, it starts the JVM and provides it with the information located in the <applet> tag. The

class loader inside the JVM looks to see which classes are needed for this applet. As part of the class loading process, the class files are run through a verifier which makes sure they are valid class files. Once verified, the applet runs [VAN96].

The advantages of Java Applets include the following aspects. Firstly, Java Applet can transform the web pages into programs interacting with messages. Secondly, Java Applets can be downloaded and run on client sides, thus web server does not need to support Java. This can be important for developers if they are writing a web application but they do not have control over the web server. Furthermore, Java Applets executive environments provide a high level of security [JAW02, SMI98].

The main disadvantage is that Java Applets are restricted writing operations in any file system on the server [JAW02].

(2) Java Plug-in and Java Applet Security

A common problem of Java Applets is that the JDK version mismatch between Java Applets and the web browser running them. Java Plug-in is the best solution of this problem [SUNPL].

Java Plug-in was designed for enterprise customers to deploy *Java 2 SDK Standard Edition* (J2SE). Java Plug-in extends functionalities of a web browser and allows Java applets to be run under *Java 2 runtime environment* (JRE). When a browser comes across a web page that requires the use of Java Plug-in, it checks to see if Java Plug-in has been installed on the same machine as the browser. If it has not, the browser must download and install the required files [SMI98].

Java Plug-in can work with different browsers in different ways. Each browser approaches Java Plug-in implementation differently. In general, Java Plug-in provides support for *Internet Explorer* and *Netscape Navigator.*

Java plug-in supports the security model of J2SE. All Java Applets run in the standard applet security manager: *java.lang.SecurityManager*. This *SecurityManager* class provides different security environments in different JVM. Java Plug-in also supports *HTTPS*, a secure version of *HyperText Transfer Protocol* (HTTP).

(3) Java Applet Implemented with HTML

Java Applet can run on web pages by different browsers and operating systems. Figure 4-9 is the basic *HyperText Markup Language* (HTML) code for the Java Applet in two browsers: *Internet Explorer* and *Netscape Navigator.*

The different browsers use different HTML tags to execute the Java Applet. The *Internet Explorer* browser uses the <OBJECT> tag, and the *Netscape Navigator* uses the <EMBED> tag in the HTML specification [SUNPL].

```
<! Internet Explorer -->
<OBJECT OBJECT classid="clsid:8AD9C840-044E-11D1-B3E9-00805F499D93"
<! -- define width and height for Java Applet -->
width = "850" height="400" align="baseline"
codebase=" http://java.sun.com/products/plugin/index.html ">
<PARAM NAME="code"    VALUE = "UserInterfaces.class">
<PARAM NAME="codebase" VALUE = "SimulationSystem/">
<COMMENT>
< ! -- Netscape Communicator -->
<EMBED type = "application/x-java-applet;version=1.3"
width = "850" height="400" align="baseline"
code = "UserInterfaces.class"
codebase ="SimulationSystem/"
pluginspage="http://java.sun.com/products/plugin/index.html ">
<NOEMBED>
No Java 2 SDK, Standard Edition v 1.4 support for Applet!
</NOEMBED>
</EMBED>
</OBJECT>
```

Figure 4-9. Java Applet with HTML using IE and Netscape browsers

Table 4-1 lists Java Plug-in supported operating systems and browsers, adapted from [SUNPL].

Table 4-1 Java Plug-in Supported Operating Systems and Browsers

	Supported
Operating Systems	Windows 98SE, ME, NT 4.0 (SP6), 2000 (SP2), and XP; Solaris 7, 8 and 9; Linux 6.0 or later.
Browsers	Internet Explorer 4 (SP2), 5.01 (SP2), 5.5 (SP2), 6 Netscape 4.5, 4.6, 4.7, 4.77, 6.2.1 and higher

4.4.3 Graphical User Interface (GUI)

As previously mentioned, *Graphical User Interface* (GUI) is designed to communicate information in two ways between the systems and the users. Java GUI is supported by *Java Foundation Classes* (JFC) which is a set of Java class libraries.

Java *Swing* is a set of lightweight GUI component toolkit. Java Swing has several benefits for Java programmers. Firstly, Java Swing can expand and simplify deployment of Java applications via providing a component set of GUI elements. Secondly, Java Swing can be run in any browser that has the appropriate version of Java Plug-in. Furthermore, Java Swing also permits a customizable look and feel without relying on any specific windowing system [SUNSW].

Appendix C introduces these GUIs of the WFSE system. These GUIs are implemented using Java Swing components such as frame, menu, toolbar, dialog, combo box, scroll pane, button, list, label, table, text, and color.

Java GUI programming is more complex than ordinary applications programming because GUI programming is driven by an event. Each event is represented by an object that gives information about the event and identifies the event source. Event sources are typically components, but other kinds of objects can also be event sources [GIL97]. Figure 4-10 is an example of defining and implementing an event handler.

```
// to declare a event handler class
public class MyButtonClass implements ActionListener {
      // to register the event handler
     myButtonComponent.addActionListener(instanceOfMyButtonClass);
      // to implement the event's action
     public void actionPerformed(ActionEvent e) {
          //code that reacts to the action...
     }
}
```

Figure 4-10. An example of Implementing an Event Handler

This example indicates that every event handler requires three bits of code. The code is to declare the event handler class implementing a listener interface; to register an instance of the event handler class as a listener component; and to implement the methods in the listener interface [SUNSW].

4.4.4 Java 2D API

Java 2D API enhances the graphics, text and imaging capabilities of Java Swing. Java Graphics2D class offers a unified interface for rendering any kind of device making the API device independent [SUN2D]. The WFSE system is implemented Java Graphics2D methods for displaying 2D coordinate systems and the computation results.

(1) Coordinate System

Java 2D API contains two coordinate systems: *User space* and *Device space.*

The user space is a device-independent and logical coordinate system; in addition, it represents a uniform abstraction of all possible device coordinate systems. The device space is a device-dependent coordinate system and it varies according to the targeting rendering device.

Java 2D API automatically performs necessary conversions between the user space and the device space of the targeting rendering device through a unified coordinate transformation model represented by AffineTransform objects [SUN2D]. The AffineTransform class defines the rules for manipulating coordinates using matrices. The

class can be used in the graphics context to rotate, scale, translate, or shear a geometric shape, text, or image when it is rendered.

Figure 4-11 is an example of a coordinate system conversion by implementing an AffineTransform object.

```
public void coordinationSystemConversion (Graphics2D g2, int width, int height,
        int setDataSize, int realDataSize, double zoom)  {
    // define an AffineTransform object and scale
    AffineTransform atObject = new AffineTransform( );
    double scale = (double)setdatasize/(double)realDataSize;
    // set Translation scope of the user space
    atObject.setToTranslation(width, height);
    // set the value of scale with x-axis and y-axis
    atObject.setToScale(scale*zoom, zoom);
    // set new screen's size with zooming
    setSize ( zoom*width, zoom*height);
    //graphics drawing
    g2.transform(atObject);
}
```

Figure 4-11. An example of Implementing an AffineTransform Object

This *coordinationSystemConversion* method can complete conversion between the device space and the user space and can enlarge or reduce the displaying arrange with a given zoom value. For example, if the device space is set to 1000, and if the user space is set 200 or 20000, then the user space can be displayed perfectly in the device space (1000). The zoom value should be -0.5 ~ +1.5.

(2) Graphics2D Class

Java Graphics 2D class creates and manipulates several kinds of objects such as shapes, text and images; additionally, it also includes image data storage, color management, font and printing.

In the Graphics 2D class, *paint (Graphics g)* method is an abstract method. In the WFSE system, the *paint (Graphics g)* method can be implemented for displaying the computation results.

Figure 4-12 shows how the *paint (Graphics g)* method should be implemented. In this *paint (Graphics g)* method, several functions can be completed such as setting a conversion of a coordinate system, drawing a curve associated with the computation results and displaying information related to the computation model.

```
public void paint (Graphics g) {
    super.paint(g);      Graphics2D g2 = (Graphics2D) g;
    // define a start point, setDataSize and zoom
    int x0_axis = 0;  int y0_axis = 250;  int j=0;   int xi_axis = 800;  int yi_axis = 500;
    int setDataSize = 1000; double zoom = getZoom();
    String info = "Information about this display results";
    int width =1100; int height =500;              // define window's size
    Vector results = estimationResults();          // get estimated results
    int realDataSize = results.size();
    coordinationSystemConversion (g2, width, height, setDataSize, realDataSize, zoom);
    drawingCoirdinationSystem(x0-axis, y0_axis, width, height);
     // drawing a curve of estimated result
     for (int i=0; i<result.size()-1; i++, j=i+1) {
         int p1 = (int) ((Double)(result.elementAt(i))).doubleValue());
         int p2 = (int) ((Double)(result.elementAt(j))).doubleValue());
         g2.setColor(Color.red);
         g2.drawLine(i+ x0-axis,-p1+ y0-axis, j+ x0-axis,-p2+ y0-axis);
      }
      drawingInformation(info, pointInfo);
}
```

Figure 4-12. An example of Implementing *paint* (Graphics g) method

4.4.5 Java Input/Output and Read/Write File Operations

Java input/output and read/write file operations are used to communicate between system and users. All of Java input /output and read/write file facilities are based on streams providing simple ways to read and write data of different types.

(1) Java Input and Output Operations

In the WFSE system, the input operations include selecting a variable or entering the variable's values. Additionally, the output operations are to manage the risk for software system or display running process.

Figure 4-13 includes examples of implementing input and output operations. Figure 4-13 (a) and (b) are the input/output dialogs; and Figure 4-13 (c) is an example of implementing the input/output operations.

In this example, the input operation is applied to enter a value by implementing a show-input-dialog window. The output is used to display an error warning message through implementing a show-message-dialog window. These dialogs are provided by Java Swing component and they are easy to be used and implemented.

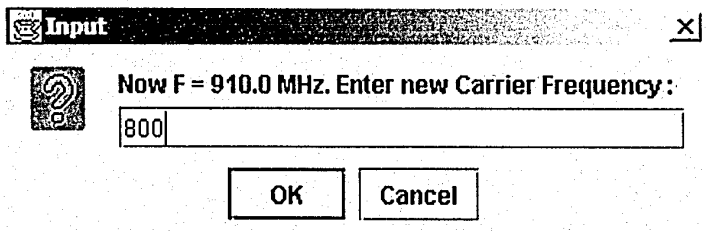

Figure 4-13 (a) An Example of an Input Dialog

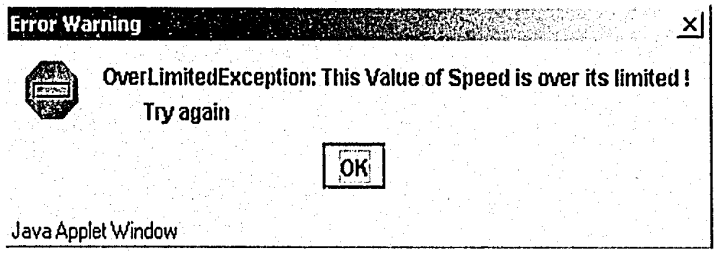

Figure 4-13 (b) An Example of an Error Warning Message Dialog

```
public double enterValue () {
    double value = 0;
    String  stringOfValue = " ";
    // input: enter value in a input dialog, return a string
    stringOfValue = JOptionPane.showInputDialog ("Please enter a value: ");
    // try {}  catch {}  in order to handle Exception
    try {
        // verify if the input includes only (0-9), (.) and (-)
        if (isValidInput(stringOfValue) == true) {
            double temp = ( double)(Double.parseDouble(stringOfValue));
        // verify if the value is over limited values (max, min)
        if (isOverLimited(temp) == false)
            value = temp;
        }
    }
    // output: Error Warning Message
    catch (InvalidInputException error1) {
        JOptionPane.showMessageDialog(null,error1.toString(),
                "Error Warning",JOptionPane.ERROR_MESSAGE);
    }
    catch (OverLimitedException error2) {
        JOptionPane.showMessageDialog(null,error2.toString(),
                "Error Warning", JOptionPane.ERROR_MESSAGE);
    }
    return value;
}
```

Figure 4-13 (c) An Example of Implementing Input and Output Operations

(2) Read File Operation

As previously mentioned in Chapter 3, the WFSE system is necessary to implement the measurement data which is stored as data files (.txt) in the web server. Therefore, a method of reading a data file is implemented. Figure 4-14 is an example of implementing a method of reading a data file operation.

```
public Vector readDataFile(String fileName) {
    Vector vector = new Vector();
    double data = 0;   String string =" ";
    String stringurl = "http://www.site.uottawa.ca/~jzhan037/SimulationSystem/datafiles/";
    // try {} .... Catch {}  to handle an Exception
    try {
       URL url = new URL(stringurl+filename);
       InputStreamReader instream = new InputStreamReader(url.openStream()));
       BufferedReader in = new BufferedReader (instream);
       while ((string = in.readLine()) != null ) {
         data = Double.valueOf(string).doubleValue();
         vector.addElement( new Double(data));
       }
      in.close();
    }
     // Exception handle
    catch (MalformedURLException e) {
       JOptionPane.showMessageDialog (null, "The file can't be found!",
           "Error Warning", JOptionPane. ERROR_MESSAGE);   }
    catch (IOException e) {      }
    return vector;
}
```

Figure 4-14. An Example of Reading a File from the Web Server

In order to read a data file from the web server, a URL referencing the data file is created, then a stream is opened and the stream is read using the stream-based method; this data file is stored in a vector.

4.4.6 Exception Handler

Java Exception handler is used to report and handle the program's errors. When an error occurs, the program throws an exception; in the same time, the normal flow of the program is interrupted and the runtime environment attempts to find the exception.

There are several good reasons for using Java Exception Handler. Firstly, the exception handling code is separated from the normal program flow; this improves

readability and maintainability of the program and system. Secondly, it is easy to find where the exception will be handled [SUNBC].

JFC provides many kinds of Java exception classes. For instance, the *FileNotFoundException* is for reading a file exception, the *MalformedURLException* is for connecting an error web site exception, the *IOException* is for invalid input/output exception, the *IndexOutOfBoundsException* is for reading or writing a vector over its size exception.

In addition, Java Exception Handler can be predefined by programmers. For instance, the WFSE system predefines several error exceptions such as *ComputationException*, *InvalidInputException*, *OverLimitedValueException* and *OverIterationException*. These predefined exception classes are subclasses of Exception class.

Figure 4-15 is an example of predefining an exception class.

```
public class OverLimitedException extends Exception {
    public OverLimitedException () {
        super();
    }
    public OverLimitedException (String error) {
        super(error);
    }
}
```

Figure 4-15 An Example of Defining an Exception Class

Error exception is handled using *try { }* and *throw { }*. Figure 4-13 and Figure 4-14 also show to how to handle these Java exceptions using try {} and catch {}.

4.4.7 Computation Methods

JFC provides some simple mathematical operations, but JFC does not provide complex computation methods. Therefore, numerous computation methods are implemented in the WFSE system. For instance, the EM algorithm and the Kalman filters are based on the matrix computations; In addition, *Fast Fourier Transforms* (FFT)

method, and *Doppler Power Spectral Density* (DPSD) method are also implemented. For instance, the simulation and estimation computation for the flat fading channel and the frequency-selective fading channel, the EM algorithm for the verification and the measurement data models, the DPSD computation and FFT function. These computation methods are based on matrix operations

Other classed and methods are defined and implemented for special requirements. For example, Date class and its methods are used to display the current date and time.

All Java source code of the WFSE system are listed in the enclosed CD-ROM

Chapter Summary

Software development process includes requirement model, analysis model, design model, implementation model, test model and maintain model.

Object-oriented programming was designed to simplify the process of building complex real-world applications.

UML is an industrial standard visual modeling language for specifying, visualizing, constructing and documenting the artifacts of a software system. Several diagrams, such as the user case diagram, sequence diagram and class diagram, are used to analyze and design software system.

Java was designed to create reliable network applications and run securely over a network. Java Plug-in is the best solution of the JDK version mismatch between Java Applets and the web browser. Java Swing provides a component set of GUI elements. Java 2D API enhances the graphics, text and imaging capabilities of Java Swing. Exception handler improves readability and maintainability of the program and system.

The Web-based simulation and estimation system can be run on the following site: http://www.site.uottawa.ca/~jzhan037/onlineSystem.html or http://www.site.uottawa.ca/~chadcha/onlineSystem.html. The operating guide is introduced in Appendix C.

Chapter 5

Summary and Future Work

This chapter summarizes my research work and discusses future work.

5.1 Summary

This thesis describes the fading channel models via the state space, estimates the inphase, quadrature, and envelope components of the received signal using the Kalman filter, and presents the EM algorithm for system identification which is based on the measurement data provided by CRC.

- *Modeling the fading channels using the discrete-time state space models.*

These models are used to analyze the characteristics of the fading channels and identify the system parameters.

- *Estimating the flat fading and the frequency-selective fading channels with the fast or slow fading using the Kalman filters.*

These fading channels are related to the motion of the receiver or transmitter. These system parameters are related to several physical factors of the mobile's motion, for example, the carried frequency, the mobile moving speed, the angle between the mobile and the base station, SNR and the interval time. Additionally, the Rayleigh fading channel, the Ricean fading channel and the N-path fading channel are examples to verify the state space models and the Kalman filters.

- Identifying system parameters using the EM algorithm together with the Kalman filter through the different orders (2^{nd}, 3^{rd} and 4^{th}) of the mathematical model.

Based on the measured data, the system identification is also applied to the flat fading and the frequency-selective fading channels. The estimated inphase and quadrature components and their Doppler power spectral densities (DPSD) are compared with those of the measurement data.

- *Design and developing a web-based software system using Java techniques to complete the fading channel modeling, simulation and system identification.*

The web-based software system is opened to all of the Internet users; and it provides friendly graphics user interface (GUI), simple operations. In addition, the software system can be also extended to add new functions easily.

5.2 Main Contributions

This web-based wireless fading simulation and estimation system is very useful to model the fading channel, to analyze the inphase, quadrature and envelope components of the received signal and to identify the system parameters based on the measurement data. The main contributions in this thesis are listed as the following:

- Analysis and design of the web-based software system
- Implementation of the EM algorithm and the Kalman filter for the discrete-time state space models
- Improvement of the computation precision for simulation and estimation
- Programming for Java source code

5.3 Future Work

In the future, the following aspects should be pursued:

- Identifying system parameters for *Multi-Input Multi-Output* (MIMO) System
- Developing the uncertainly model for the fading channels
- Developing the Jump Markov model for the fading channels

Appendix A

System Identification Results for Flat Fading Channels Based on the Measurement Data

Section 3.4 described system identification's mathematical models for the flat fading channel based on the measurement data and showed the estimated results from a data file. This appendix will illustrate many estimated results for the flat fading channel models from several data files.

Considering 2^{nd}, 3^{rd}, and 4^{th} order of the state space models based on the different measurement data files, the measurement data (the inphase components or the quadrature components) and their power spectral densities are compared between the measured data and the estimated results. In this case, Figures a) compares the output sequences; and Figures b) compares their power spectral densities.

Considering the combination of the 4^{th} order, the inphase and quadrature components and their power spectral densities are also compared between the measurement data and the estimated results. In this case, Figures (a) and (b) comprise the inphase components and their Doppler power spectral densities; Figures (c) and (d) comprise the quadrature components and their power spectral densities; and Figures (e) and (f) comprise the combination components and their power spectral densities.

In these figures, the red curves denote the measured data corresponding to the measured data files; and the blue curves denote the estimated results.

A.1 Estimated Results Based on the Data I1.4 and Q1.4

Table A.1: the Estimated Results from the data I1.4 and Q1.4 including 385 samples

Order		Estimated Model Parameters	Estimated Figures
2nd	I(k)	$\hat{A} = \begin{bmatrix} 0 & 1 \\ 1.3257 & -0.3711 \end{bmatrix}$, $\hat{BB}^T = \begin{bmatrix} 0.0035 & 0.00087 \\ 0.00087 & 0.0014 \end{bmatrix}$ $\hat{C} = [1 \;\; 0]$, $\hat{DD}^T = [0.00031]$	Figure A-1
	Q(k)	$\hat{A} = \begin{bmatrix} 0 & 1 \\ 1.3061 & -0.3476 \end{bmatrix}$, $\hat{BB}^T = \begin{bmatrix} 0.0017 & 0.0004.1 \\ 0.0004.1 & 0.0007.5 \end{bmatrix}$ $\hat{C} = [1 \;\; 0]$, $\hat{DD}^T = [0.00016]$	Figure A-2
3rd	I(k)	$\hat{A} = \begin{bmatrix} 0.0 & 1.0 & 0.0 \\ 0.0 & 0.0 & 1.0 \\ 0.6547 & 0.0425 & 0.0515 \end{bmatrix}$, $\hat{BB}^T = \begin{bmatrix} 0.0131 & 0.0046 & 0.0017 \\ 0.0046 & 0.0149 & 0.0041 \\ 0.0017 & 0.0041 & 0.0125 \end{bmatrix}$ $\hat{C} = [1 \;\; 0 \;\; 0]$, $\hat{DD}^T = [0.0074]$	Figure A-3
	Q(k)	$\hat{A} = \begin{bmatrix} 0.0 & 1.0 & 0.0 \\ 0.0 & 0.0 & 1.0 \\ 0.5208 & 0.1238 & 0.0613 \end{bmatrix}$, $\hat{BB}^T = \begin{bmatrix} 0.0087 & 0.0024 & 0.0011 \\ 0.0024 & 0.0096 & 0.0024 \\ 0.0011 & 0.0024 & 0.0087 \end{bmatrix}$ $\hat{C} = [1 \;\; 0 \;\; 0]$, $\hat{DD}^T = [0.0063]$	Figure A-4
4th	I(k)	$\hat{A} = \begin{bmatrix} 0 & 1 & 0 & 0 \\ 0 & 0 & 1 & 0 \\ 0 & 0 & 0 & 1 \\ 0.6267 & 0.1149 & -0.0479 & -0.0305 \end{bmatrix}$, $\hat{BB}^T = \begin{bmatrix} 0.0540 & 0.0019 & 0.0055 & 0.0028 \\ 0.0019 & 0.0536 & 0.0020 & 0.0057 \\ 0.0055 & 0.0020 & 0.0537 & 0.0016 \\ 0.0028 & 0.0057 & 0.0016 & 0.0512 \end{bmatrix}$ $\hat{C} = [1 \;\; 0 \;\; 0 \;\; 0]$, $\hat{DD}^T = [0.0085]$	Figure A-5
	Q(k)	$\hat{A} = \begin{bmatrix} 0 & 1 & 0 & 0 \\ 0 & 0 & 1 & 0 \\ 0 & 0 & 0 & 1 \\ 05303 & 0.1538 & -0.0299 & -0.0441 \end{bmatrix}$, $\hat{BB}^T = \begin{bmatrix} 0.0676 & -0.0005 & 0.0052 & -0.0018 \\ -0.0005 & 0.0664 & -0.0006 & 0.0053 \\ 0.0052 & -0.0006 & 0.0675 & -0.0010 \\ -0.0018 & 0.0053 & -0.0010 & 0.0642 \end{bmatrix}$ $\hat{C} = [1 \;\; 0 \;\; 0 \;\; 0]$, $\hat{DD}^T = [0.0089]$	Figure A-6
Combination		$\hat{A} = \begin{bmatrix} 0 & 1 & 0 & 0 \\ 0.8448 & 0.0715 & 0 & 0 \\ 0 & 0 & 0 & 1 \\ 0 & 0 & 0.9285 & 0.0204 \end{bmatrix}$, $\hat{BB}^T = \begin{bmatrix} 0.0091 & 0.0041 & 0.00027 & -0.0018 \\ 0.0041 & 0.0089 & 0.00034 & -0.0014 \\ 0.00027 & 0.00034 & 0.00093 & 0.00085 \\ -0.0018 & -0.0014 & 0.00085 & 0.0025 \end{bmatrix}$ $\hat{C} = [1 \;\; 0 \;\; 1 \;\; 0]$, $\hat{DD}^T = [0.0021]$	Figure A-7

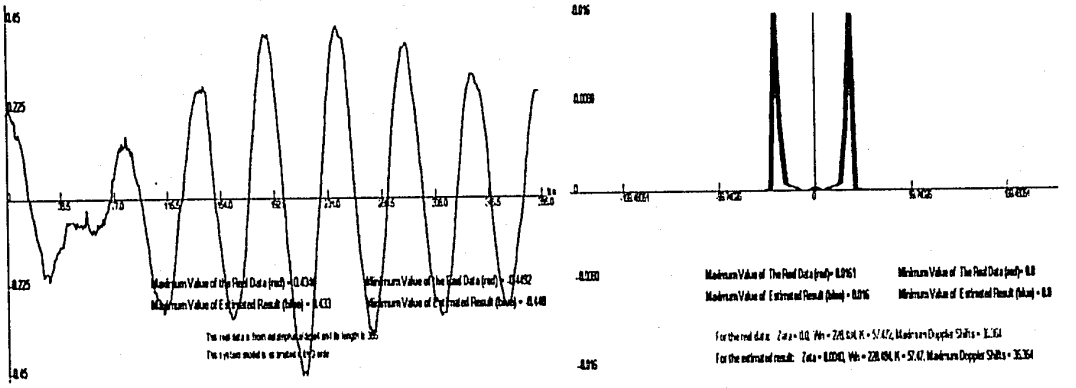

(a) Filter I(k) vs. Measured data Id(k) (b) DPSD for Filter vs. Real Data

Figure A-1. the real inphase component vs. estimate value in 2nd-order (I1.4)

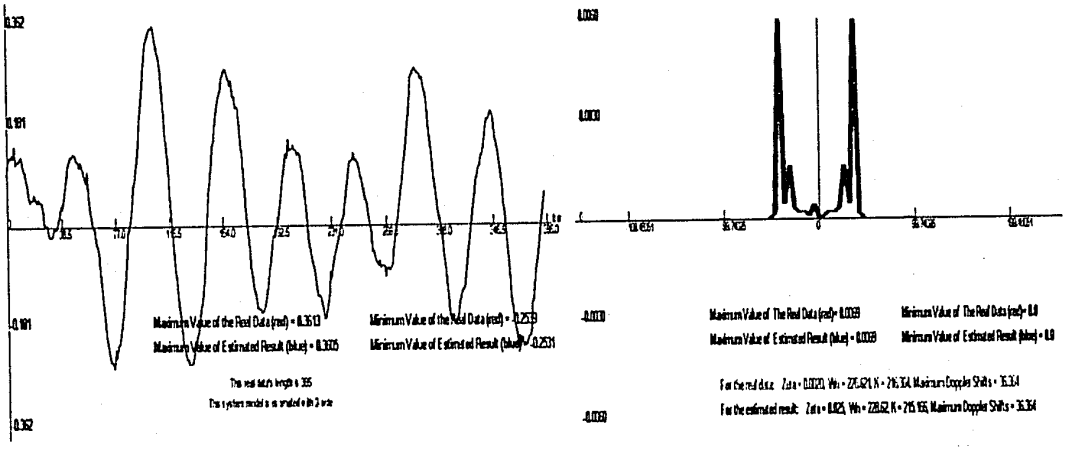

(a) Filter Q(k) vs. Measured data Qd(k) (b) DPSD for Filter vs. Real Data

Figure A-2. The real quadrature component vs. estimate result in 2nd-order (Q1.4)

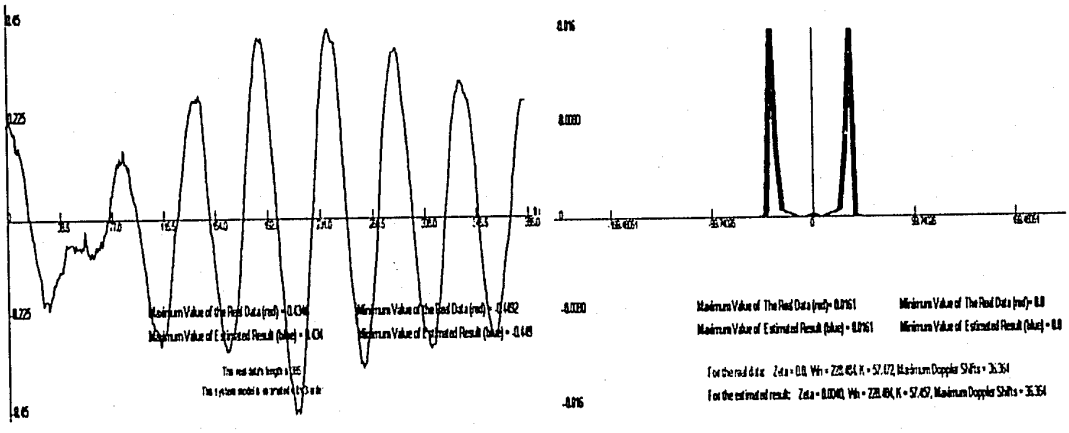

(a) Filter I(k) vs. Measured data Id(k) (b) DPSD for Filter vs. Real Data

Figure A-3. the real inphase component vs. estimate value in 3rd-order (I1.4)

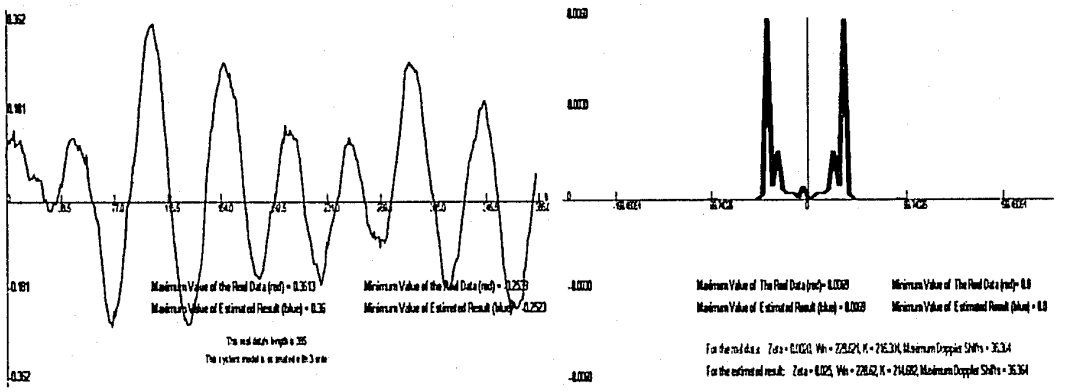

(a) Filter Q(k) vs. Measured data Qd(k) (b) DPSD for Filter vs. Real Data

Figure A-4. the real quadrature component vs. estimate value in 3rd-order (Q1.4)

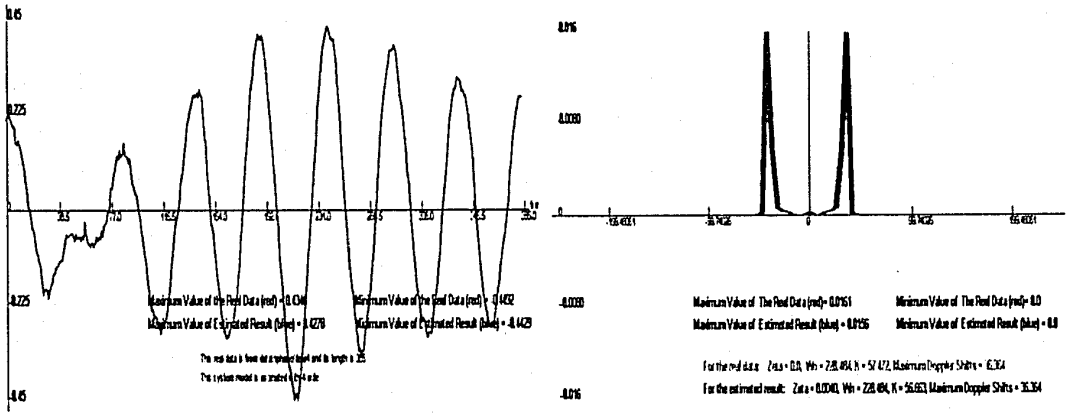

(a) Filter I(k) vs. Measured data Id(k) (b) DPSD for Filter vs. Real Data

Figure A-5. the real inphase component vs. estimate value in 4th-order (I1.4)

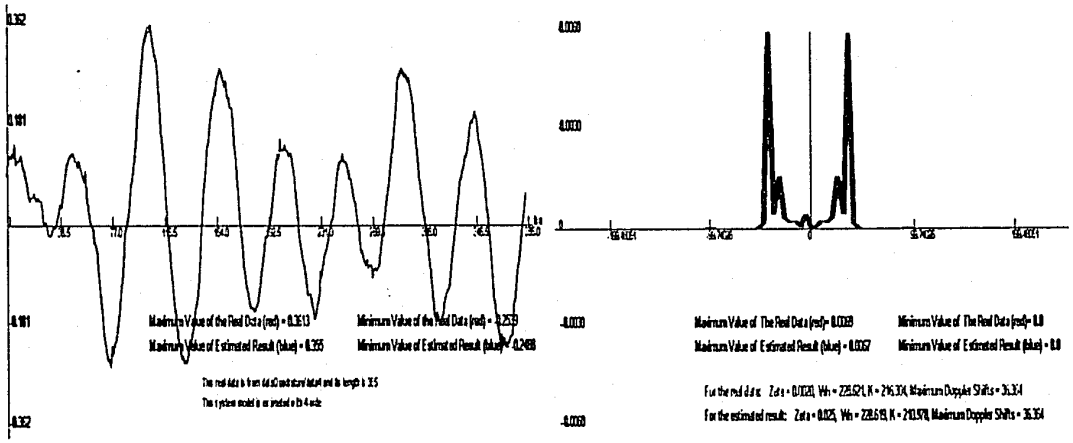

(a) Filter Q(k) vs. Measured data Id(k) (b) DPSD for Filter vs. Real Data

Figure A-6. the real quadrature component vs. estimate value in 4th-order (Q1.4)

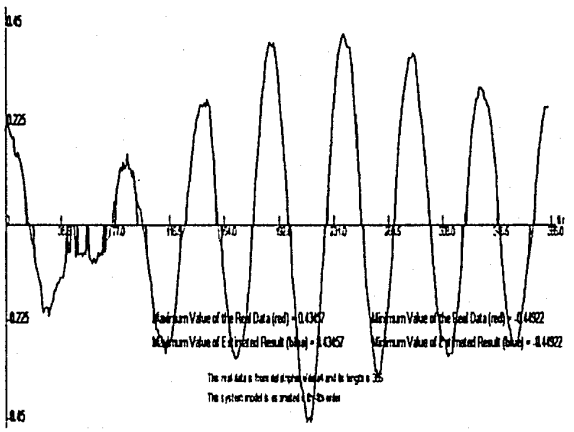

(a) Inphase Components

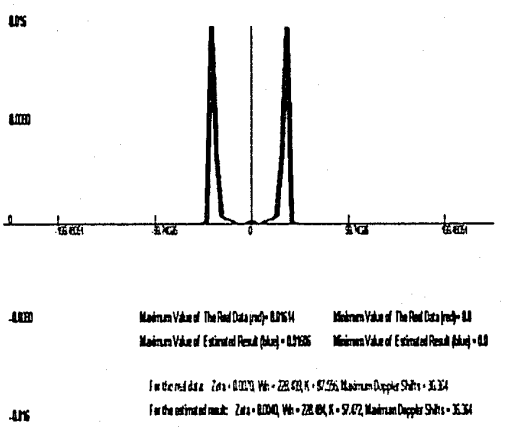

(b) DPSD for Inphase Components

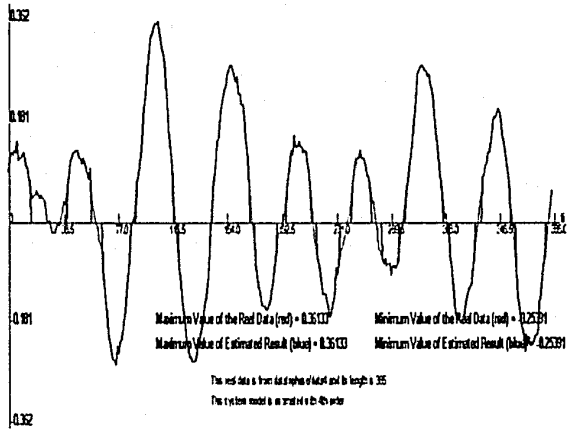

(c) Quadrature Components

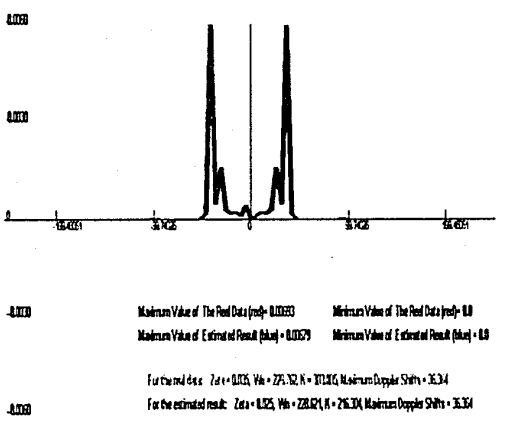

(d) DPSD for Quadrature Components

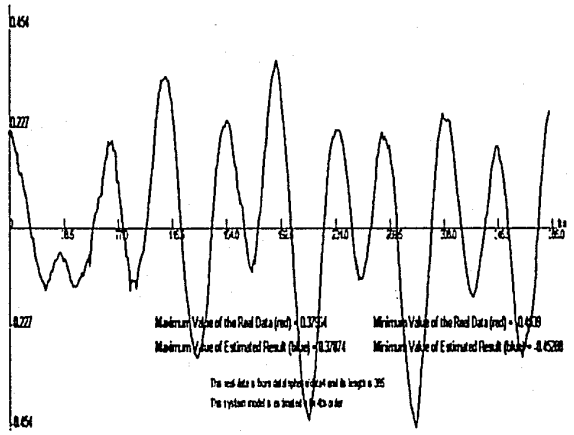

(e) Combination Components

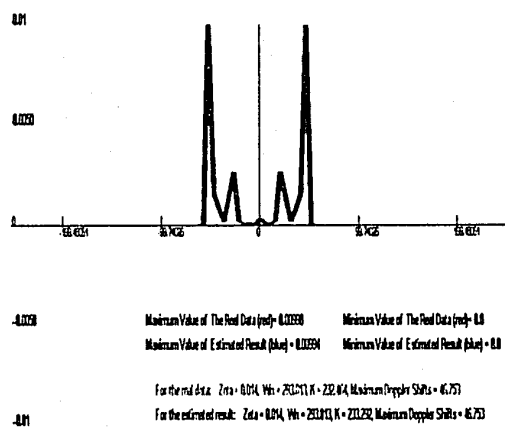

(f) DPSD for Combination Components

Figure A-7. the real inphase and quadrature components vs. estimate value in 4th-order

A.2 Estimated Results Based on the Data I2.5 and Q2.5

Table A.3: the Estimated Results from the data I2.5 and Q2.5 including 447 samples

Order		Estimated Model Parameters	Estimated Figures
I(k)	2nd	$\hat{A}=\begin{bmatrix}0 & 1\\ 1.2450 & -0.2958\end{bmatrix}$, $\hat{BB}^T=\begin{bmatrix}0.0014 & 0.0004\\ 0.0004 & 0.0007\end{bmatrix}$ $\hat{C}=\begin{bmatrix}1 & 0\end{bmatrix}$, $\hat{DD}^T=[0.0001]$	Figure A-8
	3rd	$\hat{A}=\begin{bmatrix}0.0 & 1.0 & 0.0\\ 0.0 & 0.0 & 1.0\\ 0.3789 & -0.1904 & 0.0741\end{bmatrix}$, $\hat{BB}^T=\begin{bmatrix}0.0399 & 0.0086 & 0.0080\\ 0.0086 & 0.0498 & 0.0085\\ 0.0080 & 0.0085 & 0.0509\end{bmatrix}$ $\hat{C}=\begin{bmatrix}1 & 0 & 0\end{bmatrix}$, $\hat{DD}^T=[0.0034]$	Figure A-9
	4th	$\hat{A}=\begin{bmatrix}0 & 1 & 0 & 0\\ 0 & 0 & 1 & 0\\ 0 & 0 & 0 & 1\\ 0.7178 & -0.1189 & 0.0024 & -0.0071\end{bmatrix}$, $\hat{BB}^T=\begin{bmatrix}0.0425 & 0.0010 & 0.0020 & 0.0030\\ 0.0010 & 0.0412 & 0.0020 & 0.0020\\ 0.0020 & 0.0020 & 0.0412 & 0.0010\\ 0.0030 & 0.0020 & 0.0010 & 0.0389\end{bmatrix}$ $\hat{C}=\begin{bmatrix}1 & 0 & 0 & 0\end{bmatrix}$, $\hat{DD}^T=[0.0079]$	Figure A-10
Q(k)	2nd	$\hat{A}=\begin{bmatrix}0 & 1\\ 1.3182 & -0.3917\end{bmatrix}$, $\hat{BB}^T=\begin{bmatrix}0.0041 & 0.0010\\ 0.0010 & 0.0016\end{bmatrix}$ $\hat{C}=\begin{bmatrix}1 & 0\end{bmatrix}$, $\hat{DD}^T=[0.0003]$	Figure A-11
	3rd	$\hat{A}=\begin{bmatrix}0.0 & 1.0 & 0.0\\ 0.0 & 0.0 & 1.0\\ 0.2499 & 0.06178 & 0.0433\end{bmatrix}$, $\hat{BB}^T=\begin{bmatrix}0.1476 & -0.0017 & -0.0042\\ -0.0017 & 0.1557 & 0.0014\\ -0.0042 & 0.0014 & 0.1557\end{bmatrix}$ $\hat{C}=\begin{bmatrix}1 & 0 & 0\end{bmatrix}$, $\hat{DD}^T=[0.0053]$	Figure A-12
	4th	$\hat{A}=\begin{bmatrix}0 & 1 & 0 & 0\\ 0 & 0 & 1 & 0\\ 0 & 0 & 0 & 1\\ 0.7367 & -0.1234 & -0.0024 & -0.0119\end{bmatrix}$, $\hat{BB}^T=\begin{bmatrix}0.0432 & 0.0010 & 0.0020 & 0.0030\\ 0.0010 & 0.0418 & 0.0020 & 0.0020\\ 0.0020 & 0.0020 & 0.0419 & 0.0010\\ 0.0030 & 0.0020 & 0.0010 & 0.0394\end{bmatrix}$ $\hat{C}=\begin{bmatrix}1 & 0 & 0 & 0\end{bmatrix}$, $\hat{DD}^T=[0.0079]$	Figure A-13
Combination		$\hat{A}=\begin{bmatrix}0 & 1 & 0 & 0\\ 0.7284 & 0.0779 & 0 & 0\\ 0 & 0 & 0 & 1\\ 0 & 0 & 0.7968 & 0.0339\end{bmatrix}$, $\hat{BB}^T=\begin{bmatrix}0.0114 & 0.0029 & 0.0023 & 7.3701\times10^{-4}\\ 0.0029 & 0.0112 & 0.0015 & 0.0013\\ 0.0023 & 0.0015 & 0.0059 & 0.0038\\ 7.3701\times10^{-4} & 0.013 & 0.0038 & 0.0104\end{bmatrix}$ $\hat{C}=\begin{bmatrix}1 & 0 & 1 & 0\end{bmatrix}$, $\hat{DD}^T=[0.0019]$	Figure A-14

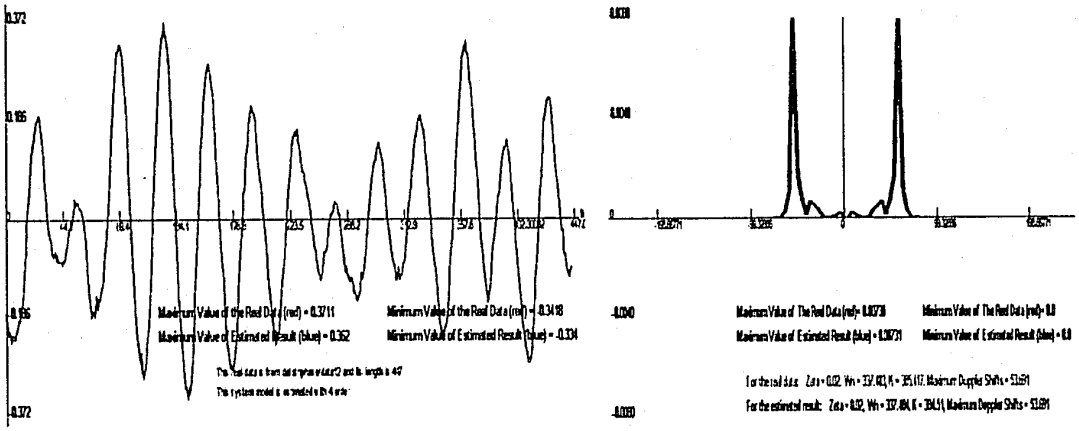

(a) Filter I(k) vs. Measured data Id(k) (b) DPSD for Filter vs. Real Data

Figure A-8 the real inphase component vs. estimate value in 2nd-order (I2.5)

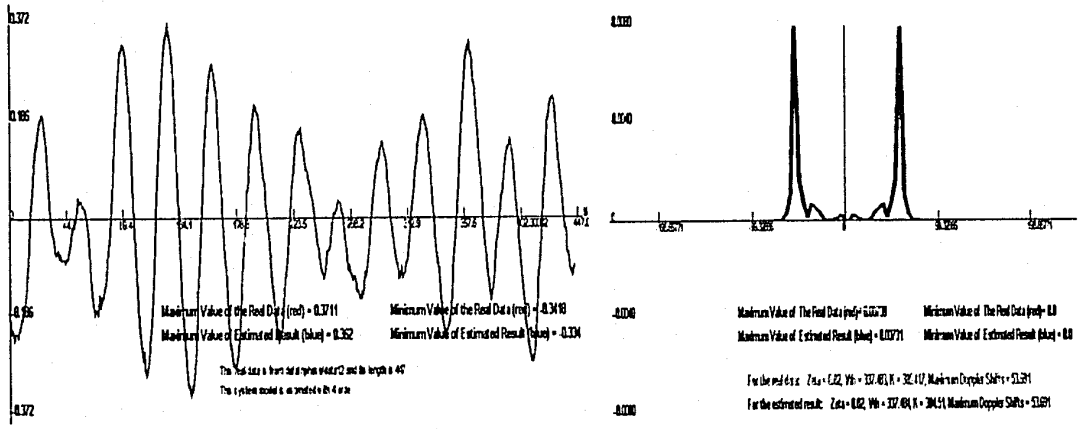

(a) Filter I(k) vs. Measured data Id(k) (b) DPSD for Filter vs. Real Data

Figure A-9. the real inphase component vs. estimate value in 3rd-order (I2.5)

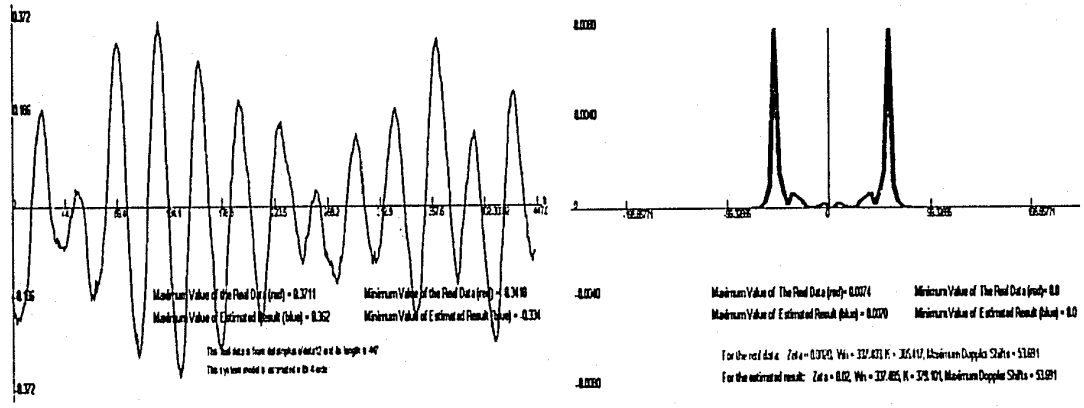

(a) Filter I(k) vs. Measured data Id(k) (b) DPSD for Filter vs. Real Data

Figure A-10. the real inphase component vs. estimate value in 4th-order (I2.5)

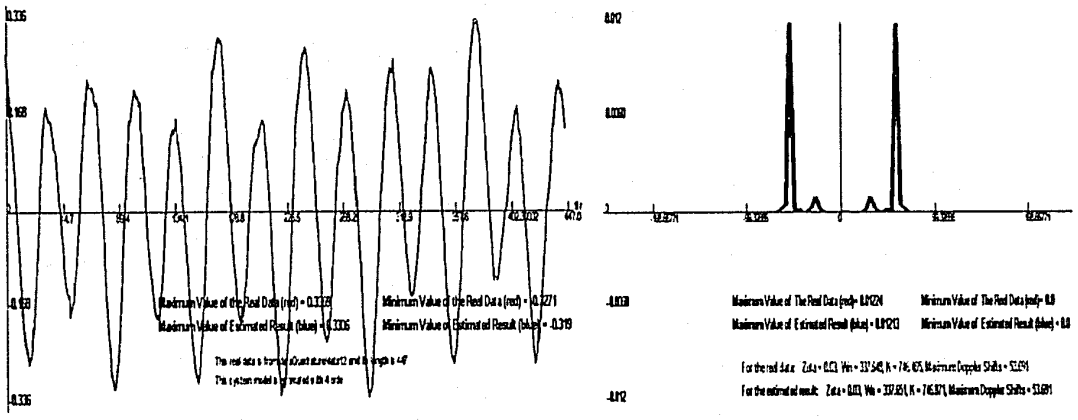

(a) Filter Q(k) vs. Measured data Qd(k) (b) DPSD for Filter vs. Real Data

Figure A-11. The real quadrature component vs. estimate result in 2nd-order (Q2.5)

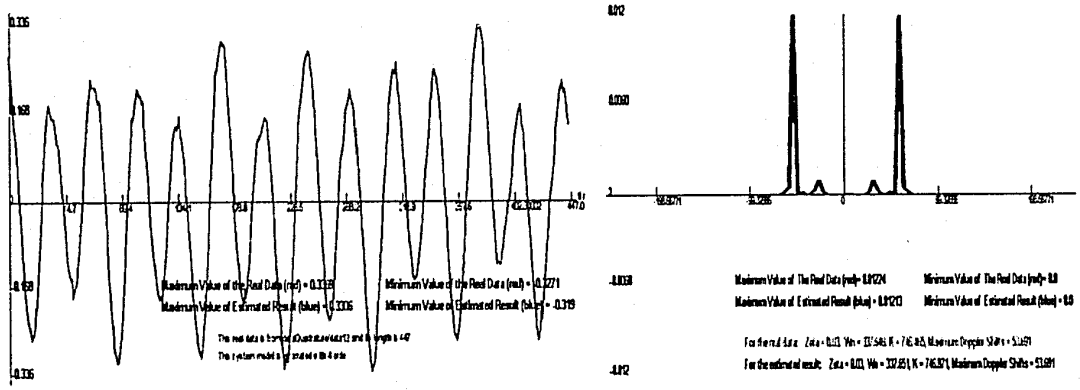

(a) Filter Q(k) vs. Measured data Id(k) (b) DPSD for Filter vs. Real Data

Figure A-12. the real quadrature component vs. estimate value in 3rd-order (Q2.5)

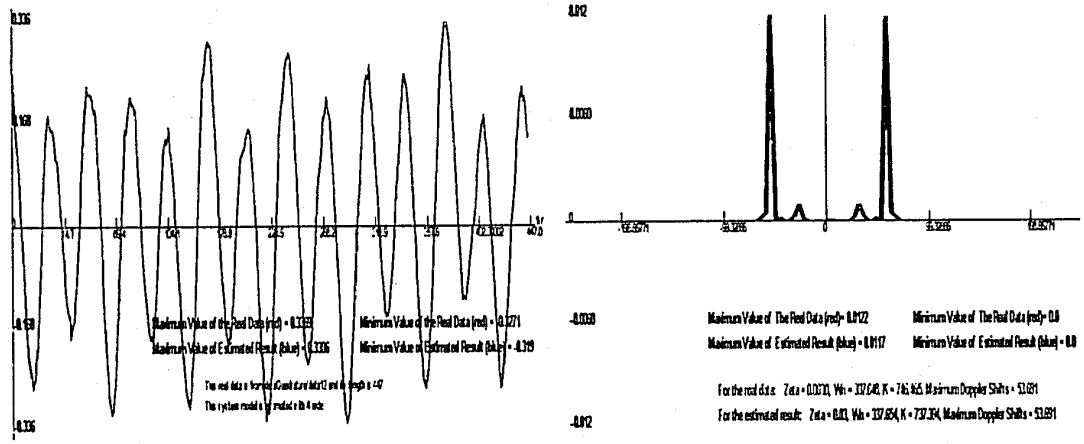

(a) Filter Q(k) vs. Measured data Qd(k) (b) DPSD for Filter vs. Real Data

Figure A-13. the real quadrature component vs. estimate value in 4th-order (Q2.5)

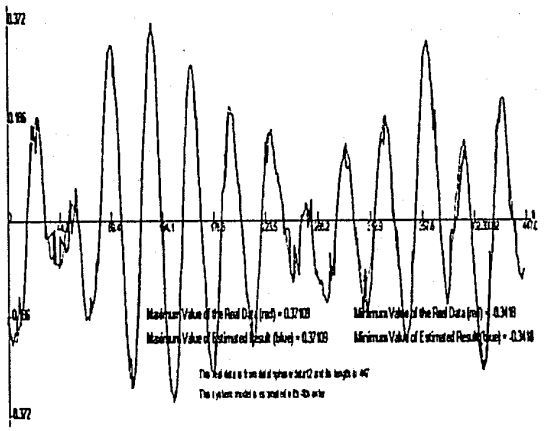

(a) Inphase Components

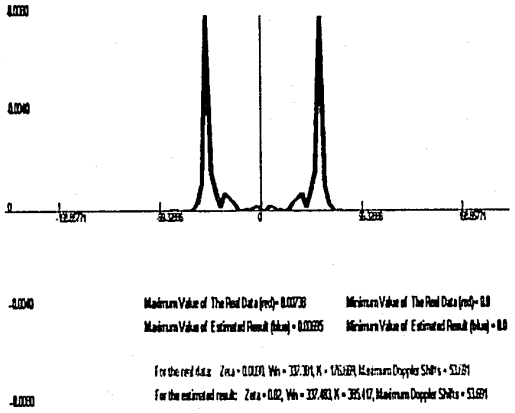

(b) DPSD for Inphase Components

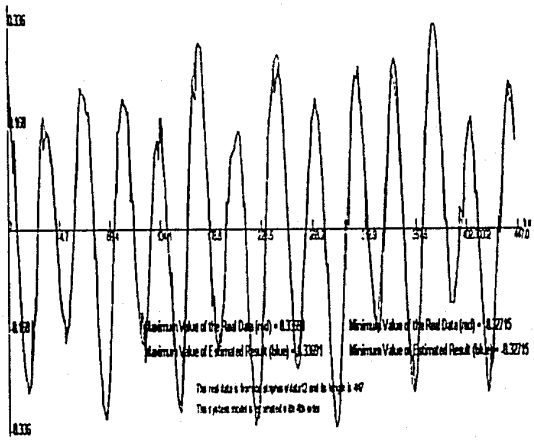

(c) Quadrature Components

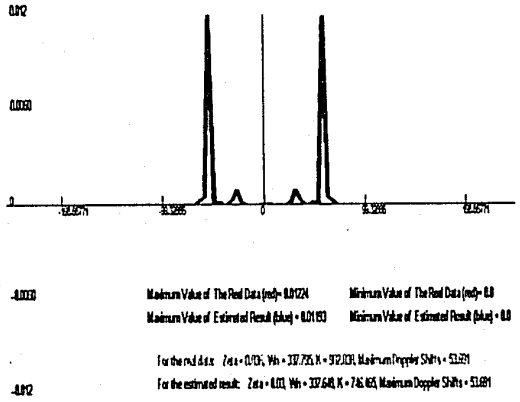

(d) DPSD for Quadrature Components

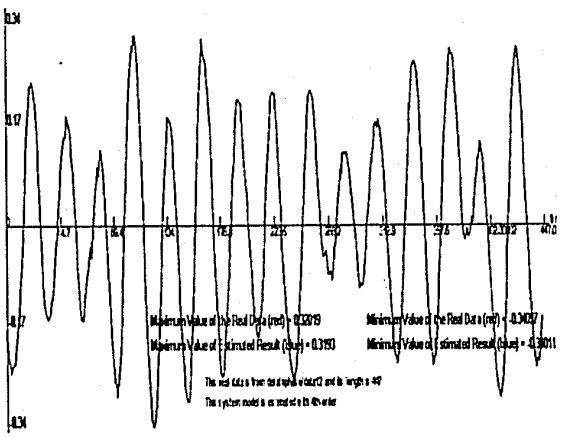

(e) Combination Components

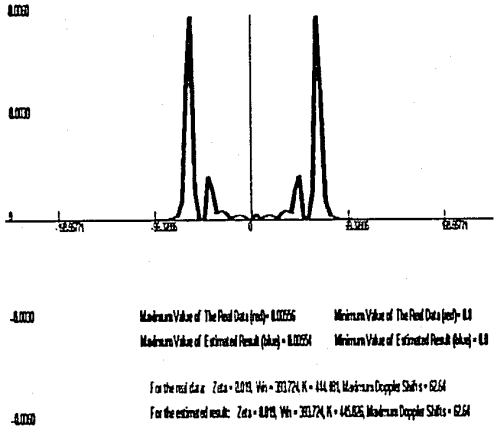

(f) DPSD for Combination Components

Figure A-14. the real inphase and quadrature components vs. estimate value in 4th-order

A.3 Estimated Results Based on the Data I3.2 and Q3.2

Table A.4: the Estimated Results from the data I3.2 and Q3.2 including 3828 samples

Order		Estimated Model Parameters	Estimated Figures
I(k)	2nd	$\hat{A}=\begin{bmatrix}0 & 1\\ 1.3357 & -0.3768\end{bmatrix}$, $\hat{BB}^T=\begin{bmatrix}0.05476 & 0.0031\\ 0.0031 & 0.0106\end{bmatrix}$ $\hat{C}=[1\ \ 0]$, $\hat{DD}^T=[7.9291\times10^{-4}]$	Figure A-15
	3rd	$\hat{A}=\begin{bmatrix}0.0 & 1.0 & 0.0\\ 0.0 & 0.0 & 1.0\\ 1.3311 & -0.5066 & 0.0754\end{bmatrix}$, $\hat{BB}^T=\begin{bmatrix}0.0491 & 0.0498 & 0.0022\\ 0.0498 & 0.0621 & 0.0044\\ 0.0022 & 0.0044 & 0.0098\end{bmatrix}$ $\hat{C}=[1\ \ 0\ \ 0]$, $\hat{DD}^T=[0.0011]$	Figure A-16
	4th	$\hat{A}=\begin{bmatrix}0 & 1 & 0 & 0\\ 0 & 0 & 1 & 0\\ 0 & 0 & 0 & 1\\ 1.3303 & -0.1151 & -0.1554 & -0.1388\end{bmatrix}$, $\hat{BB}^T=\begin{bmatrix}0.2291 & 0.0010 & 0.0020 & 0.0030\\ 0.0010 & 0.1259 & 0.0020 & 0.0020\\ 0.0020 & 0.0020 & 0.0491 & 0.0010\\ 0.0030 & 0.0020 & 0.0010 & 0.0087\end{bmatrix}$ $\hat{C}=[1\ \ 0\ \ 0\ \ 0]$, $\hat{DD}^T=[0.0022]$	Figure A-17
Q(k)	2nd	$\hat{A}=\begin{bmatrix}0 & 1\\ 1.3239 & -0.3703\end{bmatrix}$, $\hat{BB}^T=\begin{bmatrix}0.0454 & 0.0024\\ 0.0024 & 0.0086\end{bmatrix}$ $\hat{C}=[1\ \ 0]$, $\hat{DD}^T=[6.5953\times10^{-4}]$	Figure A-18
	3rd	$\hat{A}=\begin{bmatrix}0.0 & 1.0 & 0.0\\ 0.0 & 0.0 & 1.0\\ 1.4178 & -0.5212 & 0.0697\end{bmatrix}$, $\hat{BB}^T=\begin{bmatrix}0.0542 & 0.0443 & 0.0033\\ 0.0443 & 0.0514 & 0.0052\\ 0.0033 & 0.0052 & 0.0105\end{bmatrix}$ $\hat{C}=[1\ \ 0\ \ 0]$, $\hat{DD}^T=[0.0029]$	Figure A-19
	4th	$\hat{A}=\begin{bmatrix}0 & 1 & 0 & 0\\ 0 & 0 & 1 & 0\\ 0 & 0 & 0 & 1\\ 1.3306 & -0.1132 & -0.1518 & -0.1253\end{bmatrix}$, $\hat{BB}^T=\begin{bmatrix}0.1958 & 0.0010 & 0.0020 & 0.0030\\ 0.0010 & 0.1076 & 0.0020 & 0.0020\\ 0.0020 & 0.0020 & 0.0418 & 0.0010\\ 0.0030 & 0.0020 & 0.0010 & 0.0071\end{bmatrix}$ $\hat{C}=[1\ \ 0\ \ 0\ \ 0]$, $\hat{DD}^T=[0.0018]$	Figure A-20
Combination		$\hat{A}=\begin{bmatrix}0 & 1 & 0 & 0\\ 0.9226 & -0.0489 & 0 & 0\\ 0 & 0 & 0 & 1\\ 0 & 0 & 0.9208 & -0.03439\end{bmatrix}$, $\hat{BB}^T=\begin{bmatrix}0.0628 & 0.0423 & -0.0067 & -0.0164\\ 0.0423 & 0.0554 & 0.0032 & -0.0060\\ -0.0060 & 0.0032 & 0.0629 & 0.0439\\ -0.0164 & -0.0060 & 0.0439 & 0.0584\end{bmatrix}$ $\hat{C}=[1\ \ 0\ \ 1\ \ 0]$, $\hat{DD}^T=[0.0025]$	Figure A-21

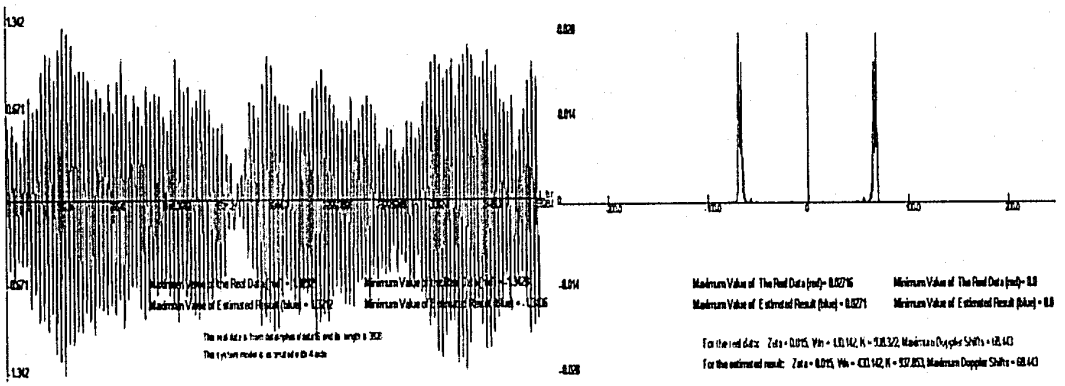

(a) Filter I(k) vs. Measured data Id(k) (b) DPSD for Filter vs. Real Data

Figure A-15. the real inphase component vs. estimate value in 2nd-order (I3.2)

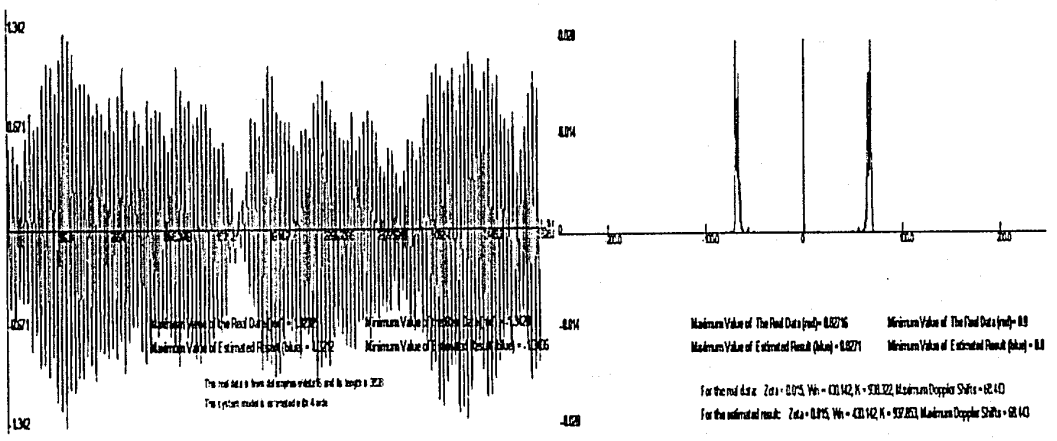

(a) Filter I(k) vs. Measured data Id(k) (b) DPSD for Filter vs. Real Data

Figure A-16. the real inphase component vs. estimate value in 3rd-order (I3.2)

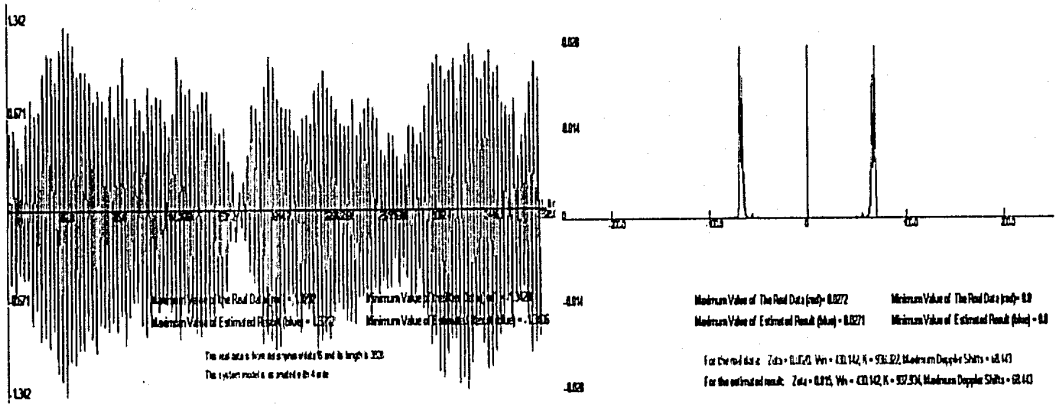

(a) Filter I(k) vs. Measured data Id(k) (b) DPSD for Filter vs. Real Data

Figure A-17. the real inphase component vs. estimate value in 4th-order (I3.2)

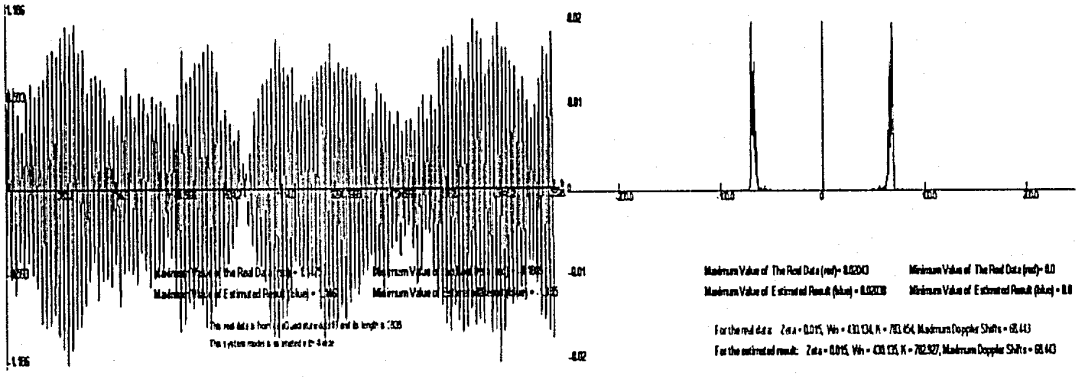

(a) Filter Q(k) vs. Measured data Qd(k) (b) DPSD for Filter vs. Real Data

Figure A-18. The real quadrature component vs. estimate result in 2nd-order (Q3.2)

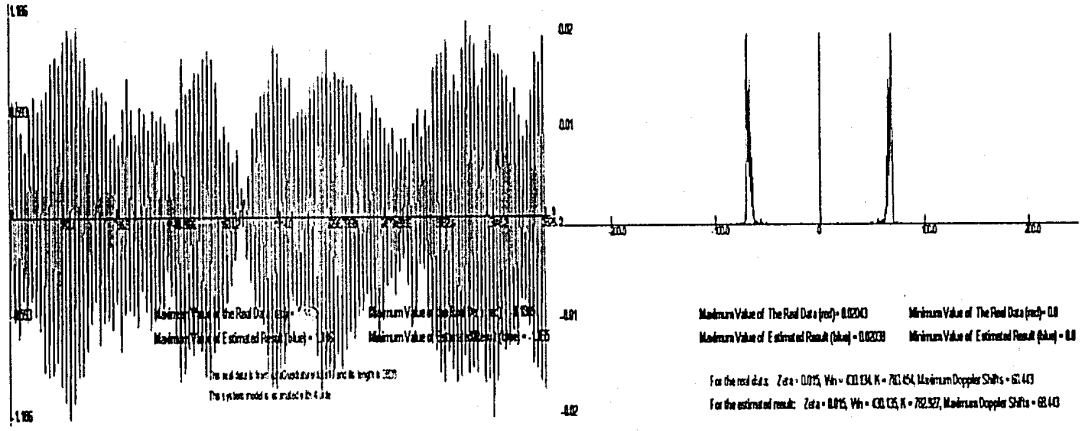

(a) Filter Q(k) vs. Measured data Id(k) (b) DPSD for Filter vs. Real Data

Figure A-19. the real quadrature component vs. estimate value in 3rd-order (Q3.2)

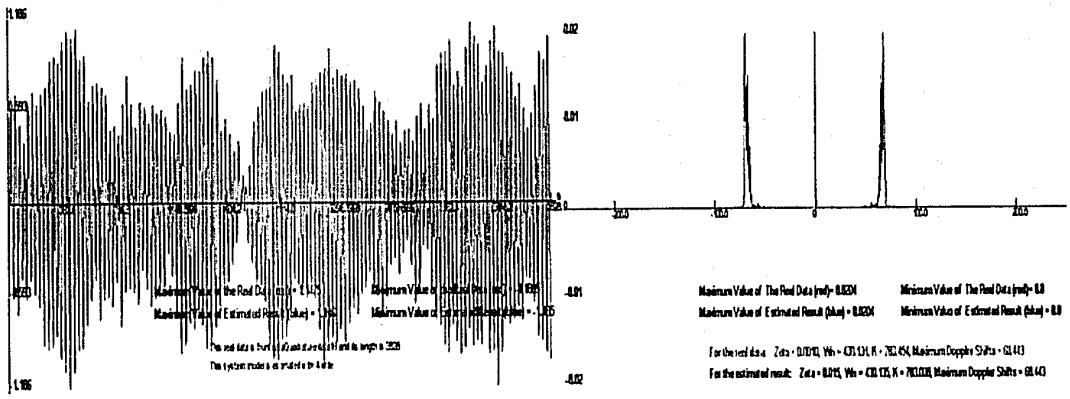

(a) Filter Q(k) vs. Measured data Qd(k) (b) DPSD for Filter vs. Real Data

Figure A-20. the real quadrature component vs. estimate value in 4th-order (Q3.2)

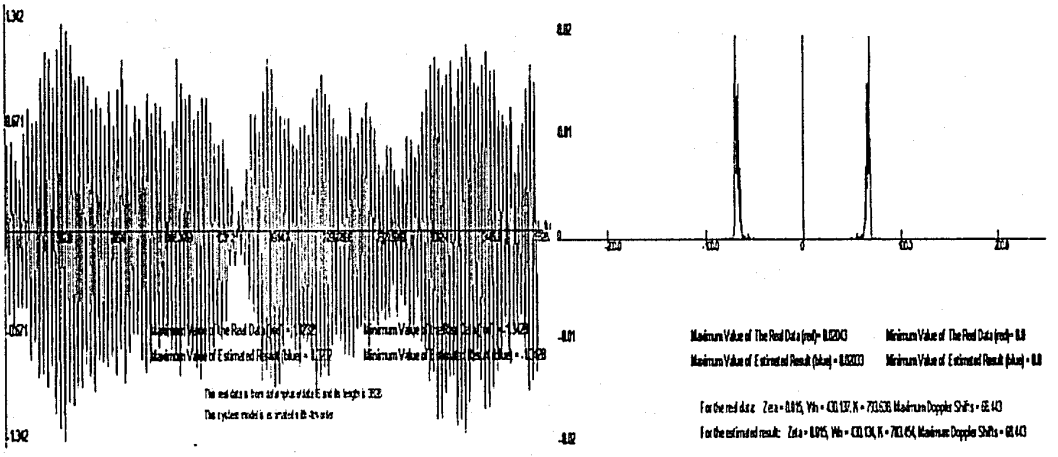

(a) Inphase Components (b) DPSD for Inphase Components

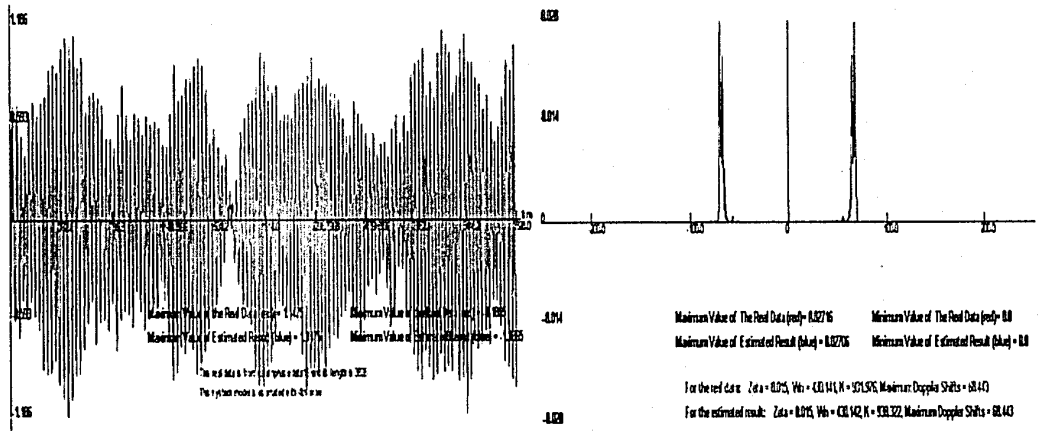

(c) Quadrature Components (d) DPSD for Quadrature Components

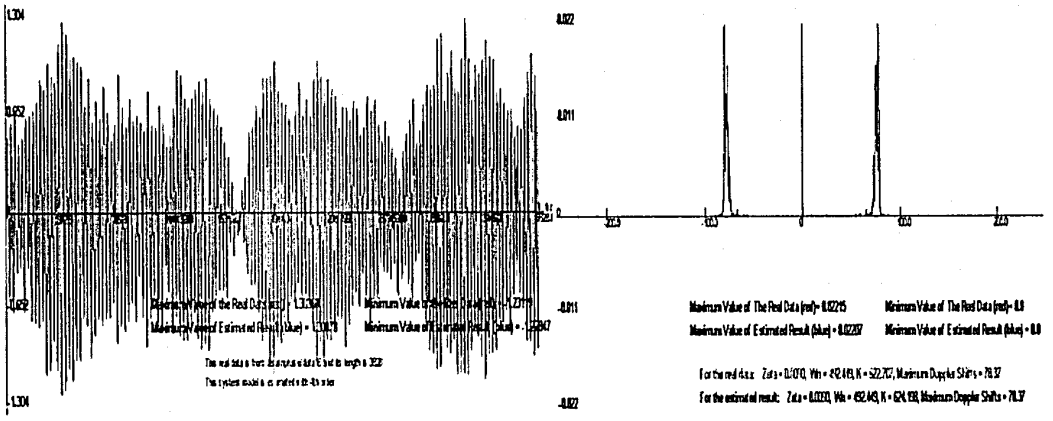

(e) Combination Components (f) DPSD for Combination Components

Figure A-21. the real inphase and quadrature components vs. estimate value in 4th-order

A.4 Estimated Results Based on the Data I4.3 and Q4.3

Table A.5: the Estimated Results from the data I4.3 and Q4.3 including 3043 samples

Order		Estimated Model Parameters	Estimated Figures
I(k)	2nd	$\hat{A}=\begin{bmatrix}0 & 1\\ 0.8723 & 0.0869\end{bmatrix}$, $\hat{BB}^T=\begin{bmatrix}0.0186 & 0.0127\\ 0.0127 & 0.0246\end{bmatrix}$ $\hat{C}=[1\ \ 0]$, $\hat{DD}^T=[0.0122]$	Figure A-22
	3rd	$\hat{A}=\begin{bmatrix}0.0 & 1.0 & 0.0\\ 0.0 & 0.0 & 1.0\\ 1.4171 & -0.7594 & 0.3067\end{bmatrix}$, $\hat{BB}^T=\begin{bmatrix}0.0135 & 0.0111 & 0.0025\\ 0.0111 & 0.0148 & 0.0004\\ 0.0025 & 0.0004 & 0.0039\end{bmatrix}$ $\hat{C}=[1\ \ 0\ \ 0]$, $\hat{DD}^T=[0.0016]$	Figure A-23
	4th	$\hat{A}=\begin{bmatrix}0 & 1 & 0 & 0\\ 0 & 0 & 1 & 0\\ 0 & 0 & 0 & 1\\ 1.3147 & -0.1884 & -0.3879 & 0.2648\end{bmatrix}$, $\hat{BB}^T=\begin{bmatrix}0.0299 & 0.0010 & 0.0020 & 0.0030\\ 0.0010 & 0.0214 & 0.0020 & 0.0020\\ 0.0020 & 0.0020 & 0.0071 & 0.0010\\ 0.0030 & 0.0020 & 0.0010 & 0.0037\end{bmatrix}$ $\hat{C}=[1\ \ 0\ \ 0\ \ 0]$, $\hat{DD}^T=[7.4679\times10^{-4}]$	Figure A-24
Q(k)	2nd	$\hat{A}=\begin{bmatrix}0 & 1\\ 1.3869 & -0.3956\end{bmatrix}$, $\hat{BB}^T=\begin{bmatrix}0.0096 & 9.1351\times10^{-4}\\ 9.1351\times10^{-4} & 0.0026\end{bmatrix}$ $\hat{C}=[1\ \ 0]$, $\hat{DD}^T=[3.4933\times10^{-4}]$	Figure A-25
	3rd	$\hat{A}=\begin{bmatrix}0.0 & 1.0 & 0.0\\ 0.0 & 0.0 & 1.0\\ 1.6074 & -0.5040 & -0.1491\end{bmatrix}$, $\hat{BB}^T=\begin{bmatrix}0.0158 & 0.0098 & 0.0009\\ 0.0098 & 0.0126 & 0.0016\\ 0.0009 & 0.0016 & 0.0037\end{bmatrix}$ $\hat{C}=[1\ \ 0\ \ 0]$, $\hat{DD}^T=[0.0013]$	Figure A-26
	4th	$\hat{A}=\begin{bmatrix}0 & 1 & 0 & 0\\ 0 & 0 & 1 & 0\\ 0 & 0 & 0 & 1\\ 1.915 & -0.3772 & -0.4186 & -0.1928\end{bmatrix}$, $\hat{BB}^T=\begin{bmatrix}0.0401 & 0.0010 & 0.0020 & 0.0030\\ 0.0010 & 0.0247 & 0.0020 & 0.0020\\ 0.0020 & 0.0020 & 0.0124 & 0.0010\\ 0.0030 & 0.0020 & 0.0010 & 0.0026\end{bmatrix}$ $\hat{C}=[1\ \ 0\ \ 0\ \ 0]$, $\hat{DD}^T=[0.0015]$	Figure A-27
Combination		$\hat{A}=\begin{bmatrix}0 & 1 & 0 & 0\\ 0.8901 & 0.0660 & 0 & 0\\ 0 & 0 & 0 & 1\\ 0 & 0 & 0.8683 & 0.0369\end{bmatrix}$, $\hat{BB}^T=\begin{bmatrix}0.0897 & 0.0569 & 0.0097 & -0.0133\\ 0.0569 & 0.0929 & 0.0175 & -0.0023\\ 0.0097 & 0.0175 & 0.0478 & 0.0098\\ -0.0133 & -0.0023 & 0.0098 & 0.0409\end{bmatrix}$ $\hat{C}=[1\ \ 0\ \ 1\ \ 0]$, $\hat{DD}^T=[0.0021]$	Figure A-28

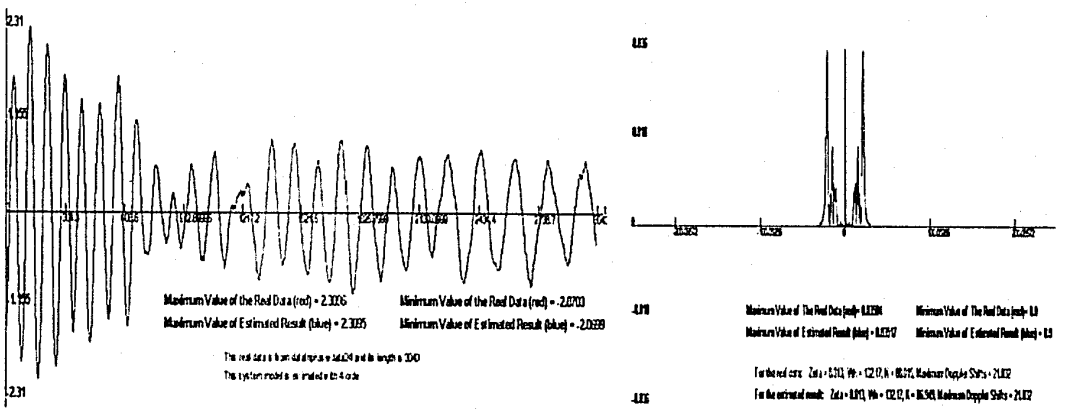

(a) Filter I(k) vs. Measured data Id(k) (b) DPSD for Filter vs. Real Data

Figure A-22. the real inphase component vs. estimate value in 2nd-order (I4.3)

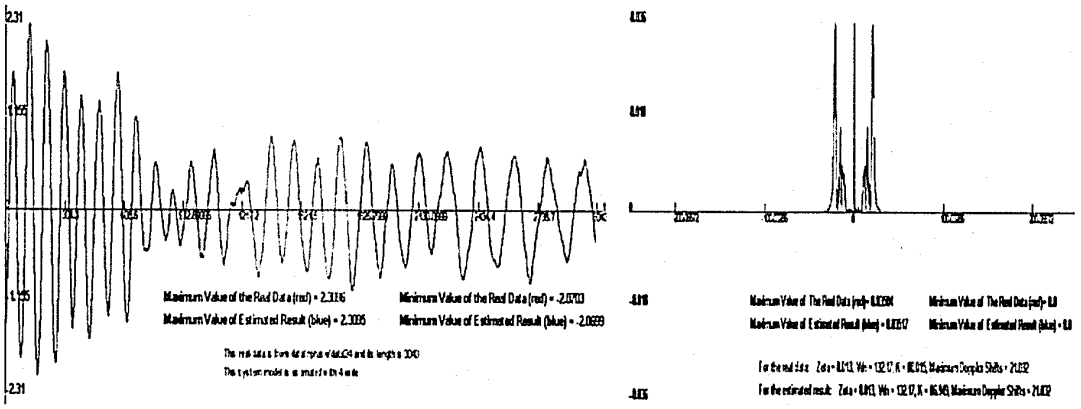

(a) Filter I(k) vs. Measured data Id(k) (b) DPSD for Filter vs. Real Data

Figure A-23. the real inphase component vs. estimate value in 3rd-order (I4.3)

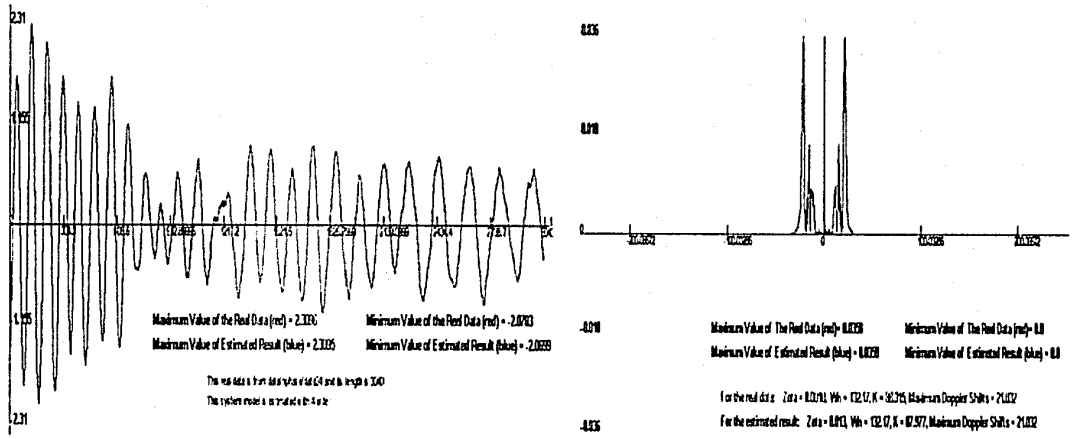

(a) Filter I(k) vs. Measured data Id(k) (b) DPSD for Filter vs. Real Data

Figure A-24. the real inphase component vs. estimate value in 4th-order (I4.3)

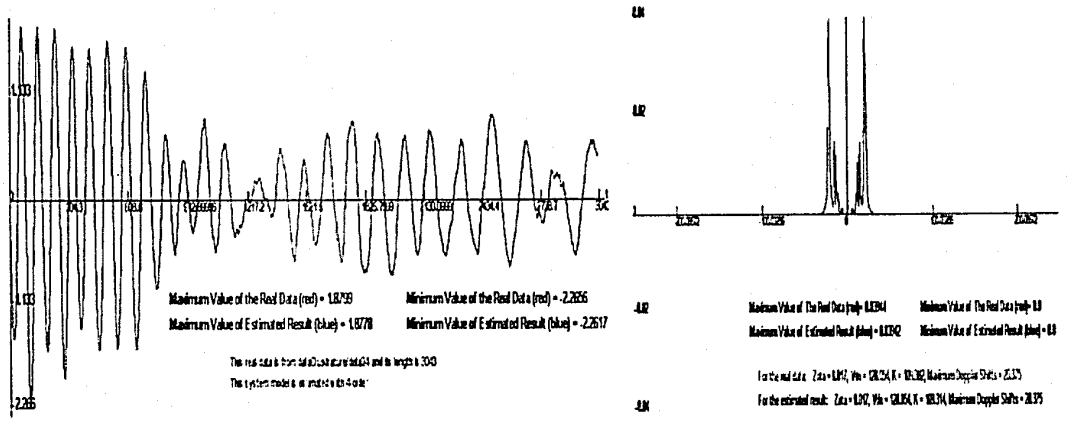

(a) Filter Q(k) vs. Measured data Qd(k) (b) DPSD for Filter vs. Real Data

Figure A-25. The real quadrature component vs. estimate result in 2nd-order (Q4.3)

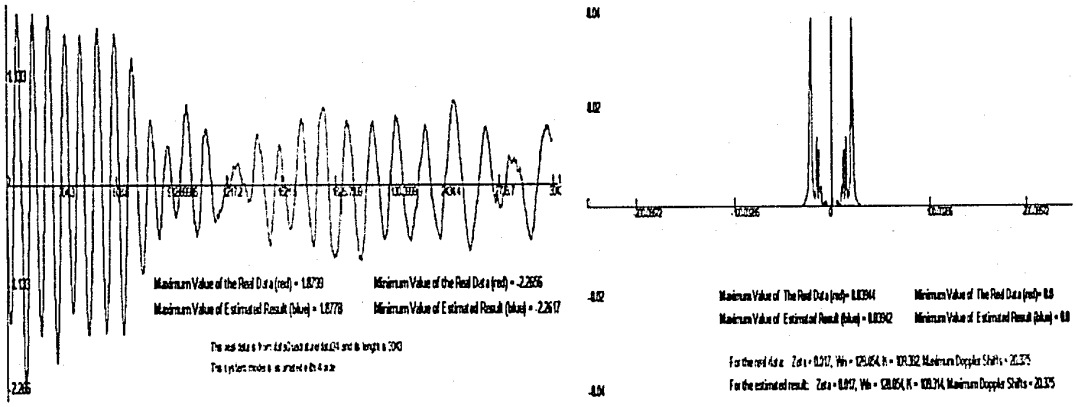

(a) Filter Q(k) vs. Measured data Id(k) (b) DPSD for Filter vs. Real Data

Figure A-26. the real quadrature component vs. estimate value in 3rd-order (Q4.3)

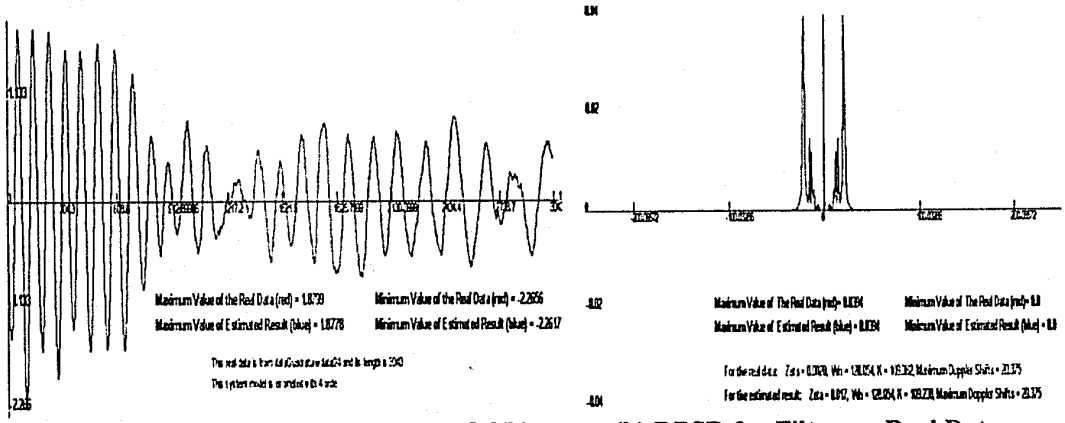

(a) Filter Q(k) vs. Measured data Qd(k) (b) DPSD for Filter vs. Real Data

Figure A-27. the real quadrature component vs. estimate value in 4th-order (Q4.3)

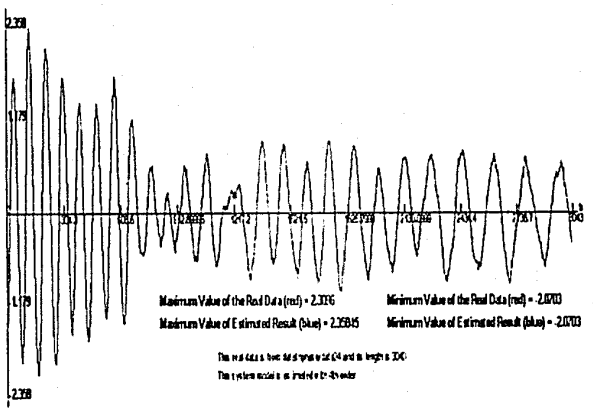

(a) Inphase Components

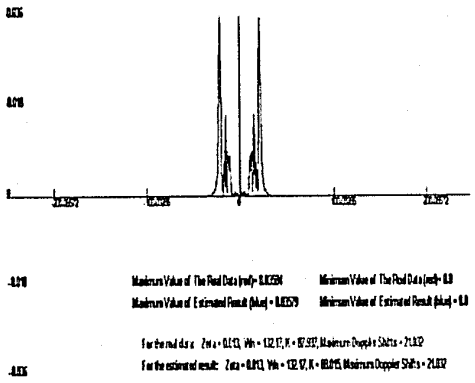

(b) DPSD for Inphase Components

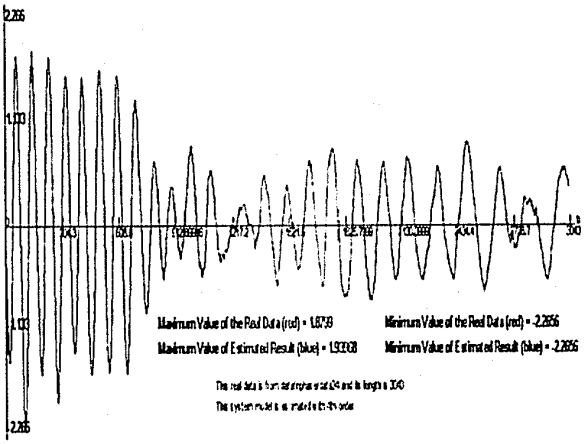

(c) Quadrature Components

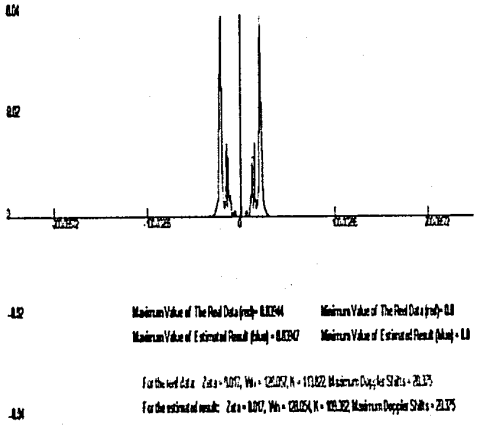

(d) DPSD for Quadrature Components

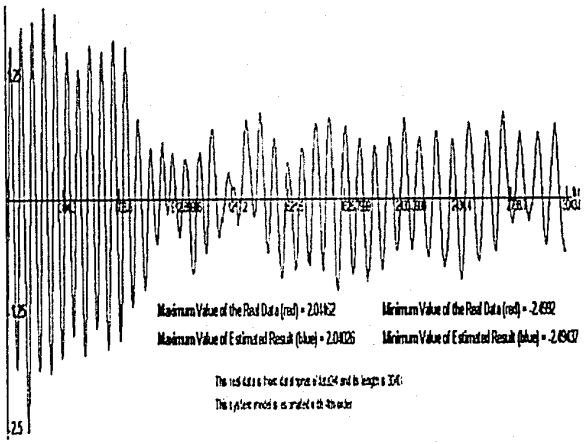

(e) Combination Components

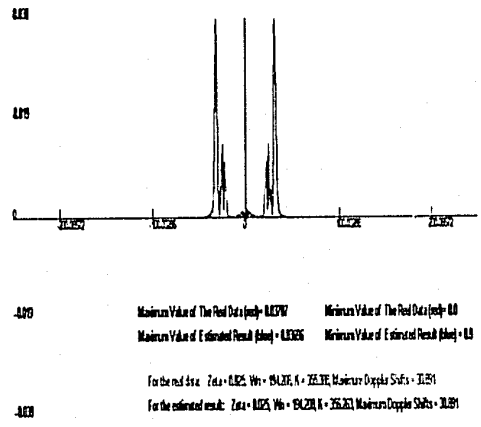

(f) DPSD for Combination Components

Figure A-28. the real inphase and quadrature components vs. estimate value in 4th-order

A.5 Estimated Results Based on the Data I5.5 and Q5.5

Table A.5: the Estimated Results from the data I5.5 and Q5.5 including 696 samples

Order		Estimated Model Parameters	Estimated Figures
I(k)	2nd	$\hat{A}=\begin{bmatrix}0 & 1\\ 1.4276 & -0.5076\end{bmatrix}$, $\hat{BB}^T=\begin{bmatrix}0.0794 & 0.0062\\ 0.0062 & 0.0145\end{bmatrix}$ $\hat{C}=[1\ \ 0]$, $\hat{DD}^T=[0.0016]$	Figure A-29
	3rd	$\hat{A}=\begin{bmatrix}0.0 & 1.0 & 0.0\\ 0.0 & 0.0 & 1.0\\ 1.4276 & -0.5721 & -0.0396\end{bmatrix}$, $\hat{BB}^T=\begin{bmatrix}0.0931 & 0.0817 & 0.0047\\ 0.0817 & 0.0959 & 0.0073\\ 0.0047 & 0.0073 & 0.0155\end{bmatrix}$ $\hat{C}=[1\ \ 0\ \ 0]$, $\hat{DD}^T=[0.0043]$	Figure A-30
	4th	$\hat{A}=\begin{bmatrix}0 & 1 & 0 & 0\\ 0 & 0 & 1 & 0\\ 0 & 0 & 0 & 1\\ 1.0719 & -0.0850 & -0.1237 & -0.0674\end{bmatrix}$, $\hat{BB}^T=\begin{bmatrix}0.3239 & 0.0010 & 0.0020 & 0.0030\\ 0.0010 & 0.1696 & 0.0020 & 0.0020\\ 0.0020 & 0.0020 & 0.0599 & 0.0010\\ 0.0030 & 0.0020 & 0.0010 & 0.0084\end{bmatrix}$ $\hat{C}=[1\ \ 0\ \ 0\ \ 0]$, $\hat{DD}^T=[0.0029]$	Figure A-31
Q(k)	2nd	$\hat{A}=\begin{bmatrix}0 & 1\\ 1.5843 & -0.6601\end{bmatrix}$, $\hat{BB}^T=\begin{bmatrix}0.0806 & 0.0161\\ 0.0161 & 0.0194\end{bmatrix}$ $\hat{C}=[1\ \ 0]$, $\hat{DD}^T=[0.0049]$	Figure A-32
	3rd	$\hat{A}=\begin{bmatrix}0.0 & 1.0 & 0.0\\ 0.0 & 0.0 & 1.0\\ 1.3309 & -1.0839 & 0.6233\end{bmatrix}$, $\hat{BB}^T=\begin{bmatrix}0.0662 & 0.0905 & 0.0104\\ 0.0905 & 0.1064 & 0.0004\\ 0.0104 & 0.0004 & 0.0125\end{bmatrix}$ $\hat{C}=[1\ \ 0\ \ 0]$, $\hat{DD}^T=[0.0025]$	Figure A-33
	4th	$\hat{A}=\begin{bmatrix}0 & 1 & 0 & 0\\ 0 & 0 & 1 & 0\\ 0 & 0 & 0 & 1\\ 1.3270 & -0.1518 & -0.2711 & -0.1788\end{bmatrix}$, $\hat{BB}^T=\begin{bmatrix}0.2611 & 0.0010 & 0.0020 & 0.0030\\ 0.0010 & 0.1621 & 0.0020 & 0.0020\\ 0.0020 & 0.0020 & 0.0602 & 0.0010\\ 0.0030 & 0.0020 & 0.0010 & 0.0196\end{bmatrix}$ $\hat{C}=[1\ \ 0\ \ 0\ \ 0]$, $\hat{DD}^T=[0.0047]$	Figure A-34
Combination		$\hat{A}=\begin{bmatrix}0 & 1 & 0 & 0\\ 08716 & -0.0194 & 0 & 0\\ 0 & 0 & 0 & 1\\ 0 & 0 & 0.8591 & -0.0478\end{bmatrix}$, $\hat{BB}^T=\begin{bmatrix}0.1256 & 0.0758 & 0.0170 & -0.0028\\ 0.0758 & 0.1203 & 0.0286 & 0.0101\\ 0.0170 & 0.0286 & 0.1046 & 0.0435\\ -0.0028 & 0.0101 & 0.0435 & 0.0767\end{bmatrix}$ $\hat{C}=[1\ \ 0\ \ 1\ \ 0]$, $\hat{DD}^T=[0.0024]$	Figure A-35

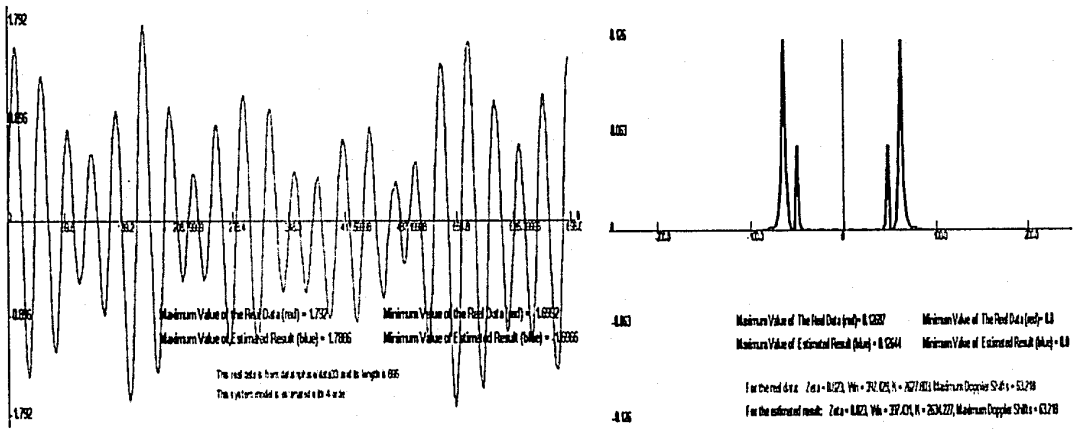

(a) Filter I(k) vs. Measured data Id(k) (b) DPSD for Filter vs. Real Data

Figure A-29. the real inphase component vs. estimate value in 2nd-order (I5.5)

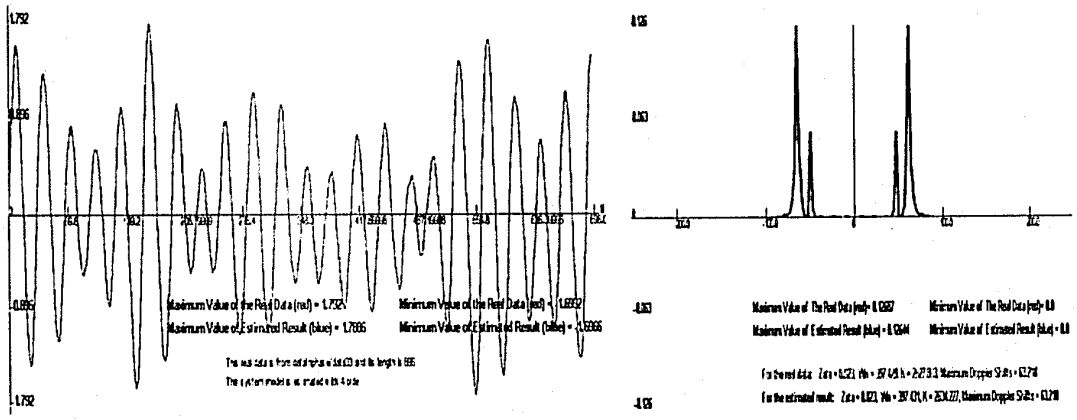

(a) Filter I(k) vs. Measured data Id(k) (b) DPSD for Filter vs. Real Data

Figure A-30. the real inphase component vs. estimate value in 3rd-order (I5.5)

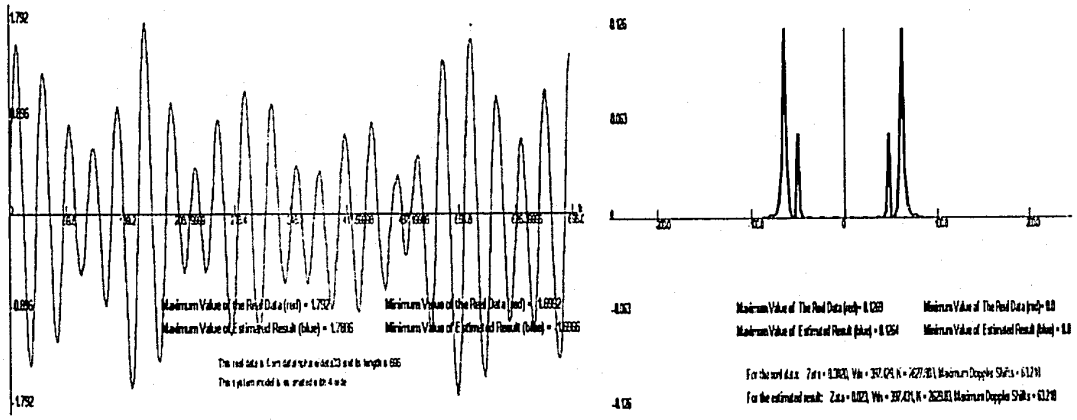

(a) Filter I(k) vs. Measured data Id(k) (b) DPSD for Filter vs. Real Data

Figure A-31. the real inphase component vs. estimate value in 4th-order (I5.5)

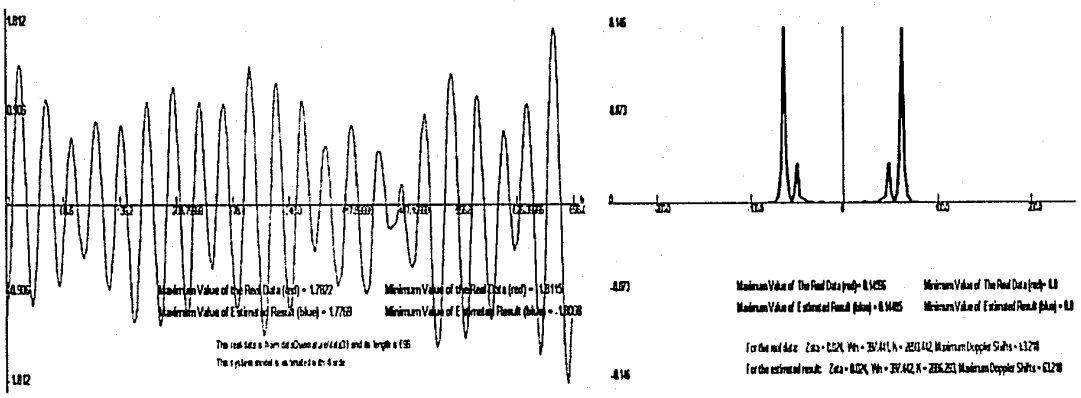

(a) Filter Q(k) vs. Measured data Qd(k) (b) DPSD for Filter vs. Real Data

Figure A-32. The real quadrature component vs. estimate result in 2nd-order (Q5.5)

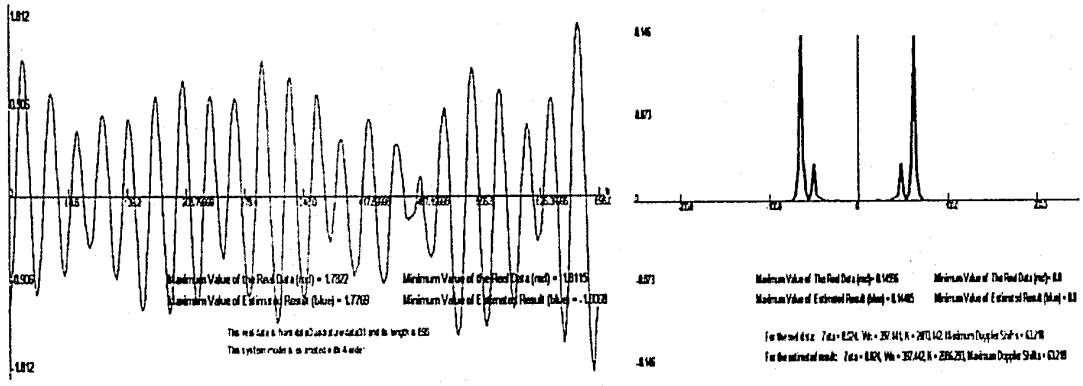

(a) Filter Q(k) vs. Measured data Id(k) (b) DPSD for Filter vs. Real Data

Figure A-33. the real quadrature component vs. estimate value in 3rd-order (Q5.5)

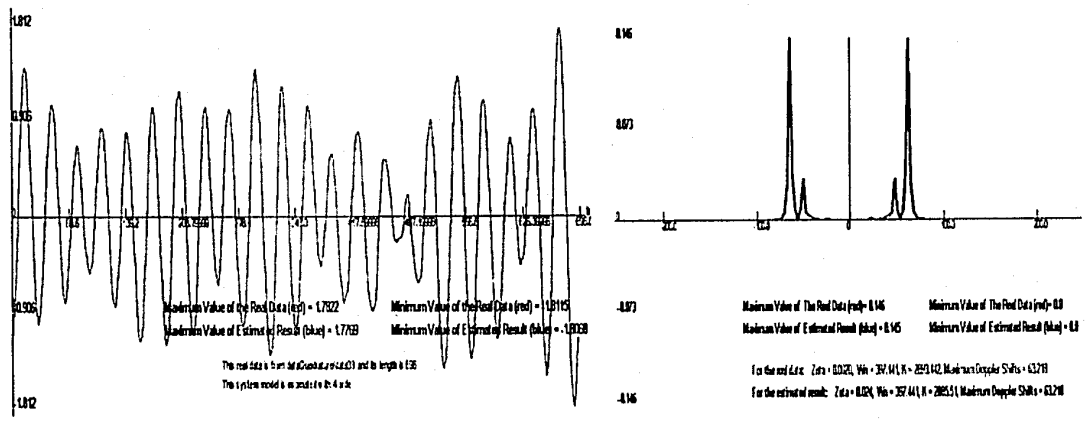

(a) Filter Q(k) vs. Measured data Qd(k) (b) DPSD for Filter vs. Real Data

Figure A-34. the real quadrature component vs. estimate value in 4th-order (Q5.5)

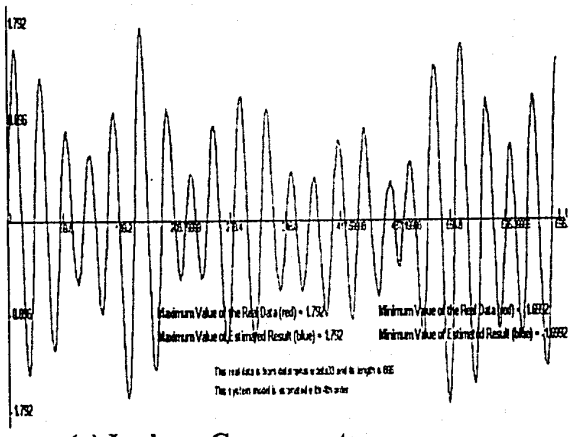

(a) Inphase Components

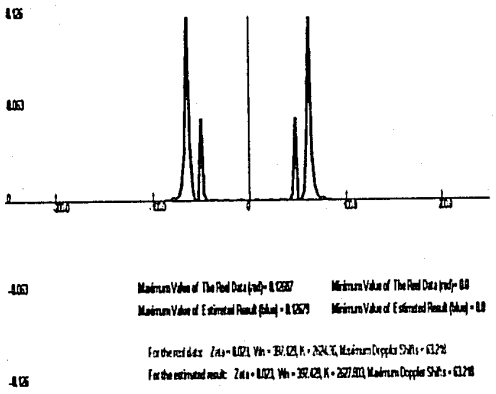

(b) DPSD for Inphase Components

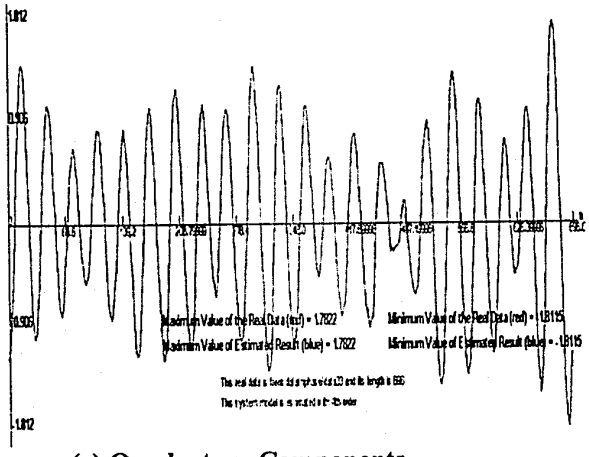

(c) Quadrature Components

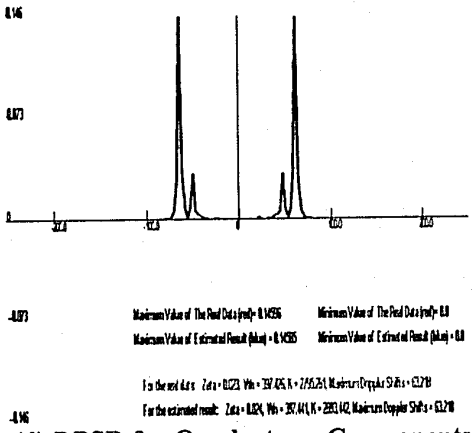

(d) DPSD for Quadrature Components

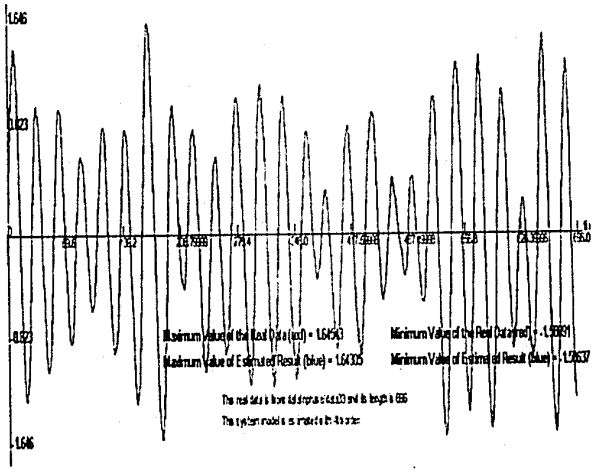

(e) Combination Components

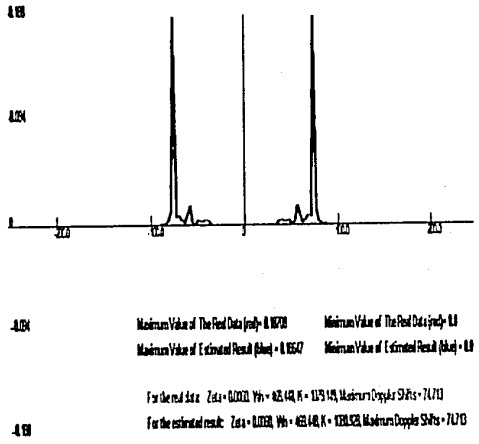

(f) DPSD for Combination Components

Figure A-35. the real inphase and quadrature components vs. estimate value in 4th-order

A.6 Estimated Results Based on the Data I6.1 and Q6.1

Table A.6: the Estimated Results from the data I6.1 and Q6.1 including 365 samples

Order		Estimated Model Parameters	Estimated Figures
I(k)	2nd	$\hat{A} = \begin{bmatrix} 0 & 1 \\ 1.4593 & -0.5285 \end{bmatrix}$, $\hat{BB}^T = \begin{bmatrix} 0.1059 & 0.0093 \\ 0.0093 & 0.0219 \end{bmatrix}$ $\hat{C} = [1 \;\; 0]$, $\hat{DD}^T = [0.0024]$	Figure A-36
	3rd	$\hat{A} = \begin{bmatrix} 0.0 & 1.0 & 0.0 \\ 0.0 & 0.0 & 1.0 \\ 1.4070 & -0.4907 & -0.0844 \end{bmatrix}$, $\hat{BB}^T = \begin{bmatrix} 0.1264 & 0.1031 & 0.0066 \\ 0.1031 & 0.1218 & 0.0116 \\ 0.0066 & 0.0116 & 0.0248 \end{bmatrix}$ $\hat{C} = [1 \;\; 0 \;\; 0]$, $\hat{DD}^T = [0.0058]$	Figure A-37
	4th	$\hat{A} = \begin{bmatrix} 0 & 1 & 0 & 0 \\ 0 & 0 & 1 & 0 \\ 0 & 0 & 0 & 1 \\ 1.2136 & -0.0917 & -0.1289 & -0.1327 \end{bmatrix}$, $\hat{BB}^T = \begin{bmatrix} 0.4199 & 0.0010 & 0.0020 & 0.0030 \\ 0.0010 & 0.2290 & 0.0020 & 0.0020 \\ 0.0020 & 0.0020 & 0.0837 & 0.0010 \\ 0.0030 & 0.0020 & 0.0010 & 0.0129 \end{bmatrix}$ $\hat{C} = [1 \;\; 0 \;\; 0 \;\; 0]$, $\hat{DD}^T = [0.0034]$	Figure A-38
Q(k)	2nd	$\hat{A} = \begin{bmatrix} 0 & 1 \\ 1.5843 & -0.6601 \end{bmatrix}$, $\hat{BB}^T = \begin{bmatrix} 0.0806 & 0.0161 \\ 0.0161 & 0.0194 \end{bmatrix}$ $\hat{C} = [1 \;\; 0]$, $\hat{DD}^T = [0.0049]$	Figure A-39
	3rd	$\hat{A} = \begin{bmatrix} 0.0 & 1.0 & 0.0 \\ 0.0 & 0.0 & 1.0 \\ 1.1139 & -0.4931 & 0.2016 \end{bmatrix}$, $\hat{BB}^T = \begin{bmatrix} 0.0759 & 0.0892 & 0.0033 \\ 0.0892 & 0.1190 & 0.0072 \\ 0.0033 & 0.0072 & 0.0145 \end{bmatrix}$ $\hat{C} = [1 \;\; 0 \;\; 0]$, $\hat{DD}^T = [0.0014]$	Figure A-40
	4th	$\hat{A} = \begin{bmatrix} 0 & 1 & 0 & 0 \\ 0 & 0 & 1 & 0 \\ 0 & 0 & 0 & 1 \\ 1.0293 & -0.0834 & -0.1152 & -0.0641 \end{bmatrix}$, $\hat{BB}^T = \begin{bmatrix} 0.3751 & 0.0010 & 0.0020 & 0.0030 \\ 0.0010 & 0.1953 & 0.0020 & 0.0020 \\ 0.0020 & 0.0020 & 0.0675 & 0.0010 \\ 0.0030 & 0.0020 & 0.0010 & 0.0099 \end{bmatrix}$ $\hat{C} = [1 \;\; 0 \;\; 0 \;\; 0]$, $\hat{DD}^T = [0.0035]$	Figure A-41
Combination		$\hat{A} = \begin{bmatrix} 0 & 1 & 0 & 0 \\ 0.9344 & -0.0509 & 0 & 0 \\ 0 & 0 & 0 & 1 \\ 0 & 0 & 0.9326 & -0.0734 \end{bmatrix}$, $\hat{BB}^T = \begin{bmatrix} 0.0959 & 0.0628 & -0.0004 & -0.0269 \\ 0.0628 & 0.0803 & 0.0202 & -0.0037 \\ -0.0004 & 0.0202 & 0.1059 & 0.0876 \\ -0.0269 & -0.0037 & 0.0876 & 0.1046 \end{bmatrix}$ $\hat{C} = [1 \;\; 0 \;\; 1 \;\; 0]$, $\hat{DD}^T = [0.0029]$	Figure A-42

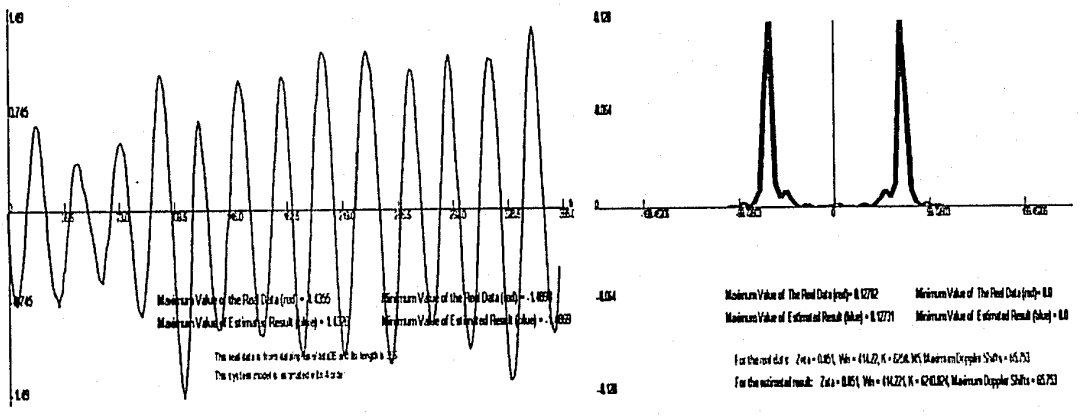

(a) Filter I(k) vs. Measured data Id(k) (b) DPSD for Filter vs. Real Data

Figure A-36. the real inphase component vs. estimate value in 2nd-order (I6.1)

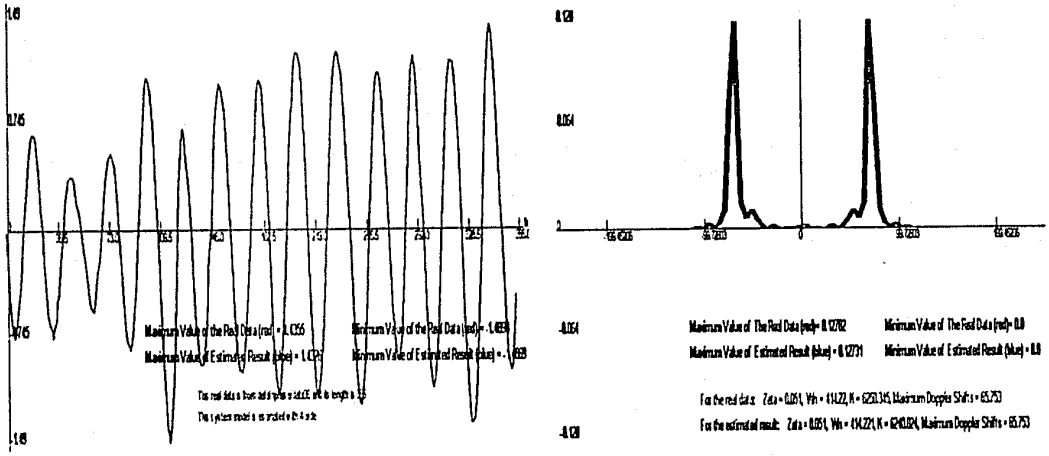

(a) Filter I(k) vs. Measured data Id(k) (b) DPSD for Filter vs. Real Data

Figure A-37. the real inphase component vs. estimate value in 3rd-order (I6.1)

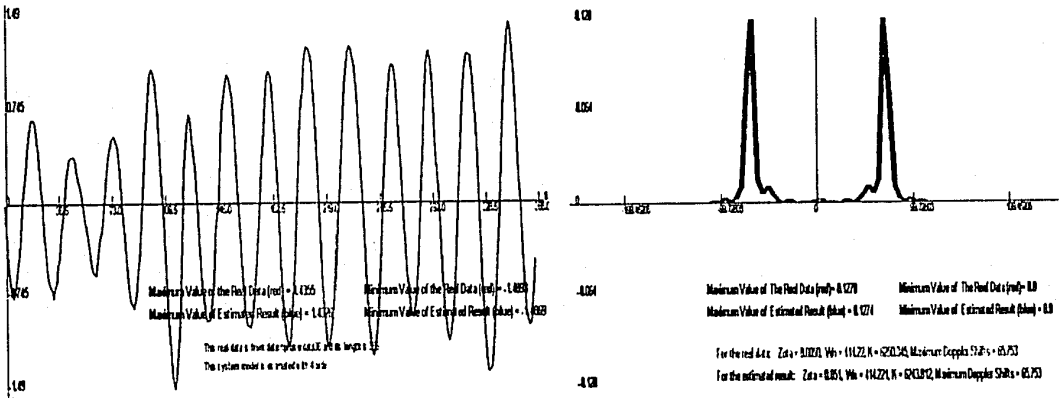

(a) Filter I(k) vs. Measured data Id(k) (b) DPSD for Filter vs. Real Data

Figure A-38. the real inphase component vs. estimate value in 4th-order (I6.1)

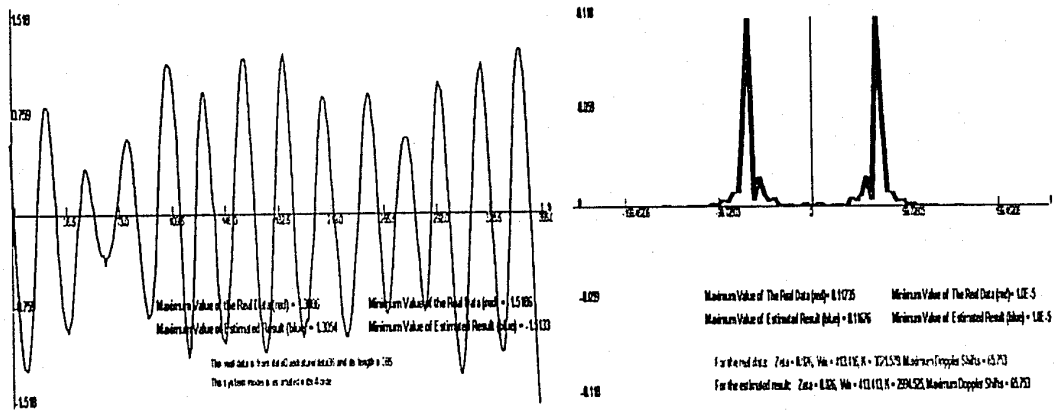

(a) Filter Q(k) vs. Measured data Qd(k) (b) DPSD for Filter vs. Real Data

Figure A-39. The real quadrature component vs. estimate result in 2nd-order (Q6.1)

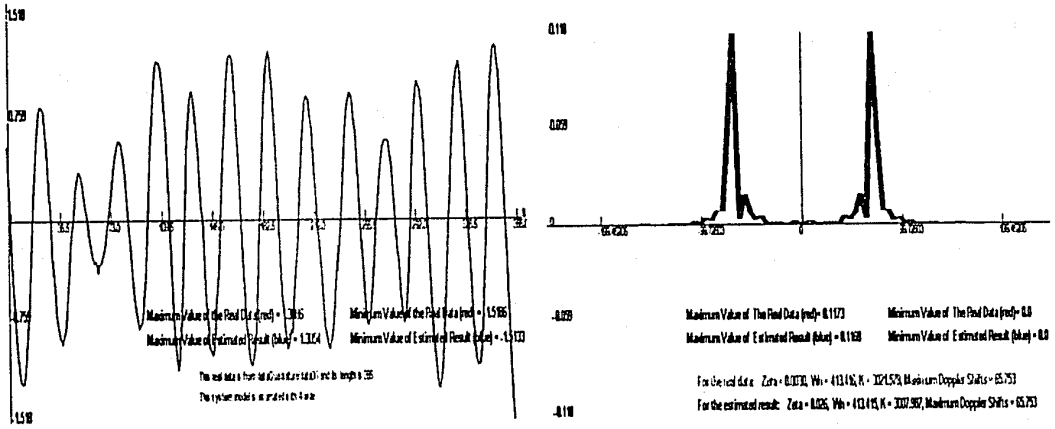

(a) Filter Q(k) vs. Measured data Id(k) (b) DPSD for Filter vs. Real Data

Figure A-40. the real quadrature component vs. estimate value in 3rd-order (Q6.1)

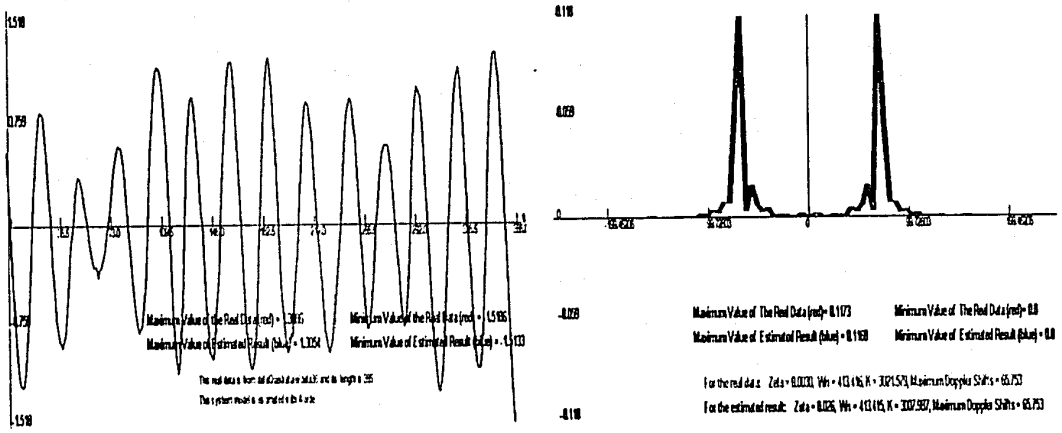

(a) Filter Q(k) vs. Measured data Qd(k) (b) DPSD for Filter vs. Real Data

Figure A-41. the real quadrature component vs. estimate value in 4th-order (Q6.1)

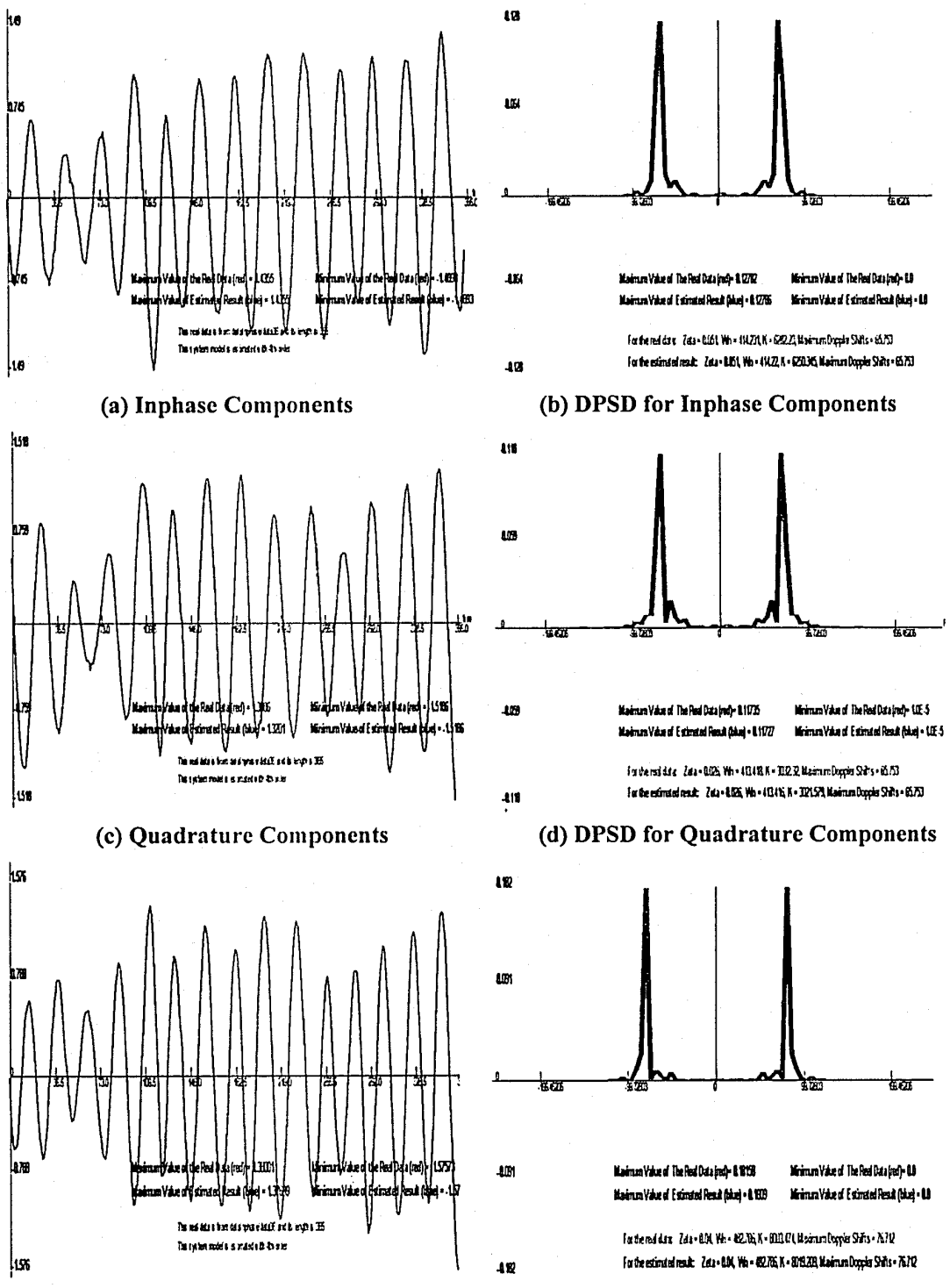

(a) Inphase Components

(b) DPSD for Inphase Components

(c) Quadrature Components

(d) DPSD for Quadrature Components

(e) Combination Components

(f) DPSD for Combination Components

Figure A-42. the real inphase and quadrature components vs. estimate value in 4th-order

A.7 Estimated Results Based on the Data I7.7 and Q7.7

Table A.7: the Estimated Results from the data I7.7 and Q7.7 including 1407 samples

Order		Estimated Model Parameters	Estimated Figures
I(k)	2nd	$\hat{A}=\begin{bmatrix}0 & 1\\ 1.3028 & -0.3431\end{bmatrix}$, $\hat{BB}^T=\begin{bmatrix}0.2128 & 0.0102\\ 0.0102 & 0.0394\end{bmatrix}$ $\hat{C}=[1\ \ 0]$, $\hat{DD}^T=[0.0029]$	Figure A-43
	3rd	$\hat{A}=\begin{bmatrix}0.0 & 1.0 & 0.0\\ 0.0 & 0.0 & 1.0\\ 1.3048 & -0.7369 & 0.3382\end{bmatrix}$, $\hat{BB}^T=\begin{bmatrix}0.1522 & 0.0214 & 0.0096\\ 0.0214 & 0.3112 & 0.0176\\ 0.0096 & 0.0176 & 0.0364\end{bmatrix}$ $\hat{C}=[1\ \ 0\ \ 0]$, $\hat{DD}^T=[0.0026]$	Figure A-44
	4th	$\hat{A}=\begin{bmatrix}0 & 1 & 0 & 0\\ 0 & 0 & 1 & 0\\ 0 & 0 & 0 & 1\\ 1.0578 & -0.0957 & -0.1299 & -0.1252\end{bmatrix}$, $\hat{BB}^T=\begin{bmatrix}0.7468 & 0.0010 & 0.0020 & 0.0030\\ 0.0010 & 0.3895 & 0.0020 & 0.0020\\ 0.0020 & 0.0020 & 0.1406 & 0.0010\\ 0.0030 & 0.0020 & 0.0010 & 0.0232\end{bmatrix}$ $\hat{C}=[1\ \ 0\ \ 0\ \ 0]$, $\hat{DD}^T=[0.0055]$	Figure A-45
Q(k)	2nd	$\hat{A}=\begin{bmatrix}0 & 1\\ 1.3061 & -0.3476\end{bmatrix}$, $\hat{BB}^T=\begin{bmatrix}0.2217 & 0.0189\\ 0.0189 & 0.0378\end{bmatrix}$ $\hat{C}=[1\ \ 0]$, $\hat{DD}^T=[0.0023]$	Figure A-46
	3rd	$\hat{A}=\begin{bmatrix}0.0 & 1.0 & 0.0\\ 0.0 & 0.0 & 1.0\\ 1.3236 & -0.7503 & 0.3298\end{bmatrix}$, $\hat{BB}^T=\begin{bmatrix}0.1699 & 0.0208 & 0.0073\\ 0.0208 & 0.2822 & 0.0068\\ 0.0073 & 0.0068 & 0.0352\end{bmatrix}$ $\hat{C}=[1\ \ 0\ \ 0]$, $\hat{DD}^T=[0.0032]$	Figure A-47
	4th	$\hat{A}=\begin{bmatrix}0 & 1 & 0 & 0\\ 0 & 0 & 1 & 0\\ 0 & 0 & 0 & 1\\ 1.1442 & -0.1154 & -0.1525 & -0.1478\end{bmatrix}$, $\hat{BB}^T=\begin{bmatrix}0.7246 & 0.0010 & 0.0020 & 0.0030\\ 0.0010 & 0.3892 & 0.0020 & 0.0020\\ 0.0020 & 0.0020 & 0.1454 & 0.0010\\ 0.0030 & 0.0020 & 0.0010 & 0.0284\end{bmatrix}$ $\hat{C}=[1\ \ 0\ \ 0\ \ 0]$, $\hat{DD}^T=[0.0055]$	Figure A-48
Combination		$\hat{A}=\begin{bmatrix}0 & 1 & 0 & 0\\ 0.8697 & -0.0320 & 0 & 0\\ 0 & 0 & 0 & 1\\ 0 & 0 & 0.8632 & -0.0612\end{bmatrix}$, $\hat{BB}^T=\begin{bmatrix}0.2632 & 0.1733 & 0.0232 & -0.0194\\ 0.1733 & 0.2499 & 0..0399 & 0.0035\\ 0.0232 & 0.0399 & 0.2429 & 0..1074\\ -0.0194 & 0.0035 & 0.1074 & 0.1787\end{bmatrix}$ $\hat{C}=[1\ \ 0\ \ 1\ \ 0]$, $\hat{DD}^T=[0.0021]$	Figure A-49

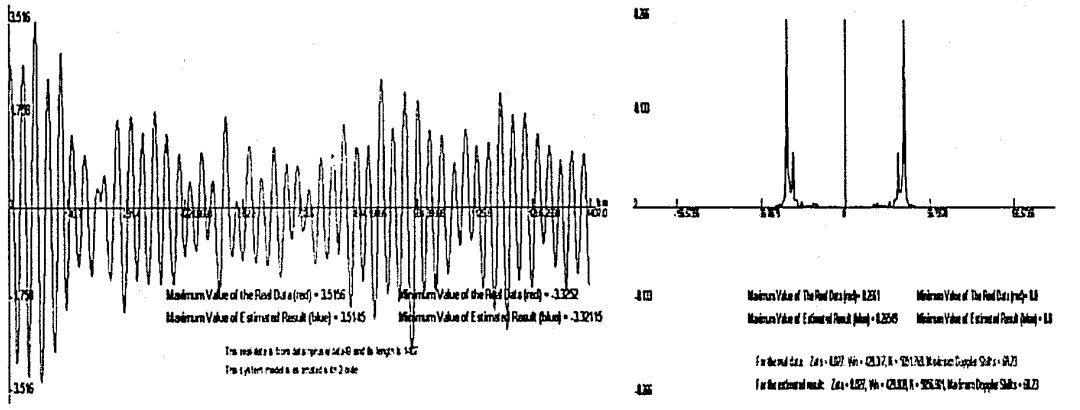

(a) Filter I(k) vs. Measured data Id(k) (b) DPSD for Filter vs. Real Data

Figure A-43. the real inphase component vs. estimate value in 2nd-order (I7.7)

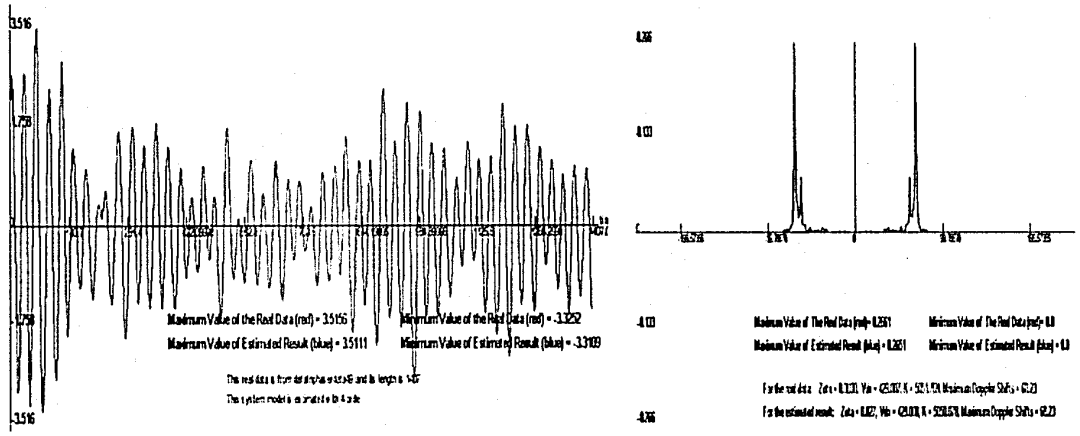

(a) Filter I(k) vs. Measured data Id(k) (b) DPSD for Filter vs. Real Data

Figure A-44. the real inphase component vs. estimate value in 3rd-order (I7.7)

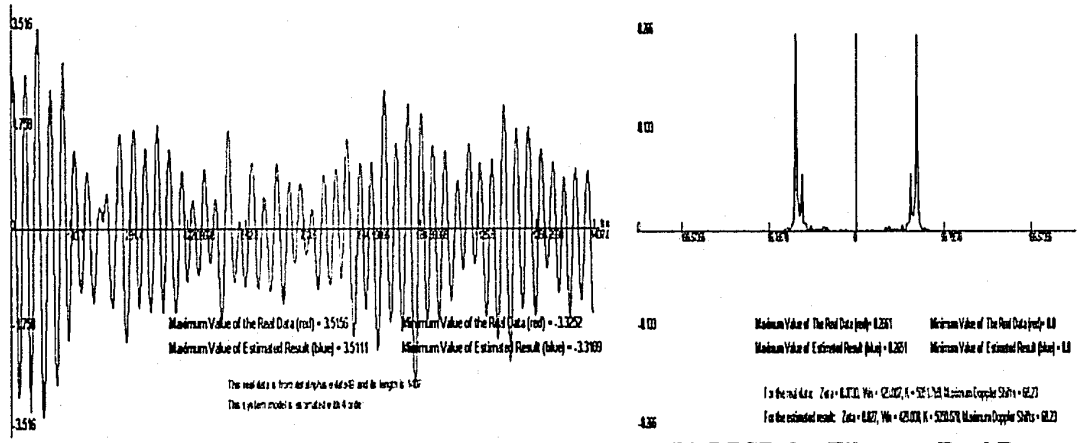

(a) Filter I(k) vs. Measured data Id(k) (b) DPSD for Filter vs. Real Data

Figure A-45. the real inphase component vs. estimate value in 4th-order (I7.7)

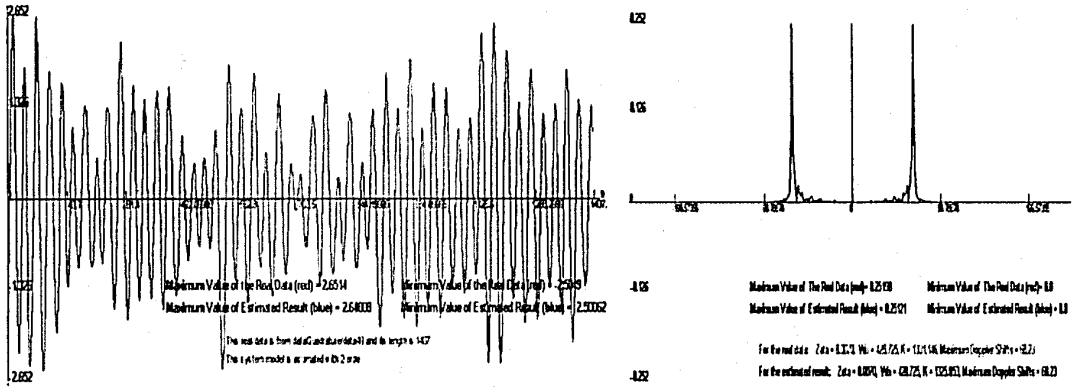

(a) Filter Q(k) vs. Measured data Qd(k) (b) DPSD for Filter vs. Real Data

Figure A-46. The real quadrature component vs. estimate result in 2nd-order (Q7.7)

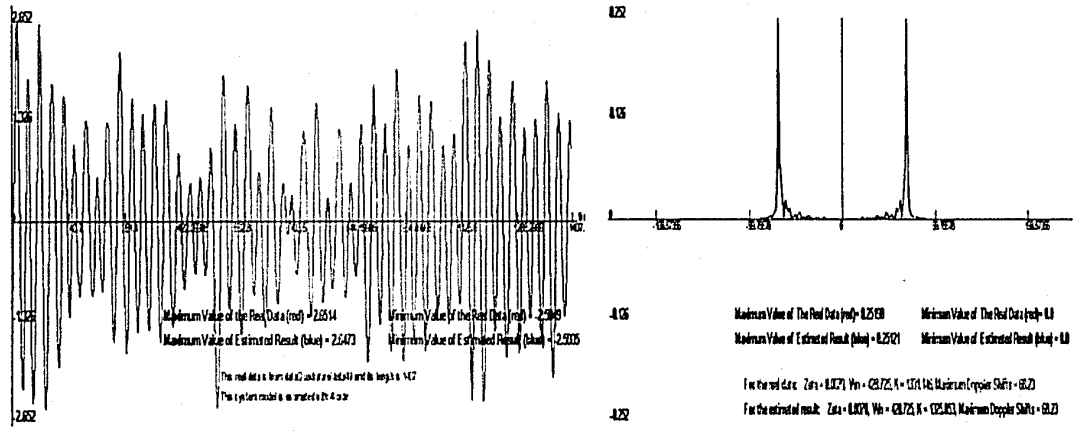

(a) Filter Q(k) vs. Measured data Qd(k) (b) DPSD for Filter vs. Real Data

Figure A-47. the real quadrature component vs. estimate value in 3rd-order (Q7.7)

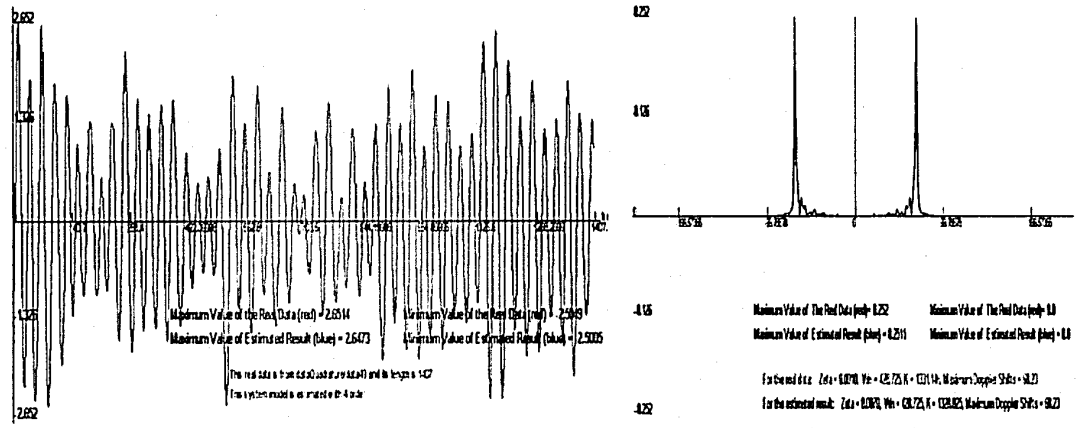

(a) Filter Q(k) vs. Measured data Qd(k) (b) DPSD for Filter vs. Real Data

Figure A-48. the real quadrature component vs. estimate value in 4th-order (Q7.7)

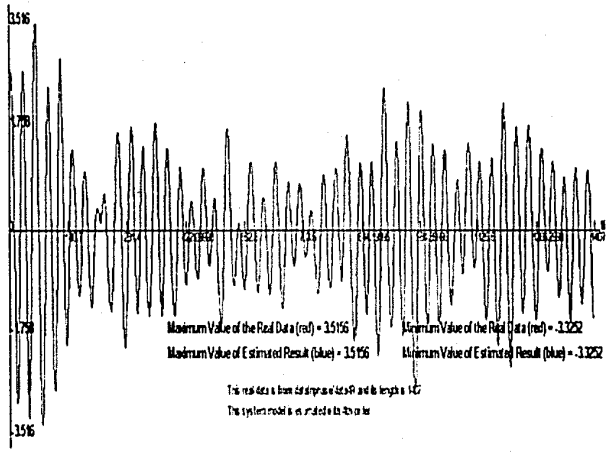

(a) Inphase Components

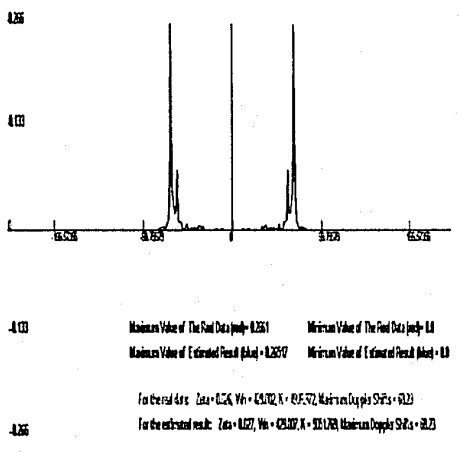

(b) DPSD for Inphase Components

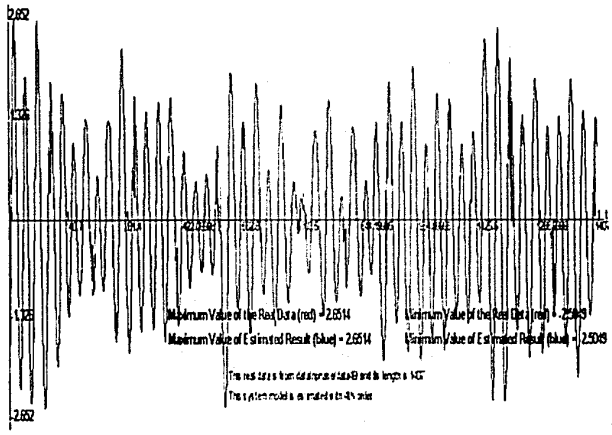

(c) Quadrature Components

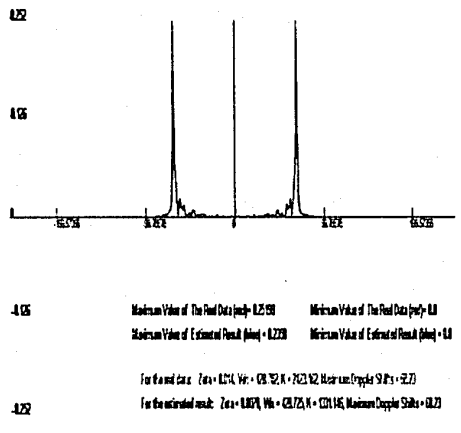

(d) DPSD for Quadrature Components

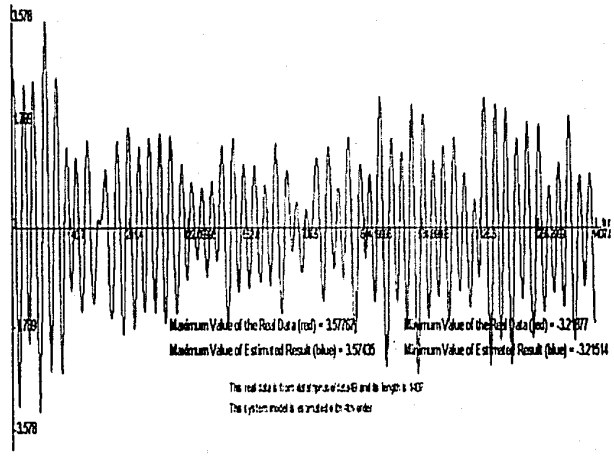

(e) Combination Components

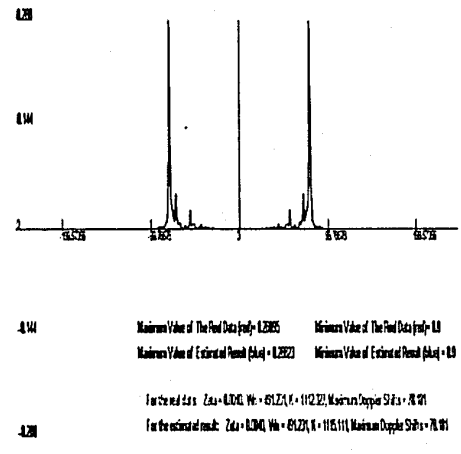

(f) DPSD for Combination Components

Figure A-49. the real inphase and quadrature components vs. estimate value in 4th-order

Appendix B

System Identification Results for Frequency-Selective Fading Channels Based on the Measurement Data

Subsection 3.5 descried the mathematical models and the estimated results for the frequency-selective fading channel models. This appendix shows many system identified esults based on the measurement data. Similarly, these models are considered the fast fading and the slow fading; the transmitted signal can be a wideband signal or a narrowband signal.

B.1 System Identification Estimated Result for N = 2 Case

In this case, the inphase and quadrature components are considered combination with two paths, and the measurement data is selected from the data group 1 including 655 samples.

(1) Wide Band Transmitted Signal

Considered the transmitted signal is a wide band signal, the estimated system parameters are computed as following:

$$\hat{A} = \begin{bmatrix} \hat{A}_1 & 0 \\ 0 & \hat{A}_2 \end{bmatrix}, \quad \hat{BB}^T = \begin{bmatrix} \hat{BB}_1^T & 0 \\ 0 & \hat{BB}_2^T \end{bmatrix}, \quad \hat{C} = \begin{bmatrix} \hat{C}_1 & \hat{C}_2 \end{bmatrix}, \quad \hat{DD}^T = 0.0027$$

Here, $\left\{ \hat{A}_i, \hat{BB}_i^T, \hat{C}_i \right\}$ are defined as the following:

$$\hat{A}_1 = \begin{bmatrix} 0 & 1 & 0 & 0 \\ 0.1760 & -0.0521 & 0 & 0 \\ 0 & 0 & 0 & 1 \\ 0 & 0 & 0.1239 & -0.0802 \end{bmatrix}, \quad \hat{A}_2 = \begin{bmatrix} 0 & 1 & 0 & 0 \\ 0.1579 & 0.0639 & 0 & 0 \\ 0 & 0 & 0 & 1 \\ 0 & 0 & -0.1522 & 0.0336 \end{bmatrix}$$

$$\hat{BB}_1^T = \begin{bmatrix} 0.0766 & 0.0049 & 0.0121 & 0.0039 \\ 0.0049 & 0.1384 & 0.0168 & -0.0167 \\ 0.0121 & 0.0168 & 0.0765 & 0.0047 \\ 0.0039 & -0.0167 & 0.0047 & 0.1870 \end{bmatrix}, \quad \hat{BB}_2^T = \begin{bmatrix} 0.1697 & 0.0018 & 0.0021 & 0.0073 \\ 0.0018 & 0.1868 & 0.0106 & -0.0032 \\ 0.0021 & 0.0106 & 0.0854 & 0.0036 \\ 0.0073 & -0.0032 & 0.0036 & 0.0583 \end{bmatrix}$$

$$\hat{C}_1 = \hat{C}_2 = \begin{bmatrix} 1 & 0 & 1 & 0 \end{bmatrix}$$

Figure B-1 shows the compared results between the measurement data and the estimated results on each path.

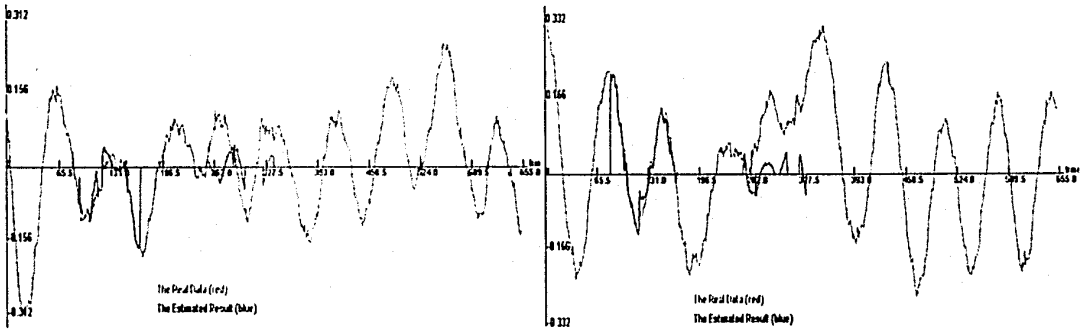

(a) Inphase Components on 1st path **(b) Quadrature Components on 1st path**

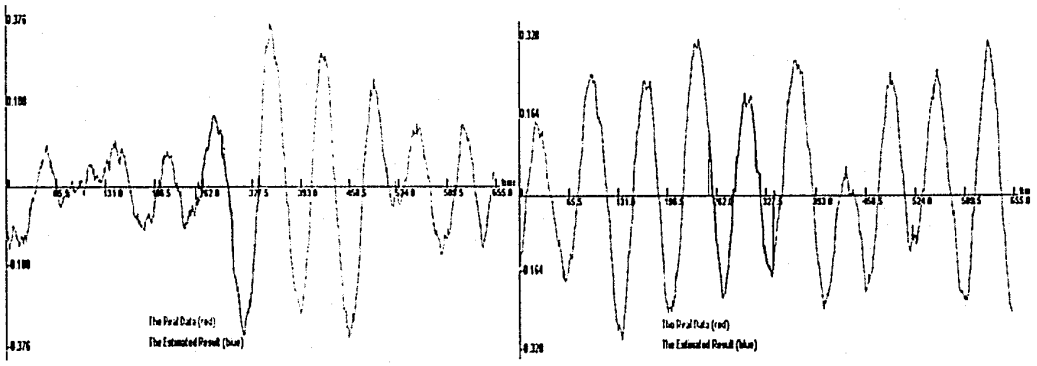

(c) Inphase Components on 2nd path **(d) Quadrature Components on 2nd path**

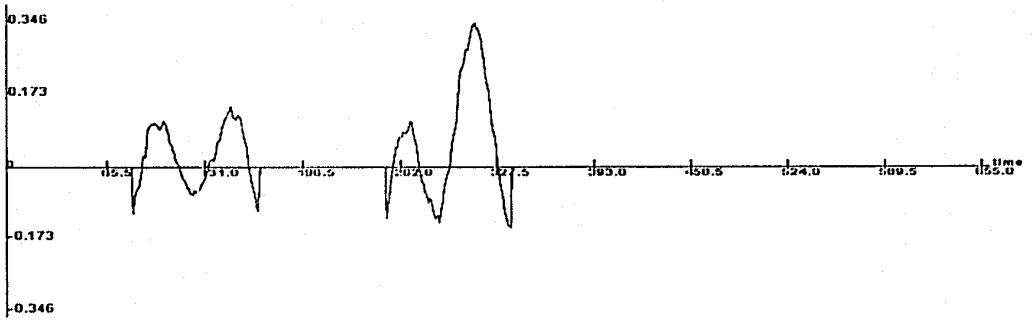

(e) the Output Sequences

Figure B-1. the Estimated Results for Frequency-selective Fading Channel (N=2 case) On the Wide Band Transmitted Signal

(2) Narrow Band Transmitted Signal

Considered the transmitted signal is a narrow band signal, the estimated system parameters are computed as following:

$$\hat{A} = \begin{bmatrix} \hat{A}_1 & 0 \\ 0 & \hat{A}_2 \end{bmatrix}, \quad \hat{BB}^T = \begin{bmatrix} \hat{BB}_1^T & 0 \\ 0 & \hat{BB}_2^T \end{bmatrix}, \quad \hat{C} = \begin{bmatrix} \hat{C}_1 & \hat{C}_2 \end{bmatrix}, \quad \hat{DD}^T = 0.0026$$

Here, $\left\{ \hat{A}_i, \hat{BB}_i^T, \hat{C}_i \right\}$ are defined as the following:

$$\hat{A}_1 = \begin{bmatrix} 0 & 1 & 0 & 0 \\ 0.1508 & -0.0809 & 0 & 0 \\ 0 & 0 & 0 & 1 \\ 0 & 0 & 0.1464 & -0.0692 \end{bmatrix}, \quad \hat{A}_2 = \begin{bmatrix} 0 & 1 & 0 & 0 \\ 0.2014 & 0.0853 & 0 & 0 \\ 0 & 0 & 0 & 1 \\ 0 & 0 & -0.1415 & 0.0358 \end{bmatrix}$$

$$\hat{BB}_1^T = \begin{bmatrix} 0.0734 & 0.0014 & 0.0101 & 0.0032 \\ 0.0014 & 0.1279 & 0.0136 & -0.0203 \\ 0.0101 & 0.0136 & 0.0755 & 0.0051 \\ 0.0033 & -0.0203 & 0.0051 & 0.1860 \end{bmatrix}, \quad \hat{BB}_2^T = \begin{bmatrix} 0.1715 & 0.0050 & 0.0029 & 0.0077 \\ 0.0050 & 0.1922 & 0.0122 & -0.0027 \\ 0.0029 & 0.0122 & 0.0867 & 0.0043 \\ 0.0077 & -0.0027 & 0.0043 & 0.0588 \end{bmatrix}$$

$$\hat{C}_1 = \hat{C}_2 = \begin{bmatrix} 1 & 0 & 1 & 0 \end{bmatrix}$$

Figure B-2 shows the compared results between the measurement data and the estimated results on each path.

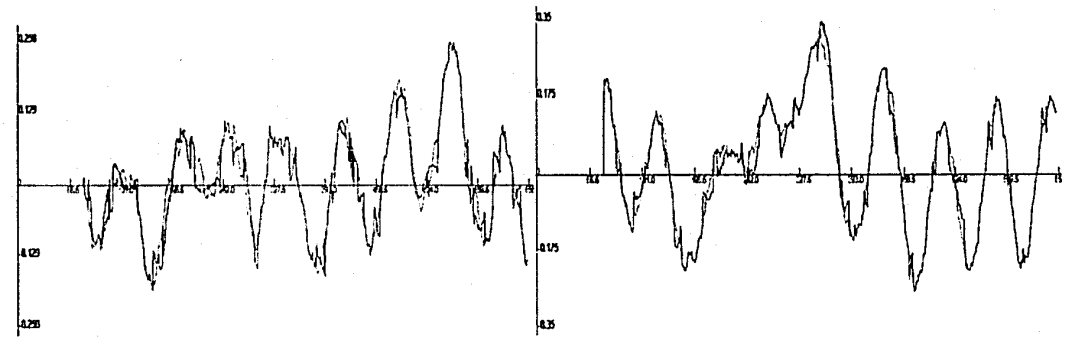

(a) Inphase Components on 1st path (b) Quadrature Components on 1st path

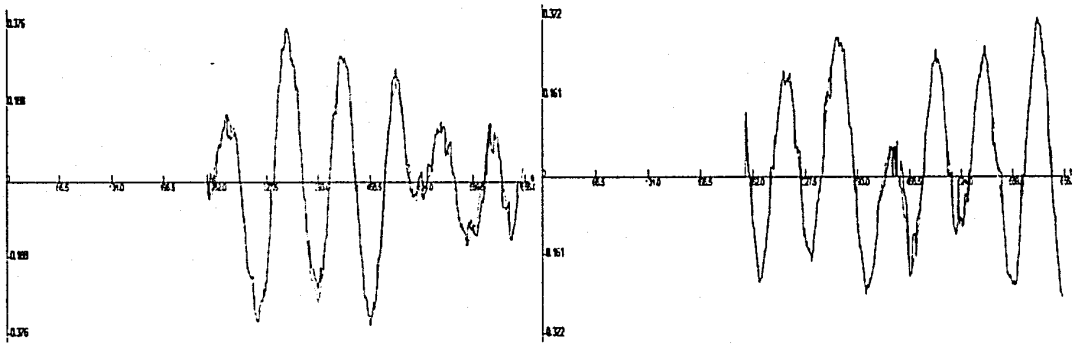

(c) Inphase Components on 2nd path (d) Quadrature Components on 2nd path

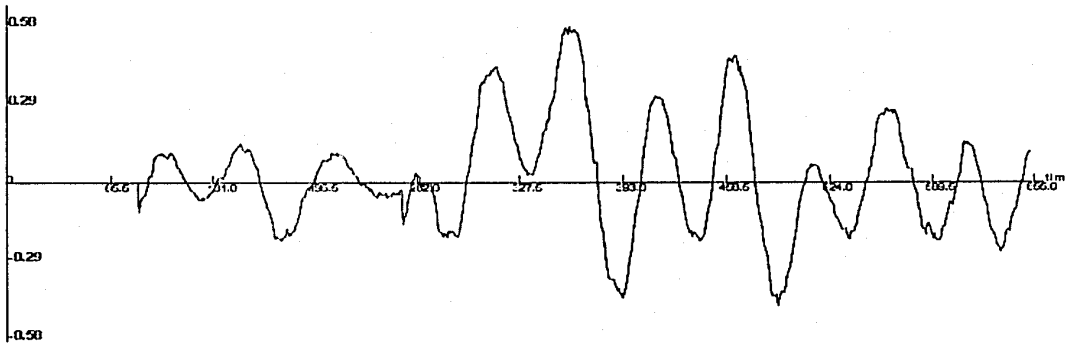

(e) the Output Sequences

Figure B-2. the Estimated Results for Frequency-selective Fading Channel (N=2 case) On the Narrow Band Signal

(3) Slow Fading with Narrow Band Transmitted Signal

The estimated system parameters of the frequency-selective slow fading are expressed as following:

$$\hat{A} = \begin{bmatrix} \hat{A}_1 & 0 \\ 0 & \hat{A}_2 \end{bmatrix}, \quad \hat{BB}^T = \begin{bmatrix} \hat{BB}_1^T & 0 \\ 0 & \hat{BB}_2^T \end{bmatrix}, \quad \hat{C} = \begin{bmatrix} \hat{C}_1 & \hat{C}_2 \end{bmatrix}, \quad \hat{DD}^T = 0.0019$$

Here, $\left\{ \hat{A}_i, \hat{BB}_i^T, \hat{C}_i \right\}$ are defined as the following:

$$\hat{A}_1 = \begin{bmatrix} 0 & 1 & 0 & 0 \\ 0.2549 & -0.1018 & 0 & 0 \\ 0 & 0 & 0 & 1 \\ 0 & 0 & 0.1735 & -0.1485 \end{bmatrix}, \quad \hat{A}_2 = \begin{bmatrix} 0 & 1 & 0 & 0 \\ 0.0846 & 0.0133 & 0 & 0 \\ 0 & 0 & 0 & 1 \\ 0 & 0 & -0.1473 & 0.0081 \end{bmatrix}$$

$$\hat{BB}_1^T = \begin{bmatrix} -0.0673 & 0.0299 & 0.0476 & 0.0061 \\ 0.0299 & 0.2210 & 0.0305 & -0.0801 \\ 0.0476 & 0.0305 & 0.0812 & 0.0139 \\ 0.0061 & -0.0801 & 0.0139 & 0.4621 \end{bmatrix}, \quad \hat{BB}_2^T = \begin{bmatrix} 0.6194 & 0.0118 & -0.1732 & -0.0269 \\ 0.0118 & 0.3195 & 0.0326 & 0.0106 \\ -0.1732 & 0.0326 & 0.1438 & 0.0236 \\ -0.0269 & 0.0106 & 0.0236 & 0.0845 \end{bmatrix}$$

$$\hat{C}_1 = \hat{C}_2 = \begin{bmatrix} 1 & 0 & 1 & 0 \end{bmatrix}$$

Figure B-3 shows the compared results between the measurement data and the estimated results on each path for the frequency-selective slow fading.

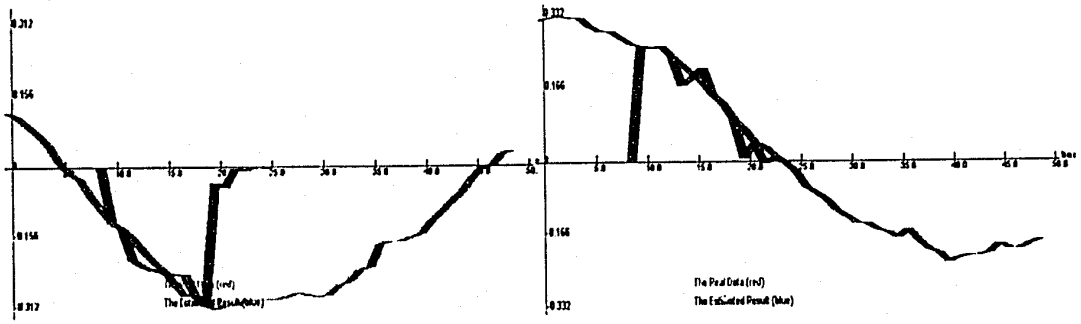

(a) Inphase Components on 1st path **(b) Quadrature Components on 1st path**

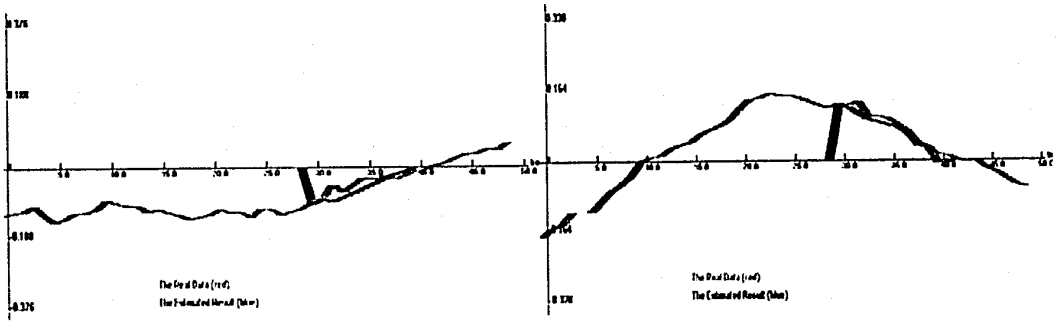

(c) Inphase Components on 2nd path **(d) Quadrature Components on 2nd path**

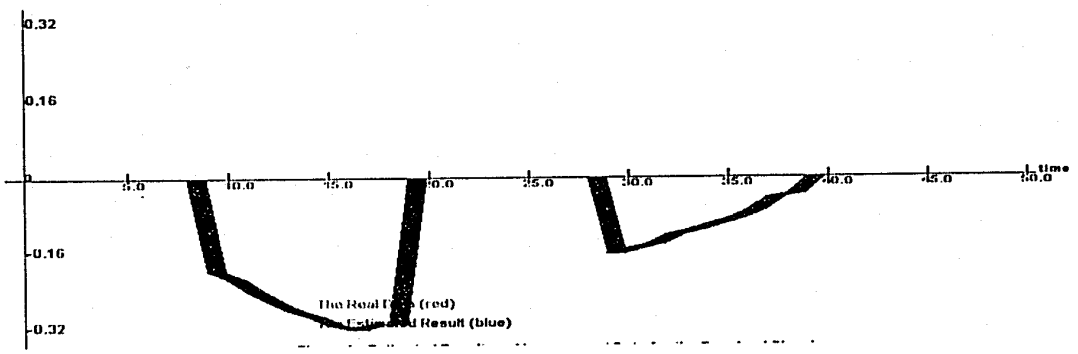

(c) the Output Sequences

Figure B-3. the Estimated Results for Frequency-selective Slow Fading Channel (N=2 case)

B.2 System Identification Estimated Result for N = 3 Case

In this case, the inphase and quadrature components are considered to contain three paths, and the measurement data is selected from the data group 3 with 554 samples.

(1) Wide Band Transmitted Signal

Considered the transmitted signal is a narrow band signal, the estimated system parameters are computed as following:

$$\hat{A} = \begin{bmatrix} \hat{A}_1 & 0 & 0 \\ 0 & \hat{A}_2 & 0 \\ 0 & 0 & \hat{A}_3 \end{bmatrix}, \quad \hat{BB}^T = \begin{bmatrix} \hat{BB}_1^T & 0 & 0 \\ 0 & \hat{BB}_2^T & 0 \\ 0 & 0 & \hat{BB}_3^T \end{bmatrix}, \quad \hat{C} = \begin{bmatrix} \hat{C}_1 & \hat{C}_2 & \hat{C}_3 \end{bmatrix}, \quad \hat{DD}^T = 0.0018$$

In addition,

$$\hat{A}_1 = \begin{bmatrix} 0 & 1 & 0 & 0 \\ 0.1846 & -0.0555 & 0 & 0 \\ 0 & 0 & 0 & 1 \\ 0 & 0 & 0.1269 & -0.0879 \end{bmatrix}, \quad \hat{A}_2 = \begin{bmatrix} 0 & 1 & 0 & 0 \\ 0.1344 & 0.0663 & 0 & 0 \\ 0 & 0 & 0 & 1 \\ 0 & 0 & -0.1512 & 0.0535 \end{bmatrix}$$

$$\hat{A}_3 = \begin{bmatrix} 0 & 1 & 0 & 0 \\ 0.1807 & -0.0573 & 0 & 0 \\ 0 & 0 & 0 & 1 \\ 0 & 0 & 0.1815 & -0.2169 \end{bmatrix}, \quad \hat{BB}_1^T = \begin{bmatrix} 0.0808 & 0.0059 & 0.0139 & 0.0043 \\ 0.0059 & 0.1556 & 0.0191 & -0.0264 \\ 0.0139 & 0.0191 & 0.0814 & 0.0068 \\ 0.0043 & -0.0264 & 0.0068 & 0.2417 \end{bmatrix},$$

$$\hat{BB}_2^T = \begin{bmatrix} 0.1819 & 0.0006 & 0.0069 & 0.0094 \\ 0.0006 & 0.2147 & 0.0158 & -0.0057 \\ 0.0069 & 0.0158 & 0.1284 & 0.0056 \\ 0.0094 & -0.0057 & 0.0056 & 0.0691 \end{bmatrix}, \quad \hat{BB}_3^T = \begin{bmatrix} 0.1447 & 0.0081 & 0.0066 & 0.0009 \\ 0.0081 & 0.1903 & 0.0056 & -0.0044 \\ 0.0066 & 0.0056 & 0.1066 & 0.0063 \\ 0.0009 & -0.0044 & 0.0063 & 0.1050 \end{bmatrix}$$

$$\hat{C}_1 = \hat{C}_2 = \hat{C}_3 = \begin{bmatrix} 1 & 0 & 1 & 0 \end{bmatrix}$$

Figure B-4 shows the compared results between the measurement data and the estimated results on each path for a wide band transmitted signal.

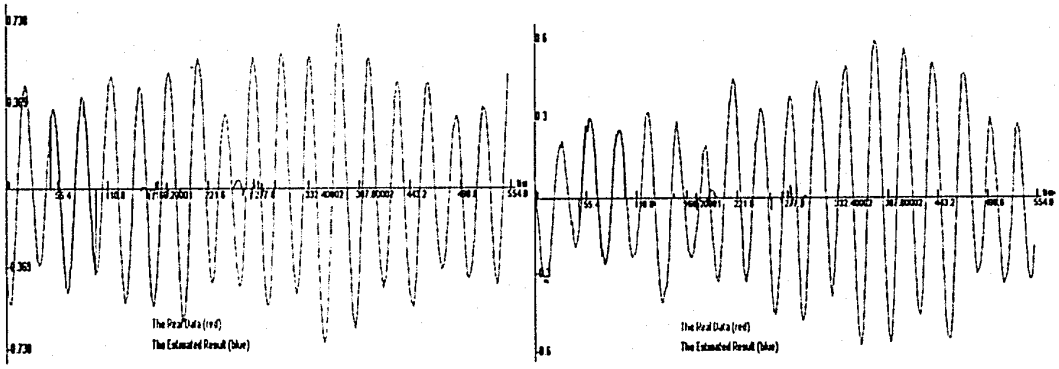

(a) Inphase Components on 1st path (b) Quadrature Components on 1st path

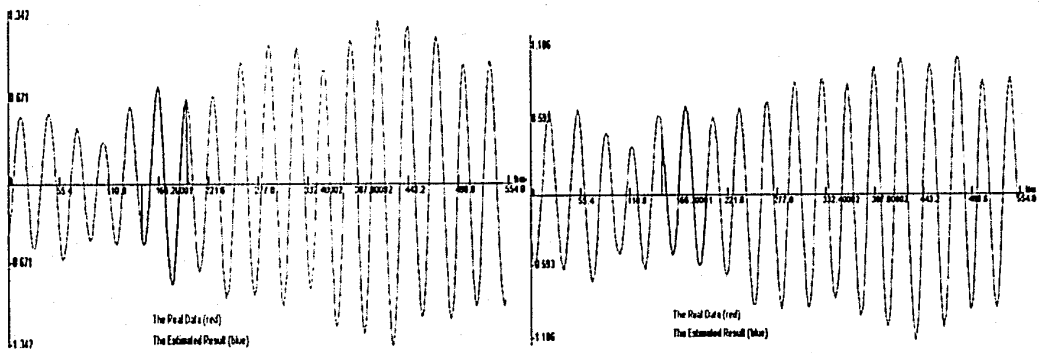

(c) Inphase Components on 2nd path (d) Quadrature Components on 2nd path

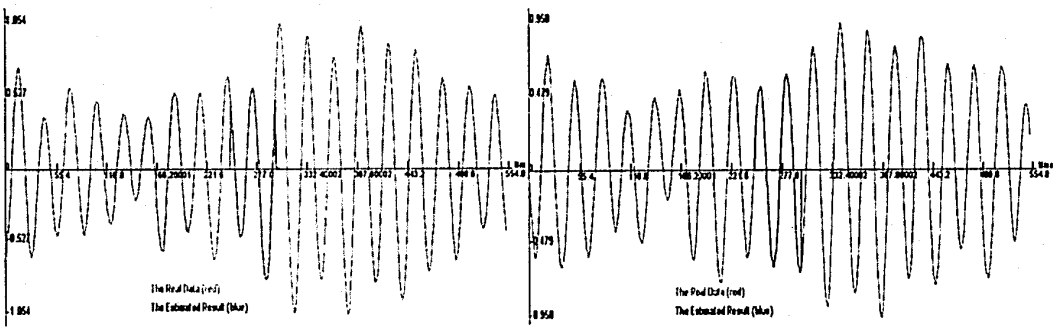

(e) Inphase Components on 3rd path (f) Quadrature Components on 3rd path

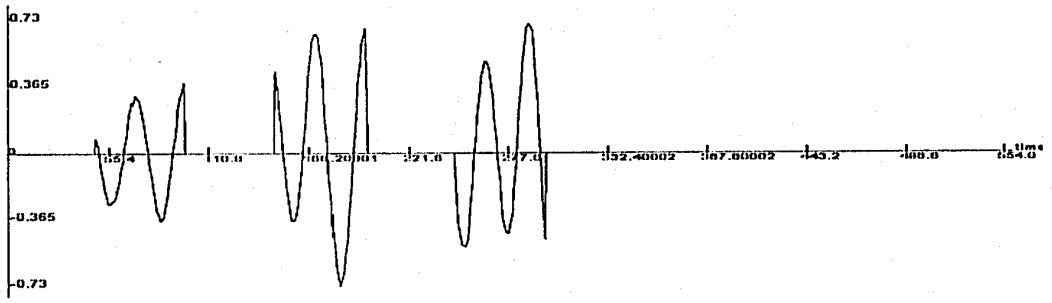

(g) the Received Signals

Figure B-4. the Estimated Results for Frequency-selective Fading Channel (N=3 case) on A Wide band Transmitted Signal

(2) Narrow Band Transmitted Signal

Considered the transmitted signal is a wide band signal, the estimated system parameters are computed as following:

$$\hat{A} = \begin{bmatrix} \hat{A}_1 & 0 & 0 \\ 0 & \hat{A}_2 & 0 \\ 0 & 0 & \hat{A}_3 \end{bmatrix}, \quad \hat{BB}^T = \begin{bmatrix} \hat{BB}_1^T & 0 & 0 \\ 0 & \hat{BB}_2^T & 0 \\ 0 & 0 & \hat{BB}_3^T \end{bmatrix}, \quad \hat{C} = \begin{bmatrix} \hat{C}_1 & \hat{C}_2 & \hat{C}_3 \end{bmatrix}, \quad \hat{DD}^T = 0.0023$$

In addition,

$$\hat{A}_1 = \begin{bmatrix} 0 & 1 & 0 & 0 \\ 0.1576 & -0.0789 & 0 & 0 \\ 0 & 0 & 0 & 1 \\ 0 & 0 & 0.1370 & -0.0885 \end{bmatrix}, \quad \hat{A}_2 = \begin{bmatrix} 0 & 1 & 0 & 0 \\ 0.1557 & 0.0746 & 0 & 0 \\ 0 & 0 & 0 & 1 \\ 0 & 0 & -0.1494 & 0.0552 \end{bmatrix}$$

$$\hat{A}_3 = \begin{bmatrix} 0 & 1 & 0 & 0 \\ 0.2047 & -0.0439 & 0 & 0 \\ 0 & 0 & 0 & 1 \\ 0 & 0 & 0.1956 & -0.2117 \end{bmatrix}, \quad \hat{BB}_1^T = \begin{bmatrix} 0.0767 & 0.0025 & 0.0127 & 0.0035 \\ 0.0025 & 0.1437 & 0.0173 & -0.0241 \\ 0.0127 & 0.0173 & 0.0805 & 0.0065 \\ 0.0035 & -0.0241 & 0.0065 & 0.2339 \end{bmatrix}$$

$$\hat{BB}_2^T = \begin{bmatrix} 0.1803 & 0.0010 & 0.0066 & 0.0094 \\ 0.0010 & 0.2146 & 0.0163 & -0.0055 \\ 0.0066 & 0.0163 & 0.1285 & 0.0059 \\ 0.0094 & -0.0055 & 0.0059 & 0.0691 \end{bmatrix}, \quad \hat{BB}_3^T = \begin{bmatrix} 0.1467 & 0.0102 & 0.0074 & 0.0013 \\ 0.0102 & 0.1945 & 0.0066 & -0.0041 \\ 0.0074 & 0.0066 & 0.1082 & 0.0074 \\ 0.0013 & -0.0041 & 0.0074 & 0.1061 \end{bmatrix}$$

$$\hat{C}_1 = \hat{C}_2 = \hat{C}_3 = \begin{bmatrix} 1 & 0 & 1 & 0 \end{bmatrix}$$

Figure B-5 shows the compared results between the measurement data and the estimated results on each path.

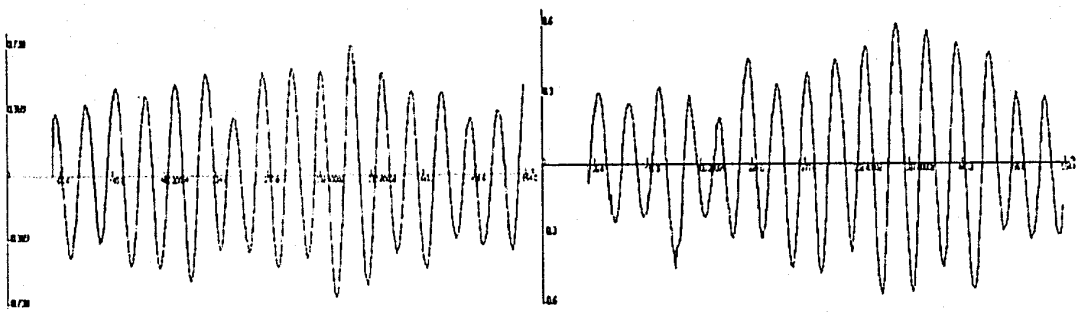

(a) Inphase Component on 1st path **(b) Quadrature Component on 1st path**

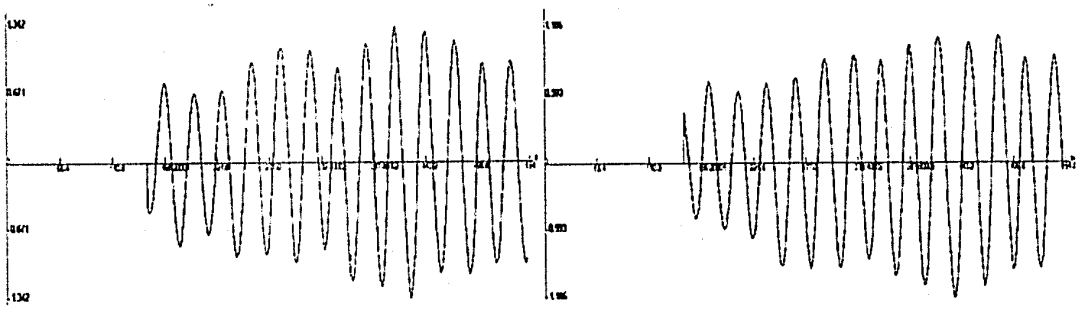

(c) Inphase Component on 2nd path **(d) Quadrature Component on 2nd path**

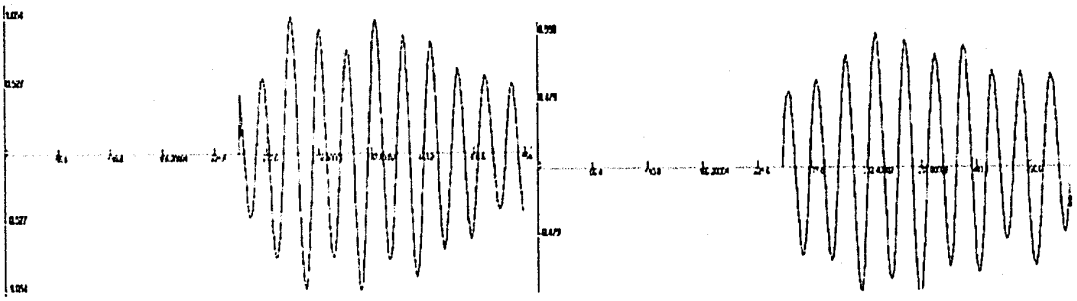

(e) Inphase Component on 3rd path **(f) Quadrature Component on 3rd path**

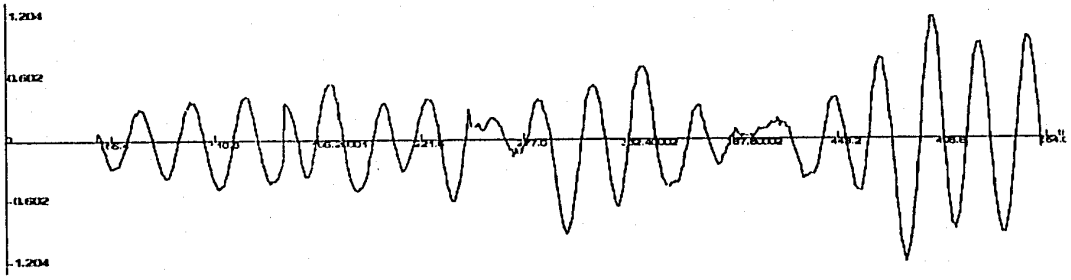

(g) the Received Signals

Figure B-5 the Estimated Results for Frequency-selective Fading Channel (N=3 case) on Narrow band Transmitted Signal

(3) Slow Fading with Narrow Band Transmitted Signal

The estimated system parameters of the frequency-selective slow fading are expressed as following:

$$\hat{A} = \begin{bmatrix} \hat{A}_1 & 0 & 0 \\ 0 & \hat{A}_2 & 0 \\ 0 & 0 & \hat{A}_3 \end{bmatrix}, \quad \hat{BB}^T = \begin{bmatrix} \hat{BB}_1^T & 0 & 0 \\ 0 & \hat{BB}_2^T & 0 \\ 0 & 0 & \hat{BB}_3^T \end{bmatrix}, \quad \hat{C} = \begin{bmatrix} \hat{C}_1 & \hat{C}_2 & \hat{C}_3 \end{bmatrix}, \quad \hat{DD}^T = 0.0022$$

In addition,

$$\hat{A}_1 = \begin{bmatrix} 0 & 1 & 0 & 0 \\ 0.0022 & -0.0572 & 0 & 0 \\ 0 & 0 & 0 & 1 \\ 0 & 0 & 0.0911 & -0.1641 \end{bmatrix}, \quad \hat{A}_2 = \begin{bmatrix} 0 & 1 & 0 & 0 \\ 0.0887 & -0.0057 & 0 & 0 \\ 0 & 0 & 0 & 1 \\ 0 & 0 & -0.1971 & -0.0836 \end{bmatrix}$$

$$\hat{A}_3 = \begin{bmatrix} 0 & 1 & 0 & 0 \\ 0.3434 & -0.2575 & 0 & 0 \\ 0 & 0 & 0 & 1 \\ 0 & 0 & 0.2762 & -0.4731 \end{bmatrix}, \quad \hat{BB}_1^T = \begin{bmatrix} -0.0070 & -0.0005 & 0.0588 & -0.0054 \\ -0.0005 & -0.0099 & -0.0027 & -0.0587 \\ 0.0588 & -0.0027 & -0.1645 & 0.0418 \\ -0.0054 & -0.0587 & 0.0418 & 0.4433 \end{bmatrix}$$

$$\hat{BB}_2^T = \begin{bmatrix} 1.4832 & -0.0042 & -0.1109 & 0.0117 \\ -0.0042 & 0.3420 & 0.0214 & 0.0397 \\ -0.1109 & 0.0214 & 0.0554 & 0.0243 \\ 0.0117 & 0.0397 & 0.0243 & 0.0843 \end{bmatrix}, \quad \hat{BB}_3^T = \begin{bmatrix} -0.5756 & 0.2603 & 0.2036 & -0.1326 \\ 0.2603 & 0.4158 & -0.0264 & -0.0937 \\ 0.2036 & -0.0264 & 0.1340 & 0.0624 \\ -0.1326 & -0.0937 & 0.0624 & 0.2052 \end{bmatrix}$$

$$\hat{C}_1 = \hat{C}_2 = \hat{C}_3 = \begin{bmatrix} 1 & 0 & 1 & 0 \end{bmatrix}$$

Figure B-6 shows the compared results between the measurement data and the estimated results on each path.

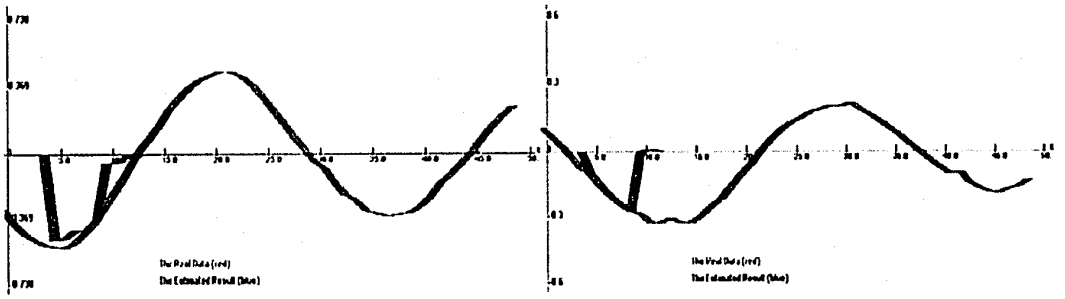

(a) Inphase Component on 1st path **(b) Quadrature Component on 1st path**

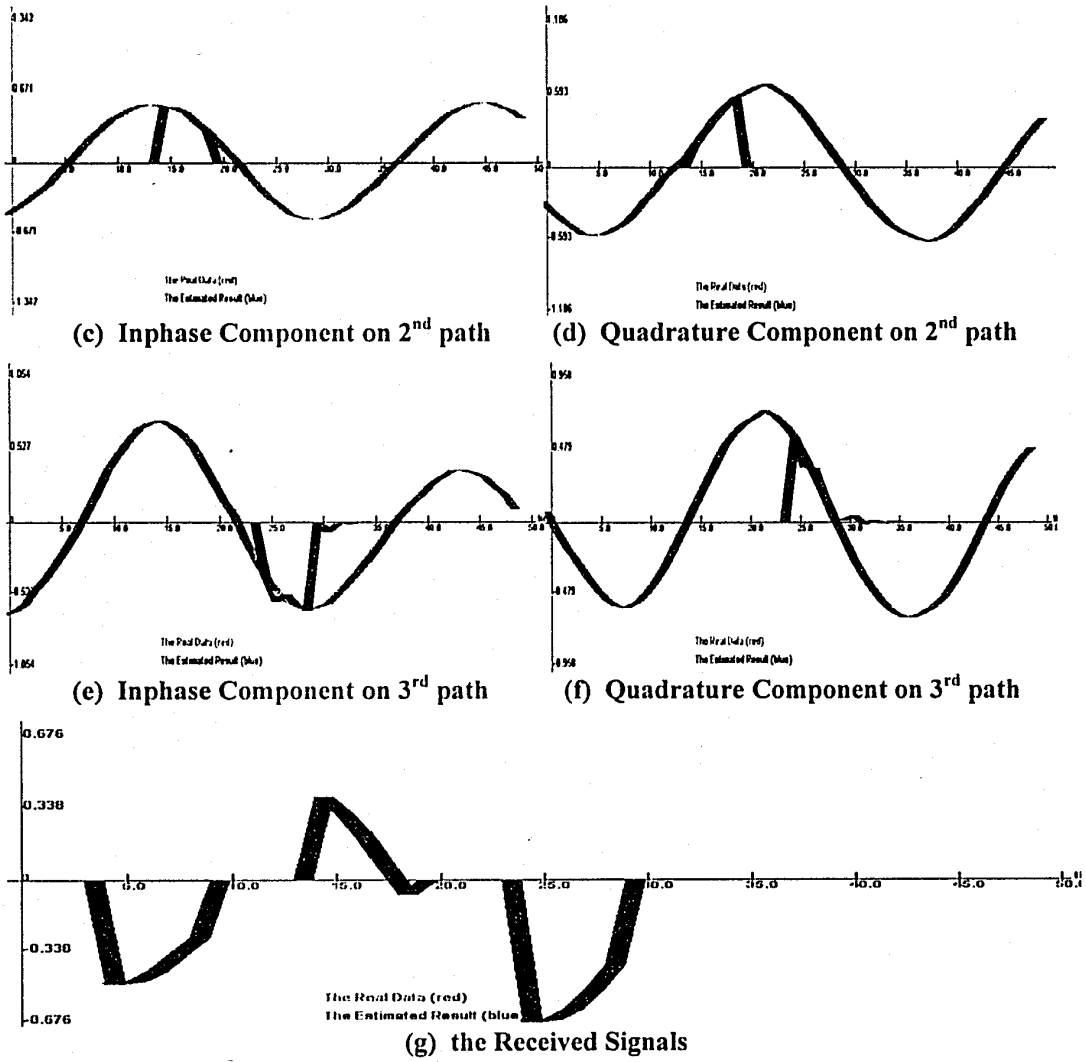

(c) Inphase Component on 2nd path (d) Quadrature Component on 2nd path

(e) Inphase Component on 3rd path (f) Quadrature Component on 3rd path

(g) the Received Signals

Figure B-6 the Estimated Results for Frequency-selective Slow Fading Channel (N=3 case)

B.3 System Identification Estimated Result for N = 4 Case

In this case, the inphase and quadrature Components are considered combination with four paths, and the measurement data is selected from the data group 3 with 554 samples.

(1) Wide Band Transmitted Signal

Considered the transmitted signal is a wide band signal, the estimated system parameters are computed as following:

$$\hat{A} = \begin{bmatrix} \hat{A}_1 & 0 & 0 & 0 \\ 0 & \hat{A}_2 & 0 & 0 \\ 0 & 0 & \hat{A}_3 & 0 \\ 0 & 0 & 0 & \hat{A}_4 \end{bmatrix}, \quad \hat{BB^T} = \begin{bmatrix} \hat{BB_1^T} & 0 & 0 & 0 \\ 0 & \hat{BB_2^T} & 0 & 0 \\ 0 & 0 & \hat{BB_3^T} & 0 \\ 0 & 0 & 0 & \hat{BB_4^T} \end{bmatrix},$$

$$\hat{C} = \begin{bmatrix} \hat{C}_1 & \hat{C}_2 & \hat{C}_3 & \hat{C}_4 \end{bmatrix}, \quad \hat{DD^T} = 0.0021$$

Here, $\left\{ \hat{A}_i, \hat{BB_i^T}, \hat{C}_i \right\}$ are defined as the following:

$$\hat{A}_1 = \begin{bmatrix} 0 & 1 & 0 & 0 \\ 0.1817 & -0.0643 & 0 & 0 \\ 0 & 0 & 0 & 1 \\ 0 & 0 & 0.1417 & -0.0959 \end{bmatrix}, \quad \hat{A}_2 = \begin{bmatrix} 0 & 1 & 0 & 0 \\ 0.1527 & 0.0690 & 0 & 0 \\ 0 & 0 & 0 & 1 \\ 0 & 0 & -0.1549 & 0.0599 \end{bmatrix}$$

$$\hat{A}_3 = \begin{bmatrix} 0 & 1 & 0 & 0 \\ 0.1772 & -0.0570 & 0 & 0 \\ 0 & 0 & 0 & 1 \\ 0 & 0 & 0.1681 & -0.2458 \end{bmatrix}, \quad \hat{A}_4 = \begin{bmatrix} 0 & 1 & 0 & 0 \\ 0.2836 & 0.0519 & 0 & 0 \\ 0 & 0 & 0 & 1 \\ 0 & 0 & 0.3558 & -0.0569 \end{bmatrix}$$

$$\hat{BB_1^T} = \begin{bmatrix} 0.0817 & 0.0055 & 0.0157 & 0.0047 \\ 0.0055 & 0.1626 & 0.0209 & -0.0282 \\ 0.0157 & 0.0209 & 0.0843 & 0.0086 \\ 0.0047 & -0.0282 & 0.0086 & 0.2776 \end{bmatrix}, \quad \hat{BB_2^T} = \begin{bmatrix} 0.2045 & 0.0020 & 0.0083 & 0.0091 \\ 0.0020 & 0.2266 & 0.0182 & -0.0049 \\ 0.0083 & 0.0182 & 0.1462 & 0.0071 \\ 0.0091 & -0.0049 & 0.0071 & 0.0724 \end{bmatrix}$$

$$\hat{BB_3^T} = \begin{bmatrix} 0.1557 & 0.0102 & 0.0094 & 0.0010 \\ 0.0102 & 0.2133 & 0.0069 & -0.0081 \\ 0.0094 & 0.0069 & 0.1481 & 0.0177 \\ 0.0010 & -0.0081 & 0.0177 & 0.1470 \end{bmatrix}, \quad \hat{BB_4^T} = \begin{bmatrix} 0.1934 & 0.0007 & 0.0063 & -0.0060 \\ 0.0007 & 0.0833 & 0.0166 & 0.0013 \\ 0.0063 & 0.0166 & 0.1976 & 0.0008 \\ -0.0060 & 0.0013 & 0.0008 & 0.1991 \end{bmatrix}$$

$$\hat{C}_1 = \hat{C}_2 = \hat{C}_3 = \hat{C}_4 = \begin{bmatrix} 1 & 0 & 1 & 0 \end{bmatrix}$$

Figure B-7 shows the compared results between the measurement data and the estimated results on each path.

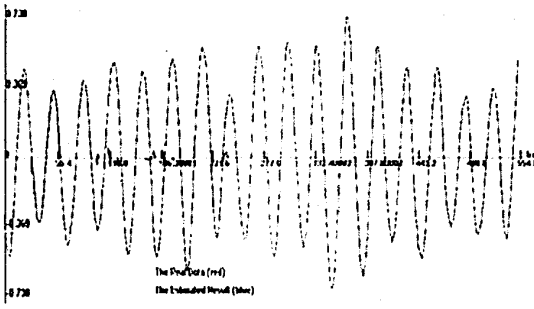

(a) Inphase Components on 1st path

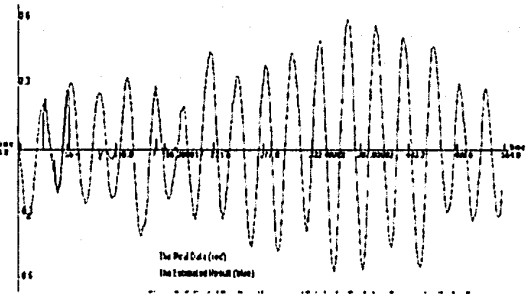

(b) Quadrature Components on 1st path

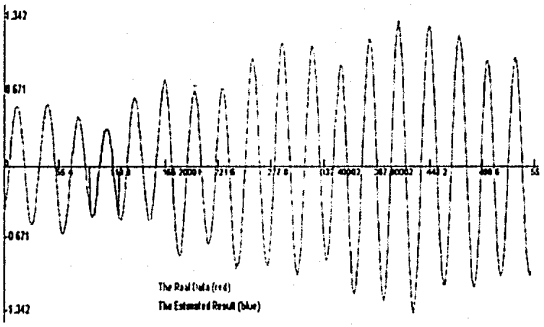

(c) Inphase Components on 2nd path

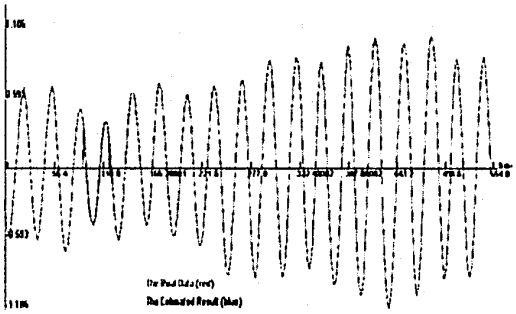

(d) Quadrature Components on 2nd path

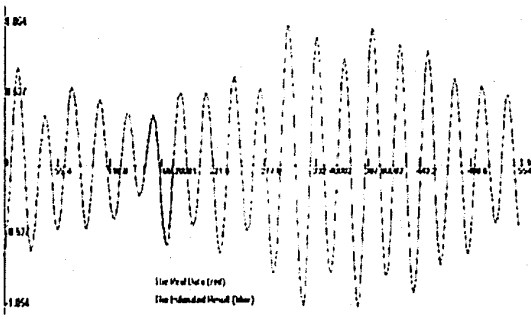

(e) Inphase Components on 3rd path

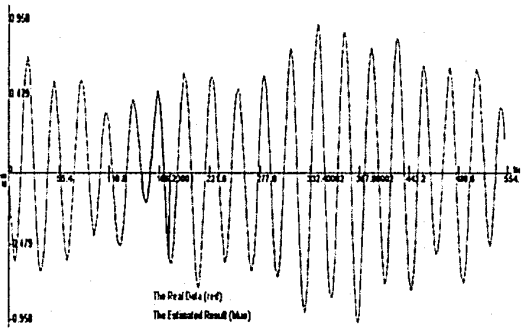

(f) Quadrature Components on 3rd path

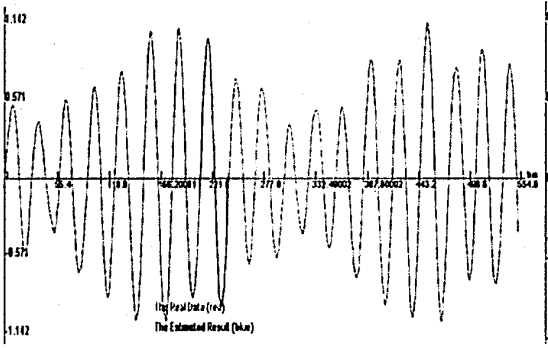

(g) Inphase Components on 4th path

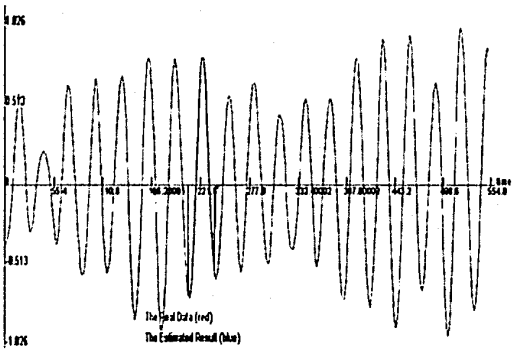

(h) Quadrature Components on 4th path

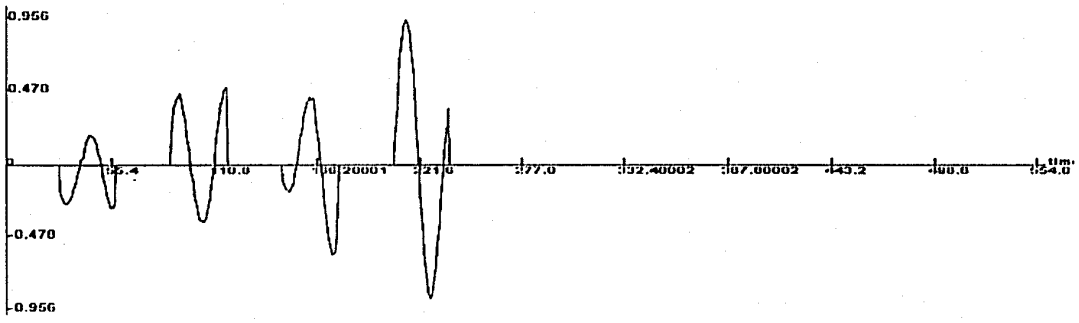

(i) the Output Sequences

Figure B-7. the Estimated Results for Frequency-selective Fading Channel (N=4 case) On the Wide Band Transmitted Signal

(2) Narrow Band Transmitted Signal

Considered the transmitted signal is a narrow band signal, the estimated system parameters are computed as following:

$$\hat{A} = \begin{bmatrix} \hat{A}_1 & 0 & 0 & 0 \\ 0 & \hat{A}_2 & 0 & 0 \\ 0 & 0 & \hat{A}_3 & 0 \\ 0 & 0 & 0 & \hat{A}_4 \end{bmatrix}, \quad \hat{BB}^T = \begin{bmatrix} \hat{BB}_1^T & 0 & 0 & 0 \\ 0 & \hat{BB}_2^T & 0 & 0 \\ 0 & 0 & \hat{BB}_3^T & 0 \\ 0 & 0 & 0 & \hat{BB}_4^T \end{bmatrix},$$

$$\hat{C} = \begin{bmatrix} \hat{C}_1 & \hat{C}_2 & \hat{C}_3 & \hat{C}_4 \end{bmatrix}, \quad \hat{DD}^T = 0.0021$$

In this case, $\left\{ \hat{A}_i, \hat{BB}_i^T, \hat{C}_i \right\}$ are defined as the following:

$$\hat{A}_1 = \begin{bmatrix} 0 & 1 & 0 & 0 \\ 0.1281 & -0.1033 & 0 & 0 \\ 0 & 0 & 0 & 1 \\ 0 & 0 & 0.1614 & -0.1178 \end{bmatrix}, \quad \hat{A}_2 = \begin{bmatrix} 0 & 1 & 0 & 0 \\ 0.1716 & 0.0613 & 0 & 0 \\ 0 & 0 & 0 & 1 \\ 0 & 0 & -0.1661 & 0.0607 \end{bmatrix}$$

$$\hat{A}_3 = \begin{bmatrix} 0 & 1 & 0 & 0 \\ 0.2135 & -0.0421 & 0 & 0 \\ 0 & 0 & 0 & 1 \\ 0 & 0 & 0.1894 & -0.2405 \end{bmatrix}, \quad \hat{A}_4 = \begin{bmatrix} 0 & 1 & 0 & 0 \\ 0.2943 & 0.0670 & 0 & 0 \\ 0 & 0 & 0 & 1 \\ 0 & 0 & 0.3883 & -0.0322 \end{bmatrix}$$

$$\hat{BB}_1^T = \begin{bmatrix} 0.0718 & 0.0002 & 0.0145 & 0.0034 \\ 0.0002 & 0.1318 & 0.0201 & -0.0059 \\ 0.0145 & 0.0201 & 0.0823 & 0.0074 \\ 0.0034 & -0.0059 & 0.0074 & 0.2374 \end{bmatrix}, \quad \hat{BB}_2^T = \begin{bmatrix} 0.1939 & -0.0028 & 0.0072 & 0.0085 \\ -0.0028 & 0.2119 & 0.0171 & -0.0042 \\ 0.0072 & 0.0171 & 0.1421 & 0.0064 \\ 0.0085 & -0.0042 & 0.0064 & 0.0711 \end{bmatrix}$$

$$\hat{BB}_3^T = \begin{bmatrix} 0.1548 & 0.0109 & 0.0096 & 0.0008 \\ 0.0109 & 0.2126 & 0.0074 & -0.0075 \\ 0.0096 & 0.0074 & 0.1467 & 0.0175 \\ 0.0008 & -0.0075 & 0.0175 & 0.1444 \end{bmatrix}, \quad \hat{BB}_4^T = \begin{bmatrix} 0.2028 & 0.0036 & 0.0118 & -0.0047 \\ 0.0036 & 0.0862 & 0.0222 & 0.0039 \\ 0.0118 & 0.0222 & 0.2137 & 0.0114 \\ -0.0047 & 0.0039 & 0.0114 & 0.2172 \end{bmatrix}$$

$$\hat{C}_1 = \hat{C}_2 = \hat{C}_3 = \hat{C}_4 = \begin{bmatrix} 1 & 0 & 1 & 0 \end{bmatrix}$$

Figure B-8 shows the compared results between the measurement data and the estimated results on each path.

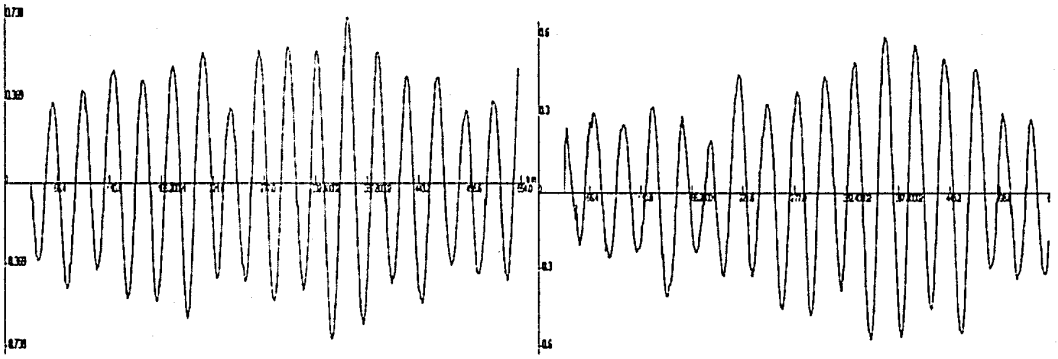

(a) Inphase Components on 1st path **(b) Quadrature Components on 1st path**

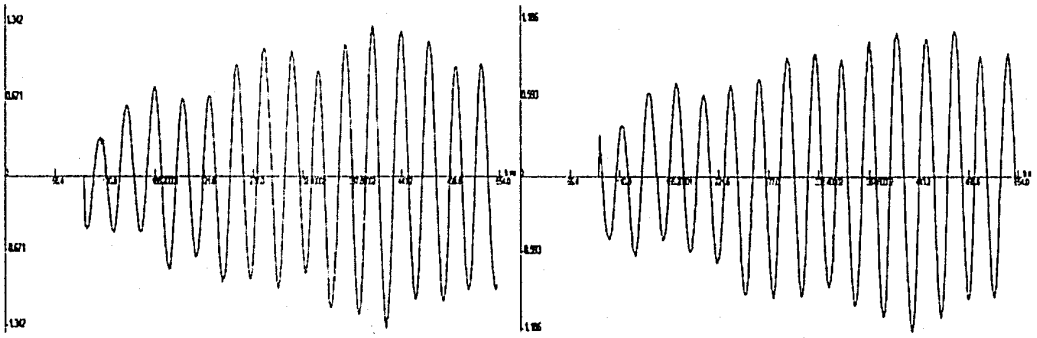

(c) Inphase Components on 2nd path **(d) Quadrature Components on 2nd path**

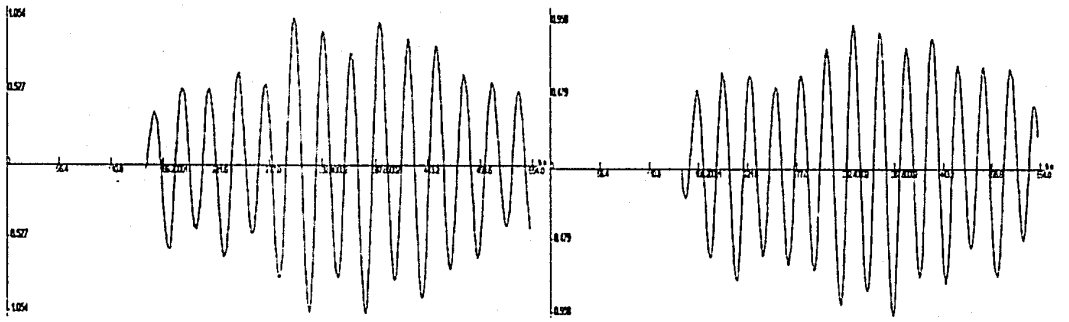

(e) Inphase Components on 3rd path **(f) Quadrature Components on 3rd path**

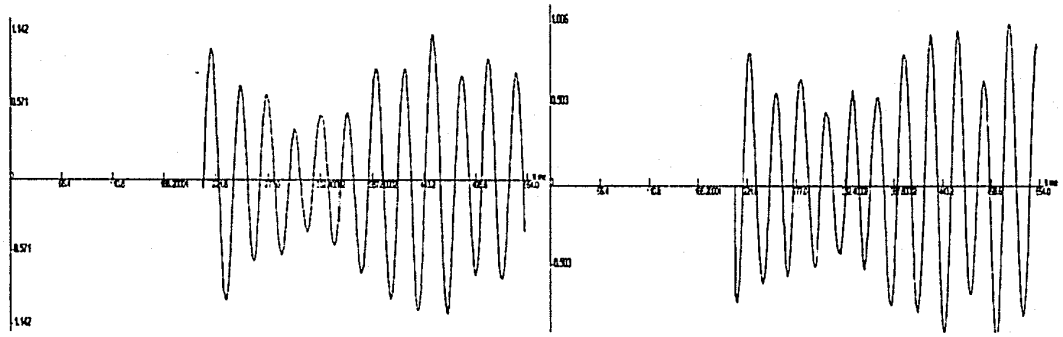

(g) Inphase Components on 4th path **(h) Quadrature Components on 4th path**

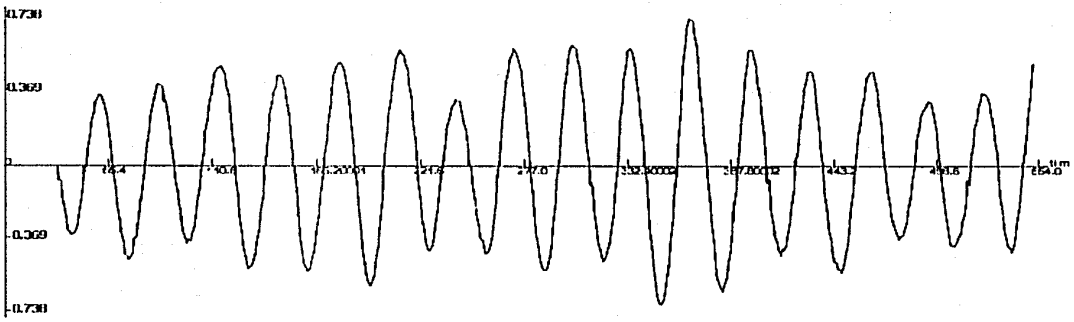

(i) the Output Sequences

Figure B-8. the Estimated Results for Frequency-selective Fading Channel (N=4 case) On the Narrow Band Transmitted Signal

(3) Slow Fading with Narrow Band Transmitted Signal

The estimated system parameters of the frequency-selective slow fading are represented as following:

$$\hat{A} = \begin{bmatrix} \hat{A}_1 & 0 & 0 & 0 \\ 0 & \hat{A}_2 & 0 & 0 \\ 0 & 0 & \hat{A}_3 & 0 \\ 0 & 0 & 0 & \hat{A}_4 \end{bmatrix}, \quad \hat{BB}^T = \begin{bmatrix} \hat{BB}_1^T & 0 & 0 & 0 \\ 0 & \hat{BB}_2^T & 0 & 0 \\ 0 & 0 & \hat{BB}_3^T & 0 \\ 0 & 0 & 0 & \hat{BB}_4^T \end{bmatrix},$$

$$\hat{C} = \begin{bmatrix} \hat{C}_1 & \hat{C}_2 & \hat{C}_3 & \hat{C}_4 \end{bmatrix}, \quad \hat{DD}^T = 0.0024$$

In this case, $\left\{ \hat{A}_i, \hat{BB}_i^T, \hat{C}_i \right\}$ are defined as the following:

$$\hat{A}_1 = \begin{bmatrix} 0 & 1 & 0 & 0 \\ 0.1769 & -0.0135 & 0 & 0 \\ 0 & 0 & 0 & 1 \\ 0 & 0 & 0.1544 & -0.1144 \end{bmatrix}, \quad \hat{A}_2 = \begin{bmatrix} 0 & 1 & 0 & 0 \\ 0.0846 & 0.0133 & 0 & 0 \\ 0 & 0 & 0 & 1 \\ 0 & 0 & -0.1474 & 0.0081 \end{bmatrix}$$

$$\hat{A}_3 = \begin{bmatrix} 0 & 1 & 0 & 0 \\ 0.2153 & -0.0708 & 0 & 0 \\ 0 & 0 & 0 & 1 \\ 0 & 0 & 0.2055 & -0.3189 \end{bmatrix}, \quad \hat{A}_4 = \begin{bmatrix} 0 & 1 & 0 & 0 \\ 0.3101 & 0.0729 & 0 & 0 \\ 0 & 0 & 0 & 1 \\ 0 & 0 & 0.3771 & -0.0906 \end{bmatrix}$$

$$\hat{BB}_1^T = \begin{bmatrix} -0.0359 & 0.0206 & 0.0394 & 0.0044 \\ 0.0206 & 0.1853 & 0.0274 & -0.0219 \\ 0.0394 & 0.0274 & 0.0641 & 0.0061 \\ 0.0044 & -0.0219 & 0.0061 & 0.2052 \end{bmatrix}, \quad \hat{BB}_2^T = \begin{bmatrix} 0.8194 & 0.0118 & -0.1724 & -0.0269 \\ 0.0118 & 0.3195 & 0.0326 & 0.0106 \\ -0.1724 & -0.0326 & 0.1438 & 0.0236 \\ -0.0269 & 0.0106 & 0.0236 & 0.0845 \end{bmatrix}$$

$$\hat{BB}_3^T = \begin{bmatrix} 0.1653 & 0.0187 & 0.0193 & 0.0008 \\ 0.0187 & 0.2882 & 0.0114 & -0.0152 \\ 0.0193 & 0.0114 & 0.1728 & 0.0378 \\ 0.0008 & -0.0152 & 0.0378 & 0.1949 \end{bmatrix}, \quad \hat{BB}_4^T = \begin{bmatrix} 0.2682 & -0.0009 & 0.0083 & -0.0205 \\ -0.0009 & 0.0952 & 0.0356 & 0.0014 \\ 0.0083 & 0.0356 & 0.3656 & 0.0099 \\ -0.0205 & 0.0014 & 0.0099 & 0.3821 \end{bmatrix}$$

$$\hat{C}_1 = \hat{C}_2 = \hat{C}_3 = \hat{C}_4 = \begin{bmatrix} 1 & 0 & 1 & 0 \end{bmatrix}$$

Figure B-9 shows the compared results between the measurement data and the estimated results on each path for the frequency-selective slow fading.

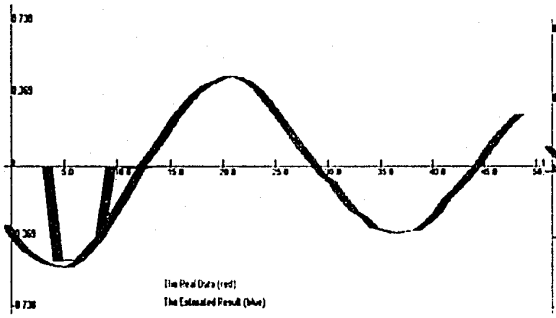

(a) Inphase Components on 1st path

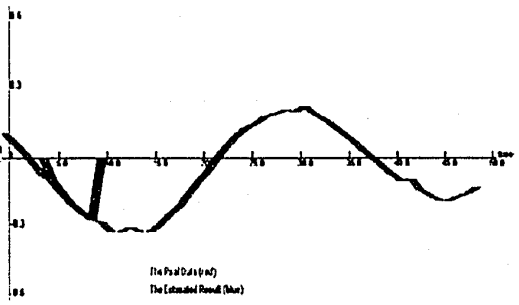

(b) Quadrature Components on 1st path

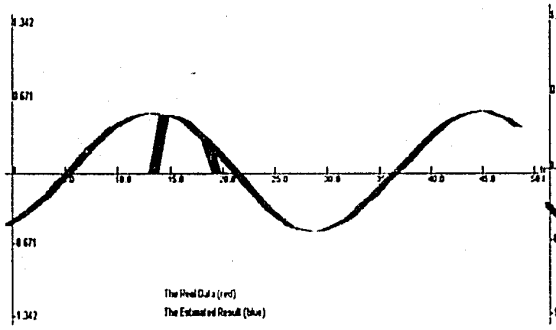

(c) Inphase Components on 2nd path

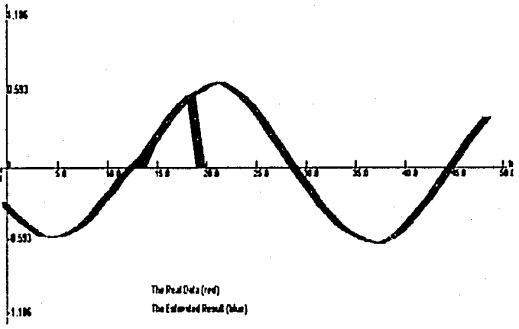

(d) Quadrature Components on 2nd path

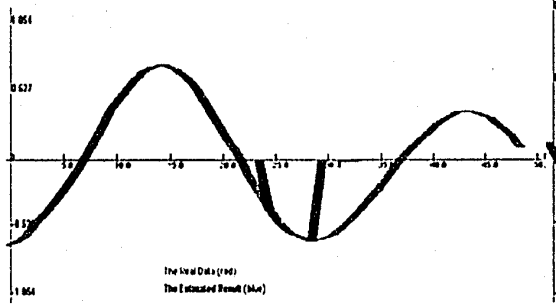

(e) Inphase Components on 3rd path

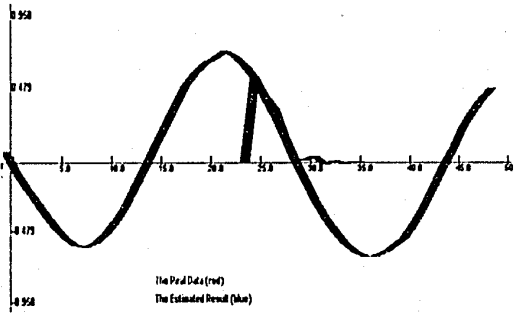

(f) Quadrature Components on 3rd path

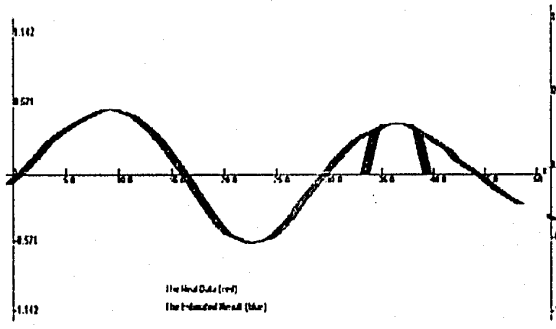

(g) Inphase Components on 4th path

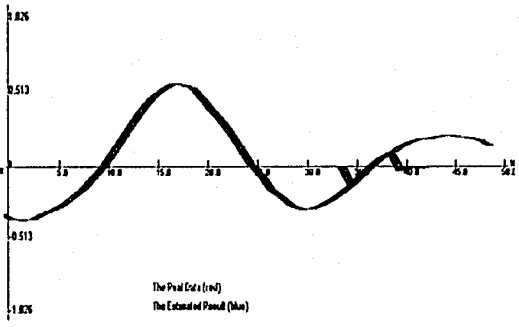

(h) Quadrature Components on 4th path

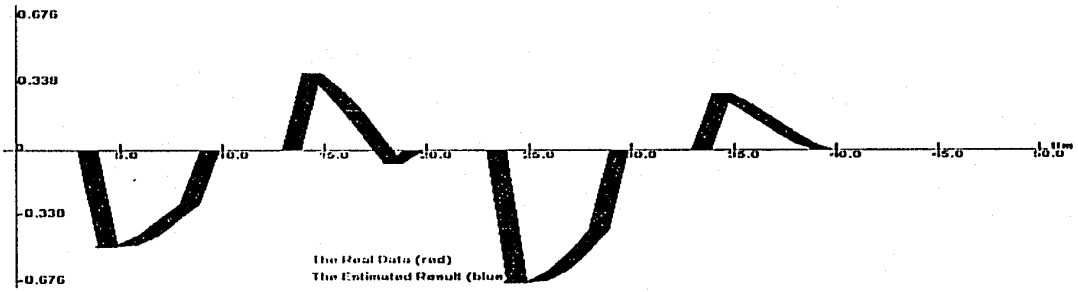

(i) the Output Sequences

Figure B-9. the Estimated Results for Frequency-selective Slow Fading Channel (N=4 case)

B.4 System Identification Estimated Result for N = 5 Case

In this case, the inphase and quadrature Components are considered combination with five paths, and the measurement data is selected from the data group 2 with 338 samples.

(1) Wide Band Transmitted Signal

Considered the transmitted signal is a wide band signal, the estimated system parameters are computed as following:

$$\hat{A} = \begin{bmatrix} \hat{A}_1 & 0 & \dots & 0 \\ 0 & \hat{A}_2 & \dots & 0 \\ \vdots & \vdots & \vdots & 0 \\ 0 & 0 & \dots & \hat{A}_5 \end{bmatrix}, \quad \hat{BB^T} = \begin{bmatrix} \hat{BB_1^T} & 0 & \dots & 0 \\ 0 & \hat{BB_2^T} & \dots & 0 \\ \vdots & \vdots & \dots & 0 \\ 0 & 0 & \cdots & \hat{BB_5^T} \end{bmatrix},$$

$$\hat{C} = \begin{bmatrix} \hat{C}_1 & \hat{C}_2 & \dots & \hat{C}_5 \end{bmatrix}, \quad \hat{DD^D} = 0.0019$$

In this case, $\left\{ \hat{A}_i, \hat{BB_i^T}, \hat{C}_i \right\}$ are defined as the following:

$$\hat{A}_1 = \begin{bmatrix} 0 & 1 & 0 & 0 \\ 0.1873 & -0.0579 & 0 & 0 \\ 0 & 0 & 0 & 1 \\ 0 & 0 & 0.1389 & -0.0962 \end{bmatrix}, \quad \hat{A}_2 = \begin{bmatrix} 0 & 1 & 0 & 0 \\ 0.2507 & 0.0514 & 0 & 0 \\ 0 & 0 & 0 & 1 \\ 0 & 0 & -0.1561 & 0.0511 \end{bmatrix}$$

$$\hat{A}_3 = \begin{bmatrix} 0 & 1 & 0 & 0 \\ 0.1860 & -0.0606 & 0 & 0 \\ 0 & 0 & 0 & 1 \\ 0 & 0 & 0.1804 & -0.2577 \end{bmatrix}, \quad \hat{A}_4 = \begin{bmatrix} 0 & 1 & 0 & 0 \\ 0.2883 & 0.0535 & 0 & 0 \\ 0 & 0 & 0 & 1 \\ 0 & 0 & 0.3600 & -0.0762 \end{bmatrix}$$

$$\hat{A}_5 = \begin{bmatrix} 0 & 1 & 0 & 0 \\ 0.1995 & -0.0624 & 0 & 0 \\ 0 & 0 & 0 & 1 \\ 0 & 0 & 0.1935 & -0.2721 \end{bmatrix}, \quad \hat{BB}_1^T = \begin{bmatrix} 0.0795 & 0.0066 & 0.0153 & 0.0042 \\ 0.0066 & 0.1648 & 0.0208 & -0.0286 \\ 0.0153 & 0.0208 & 0.0810 & 0.0068 \\ 0.0042 & -0.0286 & 0.0068 & 0.2527 \end{bmatrix}$$

$$\hat{BB}_2^T = \begin{bmatrix} 0.2729 & 0.0024 & -0.0017 & 0.0048 \\ 0.0024 & 0.2262 & 0.0181 & -0.0023 \\ -0.0017 & 0.0181 & 0.1392 & 0.0079 \\ 0.0048 & -0.0023 & 0.0079 & 0.0717 \end{bmatrix}, \quad \hat{BB}_3^T = \begin{bmatrix} 0.1614 & 0.0113 & 0.0095 & 0.0006 \\ 0.0113 & 0.2287 & 0.0075 & -0.0101 \\ 0.0095 & 0.0075 & 0.1523 & 0.0188 \\ 0.0006 & -0.0101 & 0.0188 & 0.1533 \end{bmatrix}$$

$$\hat{BB}_4^T = \begin{bmatrix} 0.2530 & 0.0011 & 0.0095 & -0.0136 \\ 0.0011 & 0.0917 & 0.0250 & 0.0017 \\ 0.0095 & 0.0250 & 0.2979 & 0.0047 \\ -0.0136 & 0.0017 & 0.0047 & 0.3000 \end{bmatrix}, \quad \hat{BB}_5^T = \begin{bmatrix} 0.1682 & 0.0122 & 0.0137 & 0.0012 \\ 0.0122 & 0.2414 & 0.0087 & -0.0092 \\ 0.0137 & 0.0087 & 0.1638 & 0.0213 \\ 0.0012 & -0.0092 & 0.0213 & 0.1650 \end{bmatrix}$$

$$\hat{C}_1 = \hat{C}_2 = \hat{C}_3 = \hat{C}_4 = \hat{C}_5 = \begin{bmatrix} 1 & 0 & 1 & 0 \end{bmatrix}$$

Figure B-10 shows the compared results between the measurement data and the estimated results on each path.

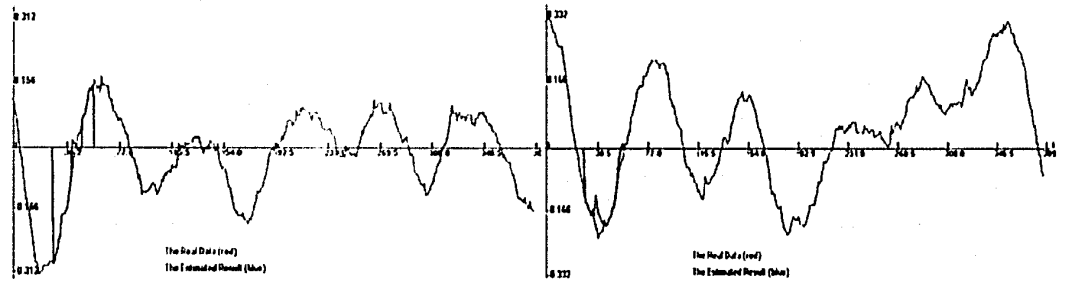

(a) Inphase Components on 1st path **(b) Quadrature Components on 1st path**

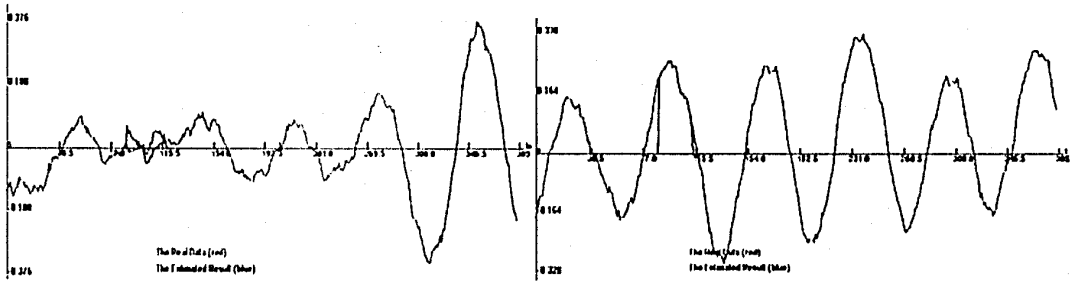

(c) Inphase Components on 2nd path **(d) Quadrature Components on 2nd path**

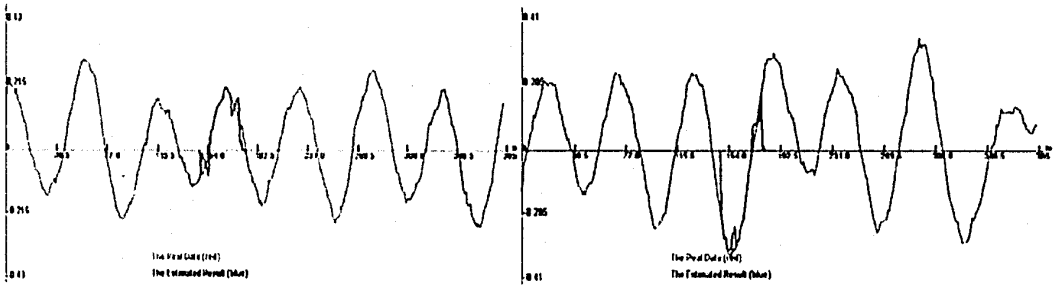

(e) Inphase Components on 3rd path (f) Quadrature Components on 3rd path

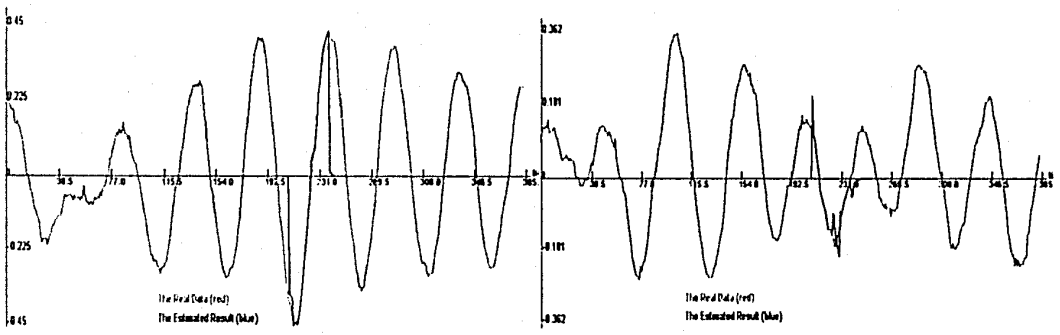

(g) Inphase Components on 4th path (h) Quadrature Components on 4th path

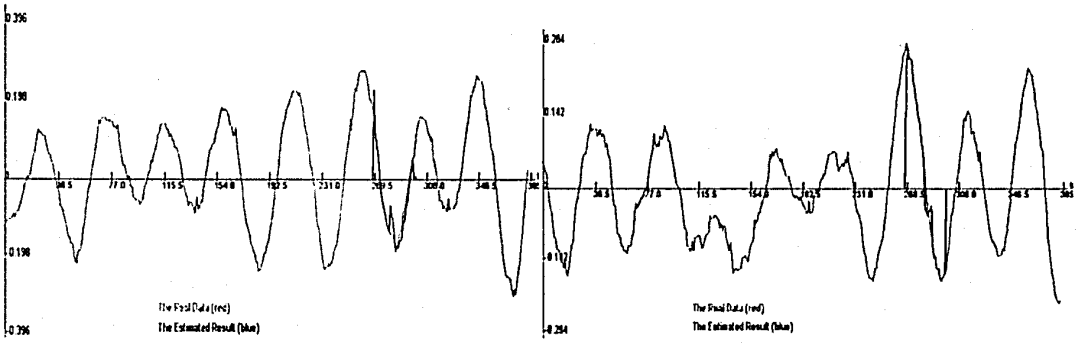

(i) Inphase Components on 5th path (j) Quadrature Components on 5th path

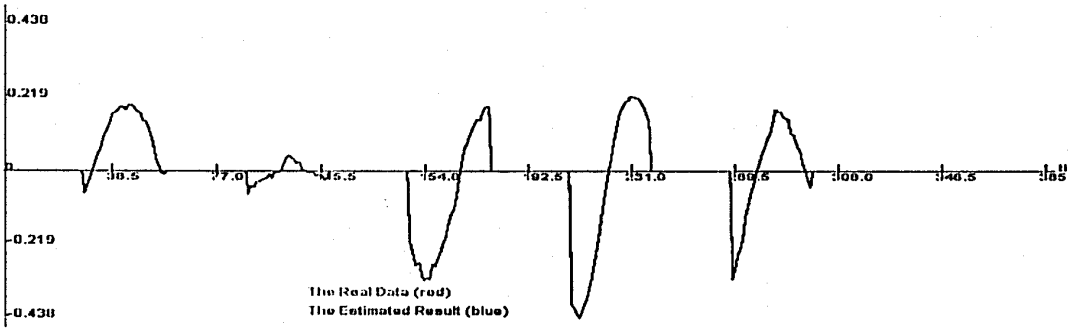

(k) the Output Sequences

Figure B-10. the Estimated Results for Frequency-selective Fading Channel (N=5 case) On the Wide Band Transmitted Signal

(2) Narrow Band Transmitted Signal

Considered the transmitted signal is a narrow band signal, the estimated system parameters are computed as following:

$$\hat{A} = \begin{bmatrix} \hat{A}_1 & 0 & \dots & 0 \\ 0 & \hat{A}_2 & \dots & 0 \\ \vdots & \vdots & \vdots & 0 \\ 0 & 0 & \dots & \hat{A}_5 \end{bmatrix}, \quad \hat{BB^T} = \begin{bmatrix} \hat{BB_1^T} & 0 & \dots & 0 \\ 0 & \hat{BB_2^T} & \dots & 0 \\ \vdots & \vdots & \dots & 0 \\ 0 & 0 & \cdots & \hat{BB_5^T} \end{bmatrix},$$

$$\hat{C} = \begin{bmatrix} \hat{C}_1 & \hat{C}_2 & \dots & \hat{C}_5 \end{bmatrix}, \quad \hat{DD^T} = 0.0019$$

Here, $\left\{ \hat{A}_i, \hat{BB_i}^T, \hat{C}_i \right\}$ are defined as the following:

$$\hat{A}_1 = \begin{bmatrix} 0 & 1 & 0 & 0 \\ 0.1820 & -0.0657 & 0 & 0 \\ 0 & 0 & 0 & 1 \\ 0 & 0 & 0.1479 & -0.0953 \end{bmatrix}, \quad \hat{A}_2 = \begin{bmatrix} 0 & 1 & 0 & 0 \\ 0.1966 & 0.0556 & 0 & 0 \\ 0 & 0 & 0 & 1 \\ 0 & 0 & -0.1564 & 0.0554 \end{bmatrix}$$

$$\hat{A}_3 = \begin{bmatrix} 0 & 1 & 0 & 0 \\ 0.1898 & -0.0596 & 0 & 0 \\ 0 & 0 & 0 & 1 \\ 0 & 0 & 0.1795 & -0.2547 \end{bmatrix}, \quad \hat{A}_4 = \begin{bmatrix} 0 & 1 & 0 & 0 \\ 0.2919 & 0.0570 & 0 & 0 \\ 0 & 0 & 0 & 1 \\ 0 & 0 & 0.3575 & -0.0669 \end{bmatrix}$$

$$\hat{A}_5 = \begin{bmatrix} 0 & 1 & 0 & 0 \\ 0.2004 & -0.0589 & 0 & 0 \\ 0 & 0 & 0 & 1 \\ 0 & 0 & 0.1943 & -0.2579 \end{bmatrix}, \quad \hat{BB_1^T} = \begin{bmatrix} 0.0794 & 0.0055 & 0.0156 & 0.0043 \\ 0.0055 & 0.1626 & 0.0217 & -0.0251 \\ 0.0156 & 0.0217 & 0.0821 & 0.0075 \\ 0.0043 & -0.0251 & 0.0075 & 0.2558 \end{bmatrix}$$

$$\hat{BB_2^T} = \begin{bmatrix} 0.2533 & 0.0017 & 0.0004 & 0.0061 \\ 0.0017 & 0.2289 & 0.0180 & -0.0032 \\ 0.0004 & 0.0180 & 0.1411 & 0.0076 \\ 0.0061 & -0.0032 & 0.0076 & 0.0718 \end{bmatrix}, \quad \hat{BB_3^T} = \begin{bmatrix} 0.1632 & 0.0114 & 0.0091 & 0.0004 \\ 0.0114 & 0.2318 & 0.0076 & -0.0106 \\ 0.0091 & 0.0076 & 0.1520 & 0.0187 \\ 0.0004 & -0.0106 & 0.0187 & 0.1524 \end{bmatrix}$$

$$\hat{BB_4^T} = \begin{bmatrix} 0.2539 & 0.0013 & 0.0074 & -0.0126 \\ 0.0013 & 0.0917 & 0.0249 & 0.0016 \\ 0.0074 & 0.0249 & 0.2872 & 0.0058 \\ -0.0126 & 0.0016 & 0.0058 & 0.2889 \end{bmatrix}, \quad \hat{BB_5^T} = \begin{bmatrix} 0.1667 & 0.0123 & 0.0102 & 0.0006 \\ 0.0123 & 0.2386 & 0.0081 & -0.0096 \\ 0.0102 & 0.0081 & 0.1470 & 0.0164 \\ 0.0006 & -0.0096 & 0.0164 & 0.1476 \end{bmatrix}$$

$$\hat{C}_1 = \hat{C}_2 = \hat{C}_3 = \hat{C}_4 = \hat{C}_5 = \begin{bmatrix} 1 & 0 & 1 & 0 \end{bmatrix}$$

Figure B-11 shows the compared results between the measurement data and the estimated results on each path.

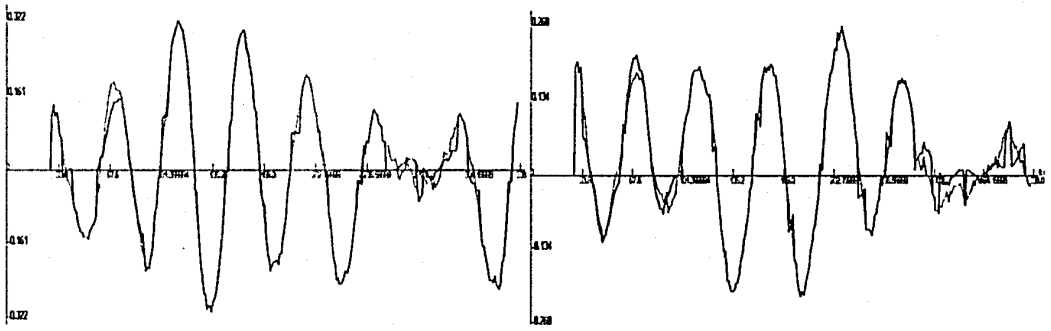

(a) Inphase Components on 1st path **(b) Quadrature Components on 1st path**

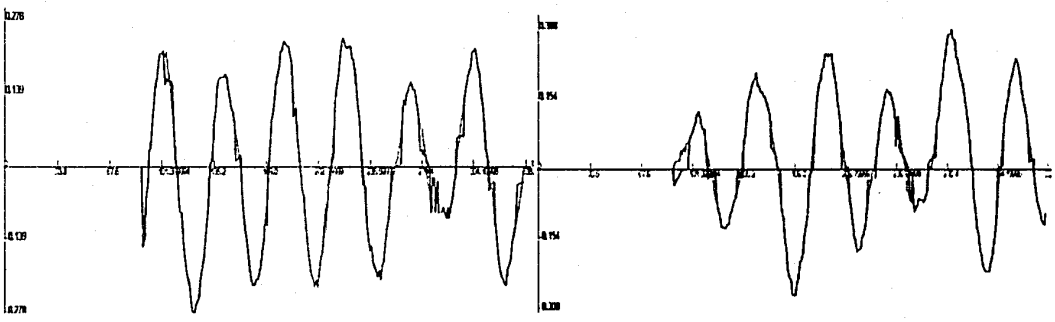

(c) Inphase Components on 2nd path **(d) Quadrature Components on 2nd path**

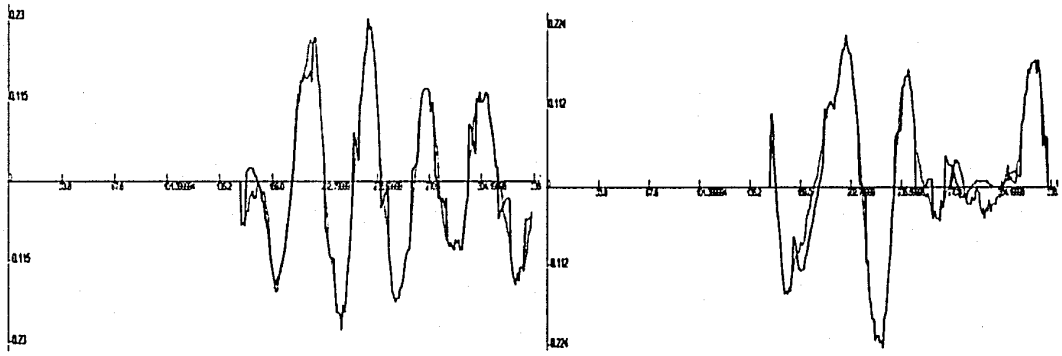

(e) Inphase Components on 3rd path **(f) Quadrature Components on 3rd path**

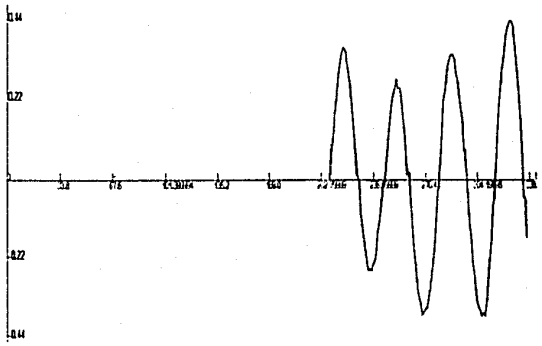

(g) Inphase Components on 4th path

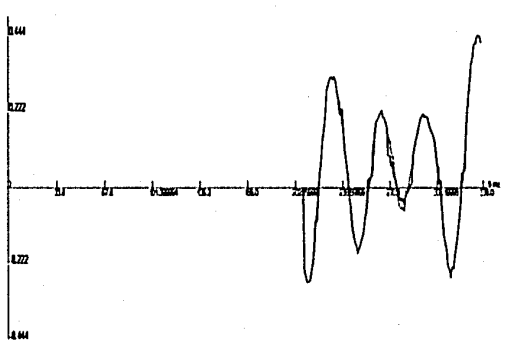

(h) Quadrature Components on 4th path

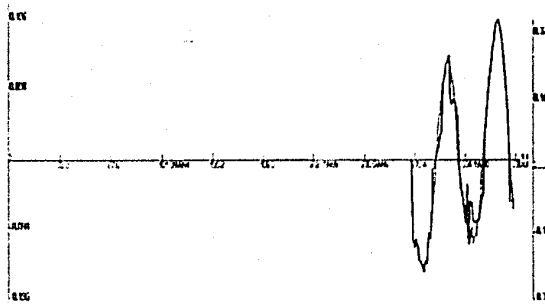

(i) Inphase Components on 5th path

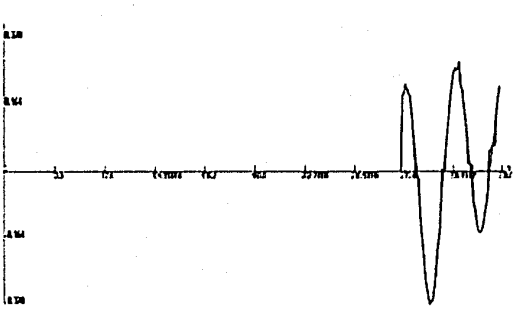

(j) Quadrature Components on 5th path

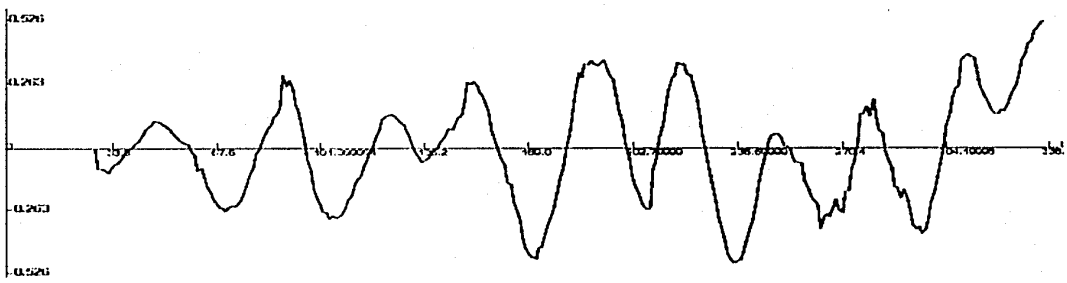

(k) the Output Sequences

Figure B-11. the Estimated Results for Frequency-selective Fading Channel (N=5 case) On the Narrow Band Transmitted Signal

(3) Slow Fading with Narrow Band Transmitted Signal

The estimated system parameters of the frequency-selective slow fading are computed as following:

$$\hat{A} = \begin{bmatrix} \hat{A}_1 & 0 & \cdots & 0 \\ 0 & \hat{A}_2 & \cdots & 0 \\ \vdots & \vdots & \vdots & 0 \\ 0 & 0 & \cdots & \hat{A}_5 \end{bmatrix}, \quad \hat{BB}^T = \begin{bmatrix} \hat{BB}_1^T & 0 & \cdots & 0 \\ 0 & \hat{BB}_2^T & \cdots & 0 \\ \vdots & \vdots & \cdots & 0 \\ 0 & 0 & \cdots & \hat{BB}_5^T \end{bmatrix},$$

$$\hat{C} = \begin{bmatrix} \hat{C}_1 & \hat{C}_2 & \cdots & \hat{C}_5 \end{bmatrix}, \quad \hat{DD}^T = 0.0019$$

Here, $\left\{ \hat{A}_i, \hat{BB}_i^T, \hat{C}_i \right\}$ are defined as the following:

$$\hat{A}_1 = \begin{bmatrix} 0 & 1 & 0 & 0 \\ 0.2357 & -0.0832 & 0 & 0 \\ 0 & 0 & 0 & 1 \\ 0 & 0 & 0.1694 & -0.1197 \end{bmatrix}, \quad \hat{A}_2 = \begin{bmatrix} 0 & 1 & 0 & 0 \\ 0.0847 & 0.0133 & 0 & 0 \\ 0 & 0 & 0 & 1 \\ 0 & 0 & -0.1474 & 0.0081 \end{bmatrix}$$

$$\hat{A}_3 = \begin{bmatrix} 0 & 1 & 0 & 0 \\ 0.2153 & -0.0708 & 0 & 0 \\ 0 & 0 & 0 & 1 \\ 0 & 0 & 0.2055 & -0.3190 \end{bmatrix}, \quad \hat{A}_4 = \begin{bmatrix} 0 & 1 & 0 & 0 \\ 0.3101 & 0.0729 & 0 & 0 \\ 0 & 0 & 0 & 1 \\ 0 & 0 & 0.3771 & -0.0906 \end{bmatrix}$$

$$\hat{A}_5 = \begin{bmatrix} 0 & 1 & 0 & 0 \\ 0.2153 & -0.0708 & 0 & 0 \\ 0 & 0 & 0 & 1 \\ 0 & 0 & 0.2055 & -0.3189 \end{bmatrix}, \quad \hat{BB}_1^T = \begin{bmatrix} -0.0239 & 0.0196 & 0.0365 & 0.0038 \\ 0.0196 & 0.1876 & 0.0259 & -0.0279 \\ 0.0365 & 0.0259 & 0.0632 & 0.0051 \\ 0.0038 & -0.0279 & 0.0051 & 0.2044 \end{bmatrix}$$

$$\hat{BB}_2^T = \begin{bmatrix} 0.928 & 0.0118 & -0.1724 & -0.0269 \\ 0.0118 & 0.3195 & 0.0326 & 0.0106 \\ -0.1724 & 0.0326 & 0.1438 & 0.0236 \\ -0.0269 & 0.0106 & 0.0236 & 0.0845 \end{bmatrix}, \quad \hat{BB}_3^T = \begin{bmatrix} 0.1653 & 0.0187 & 0.0193 & 0.0008 \\ 0.0187 & 0.2882 & 0.0114 & -0.0152 \\ 0.0193 & 0.0114 & 0.1728 & 0.0379 \\ 0.0008 & -0.0152 & 0.0379 & 0.1949 \end{bmatrix}$$

$$\hat{BB}_4^T = \begin{bmatrix} 0.2682 & -0.0009 & 0.0083 & -0.0205 \\ -0.0009 & 0.0952 & 0.0356 & 0.0014 \\ 0.0083 & 0.0356 & 0.3655 & 0.0099 \\ -0.0205 & 0.0014 & 0.0099 & 0.3821 \end{bmatrix}, \quad \hat{BB}_5^T = \begin{bmatrix} 0.1653 & 0.0187 & 0.0193 & 0.0008 \\ 0.0187 & 0.2881 & 0.0113 & -0.0152 \\ 0.0193 & 0.0113 & 0.1728 & 0.0379 \\ 0.0008 & -0.0152 & 0.0379 & 0.1949 \end{bmatrix}$$

$$\hat{C}_1 = \hat{C}_2 = \hat{C}_3 = \hat{C}_4 = \hat{C}_5 = \begin{bmatrix} 1 & 0 & 1 & 0 \end{bmatrix}$$

Figure B-12 shows the compared results between the measurement data and the estimated results on each path.

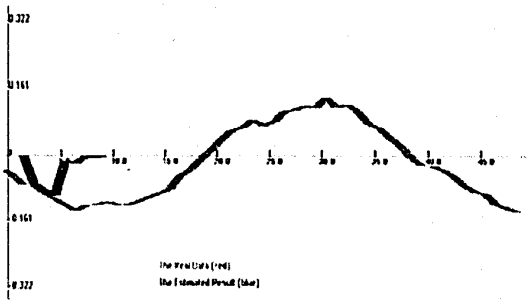

(a) Inphase Components on 1st path

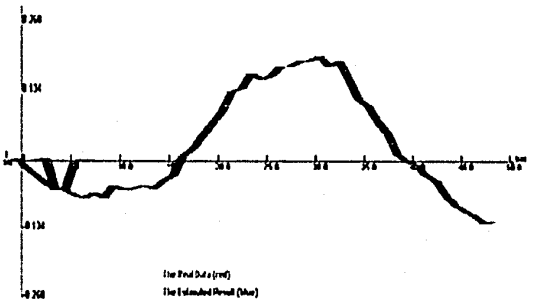

(b) Quadrature Components on 1st path

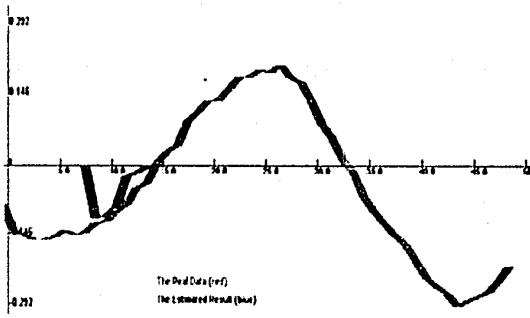

(c) Inphase Components on 2nd path

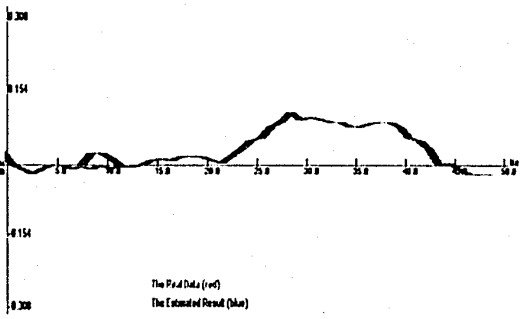

(d) Quadrature Components on 2nd path

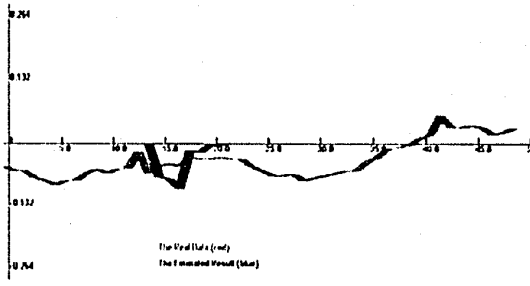

(e) Inphase Components on 3rd path

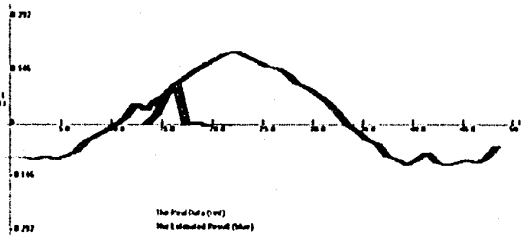

(f) Quadrature Components on 3rd path

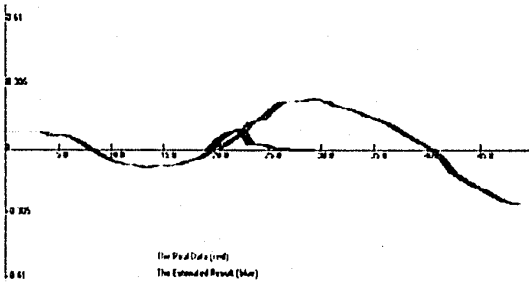

(g) Inphase Components on 4th path

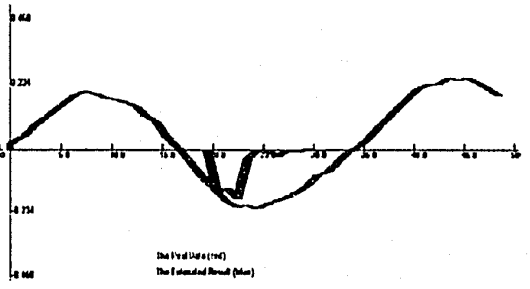

(h) Quadrature Components on 4th path

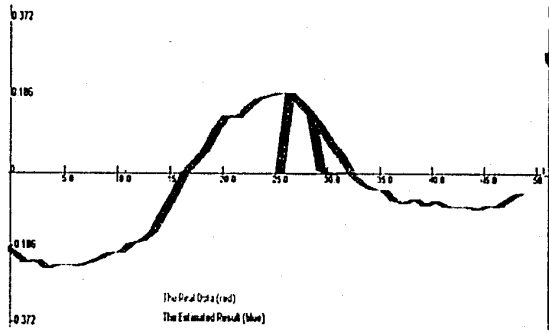

(i) Inphase Components on 5th path

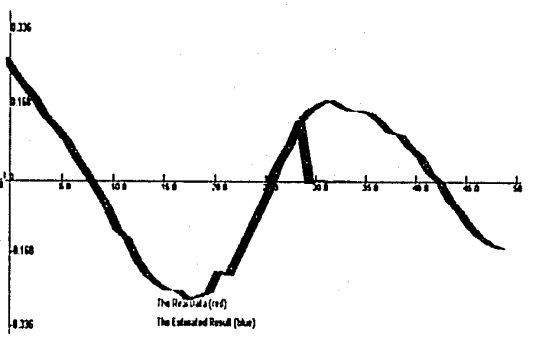

(j) Quadrature Components on 5th path

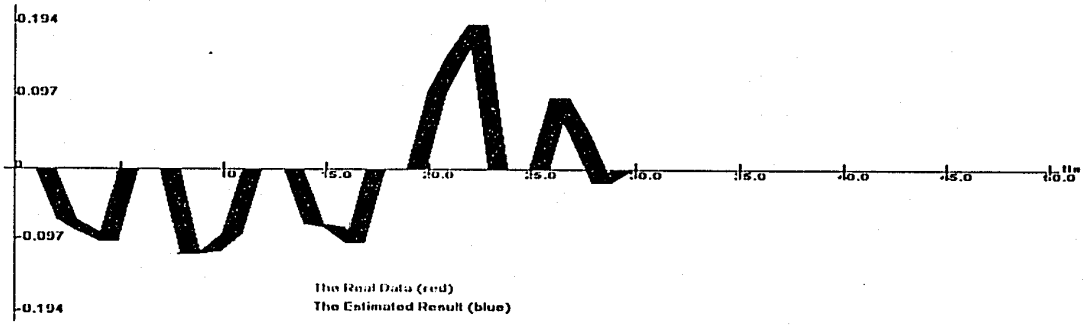

(k) the Output Sequences

Figure B-12. the Estimated Results for Frequency-selective SlowFading Channel (N=5 case)

Appendix C

The Web-based Fading Channel Simulation and Estimation (WFSE) System Operating Guide

This appendix introduces the operating guide for the web-based fading channel simulation and estimation (WFSE) system including the system's characteristics and functions, Graphics user interface and operations.

C.1 Introduction to the WFSE System

The WFSE system is designed and developed an online tool for the radio fading channel to build mathematical models, to simulate and estimate the characteristics, and to identify system parameters based on the measurement data. This section just introduces advantages and features of the WFSE system.

C.1.1 Advantages of the WFSE System

The WFSE system is a web-based application. Many Java new techniques are used in the system, thus the system has the following advantages:

- To be run on any browsers and any operating systems.
- To be used simply.
- To be added new functions.

C.1.2 Requirement of Running the WFSE System

The WFSE system is a client-side application implemented by Java Applet.

The main problem is that the JDK versions are mismatched between Java Applet and the web browsers. In order to run the WFSE system, the local computers should be installed the Java Plug-in software package that can be download free from http://java.sun.com/products/plugin/.

C.2 Introduction to Graphics User Interfaces and Operations

The WFSE system is opened to all Internet users; thus its user interfaces and operations should be simply, friendly and easily.

The WFSE system includes four subsystems presented in Chapter 4. One subsystem is used to simulate and estimate the characteristics of the fading channel related to the motion of the receiver or the transmitter; these often used fading channels can be Rayleigh fading, Ricean fading and *N*-path fading channel with known system parameters. One subsystem is applied to test success of the EM algorithm together with the Kalman filter in system identification. One subsystem is employed to identify system parameters based on the real measurement data provided by CRC. One subsystem is used to provide an online help information.

The following subsections will introduce each subsystem's GUI and its operation steps.

C.2.1 A GUI for the WFSE System

The system's GUI provides accessing to the four subsystems as Figure C-1. In this GUI, its operations are very simply. Users can access to any one subsystem by pushing a toolbars or menu operation. For example, when a user pushes the "Fading Channel Simulation & Estimation" toolbar, the user can access to this subsystem.

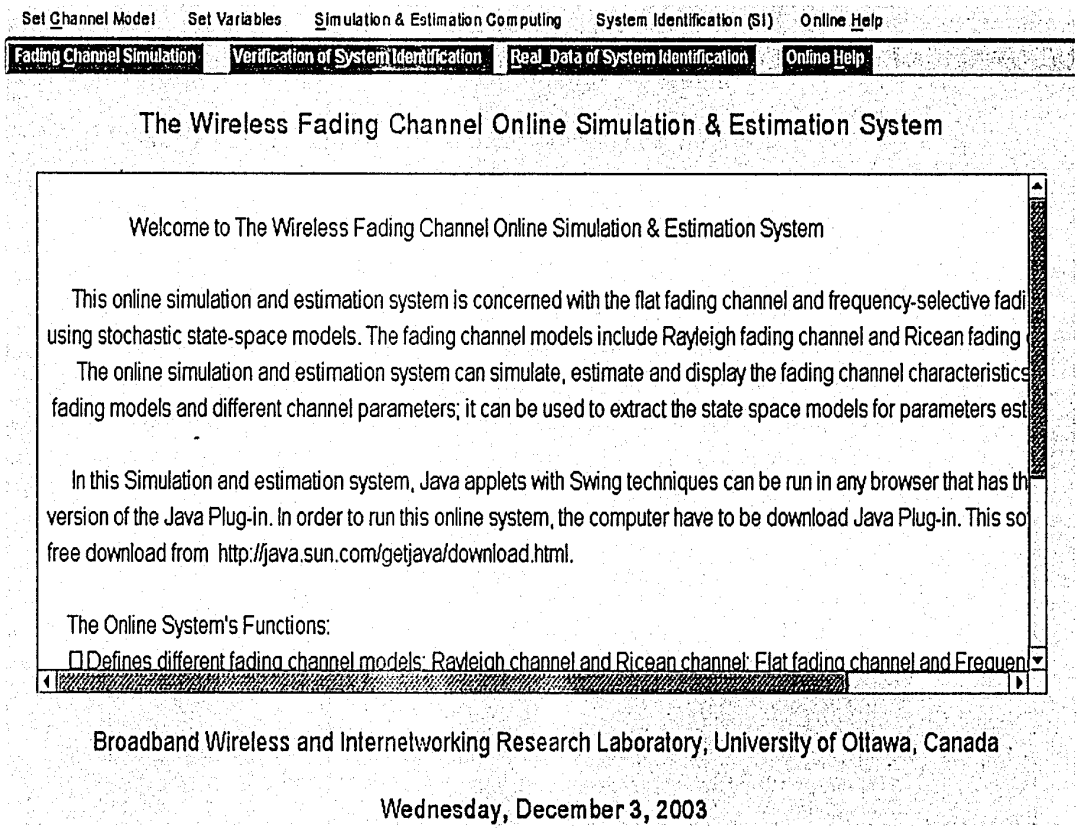

Figure C-1. The System's GUI

C.2.2 A GUI for the Fading Channel Modeling and Estimation

Figure C-2 shows a GUI for the fading channel simulation and estimation subsystem. This GUI is designed to simulate and estimate the characteristics of the flat fading and frequency-selective fading channel related to the motion of the receiver or the transmitter.

This subsystem's GUI provides the following operations:

- *Selecting a type of the fading channel models.*

The fading channel models are classified as the flat fading and the frequency-selective fading. The Rayleigh fading and the Ricean fading are often used for fading channel models; thus they are considered as two examples of the fading channel models.

The frequency-selective fading is considered as a six-path fading channel including a path of the Ricean fading and five paths of the Ricean fading.

Only one model is selected from the model list each time.

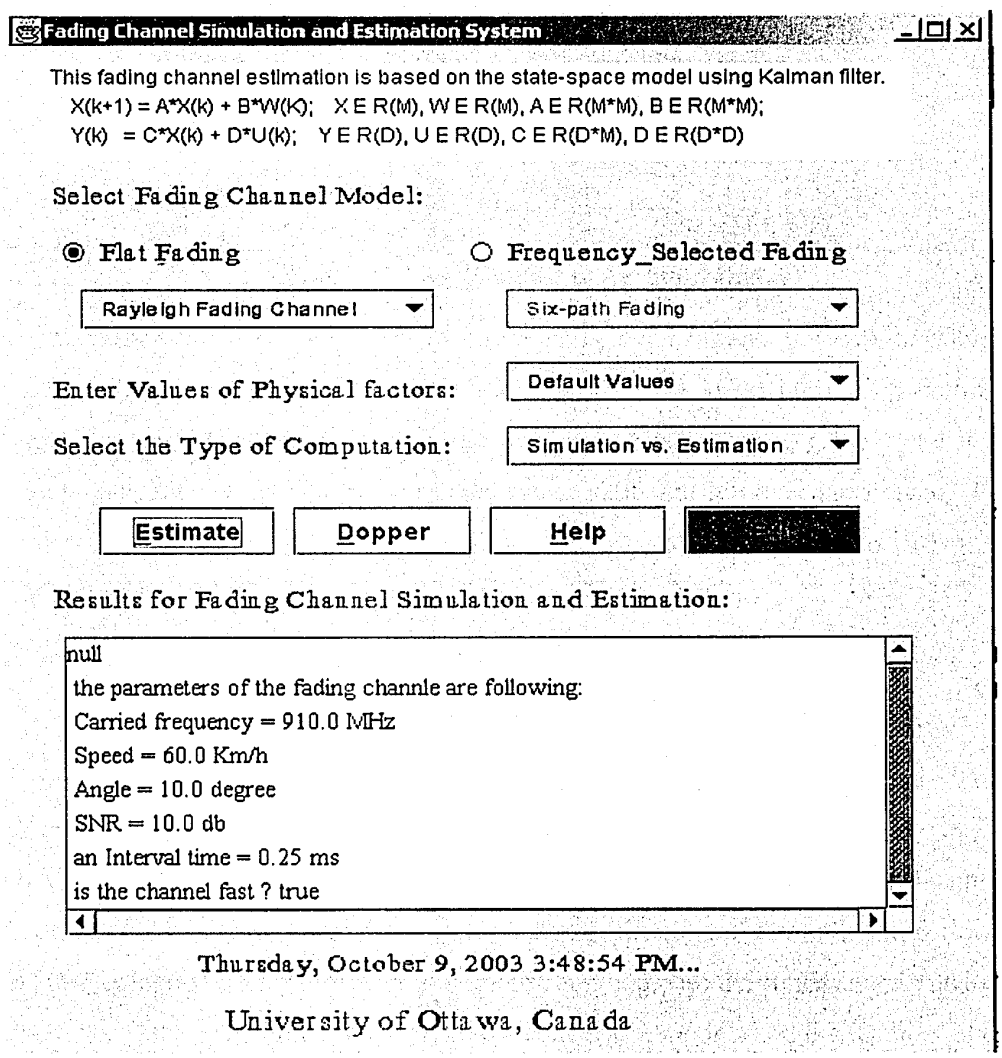

Figure C-2. The Fading Channel Simulation and Estimation Subsystem's GUI

- *Updating values of the physical factors related to the system parameters.*

The subsystem provides the default values for the physical factors related to the motion of the receiver or the transmitter described in Section 2.4. However, these values can be updated through selecting one or more variables from the physical factors list.

When one variable is selected, the input window is opened as Figure c-3. One new value can be inputted; if "OK" button is clicked, the variable is given new value; otherwise the variable keeps its old value.

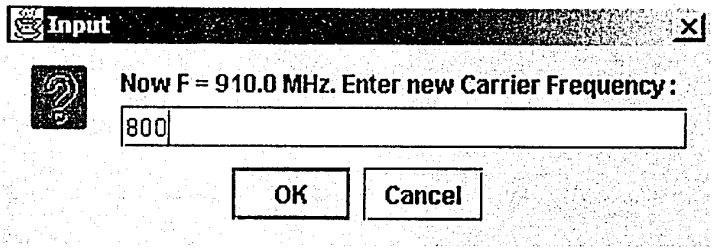

Figure C-3 An Example of An Input Dialog

When inputting a new value, the value must be valid digitals (0~9) or char (dot. or minus -), otherwise the input is invalid. Additionally, the value must keep within the setting ranges between minimal value and maximal value; otherwise, the value is over limited value. If and only if the input operation is valid and not over the limited values, the entering value can be accepted; otherwise, the value of this variable will be fixed at the default value.

- *Selecting a type of computations.*

The computations contain three types: *simulation*, *estimation* and *both simulation and estimation*. The simulation computation is applied to generate and plot the inphase and quadrature components of the fading channel using the state space models; the estimation computation is used to estimate and plot the inphase and quadrature components of the fading channel using the Kalman filters; and the both simulation and estimation computation is employed to compute and compare the inphase and quadrature components of the fading channel through the state space models and the Kalman filters.

Only one type can be selected each time.

- *Selecting an operating button.*

The four operating buttons are listed as *Estimate*, *Doppler*, *Help* and *Exit*.

The "Estimate" button is used to operate the simulation and estimation based on the selected computation type and the values of the physical factors. Once this computing process is finished, the computing results, including the inphase, quadrature, envelope,

phase and MSEs components, will display on several pages. Each page just displays one component.

User can do *Undo/Redo* (<, >), *Zoom* (+, -), *Print* and *Close* operations on each page as Figure C-7. The Undo/Redo operation is to go to next or previous page; the Zoom operation is to enlarge or reduce the size of displaying curves; the Print operation is for printing the current page; and the Close operation is to exit the current page.

The "Doppler" button is used to analyze the Doppler spread based on these values of the physical factors.

The "Help" button is getting online help; and the "Exit" button is used to exit the subsystem. The two buttons are the same operations in all subsystems.

The Sequence diagram in Figure 4-3 describes the above operation.

C.2.3 A GUI for System Identification Verification

The idea of the verification the EM algorithm is based on the following facts. A true model with known system parameters is used to generate the output sequence $\{y_t\}_{t=1}^{N}$ that is considered as the observed data. The system identification process is computed new system parameters through the EM algorithm and the Kalman filter using the observed data. If the estimated system parameters are closed to the true system parameters, it can indicate that the EM algorithm is an effect system identification method for the fading channel models.

Figure C-4 shows a GUI that is used to verify the EM algorithm for system identification.

The process of the verifying operation is showed as the following:

- *Selecting an order for the system parameters.*

The system parameters $\{A, B, C, D\}$ are described in the state space model and $A \in \Re^{n \times n}, B \in \Re^{n \times n}, C \in \Re^{d \times n}, D \in \Re^{d \times d}$ defined in Chapter 3.

In this subsystem, the order of system parameters is defined by the space model $\{n = m = i,\ d = j,\ i = j = 1,2,3,4;\ d \le m\}$.

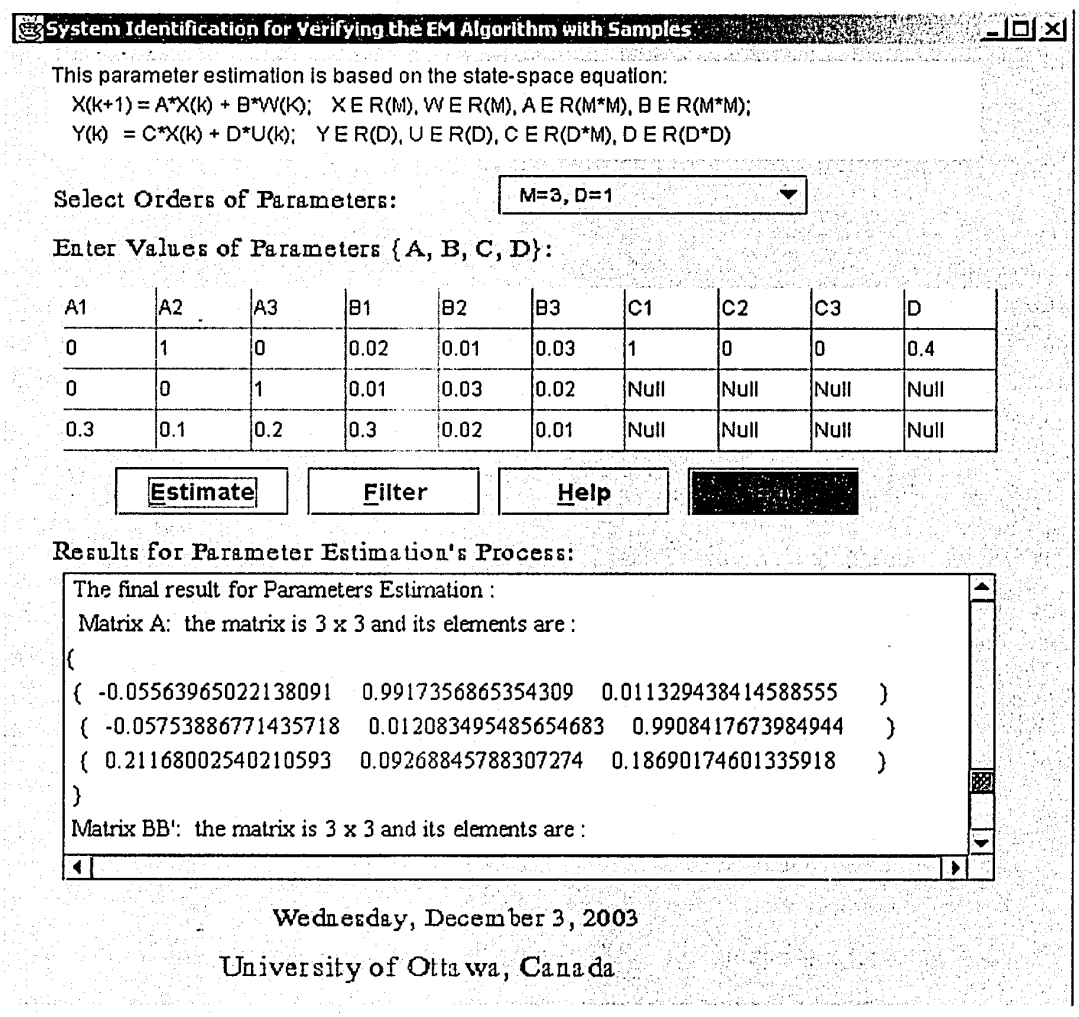

Figure C-4. A Subsystem's GUI of System Identification Verification

- *Entering system parameters* $\{A, B, C, D\}$.

A table lists default values for the different order system parameters $\{A, B, C, D\}$. However, the values can be modified or updated when the user select a cell and enter its value.

- *Selecting a type computation.*

This GUI also provides four button operations: *Estimate, Filter, Help* and *Exit.*

The "Estimate" operation is used to verify the EM algorithm. When "Estimate" button is clicked, the subsystem first checks whether the system parameters are within the range of valid inputting values; then the subsystem computes new system parameters via the EM algorithm together with the Kalman filter. If the computation process is done, the estimated new parameters will be displayed on the text area and some compared results will be plotted on another window. In the computing process, the subsystem also records the iteration counter that is used to count the times of iteration. If the counter is over its limited value, an exception will occur.

The "Filter" operation is used to compute and plot the Kalman filter's results for both the true system parameters and the estimated system parameters.

C.2.4 A GUI for System Identification Based on the Measurement Data

This subsystem is applied to identify system parameters based on the real measurement data. The mathematical models are built on the flat fading and the frequency-selective fading. Figure C-5 shows this subsystem's GUI.

C.2.4.1 Description of the Operations for the Flat Fading Channel

The operations of the flat fading are showed as the following:

- *Selecting a fading channel model.*

The fading models are also classified as the flat fading and the frequency-selective fading. Therefore, when one model is selected, other one can not be selected.

- *Selecting an order of the fading model parameters.*

The system parameters $\{A, B, C, D\}$ of the flat fading are described four cases presented in Section 3.4, thus "S*elect Model's Order*" lists these four cases.

- *Selecting a type of the data component.*

The real measurement data is classified into two components: the inphase component and the quadrature component. "*Select Data Component*" lists the two components and the default component is the inphase component.

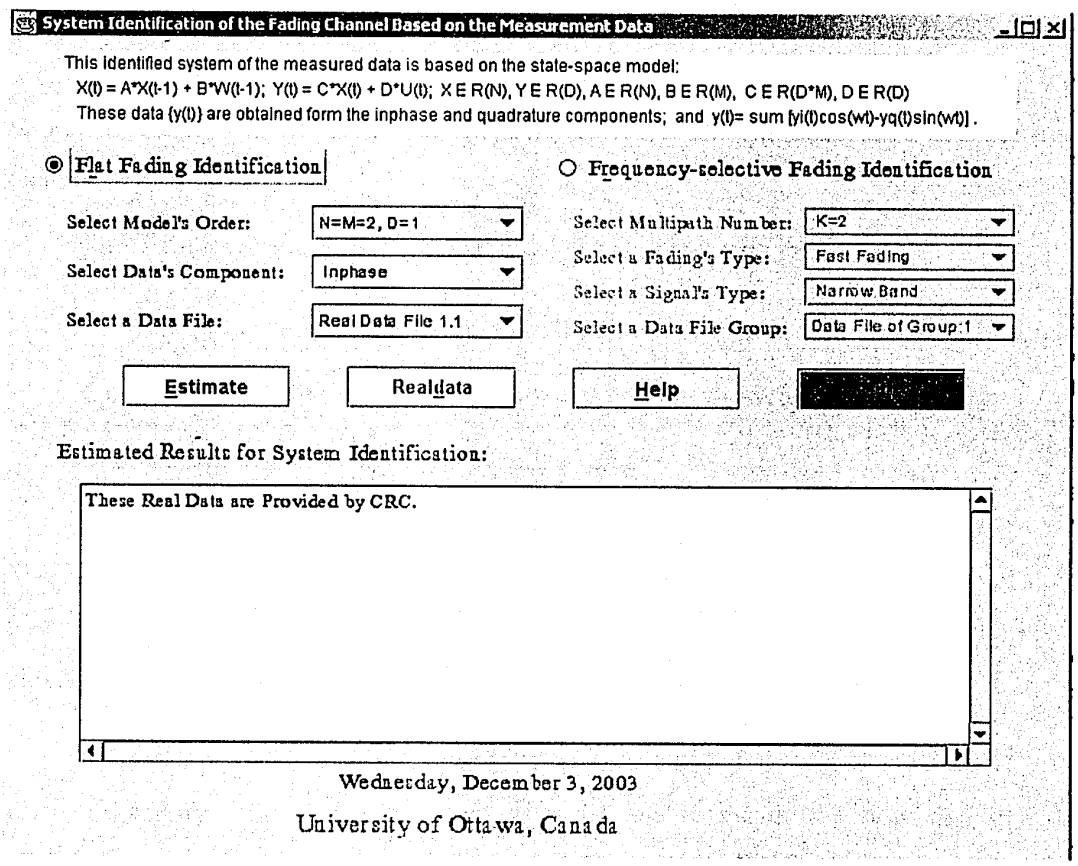

Figure C-5. A Subsystem's GUI of System Identification Based on the Measurement Data

- *Selecting a data file from the measurement data.*

The measurement data include 98 data files. The 49 data files are from the inphase components and the other 49 data files are from the quadrature component. Each 49 data files are classified as 7 groups and each group also includes 7 data files.

- *Selecting a button operation.*

The subsystem includes four button operations: *Estimate, RealData, Help* and *Exit*.

The "Estimate" button is used to estimate the model parameters based on the measurement data using the EM algorithm and the Kalman filter. When "Estimate" button is clicked, the estimating computation process starts. Firstly, the system reads the selected data file that is considered as the output sequence $\{y_t\}_{t=1}^{N}$. Secondly, the system computes new system parameters through the EM algorithm; in addition, the system also

checks the iteration counter. Finally, when the computation process is finished, the computation results will be displayed on the text area, and the comparison results will also be displayed on the other window for both the estimated parameters and the true model.

The "Realdata" button is used to plot the selected real data file.

C.2.4.2 Description of the Operations for the Frequency-selective Fading Channel

The operations of the frequency-selective fading are showed as the following:

- *Selecting a number as the multipath number.*

The multipath number can be selected N=2, 3, 4, 5, 6, 7 from "*Select Multipath Number*". Because each group of the measurement data files contains seven sets of data files. Therefore, each set of the data file can be considered as one path in the multipath fading channel.

- *Selecting a type of the fading channel.*

The fading channel can be selected as the fast fading or the slow fading from "*Select Fading Type*". In this slow fading case, the sample size is set 50.

- *Selecting a type of the transmitted signal.*

The transmitted signal can be selected a narrowband signal or a wideband signal from "*Select Transmitted Signal*".

- *Selecting a data group from the measurement data.*

The measurement data include 7 groups. Each group integrates the inphase components and the quadrature components from the measurement data files. Thus a group data file can be selected from "*Select Data File Group*".

- *Selecting a button operation.*

The subsystem includes three button operations: *Estimate, Help* and *Exit*. These operations are the same as the above descriptions.

C.2.5 GUI for Online Help

Figure C-6 shows a online help GUI which provides lots of information about the WFSE system. For example, the help information includes how to set parameters, how to enter values of variable, how to run this system, how to understand exceptions, etc. These help information is to help users to master this system and guide them to solve their problems. It is very easy for user to operate this GUI. by selecting each question and obtaining the relative help information.

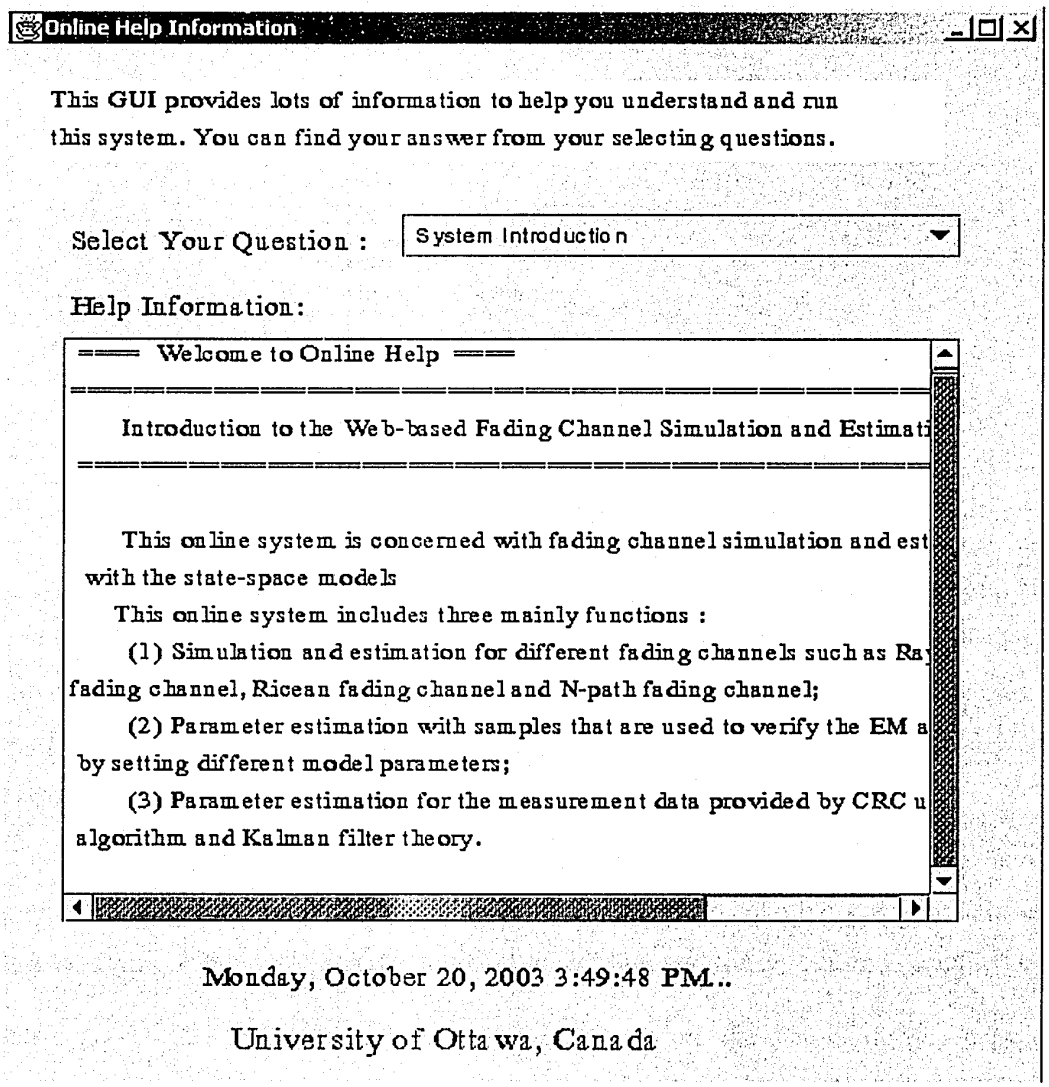

Figure C-6. A Subsystem's GUI of Online Help

C.3 Introduction to Results Plotting

In the WFSE system, a lot of computing results are plotted in 2 dimension plane. Figure C-7 is an example of plotting results.

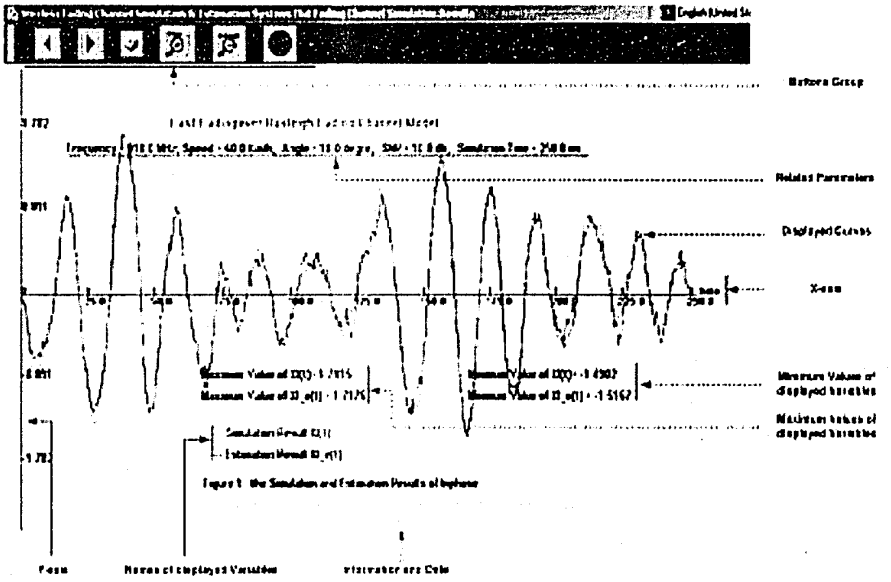

Figure C-7 An Example of Plotting Result

This figure includes six operation buttons, the important parameters description and the final simulation results. These operation buttons, such as ◀, ▶,  ,  ,  and  , provide the relative operations; and these parameters description provide the displayed variable(s), its maximum and minimum values, related system parameters, date and so on. The simulation results shows the final simulation results based on the selected parameters and types.

Users can display, zoom and print many displaying pages by these button operations. The buttons, ◀ and ▶, are used to switch the displaying page forward and backward; the ◀ button is used to go to previous page; and the ▶ button is used to go to next page. The buttons,  and  , are used to zoom the size of displayed pages; when the button  is clicked once, the size of the displayed page increases 10%; when

the button  is clicked once, the size of the page decreases 10%; the maximum limitation of zooming is 50%. The button  is used to print the current page. The button  is used to close the opening window and stop running.

Appendix D

Installing the CD-ROM

The companion CD-ROM contains all of the author's java source codes and the measurement data for the web-based fading simulation and estimation system.

D.1 Installation Instruction

The Java source code in the CD-ROM is easy to install into a local computer. The following introduces the install, compile and run the Window operating system.

- Insert the CD-ROM disc into your CD-ROM drive
- From the Windows Explorer, Set your folder at your driver
- Copy these files from CD-ROM into your folder

D.2 Compiling and Running

The Java source code can be run in any operating systems that include JDK version 1.3 or above.

D.2.1 Compiling and Running in JBuilder Tool

The software package is edited, compiled and run using JBuilder7.0 or JBuilder9.0. If the local computer is already installed with JBuiler that can be download free from http://www.borland.com/jbuilder.

In JBuilder tool, you just open this project with "WirelessSim" from "File/Open Project", the java files are listed; then you run this project from "Run/Run Project", a Java GUI will be displayed. You just follow the operating guide to run this system.

D.2.2 Compiling and Running in Windows Operating System

The source code can also be compiled and run in Window operating systems, you just use compile.bat for compiling Java source code and use run.bat for running Java source code. However you must change the class path of JDK and the source code.

These are examples for compiling and running Java source code. In these examples, it is assumed that JDK 1.4.0 is installed in C:\Java\ and the source code is installed in c:\work\.

D.2.2.1 Compiling Instruction

- path=c:\Java\jdk1.4.0\bin
- set CLASSPATH =c:\Java7\jdk1.4.0\lib\dt.jar;
  c:\Java\jdk1.4.0\lib\tools.jar;
  c:\Java\jdk1.4.0\jre\lib\jaws.jar;
  c:\work\WirelessSim\src; c:\\work\Wireless\classes;
- cd c:\work\WirelessSim\src
- javac –d c:\work\WirelessSim\classes *.java

D.2.2.2 Running Instruction

- path=c:\Java\jdk1.4.0\bin
- set CLASSPATH=c:\work\WirelessSimCopy\classes;
- cd c:\work\WirelessSim\classes
- java UserInterfaces

Note: the thesis does not include all Java source codes. If some one is interested in our research, please contact with my superior, Professor C.D Charalambos.

References

[AKA97] Y. Akaiwa. *Introduction to Digital Mobile Communication*, ISBN: 0471175455, 1st edition, Wiley-Interscience. 1997

[AUL79] T. Aulin. *A Modified Model for the Fading Signal at a Mobile Radio Channel.* IEEE Transaction on Vehicular Technology, vol. VT-28, No.3, August 1979

[BAN95] J. Bank. *Java Security.* 1995 http://swissnet.ai.mit.edu/~jbank/javapaper/javapaper.html

[BAR98] H. A. Barger. *Dynamic Characteristics of a Narrowband Land Mobile Communication Channel.* IEEE Transaction on Vehicular Technology, vol. 47, No.1, February 1998

[BIG99] E. Biglieri, G. Caire and G. Taricco. *Coding for the Fading Channel: a Survey.* Signal Processing for Multimedia, J.S. Byrnes (Ed.); IOS Press, 1999

[BORBD] Borland Software Corp. *JBuilder Tutorial.* http://www.borland.com/jbuilder

[BRO98] E. Brookkner. *Tracking and Kalman Filtering Made Easy*; ISBN 0471184071, John Wiley & Sons, 1998

[BUL00] R.J.C. Bultitude, G. Brussaard, M.H.A.J. Herben and T.J. Willink. *Radio channel modeling for terrestrial vehicular mobile application.* Proc. ICAP/JINA Millennium Symposium on Antennas and Propagation, Davos, Switzerland, April 2000

[BUL01] R.J.C. Bultitude and M.H.A.J. Herben. *Segmentation of Measured Data for Modelling of Nonstationary Narrowband Radio Channels in Urban Microcells*; EUROPEAN Cooperation in the filed of science and technical research, 2001

[BUL02] R.J.C. Bultitude, C.D. Charalambous, X. Li, M.H.A.J. Herben and G. Brussaard, *Development of a model for realistic portrayal of random time variations on mobile radio channels.* Accepted for presentation at the XXVIIth URSI General Assembly, Maastricht, The Netherlands, August 2002

[CHA98] C.D. Charalambous, A. Logothetis and R.J. Elliott. *Bank filters for ML Parameter Estimation via the Expectation-Maximization Algorithm: the continuous-time case.* IEEE Transaction on Automatic Control, Tampa, Florida, U.S.A., 1998

[CHA991] C.D. Charalambous and N. Menemenlis. *Multipath Channel Models for Short-term Fading.* 1999 International Workshop on Mobile Communications, Crete, Greece, June 1999

[CHA992] C.D. Charalambous and N. Menemenlis. *Stochastic Models for Long-term Multipath Fading Channels.* The 38th IEEE Conference on Decision and Control, Phoenix, Arizona, December 1999

[CHA00] C.D. Charalambous and A. Logothetis. *Maximum-Likelihood Parameter Estimation from Incomplete Data via the Sensitivity Equations: The continuous-time case,* IEEE Transactions on Automatic Control, Vol. 45, No. 5, May 2000.

[CHA01] C.D. Charalambous and N. Menemenlis. *A State Space Approach in Modeling Multipath Fading Channels via Stochastic Differential Equations.* IEEE International Conference on Communications, Finland, Helsinki, June 2001

[CHA03] C.D. Charalambous, J. zhan, X. Li and R.J.C. Bultitude. *Radio Channel Modeling, Estimation and Identification from Measurement Data.* EUROPEAN Cooperation in the filed of science and technical research, 2003

[CHE01] J. Cheesman and J. Daniels. *UML Components.* ISBN 0-201-70851-5, Addison-Wesley, 2001

[CLA68] R.H. Clarke. *A Statistical Theory of Mobile Radio Reception.* Bell Systems Technical Journal, vol.47 July-Aug. 1968

[CON99] J. Conallen. *Building Web Applications with UML.* ISBN 0-201-61577-0, Addison-Wesley, 1999

[COO91] J.E. Cooling. *Software Design for Real-time Systems.* ISBN 0-412-63240-3, Chapman and Hall, 1991

[DAV85] M.H.A. Davis and R.B. Vinter. *Stochastic Modeling and Control.* ISBN 0-412- 16200-8, Chapman and Hall, 1985

[DAZ95] John J.D'Azzo and C.H. Houpis. *Linear Control System Analysis and Design: Conventional and Modern.* ISBN 0-07-016321-9, McGraw-Hill, 1995

[DIN97] P.S.R Diniz. *Adaptive Filtering, Algorithm and Practical Implementation,* Kluwer Academic Publishers, Norwell, Massachusetts, 1997

[FEC93] S. A. Fechtel. *A Novel Approach to Modeling and Efficient Simulation of Frequency-Selective Fading Radio Channels.* IEEE Journal on Selected Areas in Communications, vol. 11, April 1993

[FOW99] M. Fowler. *UML Distilled: A Brief Guide to the Standard Object Modeling Language.* 2nd edition, ISBN 020165783X, Addison-Wesley, 1999

[FRI86] B. Friedland. *Control System Design: An Introduction to State Space Methods.* ISBN 0-07-022441-2, McGraw-Hill, 1986

[GAN72] M Gan. *A Power Spectral Theory of Propagation in the Mobile Radio Environment.* IEEE Transaction on Vehicular Technology, vol. VT-21, No.1, February 1972

[GAR96] V. K. Gary and J. E. Wilkes. *Wireless and Personal Communication Systems.* 1996

[GIL97] S. Gilbert and B. McCarty. *Object-Oriented Programming in Java.* ISBN 1-57169-086-7, 1997

[GRI98] M.J. Grimble and M.A. Johnson. *Optimal Control and Stochastic Estimation: Theory and Applications.* Volume 2, ISBN 0-471-91265-4, John Wiley & Sons, 1998

[HAE00] E.R. Harold. *Java Networking Programming.* 2nd edition, ISBN 1-56592-870-9, O'Reilly, 2000

[HAR01] M.V. Harmelen. *Object Modeling and User Interface Design.* ISBN 0-201-65789-9, Addison-Wesley, 2001

[IBM02] IBM. *UML Resource Center* http://www.rational.com/uml/

[JAK74] W.C. Jakes. *Microwave Mobile Communications.* IEEE Press, New York, 1974

[JAM99] J. Jaworski. *J2EE Platform Unleashed.* ISBN: 0-672-31631-5, Sams, 1999

[KAL80] G. Kallianpur. "*Stochastic Filter Theory*". ISBN 0-387-90445-X, Springer-Verlag New York, 1980

[KOM00] C. Komninakis, C. Fragouli, A. H. Sayed and R. D. Wesel. *Adaptive Multi-Input Multi-Output Fading Channel Equalization using Kalman Estimation.* PROC. ICC 2000, VOL. 3, PP. 1655–1659, NEW ORLEANS, LOUISIANA, 2000

[KOM02] C. Komninakis, C. Fragouli, A. H. Sayed and R. D. Wesel. *Multi-Input Multi-Output Fading Channel Tracking and Equalization Using Kalman Estimation.* IEEE Transactions on Signal Processing, VOL. 50, NO. 5, May 2002

[KUB99] T.E.G. Kubin, M Sternad and A. Ahlen. *Quadratic and Linear Filters for Mobile radio channel*; Extended and revised version of VTC, 1999

[LIX02] X. Li. *State Space Estimation of Wireless Fading Channels.* University of Ottawa, Master's thesis, 2002

[MUG02] K.A. Mughal and R.W. Rasnussen. *A Programmer's Guide to Java Certification.* ISBN: 0201596148, Addison-Wesley, 2002

[NES00] A Neskovic, N. Neskovic and G. Paunovic. *Modern Approaches in Mobile Radio Systems Propagation Environment.* IEEE Communications Surveys; Third Quarter 2000

[OGA02] K.Ogata. *Modern Control Engineering.* 4th edition, ISBN: 0-13-060907-2; Prentice Hall, 2002

[OSS64] J. Ossana. *A Model for Mobile Radio Fading due to Building Reflections: Theoretical and Experimental Fading Waveform Power Spectra.* Bell Systems Technical Journal, Vol. 43, No.6, pp. 2935-2971, November 1964.

[OWE97] D.H. Owens and G. S. Munde. *Stability of a Multi-Input, Multi-Output Adaptive Iterative Learning Control System.* European Control Conference (ECC), Brussels, July 1997

[PRO00] J. Proakis. *Digital Communications.* 4th edition, ISBN 0072321113, McGraw-Hill, 2000

[RAP96] T.S. Rappaport. *Wireless communications: Principles and Practice.* ISBN 0-13-375536-3, Prentice Hall, 1996

[RUM98] J. Rumbaugh, I. Jacobson and G. Booch. *The Unified Modeling Language Reference Manual.* ISBN 0-201-30998-X, Addison Wesley Longman, 1998

[SAM02] D. Samardzija & N.Mandayam. "*Pilot Assisted Estimation of MIMO Fading Channel Response and Achievable Data Rates*". DIMACS Workshop on Signal Processing for Wireless Transmission, Rutgers University, October 2002.

[SAT00] J.W. Satzinger and T.U. Orvik. *The Object-Oriented Approach: Concept, System Development, Modeling with UML.* ISBN 0-619-03390-8, Thomson, 2000

[SK971] B. Sklar. *Rayleigh Fading Channels in Mobile Digital Communication Systems Part I: Characterization.* IEEE Communications Magazine, July 1997

[SK972] B. Sklar. *Rayleigh Fading Channels in Mobile Digital Communication Systems Part II: Mitigation.* IEEE Communications Magazine, July 1997

[SMI98] D. Smith. *Java for the World Wide Web.* ISBN: 0-201-35340-7, Peachpit Press, 1998

[SUNAP] Sun Microsystem Inc. *Trail: Writing Applets*
http://java.sun.com/docs/books/tutorial/applet/

[SUNBC] Sun Microsystem Inc. *Trail: Learning the Java Language*
http://java.sun.com/docs/books/tutorial/java/index.html

[SUN2D] Sun Microsystem Inc. *Trail: 2D Graphics*
http://java.sun.com/docs/books/tutorial/2d/index.html

[SUNJF] Sun Microsystem Inc. *Trail: JAR Files*
http://java.sun.com/docs/books/tutorial/jar/index.html

[SUNPL] Sun Microsystem Inc. *Java Plug-in Developer Guide.*
http://java.sun.com/j2se/1.4/docs/guide/plugin/developer_guide/

[SUNSC] Sun Microsystem Inc. *Lesson: Java Security API Overview.*
http://java.sun.com/docs/books/tutorial/security1.1/overview/index.html

[SUNSW] Sun Microsystem Inc. *Trial: Creating a GUI with JFC/Swing*
http://java.sun.com/docs/books/tutorial/uiswing/

[SUNWB] Sun Microsystem Inc. *The Java Web Services Tutorial*
http://java.sun.com/webservices/tutorial.html

[VAN96] L. Vanhelsuwe and L. Phillips. *Mastering Java 1.1.* 2nd edition, ISBN: 0-7821-2070-9, Sybex, 1996

[ZIE96] R. E. Ziemer. *An Overview of Modulation and Coding for Wireless Communications.* IEEE, 1996